RHODES UNIVERSITY

Where leaders learn

The exploration of ARF1 screening assays to determine the drug status of ARF1 in cancer and malaria

A dissertation submitted in fulfillment of the requirements for the degree of Master of Science in Biochemistry

Apelele Ntlantsana

February 2020

Supervised by: Professor Heinrich Hoppe

ORCID: 0000-0002-1734-9925

Abstract

ARF GTPases are key regulators of the secretory and endocytic pathways. ARF1 is involved in the secretory pathway. ARF1 has been implicated in the endoplasmic reticulum to Golgi transport, function of the Golgi apparatus and transport from the trans-Golgi network to endosomes. ARFs cycle between active GTP-bound and inactive GDP-bound conformations. GDP/GTP cycling is regulated by large families of guanine nucleotide exchange factors (GEFs) and GTPase activating proteins (GAPs). ARF GEFs facilitate the activation of ARFs by mediating the exchange of GDP for GTP, while ARF GAPs terminate ARF function by stimulating the hydrolysis of the terminal phosphate group of GTP. Based on existing evidence gained from gene manipulation and cell biological investigations, ARF1 has been shown to be fundamentally important for cancer cell proliferation and metastasis and may be a promising target for the development of anti-cancer drugs. Additionally, the conservation of ARFs in eukaryotic organisms leads to an interesting question of whether a single drug target can be used to target multiple diseases. In this case, can a human cancer drug employed for cancer therapy be used in anti-malarial drug therapies? To confirm the drug target status of ARFs using chemical validation experiments, novel inhibitory compounds are needed. This requires the development of complex *in vitro* protein- protein interaction assays that can be used to screen chemical libraries for ARF GTPase inhibitors. In this study, we developed a fluorescence resonance energy transfer (FRET) assay and a novel *in vitro* colorimetric plate-based assay to detect the activation status of truncated human and *Plasmodium falciparum* ARF1. In the case of the FRET assay, active (GTP-bound) and inactive (GDP-bound) ARF1 could be distinguished with Z-factor values >0.5, suggesting that further development of the assay format to identify GEF and GAP inhibitors may be feasible. In the case of the colorimetric assay, robust signals could be detected and the assay was useful for detecting the activation status of ARF1. However, although the activation of ARF1 by the Sec7 domains of the BIG1 and ARNO was detectable, signals were not robust enough to employ in screening campaigns.

Acknowledgements

To God, the Alpha, the Omega, my shield, my glory, the One who lifts my head high… Thank you Father, thank you Jesus and thank you Holy Spirit. In times where I needed guidance, I prayed and you answered for you always answer. In times where I knew that only you could intervene, I prayed to you and you did just that. I could have never done this without you. I wrote this dissertation with the sole aim to glorify you and I hope you are pleased with my work ethic. Thank you for walking this journey with me. I have expanded my skill set and learnt soft skills in the process to equip me to be the creation you have predestined for me to be. Thank you for your GRACE and LOVE Lord.

To my supervisor, Professor Heinrich Hoppe, thank you for your supervision and guidance through my degree. I honestly have learnt to be an independent thinker. You have allowed me the freedom to express myself as a student and that allowed me to cultivate self-belief. Thank you for believing in me and trusting me as a student. Thank you for going the extra mile in making sure that I can produce the best possible outcome as I was conducting my research. The extra hours that you have put in did not go unnoticed. Thanks Smart Hoppe!

To the present and past research group members, thank you for the pleasant work environment. Special mention to Dustin Lamming and Tarryn Swart for your assistance in my research. Thank you to the academic, technical and cleaning staff of the Rhodes University Biochemistry and Microbiology department for contributing towards my educational experience.

To my family, I am so grateful to God for all of you. To my parents, Mr M.H. Ntlantsana and Mrs K.P. Ntlantsana, thank for believing in me and throughout you have never questioned me because you trust me to be able to make sound decisions. I grew up with that assurance. Thank you for providing for me, praying for me and loving me. Mama, thank you so much for everything and indeed God chose the best womb for me. To my siblings, T. Kgopa, S. Ntlantsana and N. Ntlantsana, thank you for loving me and encouraging me. To T. Kgopa, thank you for being a great example as I have been growing up. Thank you for praying for me and for your counsel. To S. Ntlantsana, so I am submitting my M.Sc dissertation and we are eagerly waiting for you to submit yours. Thank you for always checking in on me. I am proud of the man and professional you are becoming. To N. Ntlantsana, thank you for being patient with me and I always know that you are a text away. I wish you all the best in all you do. Through the pain and all that you have had to endure, you have risen and conquered. Thank you for being a great example to us.

To Ukho-Naye Ntlantsana, I still think about you every day and every milestone I achieve is a celebration for both of us. We miss you. You taught me some valuable life lessons my little champion.

To Vuyokazi Ntlantsana, thank you for your support and love. Thank you for being a great example to me. I wish you all the best with your future endeavors. Let us obtain these higher degrees. Your dedication and commitment to learning has motivated me to go for my goals.

To my Pastors, Ps I Matepo and Ps M Matepo, thank you for loving me. Throughout my journey as I have been serving thank you for sowing into me. At times where I felt discouraged, I was able to communicate and because of your counsel and prayers, I began to shake the dust off myself and walk again. The hours that you put in day after day making sure that you shepherd us in a way that pleases God is amazing and I thank you for that. May God continue to strengthen you and bless you.

To Khanyisile Ngcongco, thank you so much for the love, encouragement and the fellowship. Wow, I will miss the tea times, the jokes, the meaningful conversations we had. You have a bright future ahead of you. I have seen you emerge and I am excited for you to grow your skill set and knowledge so that you can function in the realm of greatness that was predestined for you by God.

To Farrah Khan, thank you so much for the love, encouragement. You have been part of my journey as a post graduate student and you have helped me so much. I truly would have never thought that our friendship would grow in the way it has and I thank you for that. One day, I look forward to working with you in a professional space because I see the capacity you have to impact those that work with you. You are a great example of excellence and truly any supervisor or employer is lucky to have you. All the best with your future endeavors.

To Charlie Mzimane, thank you so much for the love and encouragement. Over the past two years, you have played such a significant role in my life and I know will continue to be significant. Thank you for taking care of me. Thank you for being present in my corner.

To Armand and Kananelo Mukenge, thank you so much for your love and encouragement. I can always depend on you. Thank for interceding for me and genuinely having a heart for me and all that concerns me. You have always seen great potential in me and thank you for seeing the best in me.

To Mihlali Ntsabo, thank you for sticking with me since the earliest days of our university experience. This achievement marks something for both of us. We spoke such moments into existence and we still speak more moment into existence. I also look forward to the game changer you are becoming.

To Sandile Lubisi, thank you for supporting and cheering for me. Thank you for showing genuine and consistent interest in my wellbeing. My encounters with you are significant and you have been making an impact and you will continue to do so.

Thank you to the following for being a solid support system: Bella Boqo, Nwabisa Magengelele, Mihlali Stoffels, Vutomi Mabaso, Milisa Ganiso, Wanda Panya, Mmampe Khumalo, Akhona Ngqinambi, Mary Maluleke, Tatenda Chatikobo, Sive Maholwana, Siyolise Phunguphungu, Johanna Mothatha, Precious Makwerela, Teboho Mdiniswa and Tumelo Msutu. It was through significant encounters that I had with you that helped me to stay motivated and encouraged.

Thank you to the Pearson Young foundation for funding my studies and I look forward to partnering with you as I continue my studies. Thank you to the Bill and Melinda Gates foundation (Grand Challenges Africa award) for funding the running expenses of this project.

Table of contents

List of Abbreviations

ADAP	ARFGAP with dual PH domains
ADP	Adenosine diphosphate
AGAP	ARFGAP with GTPase domain, ankyrin repeat and PH domain
AGFG	ARFGAP domain and FG repeat-containing proteins
AP	Adaptor protein
ARAP	ARFGAP and RhoGAP with ankyrin repeat and PH domains
ASAP	ARFGAP with SH3-domain, ANK repeat and PH domain-containing protein
ARF	ADP ribosylation factor
ARF1	ADP ribosylation factor 1
ARF6	ADP ribosylation factor 6
ARL	ARF-Like
BFA	Brefeldin A
BSA	Bovine serum albumin
$CaCl_2$	Calcium chloride
cAMP	Cyclic adenosine 3′,5′-monophosphate
CDNB	2,4-Dinitrochlorobenzene
CERT	Ceramide Transport Protein
CFP	Cyan fluorescent protein
COPI/II	Coat protein complex I/II
DNA	Deoxyribonucleic acid
dNTP	Deoxyribonucleotide triphosphate
DTT	Dithiothreitol
ECFP	Enhanced cyan fluorescent protein
E. coli	*Escherichia coli*
EDTA	Ethylenediaminetetraacetic acid
ER	Endoplasmic reticulum
EYFP	Enhanced yellow fluorescent protein
FAPP2	Four-phosphate adaptor protein 2

GAP	GTPase activating protein
GDP	Guanosine diphosphate
GEF	Guanine nucleotide exchange factor
GIT	G-protein-coupled receptor kinase-interacting ARFGAPs
GLUT4	Glucose transporter 4
GST	Glutathione S Transferase
GTP	Guanosine triphosphate
HCl	Hydrochloric acid
HiFi	High fidelity
HRP	Horse radish peroxidase
Hs	*Homo sapiens*
Hz	Hertz
kB	Kilobases
KCl	Potassium chloride
IPTG	Isopropyl-β-D-thiogalactoside
$MgCl_2$	Magnesium chloride
$MnCl_2$	Manganese chloride
NaCl	Sodium chloride
NBD	7-nitrobenz-2-oxa-1,3-diazol-4-yl
Ni-NTA	Nickel- nitrilotriacetic acid
OSBP	Oxysterol-binding protein
PBS	Phosphate-buffered saline
PCR	Polymerase Chain Reaction
Pf	*Plasmodium falciparum*
PH	Pleckstrin Homology
PIP	Phosphoinositide
PMSF	Phenylmethylsulfonyl fluoride
Rac	Ras-related C3 botulinum toxin substrate
RNA	Ribonucleic acid
RNAi	Ribonucleic acid interference
ROX	Carboxy-X-rhodamine
SDS	Sodium dodecyl sulfate

SDS-PAGE	Sodium dodecyl sulfate polyacrylamide gel electrophoresis
SMAP	Small ARFGAP
TAE	Tris-Acetate EDTA
TBE	Tris-Borate EDTA
TEMED	Tetramethylethylenediamine
TMB	3,3',5,5'-Tetramethylbenzidine

List of Figures and Tables

Chapter 1: Literature Review

ADP- ribosylation factors (ARFs) are low molecular weight (~ 20-24 kDa) guanosine triphosphate (GTP) binding proteins (also referred to as GTPases) which regulate vesicular trafficking and organelle structure through the recruitment of coat proteins, regulate the metabolism of phospholipids and modulate the structure of actin below the surface of membranes. ARF GTPases act as molecular switches which cycle between two conformations: an active guanosine triphosphate (GTP)-bound state and inactive guanosine diphosphate (GDP)-bound state through the dynamic interaction of the GTPase with ARF guanine nucleotide exchange factors (ARF GEFs) and ARF GTPase- activation proteins (ARF GAPs) respectively. Active ARFs interact with effector proteins which affect cell signaling cascades that mediate downstream cellular functions. ARF GEFs and ARF GAPs are regulated through feedback loops which are fundamental for ensuring that cell signaling systems are irreversible. Feed-forward signaling mechanisms provide another dimension of added regulation wherein the case of ARF GEFs, they selectively recruit specific effector proteins for specific cellular functions. In the case of ARF GAPs, effectors are able to activate ARF GAPs which will subsequently deactivate cognate ARFs (see **Figure 1**) (Donaldson and Jackson, 2000; Bos *et al*., 2007; Cherfils and Zeghouf, 2013; Stalder and Antonny, 2013).

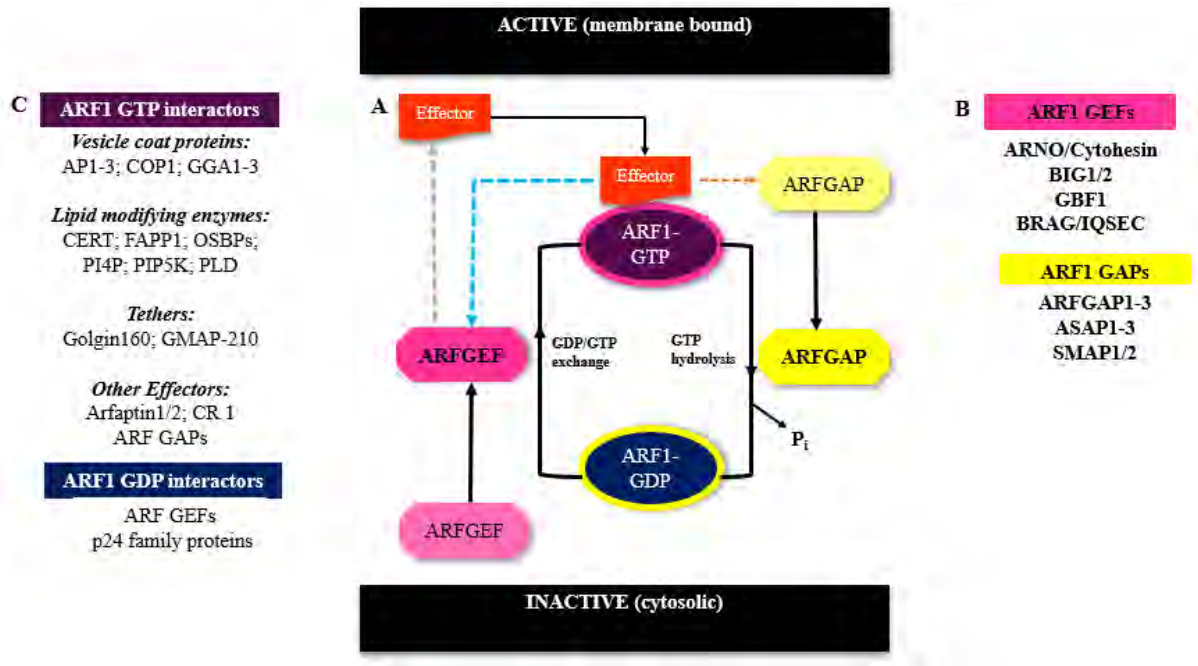

Figure 1: How ARF GTPases are regulated. A: ARF1 regulation. Weak interactions with membranes promote the activation of ARF1-GDP (*navy blue*). ARF GEFs (*pink*) promote the exchange of GDP for GTP, which causes the activation of ARF1, resulting in membrane-bound-ARF1-GTP (*purple*). Based on cellular requirements, ARF GAPs (*yellow*) promote the hydrolysis of GTP and the release of an inorganic phosphate (P_i) by ARF1, which causes the deactivation of ARF1 and results in cytosolic- ARF1-GDP (*navy blue*). Activation signals select a specific GEF (*light pink*) that will result in their active GTPase conformation. Termination signals recruit a GAP (*light yellow*) that results in their inactive GTPase conformation. GEFs and GAPs are embedded in higher-level regulatory mechanisms. This includes feedback loops for GEFs (*dotted blue line*), in which the GTPase controls the efficiency of the GEF and feed-forward mechanisms (*dotted grey line*) where GEFs contribute to the selection of an effector that will be recruited by an active GTPase. For GAPs, feed-forward mechanisms can be achieved by effectors that contribute to activating a specific GAP (*dotted orange line*). **B: ARF1 GEFs and GAPs. C: Inactive and active ARF1 interactors (effector proteins).** (Adapted from Donaldson and Jackson, 2011; Cherfils and Zeghouf, 2013).

1.0. ARF family proteins: nomenclature, classification and main functions

ARFs are a subfamily of the Ras superfamily of proteins that contains at least four different large families of regulatory guanine nucleotide-binding proteins. The ARF subfamily contains different subsets of proteins namely: ARF-like, Sar 1 and ARF proteins (Khan *et al*., 2006; Chavrier and Goud, 1999). ARF proteins are highly conserved and are ubiquitously expressed in all eukaryotic organisms examined. Three ARF subtypes (ARF1-ARF3) are expressed in the yeast *Saccharomyces cerevisiae*, whereas six (ARF1- ARF6) have been identified in mammalian cells (Donaldson and Jackson, 2000; Jackson and Casanova, 2000). Mammalian ARFs can be further classified into three distinct classes based on the amino acid sequence similarity (Tsuchiya *et al*., 1991; Jackson and Casanova, 2000). Class I contains ARF1- ARF3. Class II contains ARF4 and ARF5. Class III contains a sole member, ARF6 which is divergent in terms of function and localization. Class I and Class II ARFs mainly localize at the Golgi and endoplasmic reticulum while the Class III ARF localizes to the plasma membrane and several kinds of endosomes (Donaldson and Jackson, 2000; Hongu *et al*., 2016). Since ARF proteins were first functionally defined as a protein cofactor that is required for cholera toxin catalyzed ADP ribosylation of the stimulatory regulatory subunit (G_s) of adenylyl cyclase and then shown to be GTP binding proteins, more functions of ARFs and ARF-like proteins are being elucidated (Khan *et al.,* 1984; Khan *et al*., 2006). To date, ARF proteins function in fundamental biological processes which include: secretion, endocytosis, phagocytosis, cytokinesis, cell adhesion and tumor cell invasion. These aforementioned biological processes highlight the importance of ARF function and provide insight in the understanding of signaling pathways regulated by ARF1 and ARF6, which are the best characterized ARFs. ARF6 is implicated in the endocytic pathway. It localizes to the plasma membrane and several kinds of endosomes and mediates membrane trafficking between these cellular compartments through endocytosis, exocytosis and endosomal recycling of membrane proteins back to the plasma membrane. Additionally, ARF6 also regulates the rearrangement of the actin cytoskeleton beneath the plasma membrane. ARF1 is involved in the secretory pathway. ARF1 has been implicated in the endoplasmic reticulum to Golgi transport, function of the Golgi apparatus and transport from the *trans*-Golgi network (TGN) to endosomes. (Chavrier and Goud, 1999; Donaldson and Jackson, 2000; Randazzo and Hirsch, 2004; Hongu *et al*., 2016).

2.0. ARF GTPase protein architecture

The characteristic structural organization of ARFs in comparison with other small G-proteins has several consequences for ARF effector recruitment and interaction. ARFs possess a unique N-terminal extension that folds into an amphipathic helix and a glycine residue, at position 2, undergoes a post-translational modification by the addition of myristoyl fatty acid group. The N-terminal amphipathic helix and myristoyl group are both critical for the interaction of ARFs with membranes (Antonny *et al*., 1997; Liu *et al*., 2009; Liu *et al*., 2010). The N-terminal membrane anchoring extension is connected to the G-domain by a short flexible linker that is considerably shorter in ARFs than in other members of the GTP-binding family. The consequence is that ARFs are in close proximity to the bilayer surface which probably imposes a constraint on the orientation of ARF family proteins as well as bringing the binding partners of ARF proteins closer to the bilayer surface, consistent with the fact that ARF binding partners are coat proteins and lipid modifying enzymes that shape or alter lipid bilayers (Liu *et al*., 2007; Isabet *et al*., 2009; Cherfils, 2014). The G-domain, which is a universal feature of GTP-binding proteins, contains all the structural elements for GTP/GDP binding, namely switch 1, switch 2 and interswitch regions. The G-domain is made up of a central, six-stranded β-sheet surrounded by five α-helices. The interswitch region connects switch 1 and switch II regions and is made up of two connected β-strands (Greasley *et al*., 1995; Pasqualato *et al*., 2002). In the GDP-bound form, the interswitch region adopts an atypical retracted position and forms a pocket into which the myristoylated N-terminal helix folds back into. In the GTP-bound form, the interswitch region undergoes a shift by two residues and adopts a conformation where the interswitch obstructs the pocket where the myristoylated N-terminal helix binds, which is then free to associate with membranes through hydrophobic and lipid interactions (Ménétrey *et al*., 2000; Vetter and Wittinghofer, 2001). A unique feature of the G-domains of ARF proteins is two conserved sequences which are the nucleotide-binding sites- the N/TKxD and Gx_4GKS/T motifs. The N/TKxD binds to the base of the nucleotide while the Gx_4GKS/T interacts with the β and γ phosphates of the nucleotide (Vetter and Wittinghofer, 2001; Pasqualato *et al*., 2002).

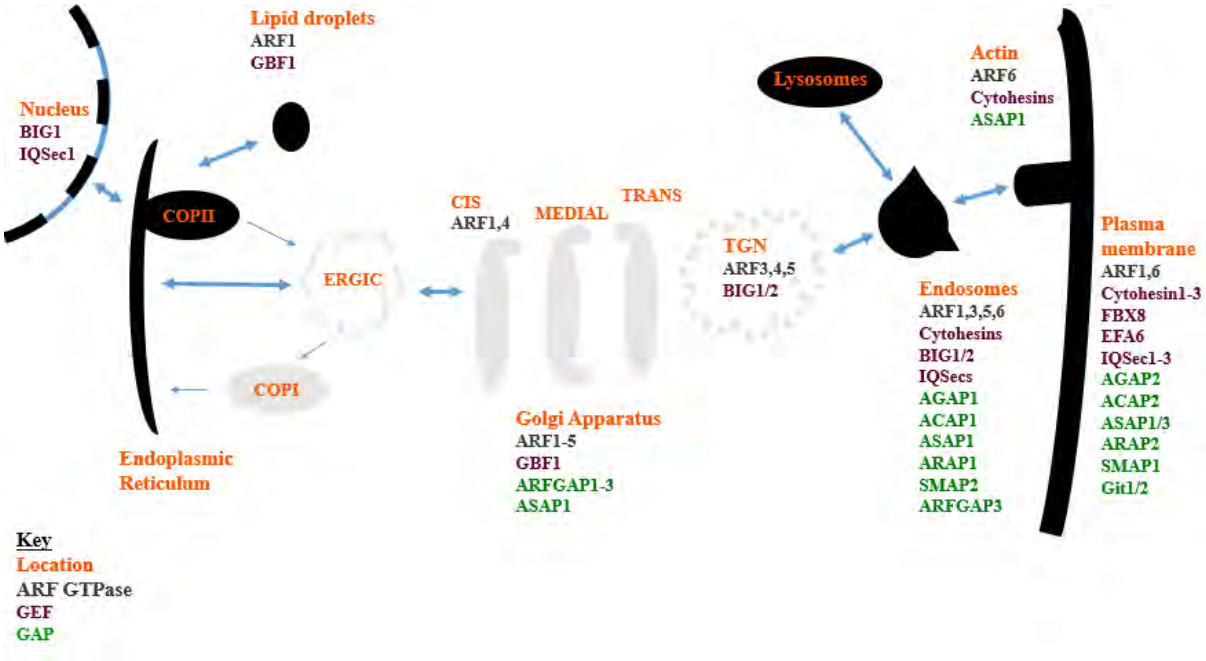

Figure 2: Subcellular localization of ARF GTPases, ARF GEFs and ARF GAPs. ARFs have distinct localization and functions in the Endoplasmic-Golgi system. A schematic representation of a cell is shown with the organelles (*orange*). The approximate localization of some ARF GTPases, relevant to this study are shown (*grey*) along with the approximate localization of some ARF GEFs (*purple*) and some ARF GAPs (*green*). Some abbreviations used: ERGIC- ER-Golgi intermediate compartment and TGN- *trans*-Golgi network (Adapted from Donaldson and Jackson, 2011; Sztul *et al*., 2019).

3.0. Expanding the roles of ARF GTPases: ADP- ribosylation factor interactions

Several studies and in some instances resolved crystal structures provide insight into how ARFs interact with effectors and the downstream effects of ARFs and effector interactions. ARF/effector interactions also provide an expansion of the roles of ARFs and this may depend on the localization of ARFs. Subtle differences in amino acid sequences remain key in governing the specificity of effectors for specific ARFs (Vetter and Wittinghofer, 2001). The localization patterns, which gives insight into the function, of ARFs, ARF GEFs and ARF GAPs are summarized in **Figure 2**. Effectors that interact with active and inactive ARF1 are summarized in **Figure 1** and described below.

3.1. ARF1 GTP interactions

Following the activation on membranes, GTP-bound ARFs recruit coat proteins, lipid-modifying enzymes, tethers and other effectors that influence organelle structure and membrane trafficking. In addition, ARF GTP interacts with ARF GAPs that stimulate GTP hydrolysis and, consequently, ARF inactivation. Considerable work is currently conducted to classify other ARF effectors which may show distinct roles and may not necessarily be classified under these broad categories mentioned above.

3.1.1. Coat complexes

ARF1 plays a crucial role in maintaining the structure and function of the Golgi apparatus. ARF1 localizes to the ER-Golgi intermediate compartment (ERGIC) through which secretory proteins travel from the ER to the Golgi, throughout the Golgi apparatus itself, and to recycling endosomes (Donaldson and Jackson, 2011; Bottanelli *et al*., 2017). As the final compartment that secretory proteins reach when they travel through the Golgi, the TGN is a major site of protein and lipid packaging for delivery to distinct subcellular localizations. At least four post-Golgi anterograde trafficking pathways exist, namely: two pathways from the TGN to the plasma membrane (constitutive and regulated secretion); a pathway from the TGN to endosomes, from where proteins travel to lysosomes; a pathway from the TGN directly to lysosomes. Transport between these compartments occurs via protein-coated membrane vesicles that bud off from the donor membrane. Protein coats have a two-fold function in that they facilitate the sorting and capture of cargo proteins into the forming vesicles as well as promoting the production of a membrane curvature which is responsible for the budding of vesicles from the donor membrane (Boman, 2001; Khan and Ménétrey, 2013). ARF1 recruits coatomer complex I (COPI) to the membranes of the Golgi, allowing for the sorting of cargo into COPI coated vesicles (Beck *et al*., 2009). ARF GTPases at the TGN also recruit heterotrimeric clathrin adaptor proteins (AP), AP1, AP2 and AP3, as well as three monomeric Golgi-localized γ-ear-containing, ADP-ribosylation factor-binding proteins (GGAs: GGA1, GGA2 and GGA3) (Bonifacino and Lippincott-Schwartz, 2003; Bonifacino and Glick, 2004; Cai and Ferro-Novick, 2007). Collectively, these coat proteins bind to and incorporate cargo proteins into forming vesicles for sorting and transporting cargo proteins to correct destinations.

3.1.2. Lipid modifying enzymes

The activation of ARFs leads to changes in membrane lipid composition through active ARF recruitment of lipid-modifying enzymes (Donaldson and Jackson, 2011). ARF proteins activate phospholipase D (PLD), which plays a role in hydrolyzing phosphatidylcholine to generate secondary lipid messenger molecules - phosphatidic acid (PA) and choline. PA serves as an effector for several physiological processes such as cell proliferation, DNA synthesis and secretory responses. ARFs also activate phosphatidylinositol 4-phosphate, 5-kinase (PIP5K), an enzyme that phosphorylates phosphatidylinositol 4-phosphate (PI4P) at the 5-position to generate phosphatidylinositol 4,5-bisphosphate ($PI4,5P_2$). ARF1 at the Golgi plays a role in the recruitment and stimulation of phosphatidylinositol 4-kinase, resulting in the formation of PI4P, an important membrane lipid for Golgi function. ARF1 also binds to PI4P-specific pleckstrin homology domains contained in a family of oxysterol-binding proteins (OSBPs), believed to function in lipid homeostasis at the Golgi (Zhang *et al*., 1995; Hong *et al*., 1998; De Matteis and Godi, 2004; D'Souza-Schorey and Chavrier, 2006). FAPP2, CERT (and OSBPs) are lipid transfer proteins that function at the contact sites of the ER-Golgi membranes where they transfer glucosylceramide, ceramide and sterol, respectively. These proteins bind to the contact sites through their PH domains but this binding requires the presence of ARF1 and PI4P (De Matteis and Godi, 2004; Raychaudhuri and Prinz, 2010).

3.1.3. Tethers

An important class of ARF effectors is long coiled Golgi tethering proteins - golgin160 and GMAP-210 – that facilitate the correct positioning of Golgi compartments and the initial binding of transport vesicles to Golgi membranes (Gillingham *et al*., 2004; Drin *et al*., 2008). Golgin160 is a membrane receptor for cytoplasmic dynein-1 (hereafter referred to as dynein) at the Golgi by directly interacting with the dynein interacting chain, which positions the Golgi next to the centrosome (Yadav *et al*., 2012). In eukaryotic cells, dynein is the major microtubule motor driving the movement of cargo along the microtubule tracks towards the minus end, by making use of the energy produced through the hydrolysis of ATP (Vallee *et al*., 2012; Carter, 2013). GMAP-210 tethers small ER-Golgi vesicles, both COPI and COPII, to flat Golgi cisternae and mediates the association of the Golgi with the centrosome. Cells that have depleted levels of GMAP-210 undergo Golgi fragmentation (Ríos *et al*., 2004; Wong and Munro, 2014).

3.1.4. Other effectors

Polymorphonuclear neutrophils (PMNs) are key cells in innate immunity as they are the first line of defense against infection (Gamara *et al*., 2015). ARF1 has a role in PMNs as it has been shown to bind to complement receptor type 1 (CR 1) storage vesicles and plays a role in the regulation of their transport (Chaudhuri *et al*., 2001).

Cross-talk between members of small G-protein families has a key role in cell signaling pathways. In particular, the coordinated action of ARF and Rho family GTPases (for example Rac) is required for the regulation of cellular processes such as cell motility, lipid signaling and Golgi function (Fensome *et al*., 1998; Bar-Sagi and Hall, 2000). Activated ARF1 is able to recruit arfaptin-1 and arfaptin-2 to the membranes of the Golgi. Arfaptins have been implicated in mediating cross-talk between small ARF GTPases and Rac (Tarricone *et al*., 2001). More recent studies have also shown that the recruitment and association of arfaptins with and the biogenesis of secretory granules at the trans-Golgi in cells is mediated by ARL1 but not other ARF proteins (Man *et al*., 2011; Gehart *et al*., 2012). This also provides evidence that emerging roles are under discovery and the classification of these other effectors could be more defined in the future.

3.2. ARF1 GDP interactions

Besides GEFs that interact with ARF1 GDP and activates it by stimulating GDP/GTP exchange, ARF1 GDP interacts with p24-family of proteins, which recruit coat proteins such as COPI and COPII via sorting signals in their cytoplasmic domains and mediate anterograde and retrograde transport in the early secretory pathway (Nie *et al*., 2003; Langhans *et al*., 2008). The selectivity of the p24-family of proteins for ARF1 GDP, as opposed to ARF1 GTP, was demonstrated in live cells using *in vitro* fluorescence resonance energy transfer (FRET) experiments (Majoul *et al*., 2001).

3.3 Other ARF1 cellular functions

The main function of ARF1 involves initiating the formation of vesicles in the Golgi apparatus by the activation of lipid-modifying enzymes and recruiting the COPI coat proteins. The COPI vesicles are responsible for retrograde transport of cargo and trafficking proteins to earlier

Golgi compartments and the endoplasmic reticulum. Additionally, ARF1 recruits clathrin adaptor proteins (AP1, AP3 and AP4) and GGA proteins to the *trans*-Golgi network, where they are involved in trapping cargo proteins and the formation of vesicles delivering secretory proteins to endosomes (Bonifacino and Lippincott-Schwartz, 2003; Beck *et al*., 2009).

The next section will focus on ARF1 cellular functions that have not yet been described in the earlier sections of this review.

3.3.1. The functional importance of ARF1 during mitosis

The levels of ARF1 change during the cell cycle and the changes in these levels have important functional consequences. When cells enter prophase the ARF1 GTP levels decrease while ARF1 GDP levels increase. ARF1 GTP is found in the lowest levels during metaphase and levels increase again when cells enter telophase. The levels of ARF1 GTP are decreased because the exchange factor activity of the ARF1 GEF GBF1 is decreased - GBF1 is phosphorylated in mitosis by AMP-activated protein kinase (AMPK) and cyclin-dependent kinase 1 (CDK1). The notion that the phosphorylation of GBF1 is of functional importance to the decrease in ARF1 GTP levels during mitosis, is supported by the finding that expression of constitutively active ARF1-Q71L prevents normal mitotic Golgi disassembly and causes defects in the segregation of chromosomes and cleavage furrow ingression during cytokinesis. While the inactivation of ARF1 contributes to Golgi disassembly through the inhibition of ARF1 effector recruitment to membranes, ARF1 activation by GBF1 is not completely blocked during mitosis (Altan-Bonnet *et al*., 2003; Morohashi *et al*., 2010; Mao *et al*., 2013). An important question, which remains to be addressed in future studies, is whether there are spatially or temporally restricted regions of complete inhibition of ARF1 activation or whether there is a partial inhibition throughout the entire cell during the stages of mitosis (Jackson, 2018).

3.3.2. The functional importance of ARF1 in lipid droplets

ARF1 promotes the formation of lipid droplets, which are neutral lipid storage organelles enclosed by a phospholipid monolayer and regulates lipid transfer proteins within the Golgi (De Matteis, and Godi, 2004; Kumari and Mayor, 2008). Lipid droplets are important in the storage of energy in the form of triacylglycerides. ARF1, along with its GEF GBF1 and effector COPI play a role in the metabolism of lipid droplets. ARF1, GBF1 and COPI associate with lipid droplets and are required to recruit a subset of lipid droplet associated proteins, namely adipose triglyceride lipase (ATGL) and perilipin 2, to the surface of lipid droplets (Ducharme

and Bickel, 2008; Soni *et al*., 2009). GBF1 is recruited to lipid droplets through the interaction of the HDS1 domain which binds to lipid droplets in cells and *in vitro* (Bouvet *et al*., 2013). ARF1 GTP and COPI can perform their functions directly on the lipid droplet surfaces and binding directly on the surfaces are important for the regulation of surface properties of lipid droplets during different stages of their metabolisms in cells (Thiam *et al*., 2013; Wilfling *et al*., 2014).

3.3.3. ARF1 works in tandem with ARF6 in actin cytoskeleton regulation

The predominant ARF GTPase in actin remodeling is ARF6. ARF proteins control the actin skeleton through the production of an important regulatory lipid - phosphatidylinositol 4,5-bisphosphate [PtdIns(4,5) P2] - and through the interaction with actin regulators such as the Rho family of GTPases (Brown *et al*., 2001; Aikawa and Martin, 2003). The ARF GEFs Cytohesins and EFA6 as well as ARF GAPs interact with the Rho GTPase family and other regulators of the actin cytoskeleton (Jiménez-Sánchez, 2016). ARF6 activates Rac (sub-family member of the Rho GTPase family) by recruiting the Rac GEF complex DOCK180/Elmo to the plasma membrane. The recruitment is mediated by Cytohesin GEFs which bind to the DOCK180 interactor (Santy *et al*., 2005). ARF1 works in conjunction with Rac to recruit efficiently WASP family verprolin-homologous protein (WAVE) regulatory complex to the plasma membrane and the WAVE regulatory complex (WRC) is a critical element in the control of actin polymerization at the eukaryotic cell membrane (Lebensohn and Kirschner, 2009; Koronakis *et al*., 2011). This highlights that some GTPases, even from different families of the Ras superfamilies, could potentially work in tandem to achieve certain cellular functions, which starts to challenge the preconceived ideas that each class of ARF GTPases works with its specific effectors to carry out cellular effects.

4.0. Activation and deactivation of ARFs by GEFs and GAPs

In the past, the activity of G-proteins has been viewed in a one-dimensional way, a linear signaling pathway, with the inactive form being the GDP-bound state and the GTP-bound state the active form, initiating effector interaction before returning to the inactive state. The GEFs and GAPs were thought of as 'activators' and 'deactivators', respectively, that control this on/off molecular switch. However, the work conducted on ARFs over the past decades has revealed that GEF and GAP signaling is more complex and GEFs and GAPs are able to initiate their own responses to changes in physiological conditions (Donaldson and Jackson, 2011). ARFs function as a network in which the regulators of ARF participate in and integrate ARF activity with other G protein signaling networks in addition to initiating their own distinct signaling pathways. Thus, new roles of ARFs are continuously emerging. Their function is under tight spatial control, mediated by ARF GEFs and ARF GAPs which promote or terminate functions of ARFs respectively. The regulation of ARFs affects their cellular function and ARFs are regulated according to cellular requirements (Bos *et al*., 2007; Donaldson and Jackson, 2011). Subtypes of the ARF family are more distantly related than other members of other small GTPases subfamilies. This gives rise to a wider array of ARF GEFs and ARF GAPs that mediate the function of each ARF subtype (Khan *et al*., 2008).

4.1. ARF GEFs: classification, mechanism and functions

4.1.1. Sec7 domain catalyzes the exchange of GDP for GTP

ARF GEFs are ubiquitously expressed in eukaryotic cells and have been found in some bacterial pathogens as well. To date, the human genome encodes for 15 ARF GEFs which are characterized into six families based on sequence relatedness, domain organization and phylogenetic analyses: BFA inhibited GEF (BIG), Golgi BFA-resistance factor 1 (GBF), ARF nucleotide-binding site opener (ARNO/Cytohesin), Exchange Factor for ARF6 (EFA6/Psd), Brefeldin-resistant ARF GEF (BRAG/IQSEC) and F-box only protein 8 (FBX8) (see **Figure 3** for GEF domain organization). Although divergent in sequence similarity, ARF GEFs share a common catalytic domain known as the Sec7 domain, which consists of approximately 200 amino acid residues (Casanova, 2007; Cherfils and Chardin, 1999; Sztul *et al*., 2019).

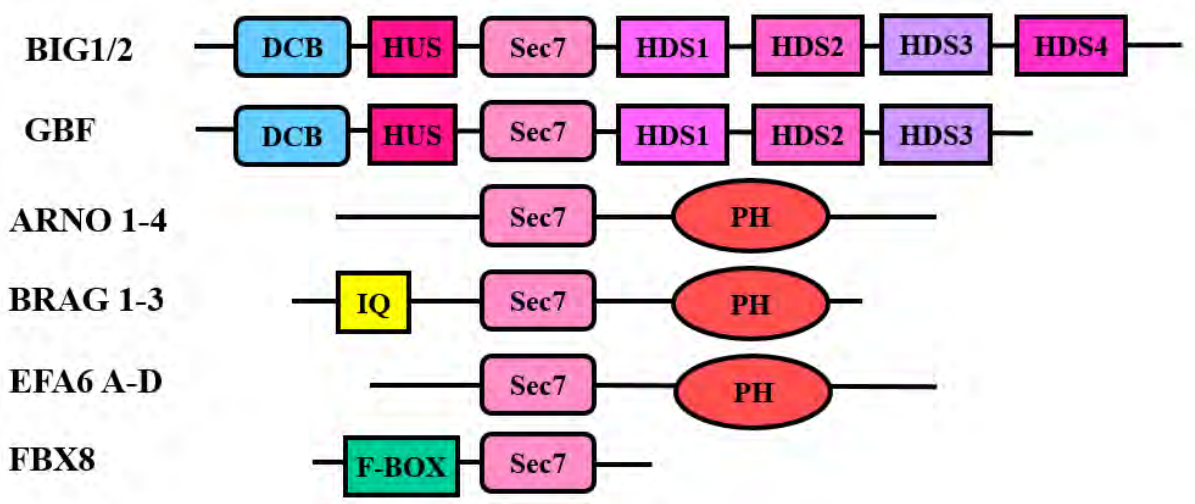

Figure 3: ARF GEF Domain organization. A schematic representation of the domains present in ARF GEF sequences. The defining Sec7 domain is aligned. Protein lengths are not drawn to scale. Abbreviations used are described in alphabetical order. DCB: Dimerization Cyclophilin Binding region; F-BOX: cyclin F protein interaction motif; HDS(1-4): Homology Downstream of Sec7; HUS: Homology Upstream of Sec7; IQ: Isoleucine/glutamine calmodulin-binding motif and PH: Pleckstrin Homology (Adapted from Gillingham and Munro, 2007; Sztul *et al*., 2019).

4.1.2. Mechanism of ARF GEFs to promote GDP/GTP nucleotide exchange

Several crystal structures that have been resolved have been fundamental in suggesting mechanisms by which ARF GEFs promote the exchange of GDP for GTP on ARFs. The Sec7 domain is the minimal fragment serving as a prerequisite to promote GEF activity on ARFs (Cox *et al*., 2004). The Sec7 domain consists of an elongated cylinder, a conserved motif, made up of transverse alpha-helices, separated into two subdomains by a deep, solvent-exposed hydrophobic groove for interaction with ARF substrates (Cherfils *et al*., 1998; Goldberg, 1998). A key feature of the catalytic mechanism is the presence of an invariant glutamate residue which forms a glutamic finger at the tip of a hydrophilic loop between helix 6 and 7. The glutamate residue inserts into the nucleotide-binding fold and through electrostatic interactions compete with the β-phosphate of the bound nucleotide. The nucleotide exchange occurs through sequential ordered steps in which the Sec7 domain institutes the opening of the ARF switch 1 and switch 2 domains, causing a rotation in the core of the ARF protein that drives the nucleotide-binding fold onto the glutamic finger, which causes GDP nucleotide displacement (Béraud-Dufour *et al*., 1998; Casanova and Jackson, 2000; Renault *et al*., 2003). The rotation in the core of the ARF protein also causes changes in the interswitch toggle leading

to an ejection and extension of the N-terminal helix away from the core of ARF protein (Mossessova *et al*., 2003; Renault *et al*., 2003).

Point mutations within the conserved motif have been shown to reduce the exchange activity of GEFs significantly, in particular, amino acid residues of the hydrophobic groove (Val187, Phe190, Ile193 and Met194) have a functional importance making up the active site of the Sec7 domain (Betz *et al.*, 1998; Mossessova *et al*., 1998). A charge reversal mutation in the glutamate residue resulted in low Sec7 exchange activity which suggests that this residue has functional importance for the catalytic activity of Sec7 domains (Cherfils *et al*., 1998; Mossessova *et al*., 1998).

4.1.3. ARF1 specific GEFs and their cellular functions

Specific GEFs stimulate nucleotide exchange on specific ARFs. Of the fifteen ARF GEFs identified, seven individual GEFs that belong to three families namely: BIG/GBF, ARNO/Cytohesin and BRAG/IQSEC stimulate nucleotide exchange on ARF1 (Donaldson and Jackson, 2011). ARNO/Cytohesins are classified as low molecular weight GEFs (45-50 kDa). They have a 77 % sequence similarity, sharing a similar domain structure consisting of an N-terminal coiled-coil domain, followed by the Sec7 domain which is immediately followed by an adjacent pleckstrin homology (PH) domain. The PH domain mediates membrane association by binding to PIP2 and PIP3 (Paris *et al*., 1997; Casanova and Jackson 2000) and localize mainly to the endosomes and regulate endosomal trafficking including the recycling of the glucose transporter GLUT4, integrins and other proteins (Oh and Santy, 2010; Li *et al*., 2012). Cytohesins are required for signaling by hormones such as insulin, epidermal growth factor (EGF) and nerve growth factor and are recruited to the plasma membrane in response to these hormones (Fuss *et al*., 2006; Hafner *et al.*, 2006; Hahn *et al.*, 2013; Pan *et al.*, 2013). Cytohesins stimulate the activation of Rac (a Rho GTPase) and actin polymerization at the cell periphery resulting in increased migration of cells (Santy and Casanova, 2001; White *et al*., 2010; Reviriego-Mendoza and Santy, 2015). Cytohesins perform these functions efficiently *in vitro* by activating ARF1 and or ARF6. However, all the ARF isoforms are activated by cytohesins *in vitro* but raises the question of how specific isoforms of ARF are selected *in vivo*.

BIG/GBF have been classified as large GEFs because they have a high molecular weight (~170-200 kDa). The BIG/GBF subfamilies are closely related sharing sequence similarity in five homology domains (Mouratou *et al.*, 2005). These domains are the DCB (Dimerization and Cyclophilin-Binding) and HUS (Homology Upstream of Sec7 domain) which are upstream

of the catalytic Sec7 domain and HDS (Homology Downstream of Sec7 domain) domains: HDS1, HDS2 and HDS3 domains which are downstream of the catalytic Sec7 domain (Bui *et al*., 2009). The N-terminus comprises of two domains with high sequence conservation across all species and phyla: DCB and HUS domains which have been suggested to play a role in membrane association. The C-terminus consists of HDS domains, which have been shown to influence membrane association as deletions of HDS1 greatly diminished membrane association (Wright *et al*., 2014).

The substrate specificity of large ARF GEFs in humans is not completely clear as *in vitro* and *in vivo* analyses have produced conflicting results. GBF1 catalyzes *in vitro* exchange on ARF1 and ARF5 (Claude *et al*., 1999) whereas ARF1 and ARF4 seem to be *in vivo* substrates for GBF1 with evidence showing a preference for ARF1 as opposed to ARF4 (Niu *et al*., 2005; Szul *et al*., 2007). Additionally, the overexpression of GBF1 recruits ARF1, ARF3 and ARF5 to the membranes of the Golgi apparatus and prevents the dissociation of ARF1 from membranes of the Golgi in response to BFA (a GEF inhibitor that disperses ARF1 into the cytoplasm and collapses the Golgi). It also causes increased expression levels of ARF3 and ARF5 at the Golgi and BFA resistance (Kawamoto *et al*., 2002). None of the large ARF GEFs appears to activate class III ARF6 (Wright *et al*., 2014).

GBF1 and BIG1/2 play a role as regulators of membrane traffic within the secretory and endosomal pathways and show distinct localization patterns (Wright *et al*., 2014). GBF1 preferentially localizes to the ERGIC and *cis*-Golgi, where it activates ARF1 required for COPI vesicle formation (Zhoa *et al*., 2006; Manolea *et al*., 2008). GBF1 also facilitates lipid droplet formation (Ellong *et al*., 2011; Bouvet *et al*., 2013). BIG1 and BIG2 localize to the TGN and endosomes, where they mediate the activation of ARFs for endosome-plasma membrane recycling, TGN-plasma membrane recycling, TGN-late endosome transport and in some cells TGN-secretory granule transport. BIG1 and BIG2 facilitate the recruitment of the clathrin adaptors AP1 and AP3 through activation of ARF1 and ARF3 (Shinotsuka *et al*., 2002; Zhoa *et al*., 2002). BIG1 and BIG2 could be involved in non-trafficking roles as they were found to be present in the nuclei of serum-starved cells (Padilla *et al*., 2004; Padilla *et al*., 2008).

BRAG/IQSEC GEFs contain a calmodulin-binding IQ motif on the N-terminus. IQSEC1/3 are highly expressed in the central nervous system while IQSEC2 is ubiquitously expressed. IQSECs mainly localize to the endosomes and plasma membrane in nonneuronal cells and to presynaptic densities in neurons (reviewed in D'Souza and Casanova, 2016). IQSECs control

the internalization of adhesive and or signaling molecules. Like Cytohesins, IQSECs activate all ARFs *in vitro* and mechanisms to determine their selectivity in cells are elusive (Peurois *et al*., 2017). IQSEC1 is found in the nucleus as well, raising the question of how its various functions are integrated and regulated (Dunphy *et al*., 2007).

Interestingly, some functions of ARF GEFs may be achieved independently without the recruitment of ARFs. Cytohesin ARF GEFs may affect signaling through the EGF or ERBB receptor Tyr kinase receptors independently of their GEF activity. EGF receptors undergo dimerization, which is induced by ligands and subsequent transphosphorylation, which is mediated by conformational changes in the cytoplasmic domains. Cytohesins bind directly to these cytoplasmic domains and promote phosphorylation. Furthermore, the function of GBF1 in poliovirus replication has been suggested to be independent of ARF1 activation (Donaldson and Jackson, 2011). This raises the question of to what extent do ARF GEFs have broader roles beyond ARF activation?

4.1.4. ARF1 GEFs and disease

IQSEC2 is mutated in X-linked nonsyndromic intellectual disability, which is a form of mental retardation (Jackson and Bouvet, 2014). Mutations in BIG1 have been linked to autosomal recessive periventricular heterotopia (ARPH) which is a disorder that leads to malformation of the cerebral cortex and severe developmental decay. Two BIG2 disease alleles have been identified, including a frameshift mutation that results in the truncation of the whole protein. The disease symptoms arise as a result of the failure of a specific class of neurons to migrate from their point of origin to the cerebral cortex due to a defect in the adhesion properties of the neurons (Sheen *et al*., 2004; Ferland *et al*., 2009). GBF1 is required for the replication of numerous plus-strand RNA viruses such as poliovirus, coxsackievirus, coronavirus and Hepatitis C virus (Wessels *et al*., 2006; Belov *et al*., 2007; Belov *et al*, 2008). BFA inhibits the replication of these viruses (Gazina *et al*., 2002; Molina *et al*., 2007; Tai *et al*., 2009). These viruses function by remodeling the ER and early secretory pathway membranes (COPI and GGA3 coats) to form replication complexes which are a function that requires GBF1 and ARF1 in coordination with lipids such as phosphatidylinositol-4-phosphate (PtdIns4P) (Bienz *et al*., 1983; Salonen *et al*., 2004). Although a major role of GBF1 has been shown in enterovirus replication, there is some considerable evidence that BIG1 and BIG2 are also involved as different viral proteins have been shown to recruit different coats to virally restructured

membranes, of which BIG1 and BIG2 are involved in the recruitment of clathrin coats (Belov *et al*., 2007; Belov *et al*., 2008). The important roles of the large ARF GEF family members - GBF1, BIG1 and BIG2 - in human disease suggests the development of drugs that specifically target these proteins may be of medical interest, which is part of the motivation for this study.

4.2. ARF GAPs: classification, mechanism and functions

The GTPase reaction for most guanine nucleotide-binding proteins is slow and would not be suitable for most biological signal transduction pathways, which require complete inactivation within minutes following GTP loading. Crystallographic studies using aluminum and beryllium fluorides, that interfere with the hydrolysis of GTP, mimic the ARF GAP transition states have been used to provide the accepted molecular mechanism of ARF GAP-stimulated GTP hydrolysis (Mittal *et al*., 1996; Hoffman *et al*., 1998).

4.2.1. GAP domain catalyzes the hydrolysis of GTP to GDP

While ARF GAPs are ubiquitously expressed across a wide array of organisms, the consensus nomenclature is based on the human GAPs. To date there are 31 genes encoding ARF GAPs in the human genome, which can be further classified under 10 subfamilies. The ten subfamilies are: ARFGAP1, ARFGAP2/3, ADAP, SMAP, AGFG, GIT, ASAP, ACAP, AGAP and ARAP (reviewed in Kahn *et al*., 2008; Shiba and Randazzo, 2014) (see **Figure 4** for ARF GAP domain organization). These proteins share a common GAP domain of ~130 amino acids, which includes a zinc finger motif of $CX_2CX_{16}CX_2CX_4R$ and a conserved arginine for GAP activity. The GAP domain is the minimal fragment that has been described to be required for GAP activity (Cukierman *et al*., 1995; Goldberg, 1999; Donaldson and Jackson, 2000). The conserved arginine is very critical for GAP activity as a mutation of arginine to lysine results in a hundred thousand-fold decrease in GAP activity for ASAP1 (Randazzo *et al*., 2000).

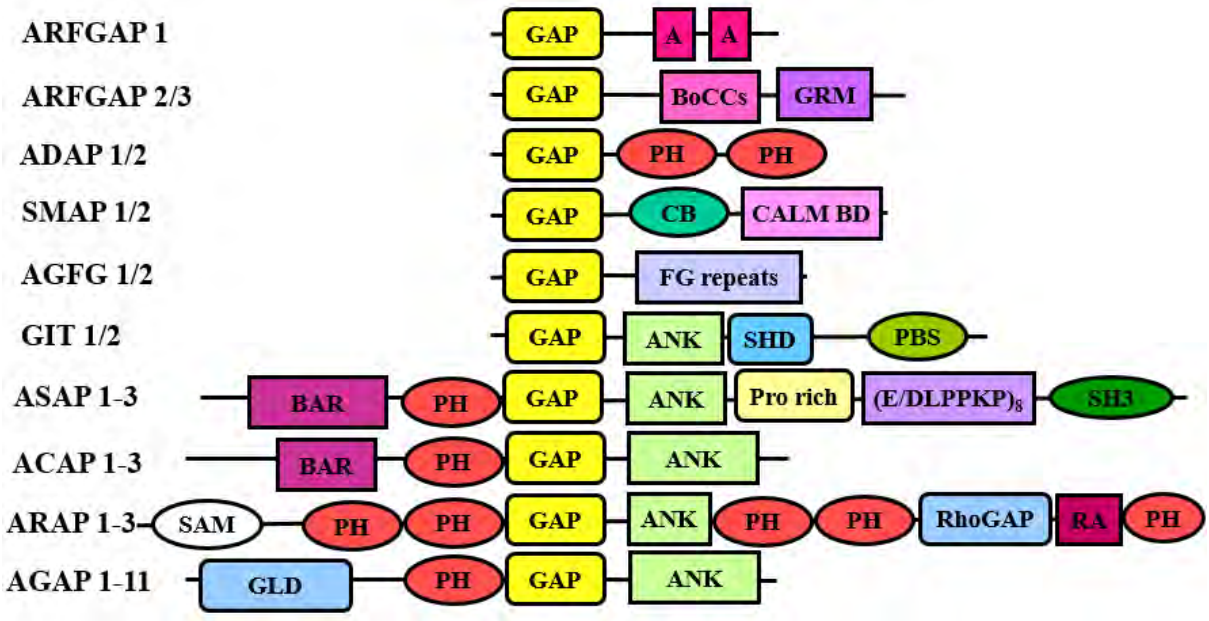

Figure 4: ARF GAP domain organization. A schematic representation of the domains present in ARF GAP sequences. The defining GAP domain is aligned. Protein lengths are not drawn to scale. Abbreviations used are described in alphabetical order. A: ARF GAP lipid-packing sensor (ALPS); ANK: Ankyrin repeat; BAR: Bin/Amphiphysin/Rvs; BoCCS: Binder of Coatomer, Cargo, and SNARE; CALM BD: CALM Binding Domain; CB: Clathrin Box; DCB: Dimerization and Cyclophilin Binding; E/DLPPKP$_8$; F-BOX, cyclin F protein interaction motif; FG repeats; GLD: GTP binding protein–Like Domain; GRM: Glo3 Regulatory Motif; PBS: Paxillin Binding Site; PH: Pleckstrin Homology; Pro rich: Proline rich; RA: Ras Association; Rho GAP: Rho GTPase-activating protein; SAM: Sterile α motif; SHD: Spa Homology Domain (Adapted from Gillingham and Munro, 2007; Sztul *et al*., 2019).

4.2.2. Mechanism of ARF GAPs to stimulate GTP hydrolysis

The GAP domain inserts the arginine finger into the nucleotide-binding site to stabilize the transition state of the reaction. The stabilization of the transition state requires the conserved glutamine in the switch 2 region of the ARFs such that it can activate a single water molecule (Ismail *et al*., 2010; Cherfils and Zeghouf *et al*., 2013). The water molecule is positioned optimally for the nucleophilic attack to the γ-phosphate of GTP opposite to the leaving group, causing dissociation inorganic phosphate from the binding site (Vetter and Wittinghofer, 2001). Effective phosphoryl transfer will occur when these three critical elements are met: correct orientation of the attacking water molecule and its polarization, occlusion of water from the active site and the stabilization of the transition state (Bos *et al*., 2007).

4.2.3 ARF1 specific GAPs and functions

ARF GAPs display varying degrees of specificity for specific members of the ARF GTPase family. To date, nine ARF GAPs belonging to four subfamilies - ARFGAP1, ARFGAP2/3, SMAP and ASAP - have *in vitro* specificity for ARF1 (Randazzo and Hirsch, 2004; Donaldson and Jackson, 2011). ARFGAP1 shuttles between the cytosol and the Golgi where it regulates the formation of the COPI coat in membrane traffic (Bigay *et al*., 2005; Mesmin *et al*., 2007). ARFGAP1 contains ALPS binding motifs that orient the protein upon binding to membranes and subsequently regulate the activity. ARFGAP1 also binds to clathrin coat proteins (including clathrin, AP1 and AP2) but the functional consequences of this interaction remain to be established (Goldberg, 1999). ARFGAP2/3 are localized to the Golgi and form strong interactions with the COPI coat. ARFGAP2 and ARFGAP3 are closely related proteins (58 % identity) with little similarity to ARFGAP1 outside the catalytic domain and lack the ALPS motif (Watson *et al*., 2004; Frigerio *et al*., 2007). SMAP1/2 have been implicated as regulators of endocytosis and oncogenesis. The two SMAP proteins share a 47 % sequence identity. SMAPs bind to clathrin heavy chain by interacting with the clathrin binding motif (LLGLD) as well as clathrin assembly protein, CALM. SMAP1 is cytosolic but is recruited to membranes where it regulates constitutive endocytosis. SMAP2 is bound to endosomes and is involved in the retrograde transport of TGN46 from early endosomes to the TGN (Natsume *et al*., 2006; Tanabe *et al*., 2006). ASAP1, ASAP2 and ASAP3 have a BAR domain that helps to regulate GAP activity (Jian *et al*., 2009; Fan *et al*., 2014). ASAPs function at the plasma membrane, localizing to specialized sites such as focal adhesions and invadopodia and regulates the endocytic pathway and actin remodeling (Nie and Randazzo, 2006; Inuoe and Randazzo, 2007; Randazzo *et al*., 2007). ASAP1 resides in focal adhesions, but when activated by Src kinase, it regulates the formation of podosomes, which are discrete actin-based structures formed at the cell substratum that degrade the matrix (Bharti *et al*., 2007).

4.2.4. ARF1 GAPs and disease

ARF1 GAPs have been implicated in various diseases. In neoplastic tissues and cancer cells, ASAPs are upregulated in renal, colorectal, gastric, gall bladder, ovarian, bladder head and neck, prostate, melanoma, esophagus, thyroid and cervical cancers (Ahn *et al*., 2004; Onodera *et al*., 2005; Junnila *et al*., 2010; Müller *et al*., 2010; Yagi *et al*., 2011; Peng *et al*., 2013; Chan *et al*., 2014; Hou *et al*., 2014; Sangar *et al*., 2014; Sirirattanakul *et al*., 2015; Chen *et al*., 2016;

Willis *et al*., 2016). ARFGAP3 is upregulated in prostate cancer (Liu *et al*., 2007; Lin *et al*., 2008; Nalla *et al*., 2016). SMAP is downregulated in colorectal cancer (Liu *et al*., 2007; Müller *et al*., 2010; Chen *et al*., 2016). Generally, ARF GAPs are implicated in cancer cell migration and cancer cell invasion with a focus on these three processes: cell-cell adhesion, integrin internalization and recycling, and actin cytoskeleton remodeling.

Interestingly, intracellular pathogens can use a fascinating GAP locking mechanism to rewire the host signaling network. Enterohemorrhagic *E. coli* produces the EspG protein, which blocks the activity of GAPs as the EspG proteins bind to active ARF1 and ARF6, blocking the accessibility to GAPs which, in turn, disrupts the function of the early Golgi and endosomes. The results of this could lead to diminished intestinal colonization (Elliot *et al*., 2001; Donaldson and Jackson, 2011; Lawley and Walker, 2013). This raises an interesting possibility that EspG may be able to assemble its own signaling complex on intracellular membranes to subvert membrane trafficking and polarity processes in host cells.

The early accepted paradigm was that because ARF GAPs can deactivate ARF GTPases they only functioned as terminators for ARF signaling but there is growing evidence that the function of ARF GAPs is far more complex than this as some are involved in scaffolding complexes. This was shown by a study conducted by Zhang *et al*. (1998) where ARF GAPs were able to compensate for ARF insufficiency in yeast. The idea that ARF GAPs could be involved in propagating an ARF signal was further supported by the discovery that a number of ARF GAPs drive the assembling of coats or cargo selection proteins when transport vesicles are being formed (Yang *et al*., 2002; Lee *et al*., 2005; Spang *et al*., 2010; Bia *et al*., 2011; Shiba and Randazzo, 2012).

5.0. Clinical significance: ARF GTPases and Cancer

There are now considerable and growing findings for a causal role of the anomalous activity of the Ras superfamily of GTPases in human cancers. A common mechanism is the deregulation of ARF GTPase expression and or activity of regulatory proteins, GEFs and GAPs (Schlienger *et al*., 2015; Casalou *et al*., 2016; Lang *et al*., 2017). A review of the relevance of ARF GTPases, and ARF GEFs in cancer will be described in this section.

Brefeldin A (BFA) impairs ARF1 activity by hindering the association of ARF1 with GEFs, thus reducing the amount of active ARF1 GTP in the cell (Mossessova *et al.*, 2003; Vigil *et al.*, 2010). The 7-hydroxyl group of BFA is pivotal to the disruption of ARF and ARF GEF association because the loss of the functional group results in weaker affinity for the ARF1-GEF complex, preventing its inhibitory action (Zeeh *et al*., 2006). Evidence shows that BFA could be used as a cancer drug lead. Firstly, BFA reduces anaplastic large cell lymphoma proliferation through the reduction of the ARF1- dependent signal transducer as well as an activator of transcription 3 (STAT 3) phosphorylation (Toda *et al*., 2015). Secondly, BFA has slight cytotoxic activity in cancers such as lung, colorectal, ovarian, breast, prostate and central nervous system (Anadu *et al*., 2006). Additionally, BFA causes tumor regression in mice models (Ohashi *et al*., 2012) but further clinical trial development has been hindered due to poor bioavailability. Further limitations include poor pharmacokinetic properties, poor solubility in biological fluids and neurotoxicity in animal studies (Sausville *et al*., 1996; Anadu *et al*., 2006). The generation of new BFA analogs with higher anticarcinogenic activity and lower off-target effects becomes very important to improve use in cancer therapy (He *et al*., 2013). New chemotypes have been reported that mimic BFA by inhibiting GEF-mediated ARF1 activation and cause potent breast cancer tumor regression in mice (Viaud *et al*., 2007; Pan *et al*., 2008; Saenz *et al*., 2009; Boal *et al*., 2010; Ohashi *et al*., 2012). For instance, acylated BFA analogs reduce the cell viability of esophagus squamous cell carcinoma by a factor of 500-fold as compared to native BFA (He *et al*., 2013). The BFA ester analogs can reduce off-target effects by lower doses administered as a result of higher potency than native BFA (Anadu *et al*., 2006). The addition of vinyl or aromatic groups to the C_{15} of BFA increases the ability to reduce HeLa cell proliferation (Seehafer *et al*., 2013).

The Golgi is responsible for the processing and sorting of numerous proteins in the cell, including cell surface-expressed receptor tyrosine kinases (RTK) (Ohashi *et al*., 2016). M-COPA, also known as AMF 26, disrupts the Golgi apparatus by inhibiting the activation of ARF1 which results in the suppression of tumor growth (Ohashi *et al*., 2012). Evaluation of

M-COPA against RTK addicted cancers suggests a novel therapeutic modality with a unique mode of action for target RTK (Ohashi *et al*., 2016). Interestingly, M-COPA has been described to affect GEF activity which impairs the formation of the ARF-GEF complex and thus presents a mode of action like BFA (Vigil *et al*., 2010; Shiina *et al*., 2013). M-COPA has greater bioavailability than BFA, increasing its potential use in cancer treatment strategies (Ohashi *et al*., 2012). M-COPA can induce complete tumor regression in breast cancer xenografts and reduce the proliferation of different cancers in different organs (Shiina *et al*., 2013; Ohashi *et al*., 2016).

Sec7 inhibitor H3 (SecinH3) is a non-specific ARF inhibitor that suppresses both ARF1 and ARF6 signaling by binding and inhibiting the Sec7 catalytic domain of ARNO and cytohesins (Hafner *et al*., 2006; Bi *et al*., 2008). SecinH3 presents great therapeutic effects in some carcinogenic diseases. For example, it is able to diminish the growth of breast xenografts and lower breast-related lung metastasis and the aggressiveness of tumors (Zhoa *et al*., 2016). It destroys the migration, invasion and proliferation of colorectal cancer cells in *in vitro* and *in vivo* models (Pan *et al*., 2014). Furthermore, it can decrease the activation of the epidermal growth factor receptor (EGFR) and induce apoptosis in both *in vitro* and in *in vivo* models which ultimately leads to reduced proliferation of some non-small cell lung cancer types and a reduction of non-small cell cancer resistance to gefitinib (Bill *et al*., 2012; Pan *et al*., 2014).

M69, an RNA aptamer, impairs the effects of ARFs by binding to the catalytic Sec7 domain of GEFs (Mayer *et al*., 2001; Germer *et al*., 2013). Experiments have been done using this inhibitor and these studies show that M69 has anti-carcinogenic effects as the expression in T lymphocytes caused rearrangements of the actin cytoskeleton and decreases the adhesion to the extracellular matrix (Mayer *et al*., 2001).

LM11 inhibits ARF1 activation in the Golgi by binding to the GEF enzyme. LM11 is very specific to ARF1 which ensures that it does not abrogate the other ARF analogs rendering it suitable to treat ARF1 overexpressing tumors (Flisiak *et al*., 2008; Xie *et al*., 2016). For example, the treatment of breast cancer tumors that overexpress ARF1 with LM11 reduces the tumor aggressiveness through the decrease in cell proliferation, invasion and inducing apoptosis. Furthermore, LM11 disrupts breast cancer adhesion to the extracellular matrix through the inhibition of paxillin translocation to the cell membrane, which is important in connecting integrins with the actin cytoskeleton (Turner, 2000; Schlienger *et al*., 2015; Xie *et al*., 2016). However, LM11 activity is hindered when tumor cells carry a K38 substitution in

ARF1 which makes it essential for tumors overexpressing ARF1 to be tested for variants before the use of this inhibitor (Flisiak *et al*., 2008).

Exo2 also inhibits ARF1 by preventing its activation by specific ARF GEFs by binding to the catalytic Sec7 domain (Bourgoin *et al.*, 2012). This inhibition results in secretory vesicles from the endoplasmic reticulum to the Golgi apparatus not being released and reduces cellular lipid storage by inhibiting perilipin-2 expression (Spooner *et al*., 2008; Sorieul *et al*., 2011; Pauloin *et al*., 2016). Experiments conducted show that Exo2 has the potential to reduce tumor growth and metastasis in prostate cells by the inhibition of ARF1-mediated ERF1/2 activation (Lang *et al*., 2017). A most recent study showed for the first time that active ARF1 is present at much higher levels in metastatic head and neck squamous cell carcinoma cells (HNSCC) in comparison with non- metastatic cells. This provides evidence for the functional importance of ARF1 activation in HNSCC metastasis. Furthermore, it has been shown that EGF induces HNSCC cell invasion through an EGFR-ARF1 signaling complex and the interruption by Exo2 deters the progression of HNSCC. Thus, this provides a rational basis for ARF1 targeted anti-HNSCC therapy (He *et al*., 2019).

6.0. Key questions and challenges

While strides have been made in developing knowledge around ARF GTPases, ARF GAPs and ARF GEFs, below are some glaring deficiencies which can be addressed experimentally to advance our understanding of underlying mechanisms and regulation of a broad array of cellular processes (reviewed in Sztul *et al*., 2019).

A. *Multiple functions of ARF GTPases in the cell:* There is oversight into how many different functions a single GTPase can perform in a cell, which GTPases support which cellular functions and the extent to which there is functional redundancy between the GTPases. This raises the following questions about a single GTPase performing multiple functions at distinct intracellular sites - how is the distribution regulated and how are the distinct functions coordinated to achieve integrated homeostasis in cells?
B. *Post-translational modifications:* ARF GTPases, ARF GEFs and ARF GAPs are subject to post-translational modifications including ubiquitination and phosphorylation. These modifications are transitory and are likely to play important roles in localization, selection of binding partners, activation and biological outputs. A

few studies have looked at the effects of these post-translational modifications on the functions of the proteins or identified the kinases responsible or other modifiers. An interesting question to answer would be how does the functional and metabolic status of a cell influence the phosphorylation of specific proteins to bring about the appropriate cellular response?

C. *The subset of ARFs, ARF GAPs and ARF GEFs used in a cellular response:* Currently, it is widely accepted that for an ARF GTPase to carry out a regulatory role, it will need to recruit an upstream ARF GEF and a downstream ARF GAP. *In vitro* studies using purified components reconstituted on membranes provide a powerful tool to study the complex regulatory properties at the molecular level, determine affinities and specificities of individual GEFs and GAPs for different ARFs and generate testable hypotheses to interrogate these mechanisms in the cell. However, *in vitro* conditions do not mimic accurately the conditions of the cell and it becomes challenging to identify how these mechanisms are mobilized, altered or combined by the cell to generate a particular response.

D. *ARF/GEF/GAP/effector interactomes:* How do the proteins that bind to ARF GTPases, GEFs and GAPs, influence the activity of the proteins and downstream events? Do the interactors differ depending on the localization and what defines the order, hierarchy and cooperativity of such interactions?

7.0. Motivation and the overall aim of the study

The potential role of ARF1 as a drug target for cancer therapy motivates this study. The pleiotropic effect of ARFs as well as their conservation in eukaryotic organisms leads to an interesting question of whether or not a single drug target can be used to target multiple diseases. In this case, can a human cancer drug employed for cancer therapy be used in anti-malarial drug therapies?

The genome of the most prevalent and most virulent of the species of the malaria parasite, *Plasmodium falciparum*, contains at least six sequences that have been identified to code for putative ARF or ARF-like proteins (www.plasmodb.com, accessed: November 2019). One of these sequences encodes for an ARF1 homologue (*Pf*ARF1) that has a high amino acid sequence conservation (76 % identity and 89 % similarity) in comparison to human ARF1. *Pf*ARF1 was shown to bind to GTP, have phospholipase D and ADP-ribosyltransferase stimulating activity and low intrinsic GTPase activity, which are all the features of ARF GTPases (Stafford *et al*., 1996; Lee *et al*., 1997; Truong *et al*., 1997). Furthermore, it is able to stimulate *P. falciparum* phosphatidylinositol 4-phosphate 5-kinase (PIP5K), which is an established role for mammalian ARF1 in regulating the levels of phosphorylated phosphatidylinositol, and consequently, membrane trafficking, regulation and actin cytoskeleton dynamics (Leber *et al*., 2009). In blood-stage parasites, *Pf*ARF fused to GFP, colocalizes with the marker for the Golgi, GRASP (Thavayogarajah *et al*., 2015), while the inhibitor for the activation of ARF, BFA, causes a disruption in the Golgi architecture and trafficking of proteins in the secretory pathway (Crary and Halder, 1992; Ogun and Holder, 1994; Hayashi *et al*., 2001; Wickham *et al*., 2001). Collectively, these studies suggest *Pf*ARF mimics the role of mammalian ARF in the secretory pathway through the Golgi apparatus.

The goals were to develop, respectively, a FRET assay and a colorimetric protein interaction assay to monitor the activation status of human and malarial ARF1. This would facilitate screening campaigns to obtain ARF1 inhibitors and confirm the drug target status of ARF1 for cancer and malarial therapeutics.

Chapter 2: Methods and materials

2.1. Preparation of DNA expression constructs

2.1.1. In vitro human and malarial ARF1 FRET assay constructs (pET-28a-CFP, pET-28a-$^{N\Delta17}$HsARF1-CFP, pET-28a-$^{N\Delta17}$PfARF1-CFP and pET-28a-YPET-GGA3^{GAT})

An mCerulean N1 plasmid used as template for amplifying the coding sequence of CFP (Cerulean variant) was obtained from Addgene (plasmid #27795, donated by Steven Vogel). The pET-28a-CFP construct encoding cyan fluorescent protein (CFP) was prepared by sub-cloning the CFP coding sequence into the BamHI/*Xho*I restriction sites of pET-28a. The template for amplifying the human ARF1 coding sequence was the pARF1-CFP-N1 plasmid (Addgene plasmid #11381, donated by Joel Swanson). The pEGFP-N1-*Pf*ARF1 plasmid used as template for amplifying the *P. falciparum* ARF1 coding sequence was prepared and donated by T. Swart, PhD thesis in preparation. It contains the *Pf*ARF1 sequence, codon optimised for human expression by Genscript, cloned between the *Xho*I/KpnI restriction sites of the pEGFP-N1 mammalian expression plasmid (Clontech). The pET-28a-$^{N\Delta17}$*Hs*ARF1-CFP and pET-28a-$^{N\Delta17}$*Pf*ARF1-CFP constructs were prepared by sub-cloning the $^{N\Delta17}$*Hs*ARF1 and $^{N\Delta17}$*Pf*ARF1 coding sequences into *Nhe*I/BamHI restriction sites of the pET-28a-CFP construct (sub-cloning experiments are described in section 2.2 below). The pEF4-myc-HisA-YPET-GGA3 construct was obtained from Addgene (plasmid #18841, donated by Martin Schwartz). The plasmid vector is a mammalian expression vector so the YPET-GGA3^{GAT} insert was sub- cloned into the *Nhe*I and *Xho*I sites of the bacterial expression plasmid, pET-28a (T. Swart, PhD thesis in preparation). The construct hereafter will be referred to as pET-28a-YPET-GGA3^{GAT}.

2.1.2. In vitro human and malarial ARF1 GEF assay constructs (pET-28a-$^{N\Delta17}$HsARF1, pET-28a-$^{N\Delta17}$PfARF1, pGEX-4T-2/hGGA3^{GAT}, pET-28a-ARNO^{Sec7}, pET-28a-BIG^{Sec7} and pET-28a-PfARFGEF^{Sec7})

The ARF1 coding sequences were ligated into the *Nhe*I/BamHI or *Nhe*I/*Xho*I sites of pET-28a for expression as His-tagged proteins. The coding sequence of human ARF1 minus the N-terminal 17 amino acids ($^{N\Delta17}$*Hs*ARF1) was PCR amplified from pARF1-CFP (Addgene plasmid #11381, donated by Joel Swanson) and the corresponding *P. falciparum* ARF1 sequence ($^{N\Delta17}$*Pf*ARF1) from the full length *Pf*ARF1 sequence (PlasmoDB ID PF3D7_1020900) codon-optimised for human expression, synthesised and cloned into

pBluescript II by GenScript (Hong Kong) (previously prepared by T. Swart, PhD thesis in preparation). The pGEX-4T-2/hGGA3^{GAT} construct (Addgene plasmid #79436, donated by Kazuhisa Nakayama) was used for the expression of GST-GGA3 GAT fusion protein (GST fused to the GAT domain- amino acids 107-286 - of human GGA3), (Addgene plasmid #79436, donated by Kazuhisa Nakayama). The protein sequences for human cytohesin-2/ARNO, human BIG1 and putative *P. falciparum* ARF GEF (Wiek *et al*., 2004) were obtained from NCBI (NP_004219.3 for cytohesin-2/ARNO and NP_006412.2 for human BIG1) and PlasmoDB (PF3D7_1442900 for putative *P. falciparum* ARF GEF). The Sec7 domain of cytohesin-2/ARNO (amino acids 51 – 253); human BIG1 (amino acids 696 – 881) and the putative *P. falciparum* ARFGEF (amino acids 1201 – 1739) were codon-optimized for expression in *E. coli* and cloned into pET-28a (*Nhe*I/*Xho*I sites) by Genscript. The constructs will hereafter be referred to as pET-28a-ARNO^{Sec7}, pET-28a-BIG1^{Sec7} and pET-28a-*Pf*ARFGEF^{Sec7} respectively.

2.2. Molecular cloning

2.2.1. PCR amplification of ^{NΔ17}HsARF1, ^{NΔ17}PfARF1 and CFP coding sequences

Forward and reverse primers were designed to amplify the CFP, *Hs*ARF1 and *Pf*ARF1 (minus the sequences encoding for the conserved N-terminal hydrophobic extension for the ARF1 coding sequences). *Xho*I/BamHI restriction sites were incorporated in the forward and reverse primers for the amplification of the CFP coding sequence to facilitate cloning into the *Xho*I/BamHI restriction sites of pET-28a. *Nhe*I/BamHI restriction sites were incorporated in the forward and reverse primers for the amplification of the ^{NΔ17}*Hs*ARF1 and ^{NΔ17}*Pf*ARF1 coding sequences to facilitate cloning into the *Nhe*I/BamHI restriction sites of pET-28a-CFP. All primers were synthesized by Integrated DNA Technologies.

In a PCR tube, a 50 µL solution containing molecular biology grade water, 1X KAPA HiFi fidelity buffer, 0.2 mM KAPA dNTP mix, 0.5 µL template DNA, 3 µM forward primer and 3 µM reverse primer (see Table 1) was heated in a PCR cycler to 94 °C for 2 minutes before 0.5 U KAPA HiFi DNA polymerase was added. Following the initial denaturation step, 30 cycles of denaturing (for 40 seconds at 94 °C), annealing (for 45 seconds at 60-65 °C, see Table 1) and extension (for 2 minutes at 70 °C) was carried out, followed by a final extension (for 5 minutes at 70 °C) (adapted from methods by Mullis *et al*., 1986). The PCR products from the

PCR reaction mixture were purified using a NucleoSpin Gel and PCR clean-up kit (Machery Nagel) according to the manufacturer's instructions. The purified PCR products were stored at 4 °C until further analysis

Table 1: Hot-Start PCR products, primers and annealing temperatures

Template DNA	Primers		Annealing Temperature used	PCR Product
mCerulean N1*	F	5'-GCTAGGATCCATGGTGAGCAAGGGCGAGGAG-3' BamHI	65 ºC	CFP
	R	5'-GCAATCTCGAGCTACTTGTACAGCTCGTCCATGCC-3' *Xho*I		
pARF1-CFP-N1#	F	5'-TCGAGCTAGCATGCGCATCCTCATGGTGGGC -3' *Nhe*I	60 ºC	$^{N\Delta17}$*Hs*ARF1
	R	5'-GCTAGGATCCCTTCTGGTTCCGGAGCTGATTG-3' BamHI		
pEGFP-N1-*Pf*ARF1+	F	5'-CGATGCTAGCGTGAGAATCCTGATGGTCGGC-3' *Nhe*I		$^{N\Delta17}$*Pf*ARF1
	R	5'-GTTGGGATCCCTTGGCGTTGTTCAGGTGGG-3' BamHI		

* Addgene plasmid #27795, donated by Steven Vogel

Addgene plasmid #11381, donated by Joel Swanson

+ Donated by Tarryn Swart

_ Restriction sites are underlined along with restriction enzyme description

2.2.2. Evaluating the DNA concentration and purity

The concentration (Absorbance 260 nm) and purity (Absorbance 260/280 nm) of purified DNA samples was determined by using a NanoDrop 2000 spectrophotometer (Thermo Fisher Scientific).

2.2.3. Ligation reactions

PCR products and target plasmids were digested with relevant New England Biolabs restriction enzymes, resolved on an agarose gel, and specific DNA fragments purified from excised gel pieces using a NucleoSpin gel and PCR clean-up kit according to the manufacturer's instructions. The purity and concentration were determined. To 100 ng of the target plasmid, 3-fold molar excess of the PCR product was added, which was determined according to the following formula:

3 fold molar excess (ng) = $3 \times \frac{size\ of\ the\ PCR\ product\ (bp)}{size\ of\ the\ target\ construct\ (bp)} \times 100$ ng

The PCR products were ligated into the target constructs containing 1X T4 DNA ligase buffer (New England Biolabs), 1U T4 DNA ligase (New England Biolabs) and molecular biology grade water. Ligation reactions were carried out overnight in a mixture of ice and water (method adapted from Western and Rose, 1991). The ligation reactions were used to transform competent *E. coli* XL-10 Gold competent cells, after which several colonies were propagated in overnight cultures and plasmids purified by alkaline lysis miniprep. Diagnostic restriction digestions were conducted using appropriate restriction enzymes and products were visualized through agarose gel electrophoresis to identify correctly ligated plasmid constructs.

2.2.4. Preparation of competent cells

T7 Express lysY/I_q *E. coli* competent cells (New England Biolabs), Rosetta (DE3) *E. coli* competent cells (Novagen), XL-10 Gold *E. coli* competent cells (Stratagene) and XL-1 Blue *E. coli* competent cells (Stratagene) were used in this study. The untransformed *E. coli* cells were propagated in Luria broth for 16 hours at 37 ℃ with continuous agitation. To 100 mL Luria broth, 2.5 mL of the untransformed *E. coli* overnight culture was added (1 in 40 inoculum) and incubated at 37 ℃ with continuous agitation until an OD_{600nm} = 0.6-0.9 was obtained. The cells were harvested by centrifugation at 2152 *g* for 10 minutes at 4 ℃ and all subsequent steps were conducted on ice. The cells were resuspended in ice cold 4 mL RF-1 buffer (100 mM KCl, 50 mM $MnCl_2$, 30 mM potassium acetate, 10 mM $CaCl_2$, 15% (w/v) glycerol, pH 5.8) and incubated on ice for 20 minutes. The cells were harvested by centrifugation at 1377 *g* for 10 minutes at 4 ℃. The cells were gently resuspended in ice cold 3 mL RF-2 buffer (10 mM HEPES, 10 mM KCl, 75 mM $CaCl_2$, 15% (w/v) glycerol, pH 6.8). Aliquots of the suspensions in cryotubes were stored at -80 °C.

2.2.5. Heat shock transformation of competent cells

A stock of competent *E. coli* cells was thawed on ice. To 50 µL *E. coli* competent cells, 10 µL alkaline lysis plasmid miniprep (or 0.5 µL pure plasmid or 10 µL ligation reaction) was added. The solution was mixed briefly and incubated on ice for 30 minutes. The mixture was heat shocked at 42.5℃ for 60 seconds and incubated on ice for 5 minutes. After incubation, 500 µl Luria broth was added and the resultant suspension was incubated at 37℃ for 60 minutes. The cells were harvested by centrifuging at 3099 *g* for 3 minutes at room temperature and cells

were resuspended in 100 µL Luria broth. Subsequently, 50 µl of the suspension was plated onto Luria-agar plates containing 50 µg. mL^{-1} kanamycin or ampicillin, depending on the plasmid resistance marker. The plates were incubated at 37℃ for 16 hours (adapted from methods of Bergmans *et al*., 1981).

2.2.6. Alkaline lysis plasmid miniprep

E. coli XL-10 Gold competent cells harbouring the target constructs stored as glycerol stocks (*E. coli* overnight cultures stored in 15% (v/v) glycerol at -80 °C) were propagated for 16 hours with agitation in Luria broth containing 50 $mg.mL^{-1}$ kanamycin or ampicillin, depending on the resistance marker. Approximately 3-5 mL of the bacterial cell culture were centrifuged in microfuge tubes at 3099 *g* for 3 minutes and the supernatant was discarded. The bacterial pellet was resuspended in GTE buffer (30 mM Glucose, 25 mM Tris, 10 mM EDTA, 10 µg. ml^{-1} RNAse, pH. 8.0). The cells were lysed by the addition of NaOH/SDS lysis solution (0.2 N NaOH, 1% (w/v) SDS). Cell lysis was terminated by the addition of neutralization buffer-potassium acetate solution (42% (v/v) acetic acid, pH 4.8 adjusted by the addition of KOH). The suspension was centrifuged at 16873 *g* for 5 minutes at room temperature to collect the cell debris. The cleared supernatant was transferred into a sterile microfuge tube and absolute ethanol was added. The plasmid DNA was pelleted by centrifugation for 6 minutes at 16873 *g* at room temperature and the pellet was washed with 70% (v/v) ethanol. A final centrifugation step was conducted at room temperature at 16873 *g* for 3 minutes. The supernatant was removed from the pellet and the pellet was air dried. The pellet was dissolved in 50 µl of molecular biology grade water and stored at 4℃ until further use.

2.2.7. Restriction digestions

2.2.7.1. Thermo Fisher Scientific Fast Digest restriction digestion

Restriction digestion reactions were conducted by incubating 10 µL target plasmid in a solution containing 1X Thermo Fisher Scientific Fast Digest buffer, molecular biology grade water and 0.5 µL of each of the Thermo Fisher Scientific Fast Digest restriction enzyme required for 3 hours at 37 ℃. The restriction digestion products were stored at 4 ℃ until further analysis.

2.2.7.2. New England Biolabs restriction digestion

Restriction digestion reactions were conducted by incubating the target plasmid (cleaned PCR products, recombinant constructs) in a solution containing an appropriate 1X New England Biolabs restriction buffer, molecular biology grade water and 0.5 µL of each of the New England Biolabs restriction enzyme required for 5 hours at 37 °C (adapted from Cohen *et al*., 1973). The restriction digestion products were stored at 4 °C until further analysis.

2.2.8. Agarose gel electrophoresis

All agarose gels were prepared by heating 0.8% (w/v) agarose (Seakem® LE) in 1X TBE buffer (22.7 mM Tris, 22.2 mM boric acid, 1.2 mM EDTA) or 1X TAE buffer (22.7 mM Tris, 22.2 mM acetate, 1.2 mM EDTA) until fully dissolved followed by the addition of 1.2 µg. mL^{-1} ethidium bromide. The solution was poured into a gel tray and allowed to cool and solidify at room temperature. The samples were prepared in sample loading buffer (5% (v/v) glycerol, 0.042% (w/v) bromophenol blue, 1X TBE or 1X TAE buffer). The samples were loaded into the wells of a gel submerged in 1X TBE or 1X TAE buffer and run alongside a 1 kbp Promega DNA marker at 95 V for 1 hour. Diagnostics gels for PCR amplification or restriction digestion were visualized and photographed under ultraviolet light using a ChemiDoc XRS + gel documentation system (Bio-Rad) (methods adapted from Meyers *et al*., 1976).

2.3. Bacterial expression and purification

2.3.1. Analytical scale bacterial expression

The expression constructs transformed into T7 Express lysY/Iq *E. coli* competent cells (New England Biolabs), Rosetta (DE3) *E. coli* competent cells (Novagen) and XL-1 Blue competent cells (Stratagene) were propagated in Luria broth containing 50 µg.ml^{-1}ampicillin or kanamycin for 14- 16 hours at 37 °C with continuous agitation. To 8.0 mL Luria broth, 0.4 mL of the relevant overnight culture (1 in 20 inoculum)-bacterial cells harbouring a plasmid encoding the appropriate fusion protein was added. The expression culture was incubated at 37 ˚C with continuous agitation at 120-184 rpm for 3 hours until an optical density (OD) at 600 nm between 0.5-0.9 was obtained. Protein expression was induced by the addition of 0.4-1 mM IPTG (Thermo Fisher Scientific) and the cells were incubated for a further 3-16 hours at 22-37℃ with continuous agitation. A parallel culture without IPTG was used as the uninduced control. The cultures were placed on ice and kept on ice for the subsequent steps. The cells

were harvested by centrifugation at 5000 *g* at 4℃ for 10 minutes and resuspended in 2 mL wash buffer (50 mM Tris-HCl, pH 8.0). The centrifugation step was repeated under the same conditions and the supernatant was discarded. The pellet was stored at -20 ˚C overnight. The pellet was thawed on ice for 12 minutes and resuspended in 1 mL wash buffer. The cells were lysed with 2 $mg.ml^{-1}$ lysozyme for 30 minutes with occasional stirring and by two cycles of sonication at a frequency of 60 Hz, interspersed with a one-minute resting period on ice. The lysate was centrifuged at 5000 *g* for 10 minutes to separate the soluble and insoluble fractions. The insoluble fraction was resuspended in 1 mL wash buffer. All samples were prepared for SDS-PAGE analysis and samples were stored at -20 °C until further use.

2.3.2. Preparative scale bacterial expression

To 250 mL Luria broth containing 50 $\mu g.ml^{-1}$ampicillin or kanamycin, 2.5 mL of the relevant overnight culture was added (1 in 100 inoculum) and incubated at 37 °C until the $OD_{600\ nm}$ value was between 0.5-0.9. Protein expression was initiated by the addition of 0.4-1 mM IPTG and followed by an incubation at 22-37 °C for 3-16 hours. The cells were harvested by centrifugation at 5000 *g* for 10 minutes and the pellet was washed using 20 mL Ni- NTA equilibration buffer (50 mM Tris-HCl with 20 mM imidazole, pH. 8.0) or 20 mL glutathione equilibration buffer (PBS, 0.2 % Triton X-100 with 1 mM PMSF, pH. 7.4) for His-tagged and GST-tagged proteins respectively. The pellet was resuspended and was centrifuged again at 5000 *g* for 10 minutes and the supernatant was discarded. The pellet was stored at -20/-80 °C overnight.

2.3.3. Cell lysis

All the steps for cell lysis were conducted on ice using ice cold buffers. The pellet was thawed on ice for 30 minutes and resuspended in 10 ml Ni-NTA equilibration buffer (50 mM Tris-HCl with 20 mM imidazole and 0.1% Triton X-100, pH. 8.0) or 10 mL glutathione equilibration buffer (PBS, 0.2 % Triton X-100 with 1 mM PMSF, pH. 7.4). Cell lysis was initiated by adding 2 ml 10 $mg.\ ml^{-1}$ lysozyme and incubating on ice for 30 minutes with occasional stirring every 10 minutes. The bacterial cells were sonicated and the sonication step was repeated (60 Hz, for 1 minute, with a 1-minute rest on ice). The lysate was centrifuged at 14 000 *g* at 4℃ for 30 minutes to separate the insoluble and soluble fractions.

2.3.4. Preparation of Ni-NTA and glutathione agarose columns for affinity chromatography

Ni-NTA fast start kit (Qiagen) columns were stored at 4 °C until use in a storage solution (50 % ethanol). The resin was resuspended in the storage solution by shaking the column gently. The storage solution was allowed to flow through and the column was washed with one volume of filter sterilized water (0.45 µM filter). Conditioning of the column was done with one volume of equilibration buffer before purification. After purification the column was washed with one volume of filter sterilized water and stored in storage solution or recharged. To prepare glutathione agarose resin, 70 mg of lyophilised glutathione agarose powder (Sigma-Aldrich) was hydrated in 14 mL water at 4℃ overnight. The agarose beads were washed with 10 volumes of water and stored in glutathione storage buffer (2 M NaCl, 1 mM sodium azide in water) at 4℃ until further use. Prior to purification, the column was washed in one volume of water and equilibrated in two volumes of glutathione equilibration buffer. After purification the column was washed with two volumes of water, one volume of glutathione cleansing buffer 1 (0.1 M borate, 0.5 M NaCl in water, pH 8.5 using NaOH), one volume of water, one volume of glutathione cleansing buffer 2 (0.1 M acetate, 0.5 M NaCl in water, pH 4.5 using acetic acid), one volume of water and stored in glutathione storage buffer at 4℃ until further use.

2.3.5. Purification of protein by Ni-NTA and glutathione affinity chromatography

The soluble fraction of an *E. coli* lysate was filtered using a 0.45 µM and 0.22 µM syringe filter consecutively and a 120 µl aliquot removed for subsequent analysis. The subsequent steps were conducted on ice at 4 ºC. The filtered lysate was applied to the equilibrated Ni-NTA column or glutathione agarose column and 120 µl was collected from the flow through. The resin was washed twice with 5 ml Ni-NTA equilibration buffer or 5 mL glutathione equilibration buffer and a 120 µl aliquot was collected from the flow through of each wash. For His-tagged proteins, bound proteins were eluted using 4 ml elution buffer (50 mM Tris-HCl, 500 mM imidazole, pH. 8.0). For GST-tagged proteins, bound proteins were eluted using 3 mL elution buffer (10 mM reduced glutathione, 50 mM Tris-HCl, pH 9.5). An aliquot of 120 µl of the eluted protein sample was removed for analysis. The remaining eluate was stored on ice for the desalting procedure (refer to section 2.3.6.). The samples collected from each step and desalted eluate were stored on ice until SDS-PAGE analysis (refer to section 2.4.1.) and protein concentration determination using a Bradford assay (refer to section 2.3.7.).

2.3.5.1. Ni-NTA column recharging for affinity chromatography

After purification, the column was washed with filter sterilised water and one volume of stripping buffer (20 mM sodium phosphate, 500 mM NaCl, 50 mM EDTA, pH 7.4) was allowed to flow through the column. One volume of filter sterilized water followed by one volume of a 0.1 M nickel sulphate solution was allowed to flow through the column. A volume of filter sterilised water was allowed to flow through the volume and the column was stored in storage solution (50 % ethanol) and kept at 4 °C until further use.

2.3.6. Desalting and storage of purified proteins

A PD-10 desalting column (GE Healthcare) containing Sephadex^{TM} G-25 M resin was equilibrated with five full volumes of assay buffer (25 mM HEPES, 150 mM KCl, 1 mM $MgCl_2$, 1 mM DTT, pH 7.4). Following column equilibration, the affinity chromatography eluate was applied to the desalting column and allowed to penetrate the resin. The bound protein was eluted using 3.5 ml assay buffer. 120 µl of the desalted protein sample was collected and set aside for SDS-PAGE analysis. The purified, desalted protein was stored in 40% (v/v) glycerol at -20 °C.

2.3.7. Bradford assay

The concentration of the desalted and purified protein was determined using a BSA standard curve. A two-fold dilution series ranging 0.075- 5.0 mg. mL^{-1} BSA in assay buffer was prepared and stored at -20 °C until use. To 5 µL of assay buffer (background), samples collected during the purification procedure, BSA standards and desalted protein, 250 µL Bradford reagent (Sigma-Aldrich) equilibrated to room temperature was added in a 96 well plate. The reactions were incubated at room temperature for 5 minutes, following which the absorbance at 595 nm was determined for all samples using a Spectramax M3 plate reader (Molecular Devices). A BSA standard curve with an $R^2 \geq 0.99$ was used for the extrapolation and determination of the concentration of the desalted proteins.

2.4. SDS-PAGE and Western blotting analysis

2.4.1. SDS- PAGE Analysis

To 60 µL of the sample to be analysed, 20 µL of 4X SDS sample loading buffer (0.25 M Tris, pH 6.5, 4.2% (w/v) SDS, 40% (v/v) glycerol, 4% (v/v) β-mercaptoethanol, 1% (w/v) bromophenol blue in water) was added and samples were incubated in boiling water for 5 minutes. The samples were loaded into the wells of a 4% (w/v) acrylamide stacking gel (0.125 M Tris, pH 6.8, 0.1% (w/v) SDS, 4% (w/v) acrylamide, 0.1% (w/v) *bis*- acrylamide, 0.05% (w/v) ammonium persulfate, 0.0012% (v/v) TEMED in water). Typically, the proteins were resolved using a 12% (w/v) acrylamide resolving gel(s) (0.38 M Tris, pH 8.8, 0.1% (w/v) SDS, 12% (w/v) acrylamide, 0.27% (w/v) *bis*- acrylamide, 0.0035% (w/v) ammonium persulfate 0.0007% (v/v) TEMED in water) alongside a colour standard broad range molecular weight marker (New England Biolabs), precision blue molecular weight marker (Bio-Rad) or an unstained molecular weight marker (New England Biolabs) until the dye front reached the bottom of the gel(s), typically for a duration of 90 minutes at 120 V, based on the method described by Laemmli [1977]. The gel(s) were run using a 1X SDS running buffer (25 mM Tris, 192 mM Glycine, 0.1% (w/v) SDS in water). The gel(s) was stained using a Coomasie brilliant blue stain (0.25% (w/v) Coomassie blue R-250, 45% (v/v) methanol, 10% (v/v) glacial acetic acid in water) overnight at room temperature with gentle agitation. The gel was destained using a destaining solution (40% (v/v) methanol, 10% (v/v) glacial acetic acid in water) until the bands were visible and gel(s) photographed using a ChemiDoc XRS + gel documentation system and software (Bio-Rad).

2.4.2. Western Blotting analysis

The proteins resolved on a polyacrylamide gel were transblotted onto an Amersham Hybond^{TM} ECL nitrocellulose blotting membrane at 95-100 V for 60 minutes at 4°C submerged in transblot buffer (25 mM Tris, 192 mM Glycine, 20% (v/v) methanol in water). Following the transblotting, the membrane was rinsed in water. The blot was incubated with Ponceau S stain solution (0.1% (w/v) Ponceau, 1% (v/v) glacial acetic acid in water) for 5 minutes and the blot was destained using Ponceau S destain solution (1% (v/v) glacial acetic acid until the bands became clear.

2.4.2.1. Detection of His-tagged proteins

The blot was blocked using 20 mL incubation buffer (0.1% (v/v) Tween-20, 10 mM Imidazole in TBS) overnight at 4 °C with gentle agitation. The blot was probed with a 1: 5000 dilution of HisDetector Nickel-HRP (SeraCare) for 1 hour at room temperature with gentle agitation. The blot was washed with three volumes of washing buffer (0.1% Tween-20, 10 mM imidazole in TBS). The blot was then covered with TMB membrane peroxidase substrate (SeraCare) and rinsed immediately with water. The bands developed following the rinsing of the blot. An image was taken using the Chemidoc XRS + gel documentation system and software (Bio-Rad).

2.4.2.2. Detection of CFP-tagged proteins and ARF1 proteins

Tris-buffer saline (40 mM Tris, 150 mM NaCl in water) was prepared and the pH was adjusted to 7.4. The blot was blocked for 40 minutes in incubation buffer (0.1 % (v/v) Tween-20, 1 % (w/v) BSA, 2 % (w/v) milk powder in TBS) at ambient temperature followed by incubation with 1 $\mu g.mL^{-1}$ B-2 mouse monoclonal anti-GFP antibodies (Santa Cruz Biotechnology) in incubation buffer overnight at 4 ºC, with gentle agitation. The membrane was washed four times in washing buffer (0.1 % (v/v) Tween-20 in TBS), each for 10 minutes with gentle agitation. The membrane was incubated with a 1: 5000 dilution of horseradish peroxidase-conjugated goat anti-mouse IgG secondary antibodies (SeraCare) in incubation buffer for 60 minutes with gentle agitation for 1 hour at room temperature. The membrane was washed five times in washing buffer (0.1 % (v/v) Tween-20 in TBS), each for 10 minutes with gentle agitation. The membrane was then covered with TMB membrane peroxidase substrate (SeraCare) and rinsed immediately with MilliQ water once appropriate bands were visible. The bands developed following the rinsing of the blot. An image was taken using the ChemiDoc XRS + gel documentation system and software (Bio-Rad). The same procedure described above was carried out for the detection of ARF1 proteins but with following modification. Following the incubation of the blot in incubating buffer to block the blot, an incubation with 1: 1000 mouse monoclonal ARF1 (1A9) antibodies (Santa Cruz Biotechnology) in incubation buffer for 60 minutes at 4 ºC, with gentle agitation was carried out.

2.5. Nucleotide exchange on ARF1 proteins and intrinsic tryptophan fluorescence

To preload $^{N\Delta17}$*Hs*ARF1-CFP, $^{N\Delta17}$*Pf*ARF1-CFP, $^{N\Delta17}$*Hs*ARF1 and $^{N\Delta17}$*Pf*ARF1 with GTP or GDP, the relevant ARF1 protein was diluted to 5 µM in assay buffer (25 mM HEPES, 150 mM KCl, 1 mM $MgCl_2$, 1 mM DTT, pH 7.4) containing 50 µM GTP or GDP and supplemented with EDTA: 5 mM for $^{N\Delta17}$*Hs*ARF1-CFP, $^{N\Delta17}$*Pf*ARF1-CFP, 2 mM for $^{N\Delta17}$*Hs*ARF1 and 20 mM for $^{N\Delta17}$*Pf*ARF1 and. The reactions were incubated at 25 ºC for 90 minutes with gentle agitation. $MgCl_2$ was added to a final concentration of 10 mM for $^{N\Delta17}$*Hs*ARF1-CFP, $^{N\Delta17}$*Pf*ARF1-CFP, 3 mM for $^{N\Delta17}$*Hs*ARF1 and 30 mM for $^{N\Delta17}$*Pf*ARF1 and incubation was carried out for a further 30 minutes at 25 ºC with gentle agitation. To monitor the nucleotide binding, the intrinsic tryptophan fluorescence was measured at an excitation wavelength of 298 nm and an emission wavelength of 340 nm in a Spectramax M3 plate reader (Molecular Devices). Each biological replicate was conducted in technical triplicate.

2.6. ARF1 interaction assays

2.6.1. ARF1 FRET assays

To a black 96-well plate, $^{N\Delta17}$*Hs*ARF1-CFP and $^{N\Delta17}$*Pf*ARF1-CFP pre-loaded with GTP or GDP were diluted in assay buffer, equilibrated to room temperature, and incubated with YPET-GGA3^{GAT} at room temperature for 20 minutes with gentle agitation (concentrations of proteins used differed from one experiment to the next and are documented in Chapter 3). The fluorescence was measured at two wavelength pairs: Ex425 nm/Em485 nm and Ex425 nm/Em535 nm. The background readings were obtained from triplicate wells by incubating GTP or GDP loaded $^{N\Delta17}$*Hs*ARF1-CFP and $^{N\Delta17}$*Pf*ARF1-CFP in the absence of YPET-GGA3^{GAT} and the mean fluorescence signal was subtracted from all experimental reactions containing YPET-GGA3^{GAT}. The FRET signal was represented by the corrected fluorescence signal measured at Ex425 nm/Em535 nm divided by the corrected fluorescence signal measured at Ex425 nm/Em485 nm.

2.6.2. Immobilised ARF1-GGA3^{GAT} interaction assays

To a pre-blocked Ni-NTA HisSorb 96-well plate (Qiagen), 50 µL of 1 µM His-tagged $^{N\Delta17}$*Hs*ARF1 and $^{N\Delta17}$*Pf*ARF1 pre-loaded with GTP or GDP, diluted in assay buffer supplemented with 1 % (w/v) bovine serum albumin (BSA), was immobilised by incubation for 30 minutes at 4 ºC with gentle agitation. GST-GGA3^{GAT} diluted in assay buffer supplemented with 1 % (w/v) BSA was added to a final concentration of 1 µM and incubation continued for a further 60 minutes at 4 ºC with gentle agitation. The protein solutions were aspirated, wells washed with two volumes (100 µL each) of assay buffer supplemented with 0.1 % (v/v) Tween-20 followed by four volumes (100 µL each) of assay buffer. GST assay buffer (2 mM reduced L-glutathione and 1 mM 1-chloro-2,4-dinitrobenzene in phosphate-buffered saline, pH 7.3), equilibrated to room temperature, was added to each well (200 µL per well) and the plate was incubated at room temperature for 30 minutes with gentle agitation. The absorbance was measured at 340 nm in a Spectramax M3 plate reader (Molecular Devices). The background readings were obtained from triplicate wells by incubating GST-GGA3^{GAT} in the absence of ARF1 and the mean absorbance was subtracted from all experimental reactions of GST-GGA3^{GAT}. Plates were prepared for reuse by rinsing the plates with 0.45 µM filter sterilised water (100 µL per well) followed by a 10-minute duplicate incubation with stripping buffer (20 mM sodium phosphate, 500 mM NaCl, 50 mM EDTA, pH 7.4) (100 µL per well), an additional wash with filter sterilised water (200 µL per well) and a 20-30 minute incubation in recharging solution (0.1 M $NiSO_4$) (100 µL per well). Wells were washed with a final volume of filter sterilised water (400 µL per well) and used immediately.

2.7. Statistical analyses

Where appropriate, comparisons between means of the datasets were made using unpaired t-tests to calculate P-values using GraphPad t-test calculator. P-values below 0.05 were regarded as indicating significant differences between compared mean values.

Chapter 3: Establishing a Fluorescence resonance energy transfer assay to confirm ARF1 as a therapeutic target for cancer and malaria.

3.1. INTRODUCTION

The research group has an interest in developing assays that can be used for medium (or high) throughput screening. A variety of assay formats are usually used for such purposes, such as colorimetric, bioluminescent and fluorescent techniques. Of interest in this chapter is the fluorescence resonance energy transfer (FRET) assay. The use of FRET over the past few years has proliferated in cell biological experiments and with the recent advances in fluorescent probes, instrumentation and methodologies, FRET is likely to continue having an increasingly significant impact in scientific research in the near future. Dynamic protein interactions play a role in many cell signalling processes and FRET is a key technique in elucidating such interactions. The majority of the FRET approaches described involve analyses conducted in cells and only a fraction involves *in vitro* biochemical assays using purified proteins. Thus, there is motivation to explore the development of a biochemical FRET assay format *in vitro* to broaden the scope of current FRET assay formats.

3.1.1. Why FRET?; physical basis of FRET

FRET is a physical phenomenon that involves transmission of energy from an excited fluorescent donor molecule to a fluorescent acceptor molecule. The energy transfer between the fluorescent molecules, which are referred to as a FRET pair, is a non-radiative process which results in an enhanced emission intensity of the acceptor molecule and a decrease in the donor fluorescence intensity (Förster, 1946; Selvin, 2000). This phenomenon is only observed when three basic requirements are met: the donor and acceptor are in close proximity (that is, the distance is less than 10 nm), the emission spectrum of the donor molecule overlaps significantly with the excitation spectrum of the acceptor molecule and favourable dipole-dipole alignment (Clegg, 1995; Selvin, 2000; Lakowicz, 2013). FRET is an appealing technique for bioanalysis because of the sensitivity to nanoscale changes in donor and acceptor separation (Song *et al*., 2011). The energy transfer efficiency, which can be used to quantitatively describe protein interactions, can be determined from steady state measurements

or time resolved measurements. This property has been used in biological research to identify protein interactions, real time monitoring of intracellular signalling activities and surveying of bioactive molecules by high throughput screening (Saucerman *et al*., 2006; Dams *et al*., 2007; Gordon *et al*., 2007). FRET offers real time monitoring and spatial extension (relationship between space, shape and area) information on molecular interactions of multicomponent structures made up of proteins, lipids, carbohydrates, nucleic acids and viruses in living cells as compared to traditional approaches to identifying protein interactions such as immunoprecipitation and yeast two hybrid assays (Clegg, 1995; Zhang *et al*., 2002; Bertolin *et al*., 2019). Another popular method to examine protein interactions *in situ* has been colocalization by immunofluorescence microscopy in fixed cells or of proteins tagged with different fluorescent proteins in live cells. Whereas most interactions between proteins are a few nanometres wide, the resolution of standard fluorescence microscopes is much lower (200-300 nm in lateral direction and 500- 700 nm in axial direction) (Huang *et al*., 2009). This presents an interesting dynamic in that, by analogy, typical fluorescence imaging experiments yield information that two students are part of a large lecture theatre but not as to whether the two students are in close proximity or interacting (Piston and Kremers, 2007). These crude measurements are suggestive but misleading at best as many signalling pathways use the same cellular machinery. FRET provides more reliable measures of interactions as information of two molecules being in close proximity and not just that the molecules are in the same neighbourhood can be obtained.

3.1.2. Existing FRET assay formats for application in cell biology

FRET constructs have been used to investigate the downstream effects of second messenger signalling. A sensor construct that targets the cAMP pathway has been designed in which the kinase-inducible domain of cAMP-responsive element binding protein forms a linker between blue fluorescent protein and green fluorescent protein. Phosphorylation causes a conformational change in the kinase inducible domain and this alters the FRET efficiency in response to cAMP signalling (DiPilato *et al*., 2004).

FRET is used to study the structure, conformation, hybridisation and automated sequencing of nucleic acids. Chromosome FISH (Fluorescence In Situ Hybridisation) based on a hybridisation mechanism of a nucleic acid with its complement has been used in gene mapping analysis, clinical diagnostics, mutation identification and studies of chromosomal and nuclear

architecture. The method is based on template-dye directed-incorporation (TDI) assay. In this method, genomic DNA fragments that are amplified contain polymorphic sites and are incubated with a 5′-fluorescein-labeled primer, which is designed to hybridize to the DNA template adjacent to the polymorphic site, the allelic ROX-labelled dideoxy terminator and Taq DNA polymerase (Klentaq1-FY). The dye-labelled primer is extended by one base by the dye-terminator which is specific for the allele that is present on the template. At the end of the genotyping reaction, the reaction mixture is analysed for changes in fluorescence intensities where the excitation is measured for fluorescein at 488 nm and the emission wavelength (due to energy transfer) of ROX at 605 nm (Chen *et al*., 1997; Sekar and Periasamy, 2003).

FRET has also been applied in membrane fusion assays. An assay for vesicle to vesicle fusion involving resonance energy transfer from NBD, the donor, to rhodamine, acceptor, has been described. Both fluorophores are coupled to the amino group of phosphatidylethanolamine to provide analogues which can be incorporated into a lipid vesicle bilayer. When both fluorescent lipids are incorporated into phosphatidylserine vesicles at appropriate surface densities (relating to the ratio of fluorescent lipid to total lipid), energy transfer can be observed. When these vesicles are fused with phosphatidylserine vesicles by the addition of calcium, the two probes mix with the other lipids present which results in the formation of a new membrane. This mixing results in the reduction of surface density of the energy acceptor which decreases resonance energy transfer efficiency which can be determined experimentally (Struck *et al*., 1981).

FRET measurements can also be employed in immunoassays. In an immunoassay, where Cy5 NH_2-terminally labelled phosphopeptide, is recognized by an antiphosphotyrosine primary mouse antibody, followed by a Cy3-labeled secondary antibody, are used to measure specific antibody and antigen interactions. FRET occurs when the antibody and antigen are bound together and excitation at wavelengths of Cy3 and emission wavelengths of Cy5. When the interaction between the phosphopeptide and primary antibody is disrupted then the FRET signal observed will reduce. This is particularly useful for studying protein kinases and their ability to phosphorylate labelled peptides (Sekar and Periasamy, 2003).

Thus, the benefits of FRET are becoming an attractive feature for researchers that seek measurements with high sensitivity, specificity, non- invasiveness, rapidity and relative simplicity.

3.1.3. FRET pairs

Genetic labelling with fluorescent proteins has been widely used in biomedical and biological research, has revolutionized live cell imaging experiments and has led to a growing interest in FRET methodology. FRET biosensors, which are proteins composed of fluorophores and sensing domains are now widely used as spectroscopic rulers to monitor biochemical activities that cause changes in molecular proximity such as protein interactions, concentrations of intracellular ions, activities of enzymes and conformational changes (Miyawaki, 2011; Lam *et al*., 2012). FRET pairs can be classified into two types. The intramolecular type, also known as a homo-FRET pair, where the donor and acceptor fluorophores are conjoined to the same molecule. The changes in FRET will be observed due to the conformational changes that occur in molecule. The intermolecular type, also known as a hetero-FRET pair, where the fluorophores are joined to different molecules and changes in FRET will be observed when the molecules interact or come in close proximity (Miyawaki, 2011). The intermolecular type approach was adopted for this study. Choosing optimal FRET pairs is of paramount importance for high performing biosensors in live cells and this can be extended to FRET approaches using biochemical assays (Piston and Kremers, 2007). All FRET measurements rely on mutants of green fluorescent protein from *Aequorea victoria,* which gave rise to different fluorescent pairs (Shaner *et al*., 2013). Currently available FRET fluorescent pairs are described below.

3.1.3.1. Cyan fluorescent protein (CFP) and Yellow fluorescent protein (YFP) FRET pairs

The first FRET pair developed was the blue fluorescent protein (BFP) coupled with green fluorescent protein (GFP) but the low photostability and low brightness of this pair, particularly that of BFP, made it nonviable for a wide array of applications. Site directed mutagenesis has been used to introduce mutations on the blue fluorescent protein to overcome these limitations to make this pair now useful for some applications (Kremers *et al*., 2006; Mena *et al*., 2006). Mutations on GFP and the discovery of coral derived proteins has led to a broad palette of different coloured proteins (Heim *et al*., 1994). To overcome the limitations of the BFP-GFP pair, cyan fluorescent protein (CFP) coupled with yellow fluorescent protein (YFP) was the first effective pair developed and has become the most popular pair (Miyawaki *et al*., 1997; Piston and Kremers, 2007). The CFP- YFP pair has been engineered starting with an ECFP-EYFP pair using site directed mutagenesis (Heim and Tsien, 1996; Kremers *et al*., 2006). CFP donor variants engineered have been proven to have high quantum yields and these include:

mCerulean (which was adopted for this study), mTurquoise2, mTFP1 and Aquamarine (Heim *et al*., 1994; Ai *et al*., 2006; Goedhart *et al*., 2012; Erard *et al*., 2013). YFPs used in applications include EYFP derivatives such as mVenus, mCitrine, sEYFP and YPET (used in this study) because of better folding at 37 ºC, more photostability and less sensitivity to pH and chlorides as compared to EYFP (Griesbeck *et al*., 2001; Koushik *et al*., 2006). However, CFP-YFP pairs have their own set of limitations which include fast photobleaching of YFP acceptor, phototoxicity from violet donor excitation, spectral cross talk and the photoconversion of YFPs to CFP like fluorescent proteins (Malkani and Schimid, 2011; Lam *et al*., 2012). Despite the limitations of the CFP-YFP pair, this pair remains the 'best' FRET pair (Piston and Kremers, 2007).

3.1.3.2. Green fluorescent protein (GFP) and Red fluorescent protein (RFP) FRET pairs

Green fluorescent protein (GFP) coupled with red fluorescent protein (RFP) have been developed to mitigate some disadvantages of the CFP-YFP FRET pairs. The excitation of GFP-RFP at longer wavelengths leads to greater spectral separation, reduces phototoxicity and reduces autofluorescence from fluorophores such as flavoproteins in cells. Despite advances that have been made in FRET based sensor applications, use of this pair in cell biology and high throughput screening is still limited due to low FRET efficiency and dynamic range (donor and acceptor emission ratio variation) (Abraham *et al*., 2015; Mastop *et al*., 2017). Brighter and more photostable green fluorescence protein donors and red fluorescence acceptors have been developed. Acceptors derived from GFP include mClover and mClover3 and mNeonGreen derived from YFP. Donors derived from RFP include mCherry, mRuby derivatives mRuby2 and mRuby3 (Piston and Kremers, 2007; Shaner *et al*., 2013; Bajar *et al*., 2016). Some examples of these GFP-RFP pairs include EGFP-mCherry, Clover-mRuby2, mClover3-mRuby3 and mNeonGreen-mRuby3 which have been specifically developed to improve FRET efficiency, improvement in dynamic range and increased application in FRET intensity-based measurements. These brighter and more photostable green donors and red acceptors have become increasingly attractive in FRET measurements in cells due to their advantages over the CFP-YFP FRET pair (Bajar *et al*., 2016).

3.1.3.3. Far-red fluorescent protein (FFP) and Infrared fluorescent protein (IFP) FRET pairs

The FFP donor coupled with IFP acceptor has been useful in deep tissue imaging owing to the low scattering of light and absorption from haemoglobin. The FFP-IFP FRET pair is more red-shifted in spectra in comparison to the GFP-RFP pair which presents an advantage for use in

the monitoring of cellular processes in mammalian tissues (Filonov *et al*., 2011; Chu *et al*., 2014). One of the few FFP-IFP FRET pairs described is the mPlum donor coupled with IFP1.4 acceptor, where IFP1.4 uses Biliverdin, a ubiquitous chromophore expressed in mammalian cells, to produce fluorescence to image both cell culture and xenograft tumours. Another IFP which has shown considerable promise is iRFP. FRET experiments do not require the addition of exogenous Biliverdin to boost the fluorescence signal and brightness because it is stable in cells and has a high binding affinity for Biliverdin. iRFP has been coupled with a range of far red fluorescent donors but in particular the coupling with eqFP650 showed the greatest dynamic range in a caspase 3 sensor but still significantly low in comparison to other dynamic ranges of FRET sensors because of the low quantum yield of the FFP donor. This presents the motivation for the development of new FFPs with higher quantum yields (Wang *et al*., 2004; Shu *et al*., 2009; Lecoq and Schnitzer, 2011).

3.1.3.4. Large Stokes Shift fluorescent protein based (LSS-FP) FRET pairs

Another class of FRET pairs include fluorescent proteins with a large stokes shift characterised by a difference in the excitation and emission maxima of more than 100 nm and have been developed based on conventional RFPs. The advantage of using such proteins is that there is a reduction in spectral cross talk between the donor and acceptor fluorescent proteins to provide larger changes in FRET for use in FRET imaging analysis and are useful for the monitoring of multiple processes in a single cell using multicolor FRET imaging analysis (Paitkevich *et al*., 2010; Wu *et al*., 2011). An orange large stokes shift fluorescent protein, LSSmOrange has a five-fold brightness in comparison the previous brightest LSS red fluorescent protein and was shown to be an effective FRET donor when coupled with far red fluorescent acceptors such as mKate2. LSSmOrange is of interest as it fills the gap between yellow and green fluorescent proteins and LSS far red fluorescent proteins with excitation and emission wavelengths of 437 nm and 572 nm respectively (Shcherbo *et al*., 2009; Shcherbakova *et al*., 2012).

3.1.3.5. Dark fluorescent protein (Dark FP) based FRET pairs

Dark fluorescent proteins have a very low quantum yield and a high absorption are valuable FRET acceptors for FLIM (fluorescent lifetime imaging microscopy) (Bajar *et al*., 2016; Murakoshi and Shibata, 2017). Dark FPs are non- fluorescent but retain their absorption properties to enable FRET and have been utilized in FLIM-FRET experiments (refer to section 3.1.4.3 for principle of FLIM-FRET). Intrinsic advantages of the darkness of dark FPs include: accurate measurement of donor fluorescence lifetime, thereby improving the FRET dynamic

range, as there is a decline in the bleed-through from the acceptor to the emission channel, decrease in probable phototoxicity by lowering the excitation intensity and the use of wider optical filters, dark FRET pairs occupy a small range of the wavelength spectrum, more fluorescent proteins of different colours can be used for dual colour imaging in FLIM-FRET (Bajar *et al*., 2016). To date, ShadowY, a dark yellow fluorescent protein, is the best dark FP developed. ShadowY has been coupled with EGFP or a mClover mutant with large FRET signal changes and less cell to cell variability which allows for precise measurements of individual cellular responses. Other dark FPs include: REACh, sREACh and ShadowG (Ganesan *et al*., 2006; Murakoshi *et al.*, 2008; Murakoshi *et al*., 2015; Murakoshi and Shibata, 2017).

3.1.3.6. Multicolor FRET pairs

The continuous development of new fluorescent proteins has created a plethora of existing FRET pairs suited for multicolor FRET. Multicolor FRET has the potential to allow the simultaneous detection or near simultaneous detection of different cellular processes with the same cell (Bajar *et al*., 2016). The FRET pair used in this study has been used in multicolor FRET. DsRed, RFP from *Discosoma*, has great spectral overlap with YFP and CFP and this enables it to be a great candidate acceptor to YFP and CFP and by using CFP-DsRed and YFP-DsRed, near-simultaneous FRET imaging of initiator and effector caspases in the same cell was reported (Kawai *et al*., 2005). There are many other multicolor FRET pairs described in literature and are used for a variety of applications in cell biology.

3.1.4. Detection methods of FRET commonly used

Some methods in FRET analysis have been developed for use in imaging analysis on microscopes. However, some of the detection methods can be applied for *in vitro* analysis using biochemical assays.

3.1.4.1. Sensitized emission

Sensitized emission, also known as two color ratio imaging, is the simplest method to detect FRET. The donor is excited by light of a specific wavelength and the signal is collected using emission filters chosen for the donor fluorescence and acceptor fluorescence. This would be the perfect method if there was no fluorescence cross-talk from the donor and acceptor fluorescence. The background signal known as spectral bleedthrough and appropriate controls

are needed to account for the cross-talk. The strength of this method is that it allows for both the quenched donor and sensitized acceptor signal to be measured continuously. Thus, the FRET signal from the acceptor is instantly confirmed from measuring the quenched donor signal. Additionally, measurements are rapid, conducted in seconds (Berney and Danuser, 2003; Day and Davidson, 2012). This method was employed in this study to measure FRET.

3.1.4.2. Acceptor photobleaching

Acceptor photobleaching or donor dequenching is also a simple method but limited to a single measurement. The concept involves the quenching of the donor fluorescence when FRET occurs. Photobleaching the acceptor releases quenching and increases the donor fluorescence. If FRET is present, the donor fluorescence will increase when the acceptor is removed. For these experiments, it is important to ensure that the acceptor photobleaching does not cause degradation. The weakness of this approach is that photobleaching can take a significant amount of time, a limitation in localisation experiments where changes occur over relatively short periods and some fluorophores can convert to other spectral forms which can lead to the overestimation of donor dequenching. The strength of this approach is that it is straightforward, quantitative and performed on the same sample (Kremers *et al*., 2009; Malkani and Schmid, 2011).

3.1.4.3. Fluorescence lifetime imaging microscopy (FLIM)

FLIM is the most rigorous method used in imaging experiments and a relatively newly developed approach. FLIM measures the fluorescence decay time of the donor. When FRET occurs between the fluorescent proteins, donor fluorescence is quenched and the decaying time of the donor is shortened, allowing for measurements of FRET efficiency. FLIM-FRET measurements are not as sensitive to direct acceptor excitation and can be used with acceptors that are not fluorescent giving rise to the expansion the number of useful fluorescent FRET pairs. Limitations include slower imaging which limits applicability and measurements of nanosecond lifetimes are complicated and thus the instrumentation used is expensive to obtain and maintain (Day and Davidson, 2012).

3.1.4.4. Spectral imaging

Spectral imaging is a recent method for the improvement of imaging systems. The concept involves the collection of the whole fluorescence spectrum which enables overlapping spectra to be separated by using the peak of the fluorescence emission as well as distinct shapes of

spectral tails (known as lambda stacks). Collection of both donor and acceptor fluorescence makes it possible to determine the amount of donor fluorescence and acceptor fluorescence. The strength of this method is that it allows for both the quenched donor and sensitized acceptor signal to be measured continuously in living specimens. Thus, the FRET signal from the acceptor is instantly confirmed from measuring the quenching of the donor signal. Additionally, measurements are taken rapidly, in seconds, which allows for dynamic measurements. The drawback is that separate measurements from control cells need to be taken to obtain corrections to quantify FRET accurately. As more commercial systems are being developed, the use of spectral imaging for FRET is increasing and may become one of the main methods for performing FRET imaging experiments (Dickinson *et al*., 2001; Zimmermann *et al*., 2003; Chen *et al*., 2006; Chen *et al*., 2007).

3.1.5. Conceptualisations of assay formats

As previously reviewed, all ARF GTPases, including ARF1, undergo an activation/deactivation cycle to perform their functions. They are inactive cytoplasmic proteins when bound to GDP. Exchange of GDP for GTP activates them and causes them to bind to organelle membranes and recruit effector proteins. Hydrolysis of the bound GTP to GDP deactivates them and returns them to the cytoplasm. GDP/GTP exchange is triggered by a family of ARF guanine nucleotide exchange factors (ARF GEFs), while GTP hydrolysis is stimulated by GTPase activating proteins (ARF GAPs). Recombinant ARF GTPases produced in bacteria, yeast or mammalian cells are purified in a GTP or GDP bound form (Macia *et al*., 2001), thus it is necessary to prepare GTP loaded and GDP loaded ARFs for studying the activation status of ARF GTPases, particularly for developing assays that measure the activation or deactivation of ARF as is the case in this chapter. The activation status can be manipulated using EDTA-mediated nucleotide exchange and monitored using intrinsic tryptophan fluorescence (Bigay and Antonny, 2005). In EDTA-mediated nucleotide exchange, ARF GTPases are incubated with an excess of GTP or GDP in the presence of EDTA, which is a chelator of the Mg^{2+} ions that stabilise the bound nucleotides, giving rise to the inactive and active forms of ARFs. The ARFs will bind the nucleotide that is present in excess concentrations. The resulting GDP or GTP-ARF GTPase complex is subsequently stabilized by the addition of $MgCl_2$. The stabilized complexes are employed in assessing the effects of ARF GEFs and ARF GAPs on the activation status of ARF GTPases. Nucleotide exchange is

monitored by intrinsic tryptophan fluorescence as an invariant tryptophan residue within the switch II region of ARF GTPases is exposed upon the binding of GTP when ARF GDP transitions to ARF GTP. Upon deactivation, the invariant residue is hidden within the core of the protein. Thus, the tryptophan residue can be used as an intrinsic probe for protein conformation and hence the GTP vs. GDP-bound status of ARF (Béraud-Dufour *et al*., 1998; Goldberg, 1998; Bigay and Antonny, 2005). Changes in the activation status of ARFs by ARF GEFs and ARF GAPs could be assessed using real time measurements of intrinsic tryptophan fluorescence, but this method is not amenable to high throughput screening assays due to the possibility of background fluorescence produced by test compounds.

3.1.5.1. Principle of assay formats

The basis for the assay explored in this chapter is that ARF1, when active (bound to GTP), should bind to an effector protein (the GAT domain of GGA3), but not when it is inactive (bound to GDP). By fusing ARF1 to a fluorescent tag, cyan fluorescent protein (CFP), and GGA3 to yellow fluorescent protein (YFP), binding interaction of active ARF1 to GGA3 should produce a FRET signal (excitation of CFP at 425 nm should produce fluorescence emission at 485 nm which, in turn, should excite the YFP in proximity to emit fluorescence at 535 nm) (**Figure 5**). The consequence is that the FRET signal should correlate with the activation status of ARF1: increase when ARF1 is active (GTP bound) and decrease when it is inactive (GDP bound). In addition to human (*Homo sapiens*) ARF1, putative *P. falciparum* ARF1 was used in an attempt to develop the assay. The motivation was to address the question of whether ARF1 inhibitors aimed at cancer therapy may also be useful as an anti-malarial strategy, due to the high level of homology between the two proteins.

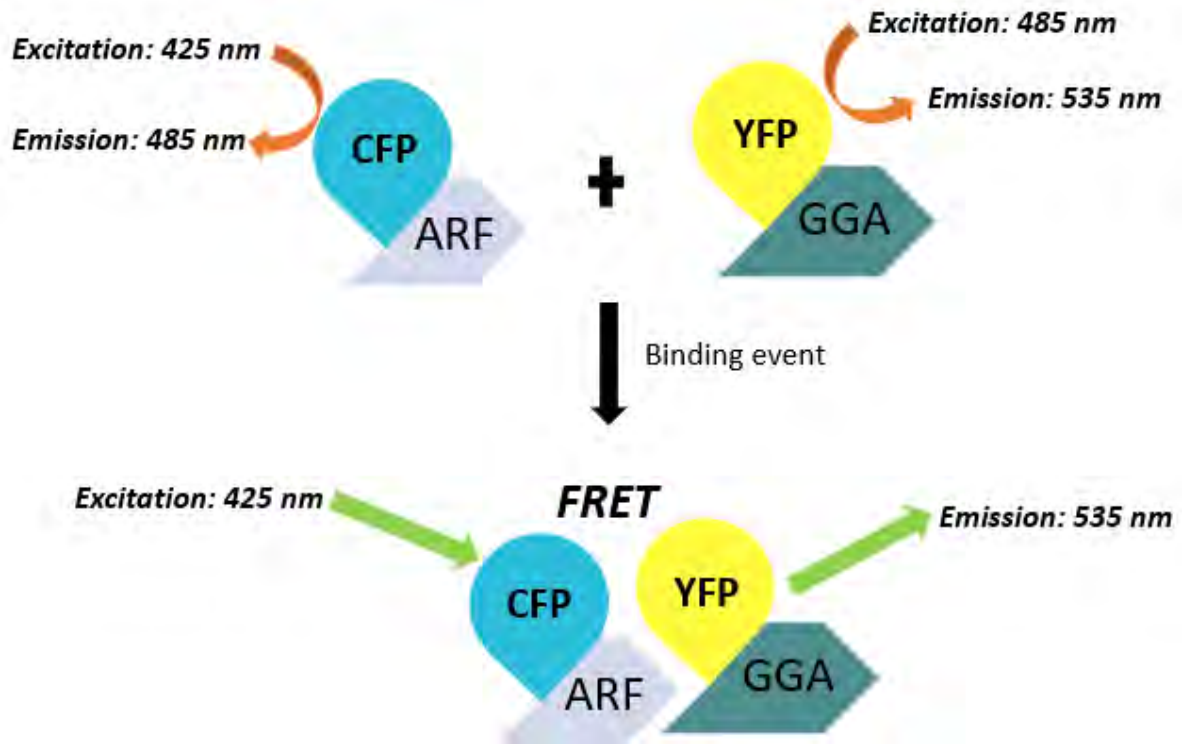

Figure 5: The principle of FRET. Before a binding event, the recombinant proteins are in solution with different excitation and emission spectra and no FRET signal, an increase in fluorescence emission at 535 nm when excited at 425 nm, is observed. The human and *Plasmodium falciparum* ARF1 protein fused to CFP excitation and emission wavelengths are 425 nm and 485 nm respectively. The GGA3^{GAT} protein fused to YFP excitation and emission wavelengths are 485 nm and 535 nm respectively. When a binding event occurs between active ARF1 and GGA3, a FRET signal, an increase in fluorescence emission at 535 nm when excited at 425 nm, is observed, and fluorescence is measured at excitation and emission wavelengths of 425 nm and 535 nm respectively.

3.2. AIMS AND OBJECTIVES

Aim of the study: The research question that motivates the project is: if ARF1 is so widely regarded as a potential drug target, why are there so few publications describing drug discovery projects aimed at ARF1, and relatively few ARF1 inhibitors that can be used to validate it as a therapeutic target? Our hypothesis is that it is due to the lack of a convenient assay that can be used for drug screening purposes (an essential feature of a drug target is a multiwell plate-based assay that can be used to screen large numbers of chemical compounds in order to identify inhibitors). The overall aim of this chapter was to attempt the development of a FRET assay to measure the activation status of ARF1 and that can be potentially applied for use in compound drug screening campaigns, i.e. identify novel compounds capable of preventing the activation or deactivation of ARF1. Specific aims and experimental objectives are described below.

Specific aims/ questions and objectives:

1. Prepare DNA plasmid constructs for expressing human and *P. falciparum* ARF1 (*Hs*ARF1 and *Pf*ARF1, respectively) fused to CFP.
2. Express and purify human and *Pf*ARF1 fused to CFP using *E. coli* following the determination of optimal expression conditions by conducting induction studies at different concentrations of IPTG and temperatures.
3. Express and purify the GAT domain of GGA3 fused to YFP using *E. coli* and a previously prepared construct (T. Swart, PhD thesis in preparation). Can the protein be expressed in a sufficiently soluble and pure form?
4. Establish optimal conditions for EDTA mediated nucleotide exchange for plate reader measurement of tryptophan fluorescence as an indicator of the activation status of *Hs*ARF1-CFP and *Pf*ARF1-CFP.
5. Determine whether a FRET signal between ARF1-CFP and YFP-GGA3^{GAT} can be detected by using ARF1-CFP pre-loaded with GTP (active ARF1) *vs.* a negative control consisting of ARF1 pre-loaded with GDP (inactive ARF1).

3.3. RESULTS

Preparation of DNA constructs used in the development of an ARF1 FRET assay. The main objective of this part of the work was to prepare DNA constructs that could be used to express and purify the proteins required to develop the ARF1-CFP interaction with YPET-GGA3^{GAT} FRET assay. For the expression of both the $^{N\Delta17}$*Hs*ARF1-CFP and $^{N\Delta17}$*Pf*ARF1-CFP in *E.coli*, the general cloning strategy is described below (note that the NΔ17 prefix indicates the absence of the N-terminal 17 amino acids of the native ARF1 proteins – these form an amphipathic α-helix that hampers soluble expression in *E. coli*). The pET-28a plasmid containing the coding sequence of *E. coli* 6-Hydroxymethyl-7,8-dihydropterin pyrophosphokinase (HPPK) inserted between the BamHI and *Xho*I sites was custom prepared and provided by Genscript (Hong Kong) for a previous study. To remove the HPPK sequence, the plasmid was digested using BamHI and *Xho*I. An mCerulean N1 plasmid was used as template for amplifying the coding sequence of CFP (cerulean variant) and was obtained from Addgene (plasmid #27795, donated by Steven Vogel). The PCR amplicon and the restriction digested pET-28a-HPPK plasmid were analysed by agarose gel electrophoresis (*results not shown*). The approximate sizes of the PCR amplicon and restriction digestion products were determined using a standard curve of log (size in bp) versus relative migration distance of DNA molecular weight markers used (*results not shown*). The template for amplifying the human ARF1 coding sequence was pARF1-CFP-N1 (Addgene plasmid #11381, donated by Joel Swanson). The pEGFP-N1-*Pf*ARF1 plasmid used as template for amplifying the *P. falciparum* ARF1 coding sequence was prepared and donated by Tarryn Swart (T. Swart, PhD thesis (in preparation)). The plasmid contains the *Pf*ARF1 sequence, codon optimised for human expression by Genscript, cloned between the *Xho*I/*Kpn*I restriction sites of the pEGFP-N1 mammalian expression plasmid (Clontech). To prepare N terminal truncated $^{N\Delta17}$*Hs*ARF1 and $^{N\Delta17}$*Pf*ARF1 coding sequences, a forward primer that omitted the coding sequence for the first 17 amino acids was used in the PCR amplification. The PCR amplicons were analysed by agarose gel electrophoresis. The $^{N\Delta17}$*Hs*ARF1 and $^{N\Delta17}$*Pf*ARF1 PCR amplicons digested with BamHI and *Nhe*I were subcloned into pET-28a-CFP plasmid digested with BamHI and *Nhe*I. The ligation reactions were transformed into XL-10 Gold competent *E. coli* cells, colonies cultured overnight and plasmids purified using alkaline lysis miniprep. Double restriction digestions were done using BamHI and *Nhe*I and triple restriction digestions were done using BamHI, *Nhe*I and *Xho*I. Triple digestions were conducted as an additional diagnostic as the CFP coding sequence has a flanking *Xho*I restriction site and a digestion along with BamHI

and *Nhe*I should release both the ARF1 and CFP coding sequences from the plasmid backbone. Restriction digestion products were analysed by agarose gel electrophoresis. Theoretically, digestions of pET-28a-$^{N\Delta17}$*Hs*ARF1-CFP and pET-28a-$^{N\Delta17}$*Pf*ARF1-CFP constructs by BamHI and *Nhe*I should result in two linearized bands which represent the pET-28a vector fused with CFP (6119 bp) and respectively the $^{N\Delta17}$*Hs*ARF1 or $^{N\Delta17}$*Pf*ARF1 (510 bp) coding sequences. Two digestion products of approximately 6100 bp and 500 bp were obtained which corresponded with the predicted digestion pattern (**Figure 6A**, Lane 2 for pET-28a-$^{N\Delta17}$*Hs*ARF1-CFP and **Figure 6B,** Lane 2 for pET-28a-$^{N\Delta17}$*Pf*ARF1-CFP). Theoretically, triple digestions of the two constructs by BamHI, *Nhe*I and *Xho*I should have resulted in three linearized bands which represent the pET-28a vector (5369 bp), CFP (740 bp) and the respective $^{N\Delta17}$ARF1 (510 bp) coding sequences. Three digestion products of approximately 5200 bp, 740 bp and 500 bp were obtained which corresponded with the digestion pattern predicted (**Figure 6B**, Lane 3 for pET-28a-$^{N\Delta17}$*Hs*ARF1-CFP and **Figure 6B,** Lane 3 for pET-28a-$^{N\Delta17}$*Pf*ARF1-CFP). The cloned plasmids were further verified by sequencing analysis by Inqaba Biotech (**Figure S36 and S37**, *see supplementary information*).

The pEF4-myc-HisA-YPET-GGA3 construct was obtained from Addgene (plasmid #18841, donated by Martin Schwartz). It contains the coding sequence of YPET (a YFP variant) fused to the 5' end of the coding sequence for the GAT domain (amino acids 148-303) of human GGA3. The plasmid vector is a mammalian expression vector. Protein expression is done in *E.coli* in the research group so to solve this, the YPET-GGA3^{GAT} insert was sub- cloned into the *Nhe*I and *Xho*I sites of the bacterial expression plasmid, pET-28a (T. Swart, PhD thesis (in preparation)). Plasmids were purified by alkaline lysis miniprep from the supplied glycerol stock. The plasmid construct was retransformed into XL-10 Gold competent *E. coli* cells, colonies cultured overnight and plasmids purified using alkaline lysis miniprep. A restriction digestion was done using *Nhe*I and *Xho*I. Theoretically, digestions of pET-28a-YPET-GGA3^{GAT} should result in two linearized bands which represent the pET-28a backbone (5369 bp) and the YPET-GGA3^{GAT} coding sequence (1209 bp). Two digestion products of 5400 bp and 1300 bp were obtained which corresponded with the digestion pattern predicted (**Figure 6C**, Lane 2).

In summary, the results suggested that plasmid constructs were successfully prepared for protein expression in *E.coli* cells.

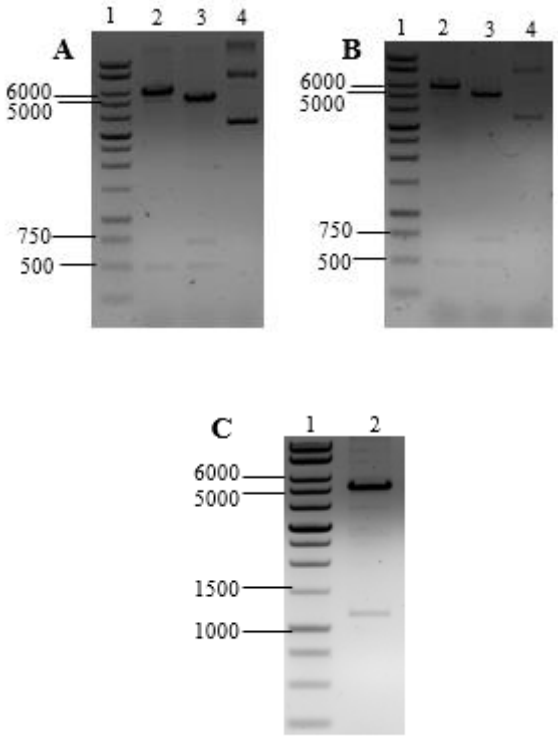

Figure 6: Diagnostic restriction digestion analysis of pET-28a- $^{N\Delta17}$*Hs*ARF1-CFP and pET-28a-$^{N\Delta17}$*Pf*ARF1-CFP and pET-28a-YPET-GGA3^{GAT} constructs. All the restriction digestion products were run on a 0.8 % (w/v) agarose gel at 95 V for approximately 75 minutes and stained with ethidium bromide. The DNA bands were visualized under UV light and photographed using a ChemiDoc XRS+ system (Bio-Rad). For all gels: Lane 1: Promega 1 kbp DNA ladder (molecular weight shown in bp) **A: $^{N\Delta17}$*Hs*ARF1 coding sequence cloned into pET-28a-CFP construct.** Lane 2: pET-28a- $^{N\Delta17}$*Hs*ARF1-CFP construct double digest using BamHI and *Nhe*I; Lane 3: pET-28a- $^{N\Delta17}$*Hs*ARF1 -CFP construct triple digest using BamHI, *Nhe*I and *Xho*I and Lane 4: Uncut pET-28a- $^{N\Delta17}$*Hs*ARF1-CFP construct. **B: $^{N\Delta17}$*Pf*ARF1 coding sequence cloned into pET-28a-CFP construct.** Lane 2: pET-28a- $^{N\Delta17}$*Pf*ARF1-CFP construct double digest using BamHI and *Nhe*I; Lane 3: pET-28a- $^{N\Delta17}$*Pf*ARF1-CFP construct triple digest using BamHI, *Nhe*I and *Xho*I and Lane 4: Uncut pET-28a-CFP- $^{N\Delta17}$*Pf*ARF1-CFP construct. **C: pET-18a-YPET-GGA3^{GAT}.** Lane 2: double digestion of YPET-GGA3 construct using *Nhe*I and BamHI.

Analytical scale expression of the recombinant proteins used in the FRET assays for ARF1. The main objective of this part of the work was to establish the conditions that are required to express soluble proteins required for the ARF1 FRET assay. The expression constructs, previously used to transform XL-10 Gold competent *E. coli* for cloning and storage purposes, were transformed into T7 Express lysY/I_q competent *E. coli* cells and the cells cultured overnight at 37 ºC. The analytical scale expression cultures were prepared by inoculating (1 in 20 inoculum) 8 mL Luria broth containing kanamycin with the overnight starter culture. Once the bacterial expression cultures had achieved a bacterial density with an OD_{600} reading of 0.5-0.9, protein expression was induced by the addition of IPTG to final concentrations between 0.4- 1 mM and by incubation for 3, 6,16 and 18 hours at 37, 30, 25 and 18 ºC respectively to optimize protein expression conditions. Soluble and insoluble bacterial fractions were prepared and analysed by SDS-PAGE. The molecular mass of the recombinant proteins was determined by preparing a standard curve of log molecular weight versus migration distance of the molecular weight marker used (*results not shown*). The His-tagged CFP recombinant protein had a predicted molecular mass of 26 kDa. The protein was concluded to be soluble as an overexpressed protein band with a molecular mass of 26 kDa in the induced soluble fraction of the analytical scale expression profile of *E. coli* cells harbouring the pET-28a-CFP construct **(Figure 7,** Lane 6 *indicated by arrow*). The overexpressed protein band was not present in the uninduced insoluble and soluble fractions.

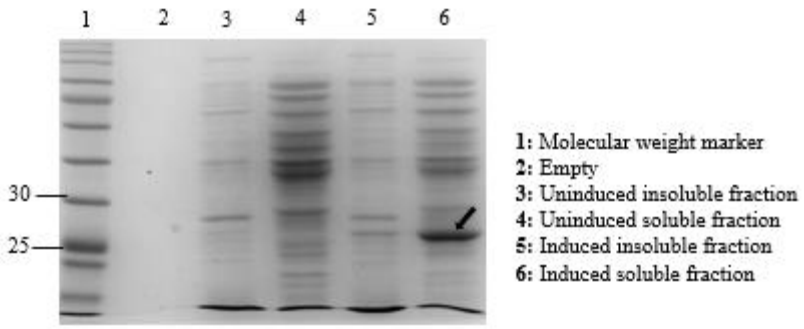

Figure 7: Analytical scale protein expression analysis of His-tagged CFP. All expression constructs were transformed into competent *E. coli* (T7 Express LysY/I_q). The transformed cells were cultured at 37 °C until the logarithmic growth phase. Protein expression was induced by the addition of 1 mM IPTG at 37 °C for 3 hours. The uninduced and induced protein expression cultures were lysed and soluble and insoluble protein fractions were obtained by centrifugation. All samples were prepared in SDS sample loading buffer and resolved on a 12% SDS- PAGE gel run at 120 V for approximately 1.5 hours. Molecular weight marker (kDa): Unstained protein standard (New England Biolabs #P7704S).

Preliminary analysis of the analytical scale expression of the $^{N\Delta17}$*Hs*ARF1-CFP recombinant protein induced at 1 mM IPTG at 37 ºC suggested that these conditions were unfavourable for optimum expression of proteins due to low expression levels. To overcome this problem, protein expression was conducted using different concentrations of IPTG at different temperatures. This strategy was also employed for the analytical scale expression of the $^{N\Delta17}$*Pf*ARF1-CFP recombinant protein. The His-tagged $^{N\Delta17}$*Hs*ARF1-CFP recombinant protein had a predicted molecular mass of 49.7 kDa. At all IPTG concentrations used, expression at 37 degrees for 3 hours (**Figure 8A**), 30 degrees for 6 hours (**Figure 8B**) and 25 degrees for 26 hours (**Figure 8C**) yielded dark protein bands with a molecular mass of 48 kDa in the induced soluble and insoluble fractions that were not present in the corresponding uninduced fractions and likely represents the $^{N\Delta17}$*Hs*ARF1-CFP protein. To confirm the presence of $^{N\Delta17}$*Hs*ARF1-CFP, a western blotting analysis on the samples of the analytical scale expression profile was done. The proteins resolved on a SDS-PAGE gel were transferred to a nitrocellulose membrane probed for CFP-tagged proteins using anti-GFP mouse primary antibodies and anti-mouse secondary antibodies conjugated to HRP followed with an incubation in TMB membrane peroxidase substrate. Prominent bands with a molecular mass of 50 kDa were present in the induced soluble fractions and induced insoluble fractions at most of the concentrations of IPTG used to induced protein expression. There are bands detected in the uninduced insoluble and soluble protein fractions probably due to leaky expression (**Figure 8D**). In addition, expression

at 25 degrees Celsius appeared to increase the proportion of the protein present in the soluble vs. insoluble fractions compared to expression at higher temperatures.

The His-tagged $^{N\Delta17}$*Pf*ARF1-CFP recombinant protein had a predicted molecular mass of 49.9 kDa. Analytical scale expression profiles of *E.coli* cells harbouring the pET-28a-$^{N\Delta17}$*Pf*ARF1-CFP construct conducted at 37, 30, 25 and 18 ºC for 3, 6, 16, and 18 hours respectively with IPTG concentrations ranging from 0.4 – 1 mM showed no prominent discernible bands at the expected size in the induced samples compared to the uninduced controls lacking IPTG. At 30 ºC, there was a faint protein band with a molecular mass of 46 kDa present in the induced insoluble and soluble fractions but a band at the same position seemed to be present in the uninduced soluble and insoluble fractions as well (**Figure 9C**). Due to the difficulty in detecting $^{N\Delta17}$*Pf*ARF1-CFP expression in the Coomassie stained gels, a western blot to analyse the samples of the 30°C analytical scale expression profile was done. The proteins resolved on a SDS-PAGE gel were transferred to a nitrocellulose membrane probed for CFP-tagged proteins using anti-GFP mouse primary antibodies and anti-mouse secondary antibodies conjugated to HRP followed with an incubation in TMB membrane peroxidase substrate. Prominent bands with an approximate molecular mass of 50 kDa were present in the induced soluble fractions and induced insoluble fractions at the chosen concentrations of IPTG used to induced protein expression (**Figure 9E** *indicated by arrow*). The bands were not present in the uninduced insoluble and soluble fractions.

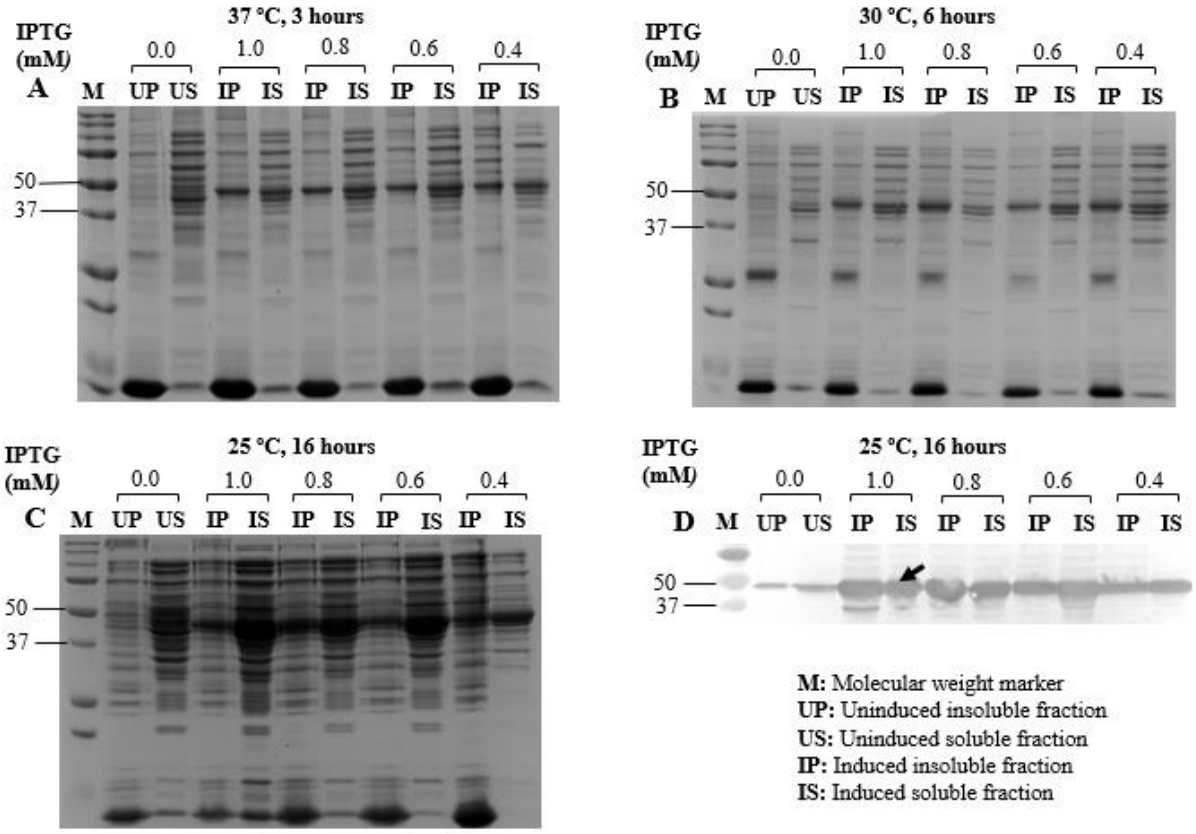

Figure 8: Analytical scale protein expression analysis of $^{N\Delta17}$*Hs*ARF1-CFP. *E. coli* (T7 Express lysY/I_q) was transformed with pET-28a-$^{N\Delta17}$*Hs*ARF1-CFP. The transformed cells were cultured at 37 °C until the logarithmic growth phase. Protein expression was induced by the addition of IPTG to final concentrations ranging from 0.4- 1.0 mM, while parallel cultures lacking IPTG served as uninduced controls. The uninduced and induced cultures were lysed and soluble and insoluble protein fractions were obtained by centrifugation. All samples were prepared in SDS sample loading buffer and resolved on a 12% SDS- PAGE gel run at 100 V for approximately 1.5 hours. For all gels: **M:** Molecular weight marker: Precision Plus protein standard (Bio-Rad #161-0373) (molecular mass shown in kDa). **Expression conducted: A:37 ºC, B: 30 ºC and C: 25 ºC. D: Western Blotting analysis of $^{N\Delta17}$*Hs*ARF1-CFP expressed at 25 °C.**

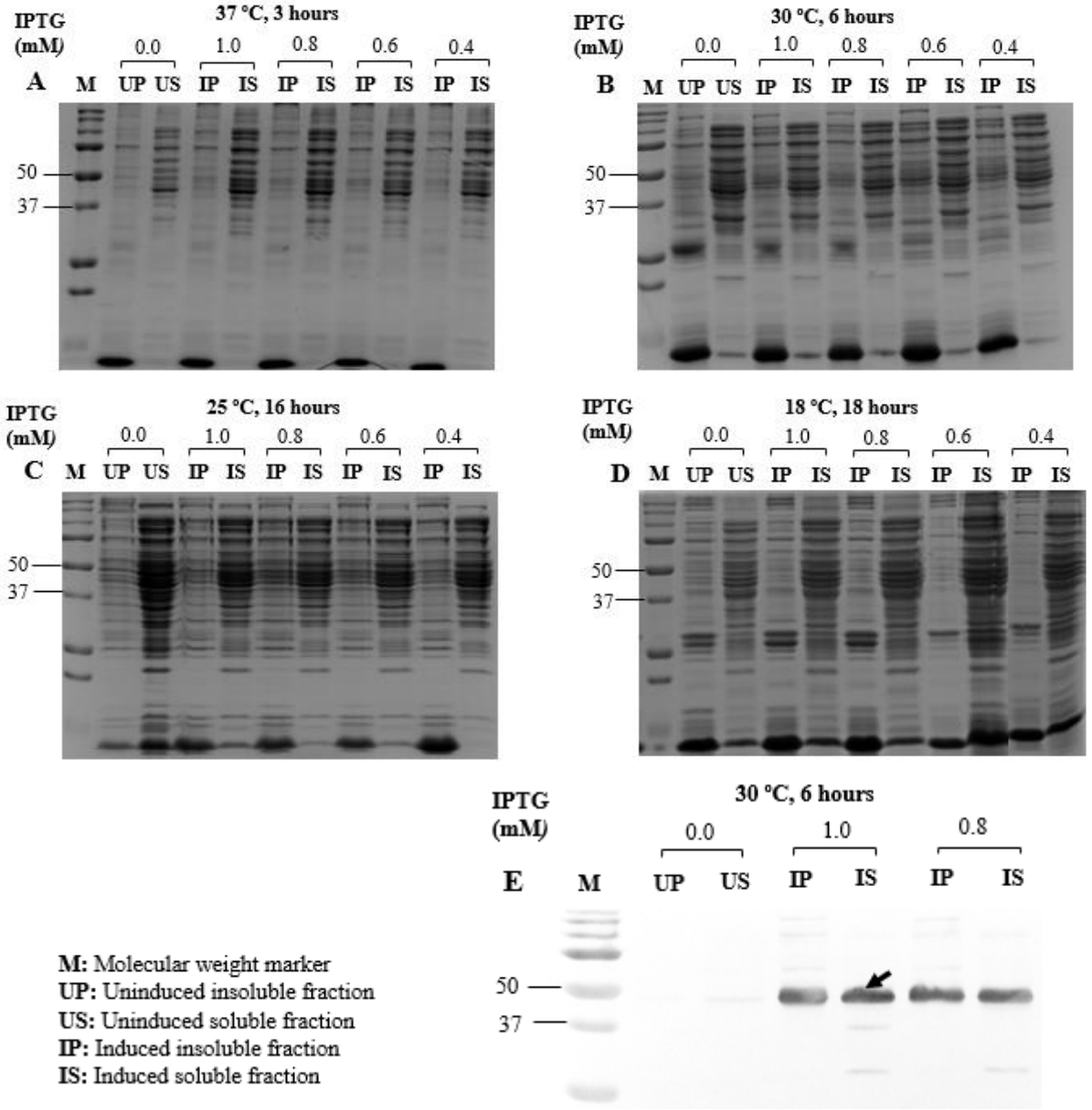

Figure 9: Analytical scale protein expression analysis of $^{N\Delta17}$*Pf*ARF1-CFP. The pET-28a-$^{N\Delta17}$*Pf*ARF1-CFP construct was transformed into competent *E. coli* (T7 Express lysY/I_q). The transformed cells were cultured at 37 °C until the logarithmic growth phase. Protein expression was induced by the addition of IPTG to final concentrations ranging from 0.4- 1.0 mM. The bacteria were lysed and soluble and insoluble protein fractions were obtained by centrifugation. All samples were prepared in SDS sample loading buffer and resolved on a 12% SDS- PAGE gel run at 100 V for approximately 1.5 hours. For all gels: **M:** Molecular weight marker: Precision Plus protein standard (Bio-Rad #161-0373) (molecular mass shown in kDa). **Expression conducted: A: 37 ºC, B: 30 ºC, C: 25 ºC and 18 ºC. E: Western Blotting analysis of $^{N\Delta17}$*Pf*ARF1-CFP expressed at 30 ºC.**

The His-tagged YPET-GGA3^{GAT} had a predicted molecular mass of 46 kDa. Analytical scale expression profiles of *E. coli* cells harbouring the pET-28a-YPET-GGA3^{GAT} construct conducted at 37°C and 30 ºC showed no prominent bands at the expected molecular mass that were not present in the uninduced samples as well. A western blot to analyse the samples of the analytical scale expression profile was done. The proteins resolved on a SDS-PAGE gel were transferred to a nitrocellulose membrane, probed for His-tagged proteins using HisDetector (HRP conjugated to nickel) and incubated in TMB membrane peroxidase substrate. The presence of multiple proteins in the induced and uninduced soluble fractions that reacted with the nickel-HRP probe complicated data interpretation. However, there was an additional band in the induced soluble fractions that appeared to be present at a higher concentration than in the corresponding uninduced sample (**Figure 10E** *indicated by arrow*). For this reason, it was decided to attempt purification of YPET-GGA3^{GAT} from larger cultures using nickel affinity chromatography. In retrospect, the anti-GFP antibody could have been used to detect the presence of YPET-GGA3^{GAT}.

In summary, analytical protein expression analysis for $^{N\Delta17}$*Hs*ARF1-CFP, $^{N\Delta17}$*Pf*ARF1-CFP and YPET-GGA3^{GAT} conducted at 25, 30 and 37 ºC for 16, 6 and 3 hours respectively at 1 mM IPTG concentration suggested that these conditions could be scaled up for preparative scale purification to obtain sufficient amounts of each recombinant protein to use to set up the human and malarial ARF1 FRET assays.

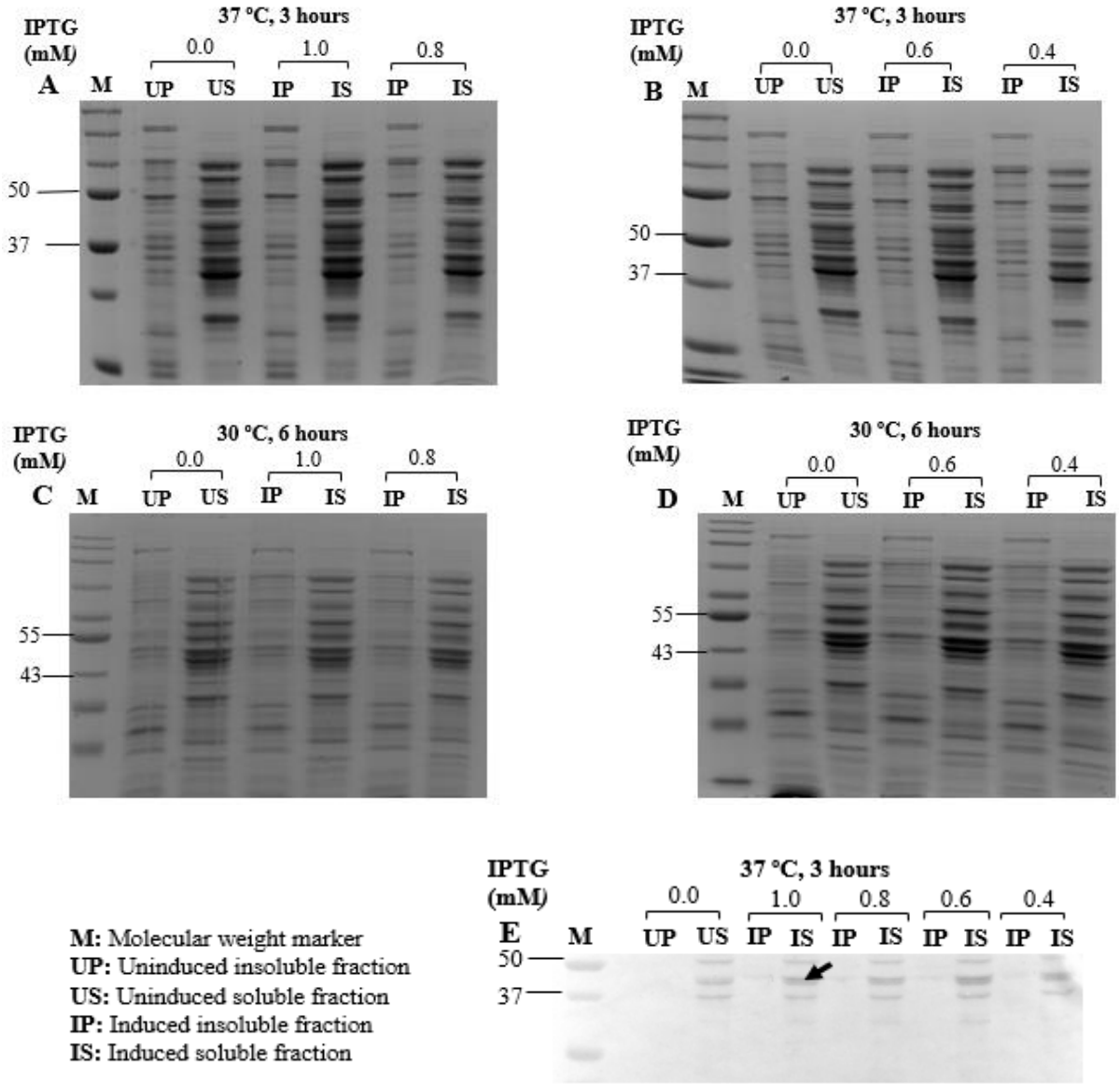

Figure 10: Analytical scale protein expression analysis of YPET-GGA3^{GAT}. *E. coli* (T7 Express lysY/I_q) cells were transformed with pET-28a-YPET-GGA3^{GAT}. The transformed cells were cultured at 37 °C until the logarithmic growth phase. Protein expression was induced by the addition of IPTG to final concentrations ranging from 0.4- 1.0 mM, while an uninduced control lacking IPTG was cultured in parallel. The bacteria were lysed and soluble and insoluble protein fractions were obtained by centrifugation. All samples were prepared in SDS sample loading buffer and resolved on a 12% SDS- PAGE gel run at 100 V for approximately 1.5 hours. For **A, B and D: M:** Molecular weight marker: Precision Plus protein standard (Bio-Rad #161-0373) (molecular mass shown in kDa). For **C and D: M:** Molecular weight marker: Blue prestained protein standard (NEB #P7718S) (molecular mass shown in kDa). **A and B: Expression analysis of YPET-GGA3^{GAT} conducted at 37 ºC. C and D: Expression analysis YPET-GGA3^{GAT} conducted at 30 ºC. D: Western Blotting analysis of YPET-GGA3^{GAT} expressed at 37 °C.**

Preparative scale heterologous production and purification of the recombinant proteins required for the ARF1 FRET assays. The main objective of this part of the project was to produce $^{N\Delta17}$*Hs*ARF1-CFP, $^{N\Delta17}$*Pf*ARF1-CFP, YPET-GGA3^{GAT} and CFP as His-tagged recombinant proteins that can be used in setting up the human and malarial ARF1 protein interaction FRET assays. $^{N\Delta17}$*Hs*ARF1-CFP, $^{N\Delta17}$*Pf*ARF1-CFP, CFP and YPET-GGA3^{GAT} were expressed at 25 ºC, 30 ºC, 37 ºC and 37 ºC for 16, 6, 3 and 3 hours respectively using a 1 mM IPTG concentration. The analytical scale conditions were adopted for preparative scale expression and purification in 250 mL, 500 mL or 1000 mL cultures. The *E. coli* from the overnight cultures was harvested, lysed and the soluble fraction was prepared. $^{N\Delta17}$*Hs*ARF1-CFP, $^{N\Delta17}$*Pf*ARF1-CFP, YPET-GGA3^{GAT} and CFP were successfully purified using Ni-NTA chromatography, desalted into assay buffer using size exclusion chromatography and protein concentration was determined using a Bradford assay (BSA standard curve with $R^2 \geq 0.99$). SDS-PAGE analysis was conducted to assess the purification profiles of the recombinant proteins and assess the purity of the final desalted eluate. The molecular masses of the purified recombinant proteins were determined by a standard curve of Log (molecular weight) versus relative migration distance of the molecular weight marker used (*results not shown*). The average protein concentrations of all the recombinant proteins are described below as some were expressed and purified on multiple occasions.

A protein product for the $^{N\Delta17}$*Hs*ARF1-CFP recombinant protein was expected at 49.7 kDa and sufficient soluble protein was purified as there is a prominent band present at 50 kDa (**Figure 11A**, Lane 7 *indicated by arrow*). In the wash steps, there was some unbound protein that was eluted as there are dark bands of protein of expected molecular mass, possibly due to oversaturation of the column (**Figure 11A**, Lanes 4-5). The banding pattern showed minimal amounts of non-specific proteins in both of the eluate and desalted fractions and a dark band was observed corresponding to high yields of recombinant protein in the eluate and desalted samples (**Figure 11A**, Lanes 6-7). A total of 3.5 mL $^{N\Delta17}$*Hs*ARF1-CFP at a concentration of 3.24 mg. mL^{-1} was purified from a 250 mL protein expression culture. A protein product for the $^{N\Delta17}$*Pf*ARF1-CFP recombinant protein was expected at 49.9 kDa and sufficient soluble protein was purified as there is a prominent band present at 47 kDa (**Figure 11B**, Lane 7 *indicated by arrow*). A similar purification profile was obtained for $^{N\Delta17}$*Pf*ARF1-CFP as compared to $^{N\Delta17}$*Hs*ARF1-CFP, except that the yield was lower than that obtained for the human protein. A total of 3.5 mL $^{N\Delta17}$*Pf*ARF1-CFP at a concentration of 1.02 mg. mL^{-1} was purified from a 500 mL protein expression culture. A protein product for the YPET-GGA3^{GAT}

recombinant protein was expected at 46 kDa and sufficient soluble protein was purified as there is a prominent band present at that position in the column eluate and desalted sample (**Figure 12C**, Lane 6-7). As expected from the analytical scale expression analysis, the yield of YPET-GGA3^{GAT} was lower than that of the ARF1 proteins. A total of 3.5 mL YPET-GGA3^{GAT} at a concentration of 0.36 mg. mL^{-1} was purified from a 1000 mL protein expression culture. The YPET-GGA3^{GAT} was poorly expressed and as a result of that, metal affinity chromatography preparations contained contaminating proteins. As a result, this amount is an overestimate, due to the presence of significant additional protein bands in the eluate and desalted protein samples (**Figure 11C**, lanes 6-7). In retrospect, the actual concentration and purity of the protein could have been estimated by SDS-PAGE analysis in which band intensities of different amounts of YPET-GGA3^{GAT} preparation could be compared with those of a pure protein preparation of known concentration (for example His-tagged $^{N\Delta17}$*Hs*ARF1-CFP).

A protein product was expected at 26.7 kDa for the His-tagged CFP protein and sufficient soluble amounts of target protein were purified as there was a prominent band present at 28 kDa in the eluate and desalted samples (**Figure 11D**, Lane 7 *indicated by arrow*), with negligible amounts of non-specific proteins. A total of 3.3 mL CFP at a concentration of 0.89 mg. mL^{-1} was purified from a 250 mL protein expression culture. All purified proteins were stored in 40 % (v/v) glycerol at -20 ºC.

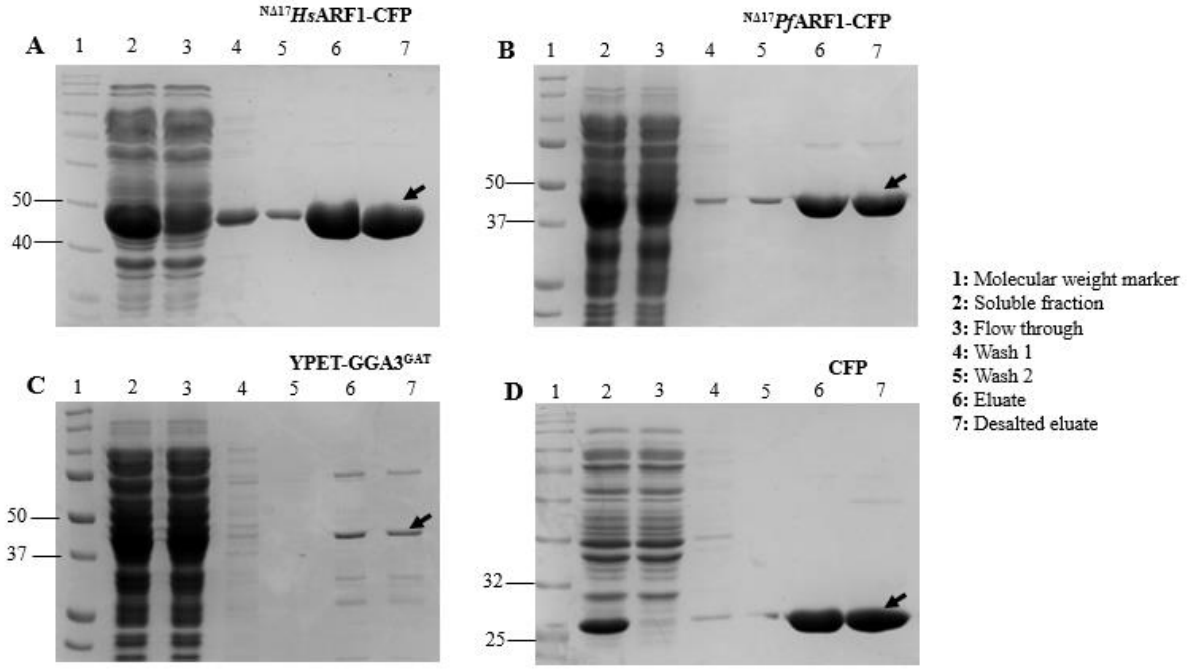

Figure 11: Preparative scale purification of $^{N\Delta17}$*Hs*ARF1-CFP, $^{N\Delta17}$*Pf*ARF1-CFP, YPET-GGA3^{GAT} and CFP by Ni-NTA affinity chromatography. All expression constructs were transformed into competent *E. coli* (T7 Express lysY/I_q cells). The transformed cells were cultured until the logarithmic growth phase and protein expression was induced by the addition of 1 mM IPTG: at 37 ºC for 4 and 3 hours for the expression of YPET-GGA3^{GAT} and CFP respectively, at 25 ºC for 16 hours for the expression of $^{N\Delta17}$*Hs*ARF1-CFP and at 30 ºC for 6 hours for the expression of $^{N\Delta17}$*Pf*ARF1-CFP. The cells were harvested by centrifugation, lysed and soluble fractions were prepared by centrifugation and filtration for purification by Ni-NTA affinity chromatography. All samples were prepared in SDS sample loading buffer and resolved on a 12% SDS-PAGE gel run at approximately 115- 120 V for approximately 1.5 hours. For **A**: Lane 1: Unstained protein standard (NEB #P7717) (molecular mass shown in kDa). For **B and C:** Lane 1: Precision Plus protein standard (Bio-Rad #161-0373) (molecular mass shown in kDa). **D:** Lane 1: Colour protein standard (NEB #P7712S) (molecular mass shown in kDa). **A: Purification profile of His-tagged $^{N\Delta17}$*Hs*ARF1-CFP. B: Purification profile of His-tagged $^{N\Delta17}$*Pf*ARF1-CFP. C: Purification profile of His-tagged YPET-GGA3^{GAT}. D: Purification profile of His-tagged CFP.**

Nucleotide binding reaction. For the sake of clarification, the active forms of the recombinant proteins will be referred to as $^{N\Delta17}$*Hs*ARF1-CFP GTP and $^{N\Delta17}$*Pf*ARF1-CFP GTP and inactive forms will be referred to as $^{N\Delta17}$*Hs*ARF1-CFP GDP and $^{N\Delta17}$*Pf*ARF1-CFP GDP. The extent to which ARF GTPases are purified as GTP or GDP bound from *E.coli* differs from one purification to the next. It was necessary to prepare sufficiently GTP loaded, active $^{N\Delta17}$*Hs*ARF1-CFP and $^{N\Delta17}$*Pf*ARF1-CFP forms for the FRET interaction assay, as well as GDP loaded inactive forms of the proteins as negative controls. Effectors of ARF GTPases (like the GAT domain of GGA3) will bind only to active ARFs (Jackson, 2018). As a starting point to develop the optimum conditions for loading the ARF proteins with GTP and GDP, a protocol developed by members of the research group - T. Swart, PhD thesis (in preparation) and F.Khan, M.Sc dissertation - was utilized. To provide context for the procedure, ARF1 nucleotide loading is typically carried out by incubating the protein with an excess of the desired nucleotide in the presence of EDTA to destabilise the binding of the existing nucleotide to ARF1 through Mg^{2+} chelation, followed by the introduction of Mg^{2+}. Compared to the GDP-bound form, binding of ARF1 to GTP causes a significant conformational change that solvent exposes a tryptophan residue (W66), thus increasing the intrinsic tryptophan fluorescence of the protein (Richardson and Fromme, 2015). For the EDTA mediated nucleotide exchange, 5 µM $^{N\Delta17}$*Hs*ARF1-CFP or $^{N\Delta17}$*Pf*ARF1-CFP was incubated in assay buffer with various concentrations of EDTA (2.5, 5, 10 and 20 mM) in the presence of 50 µM GTP or GDP at 25 ºC for 90 minutes with gentle agitation. Nucleotide exchange was assessed by measuring the end point tryptophan fluorescence signal at an excitation wavelength of 298 nm and an emission wavelength of 340 nm at the end of the 90-minute incubation. The difference in signals between $^{N\Delta17}$*Hs*ARF1-CFP GTP and $^{N\Delta17}$*Hs*ARF1-CFP GDP as well as $^{N\Delta17}$*Pf*ARF1-CFP GTP and $^{N\Delta17}$*PF*ARF1-CFP GDP were approximately two-fold at all concentrations of EDTA tested (**Figure 12A** and **12B**, respectively). These results suggested that EDTA was able to successfully promote nucleotide exchange on $^{N\Delta17}$*Hs*ARF1-CFP and $^{N\Delta17}$*Pf*ARF1-CFP at concentrations ranging from 2.5- 20 mM. A 5 mM EDTA concentration was chosen to promote nucleotide exchange on $^{N\Delta17}$*Hs*ARF1-CFP and $^{N\Delta17}$*Pf*ARF1-CFP in subsequent experiments. Taking into consideration that this assay would be employed for compound library screening purposes, it could be important to use lower concentrations to minimise the presence of additional buffer components that could affect compound binding. The next question we sought to investigate is what concentration of $MgCl_2$ stabilise the nucleotide complexes optimally. After EDTA-mediated nucleotide exchange, $MgCl_2$ is typically added to the ARF1 to stabilise its binding to the appropriate nucleotide. To confirm that the ARF1-CFP conformations are

maintained after $MgCl_2$ addition, EDTA mediated nucleotide exchange was carried out as described above using 5 mM EDTA and following the 90-minute incubation, $MgCl_2$ was added to final concentrations of 5, 10 and 20 mM followed by an additional incubation for 30 minutes at 25 ºC with gentle agitation. Maintenance of nucleotide bound complexes was assessed by measuring the end point tryptophan fluorescence. The difference in signals between $^{N\Delta17}$*Hs*ARF1-CFP GTP and $^{N\Delta17}$*Hs*ARF1-CFP GDP as well as $^{N\Delta17}$*Pf*ARF1-CFP GTP and $^{N\Delta17}$*Pf*ARF1-CFP GDP were approximately two-fold at all concentrations of magnesium chloride tested (**Figure 13A** and **13B**, respectively). A 10 mM $MgCl_2$ concentration was chosen to conduct all future experiments as a molar excess of $MgCl_2$ to EDTA concentration was desired. Finally, to confirm nucleotide loading under the conditions chosen, kinetic studies were performed. Of additional interest was whether the purified $^{N\Delta17}$*Hs*ARF1-CFP and $^{N\Delta17}$*Pf*ARF1-CFP were GTP- or GDP-bound prior to EDTA-mediated nucleotide exchange. Thus, the purified recombinant $^{N\Delta17}$*Hs*ARF1-CFP and $^{N\Delta17}$*Pf*ARF1-CFP in the absence of additional excess nucleotide were assayed kinetically as well. For 5 mM EDTA-mediated nucleotide exchange in the presence of 50 µM GTP or GDP, interval tryptophan fluorescence readings were taken every 5 minutes for a 90-minute duration (**Figure 14A** and **15A**). After addition of 10 mM $MgCl_2$, readings were taken every 2 minutes for a 30-minute duration (**Figure 14B** and **15B**). An end point reading assessing the intrinsic tryptophan fluorescence was taken after the completion of the nucleotide binding reaction. **Figure 14** and **Figure 15** for $^{N\Delta17}$*Hs*ARF1-CFP and $^{N\Delta17}$*Pf*ARF1-CFP respectively show the results of the kinetic assays which show successful nucleotide exchange by EDTA and stabilisation of nucleotide bound complexes by $MgCl_2$, indicated by the increased tryptophan fluorescence of the GTP- vs. GDP-bound forms of the two ARF1-CFP proteins. The results also suggest $^{N\Delta17}$*Hs*ARF1-CFP and $^{N\Delta17}$*Pf*ARF1-CFP were purified from *E. coli* predominantly in a GTP bound form and loading with GTP may not be necessary for use in subsequent assays. This is indicated by the similarity of the tryptophan fluorescence signals obtained between $^{N\Delta17}$*Hs*ARF1-CFP and $^{N\Delta17}$*Pf*ARF1-CFP incubated without the addition of nucleotides (the blue lines in **Figure 14** and **15**) and the corresponding GTP loading reactions. Nucleotide exchange of $^{N\Delta17}$*Hs*ARF1-CFP and $^{N\Delta17}$*Pf*ARF1-CFP was reproducible using the aforementioned methods for the remainder of this study. GTP- and GDP-loaded forms of the proteins were prepared and stored on ice prior to use in subsequent assays.

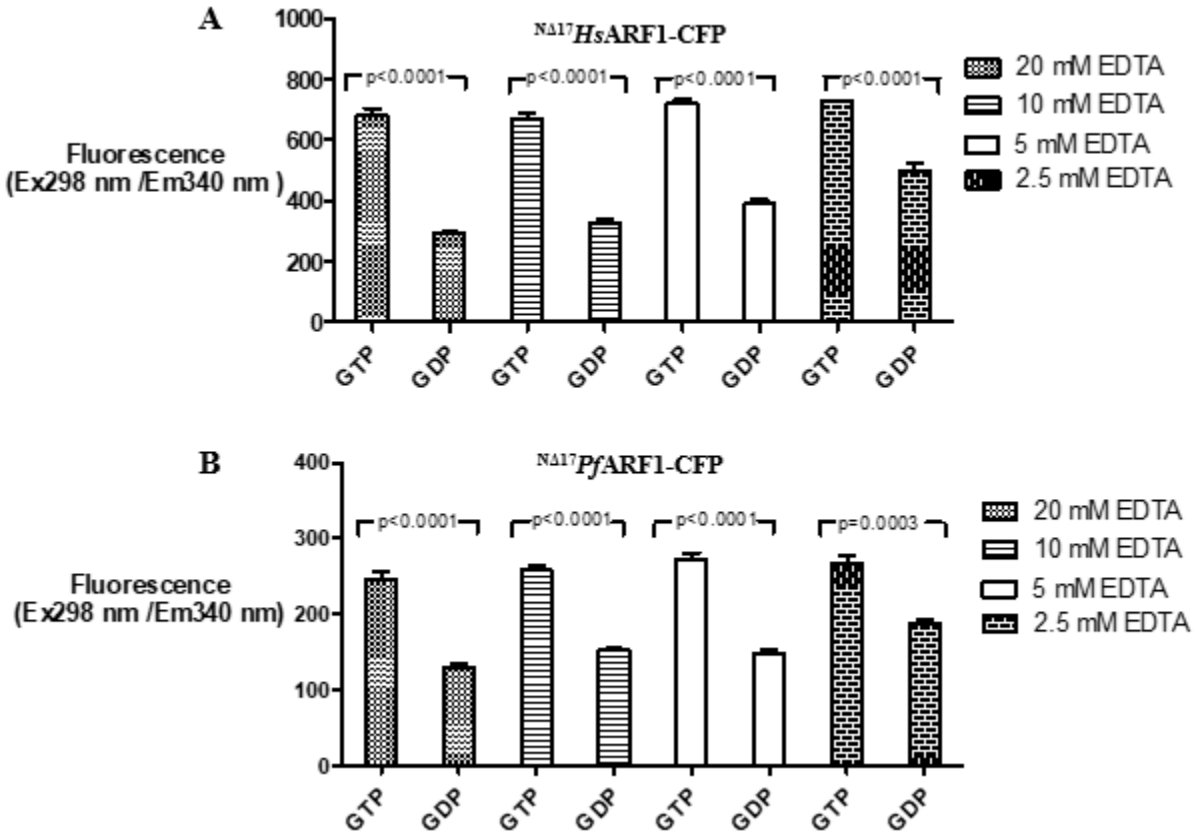

Figure 12: Detection of EDTA mediated nucleotide exchange on $^{N\Delta17}$*Hs*ARF1-CFP and $^{N\Delta17}$*Pf*ARF1-CFP by intrinsic tryptophan fluorescence. Background controls contained GTP or GDP and all reaction components without the recombinant protein. 5 µM $^{N\Delta17}$*Hs*ARF1-CFP and $^{N\Delta17}$*Pf*ARF1-CFP was incubated at 25 ºC with 50 µM GTP or GDP in the presence of 2.5, 5, 10 and 20 mM EDTA in a black 96 well plate and the tryptophan fluorescence (Ex298 nm/ Em340 nm) was measured in a plate reader as endpoint readings following at 90 minute incubation with gentle agitation. **A: Intrinsic tryptophan fluorescence of $^{N\Delta17}$*Hs*ARF1-CFP. B: Intrinsic tryptophan fluorescence of $^{N\Delta17}$*Pf*ARF1-CFP.** The intrinsic fluorescence readings were corrected by subtracting the signals measured in the corresponding background controls. The nucleotide exchange reactions were conducted in triplicate wells and all data points represent the mean fluorescence ± standard deviations. p-values calculated using a Student t-test are shown above the bars.

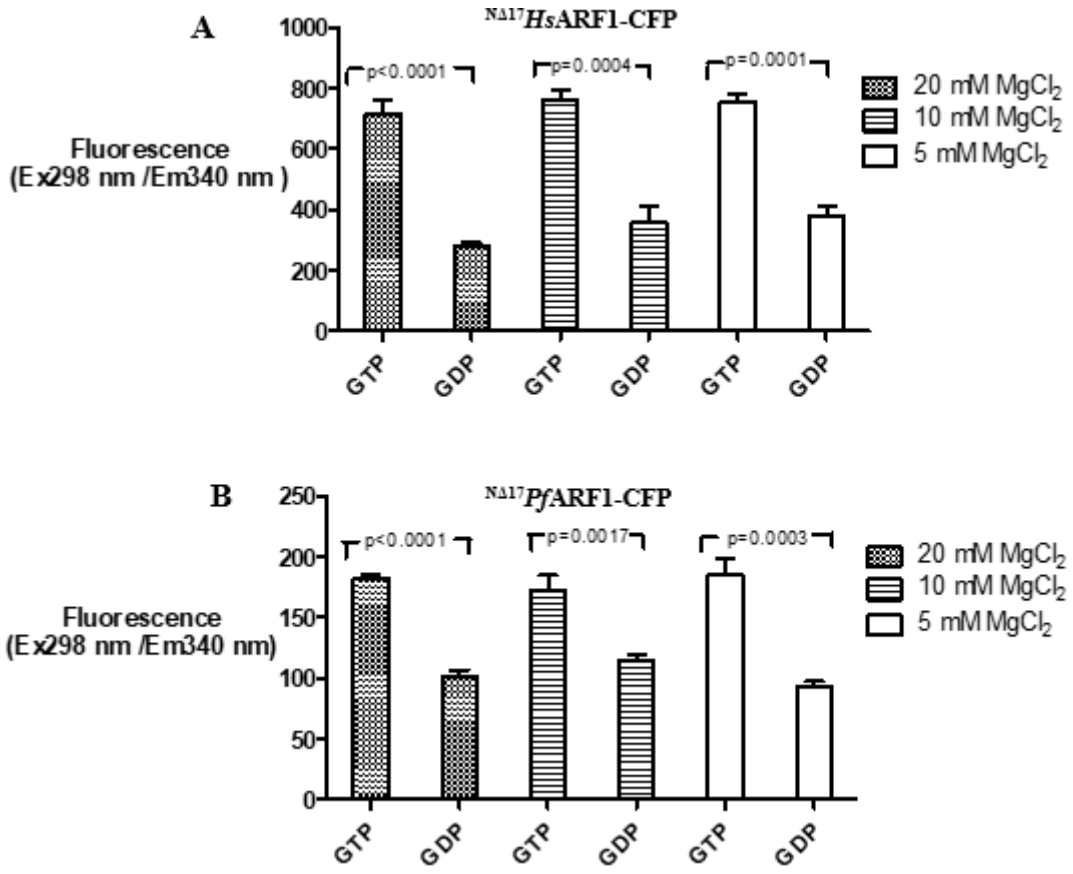

Figure 13: Detection of the stabilisation of EDTA mediated nucleotide exchange on $^{N\Delta17}$*Hs*ARF1-CFP and $^{N\Delta17}$*Pf*ARF1-CFP by magnesium chloride. 5 µM $^{N\Delta17}$*Hs*ARF1-CFP and $^{N\Delta17}$*Pf*ARF1-CFP were incubated at 25 ºC with 50 µM GTP or GDP in the presence of 5 mM EDTA in a black 96 well plate for 90 minutes with gentle agitation. Magnesium chloride was added to final concentrations of 5, 10 and 20 mM and a further incubation for 30 minutes with gentle agitation was conducted. The tryptophan fluorescence (Ex298 nm/ Em340 nm) was measured in a plate reader as endpoint readings. Background controls contained GTP or GDP and all reaction components without the recombinant protein **A: Intrinsic tryptophan fluorescence of $^{N\Delta17}$*Hs*ARF1-CFP at different concentrations of magnesium chloride. B: Intrinsic tryptophan fluorescence of $^{N\Delta17}$*Pf*ARF1-CFP at different concentrations of magnesium chloride.** The intrinsic fluorescence readings were corrected by subtracting the signals measured in the corresponding background controls. The nucleotide exchange reactions were conducted in triplicate wells and all data points represent the mean fluorescence ± standard deviations. The p-values obtained by Student t-tests are indicated above the bars.

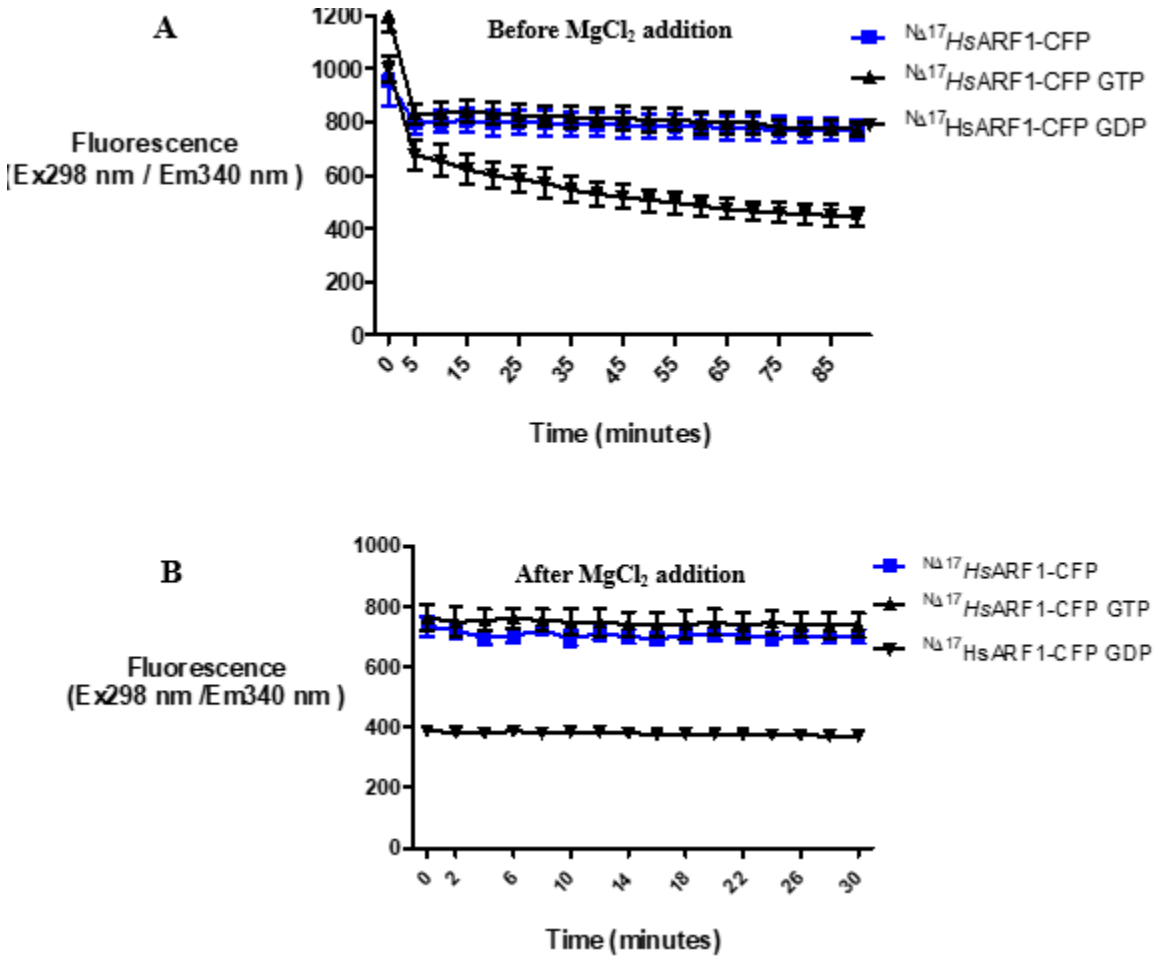

Figure 14: Optimised conditions for nucleotide exchange on $^{N\Delta17}$*Hs*ARF1-CFP. A: Intrinsic tryptophan fluorescence profile of $^{N\Delta17}$*Hs*ARF1-CFP before the addition of magnesium chloride. 5 µM $^{N\Delta17}$*Hs*ARF1-CFP was incubated at 25 ºC with 50 µM GTP or GDP in the presence of 5 mM EDTA in a black 96 well plate and the tryptophan fluorescence (Ex298 nm/ Em340 nm) was measured in a plate reader for 90 minutes at 5-minute intervals. 5 µM $^{N\Delta17}$*Hs*ARF1-CFP without the addition of GTP and GDP was also included and was incubated in assay buffer only. Background controls contained GTP or GDP and all reaction components without the recombinant protein. Readings obtained from these wells were subtracted from the $^{N\Delta17}$*Hs*ARF1-CFP GTP and $^{N\Delta17}$*Hs*ARF1-CFP GDP signals respectively. The nucleotide exchange reactions were conducted in triplicate wells and all data points represent the mean fluorescence ± standard deviations. **B: Intrinsic tryptophan fluorescence profile of $^{N\Delta17}$*Hs*ARF1-CFP after the addition of magnesium chloride.** Following the addition of 10 mM $MgCl_2$, a further incubation was conducted and the tryptophan fluorescence was measured in a plate reader for 30 minutes at 2-minute intervals.

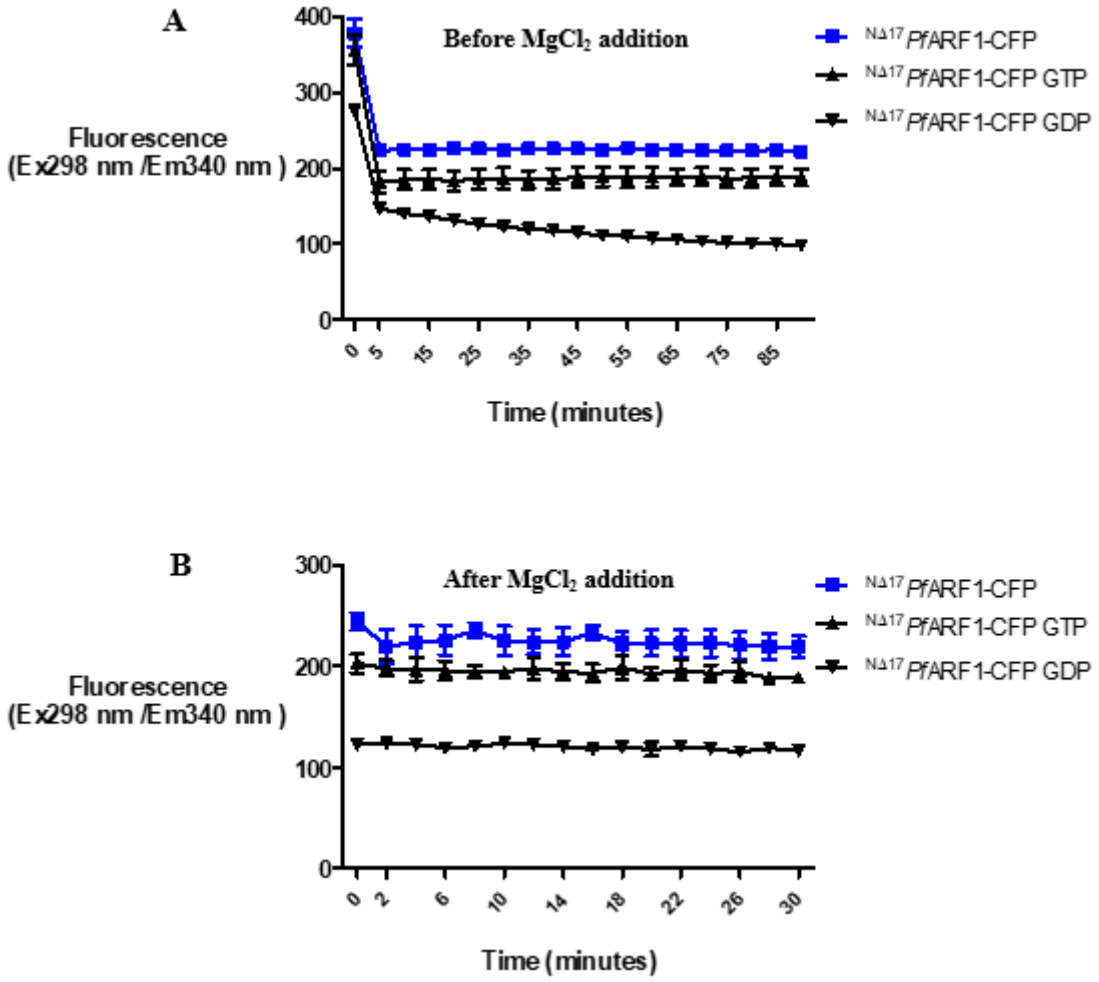

Figure 15: Optimised conditions for nucleotide exchange on $^{N\Delta17}$*Pf*ARF1-CFP. A: Intrinsic tryptophan fluorescence profile of $^{N\Delta17}$*Pf*ARF1-CFP before the addition of magnesium chloride. 5 µM $^{N\Delta17}$*Pf*ARF1-CFP was incubated at 25 ºC with 50 µM GTP or GDP in the presence of 5 mM EDTA in a black 96 well plate and the tryptophan fluorescence (Ex298 nm/ Em340 nm) was measured in a plate reader for 90 minutes at 5-minute intervals. 5 µM $^{N\Delta17}$*Pf*ARF1-CFP without the addition of GTP and GDP was also included and was incubated in assay buffer only. Background controls contained GTP or GDP and all reaction components without the recombinant protein. Readings obtained from these wells were subtracted from the $^{N\Delta17}$*Pf*ARF1-CFP GTP and $^{N\Delta17}$*Pf*ARF1-CFP GDP signals respectively. The nucleotide exchange reactions were conducted in triplicate wells and all data points represent the mean fluorescence ± standard deviations. **B: Intrinsic tryptophan fluorescence profile of $^{N\Delta17}$*Pf*ARF1-CFP after the addition of magnesium chloride.** Following the addition of 10 mM $MgCl_2$, a further incubation was conducted and the tryptophan fluorescence was measured in a plate reader for 30 minutes at 2 minute intervals.

Assessment of FRET signals produced by ARF-GGA3 interaction. Having prepared the necessary protein reagents, the next question was whether YPET-GGA3^{GAT} could distinguish between GTP- and GDP-bound ARF1 and its expected preferential binding to active ARF1 could be detected as a FRET signal. The first step that would aid in the detection of a FRET signal was to establish the analyte concentrations of the recombinant proteins that would give the same fluorescence yield. Additionally, both acceptor and donor molecules need to be present in sufficient concentration for FRET to take place. In preliminary analyses, incubations of YPET-GGA3^{GAT} with GDP loaded $^{N\Delta17}$*Hs*ARF1-CFP gave higher readings than when GTP loaded $^{N\Delta17}$*Hs*ARF1-CFP was used, which was not expected (*results not shown*). Optimising the concentration of each recombinant protein was therefore attempted to avoid the fluorescence emitted by the CFP recombinant protein from dominating the fluorescence emitted by YPET and obscuring FRET signals. A range of different concentrations were prepared through serial dilutions of the proteins and incubated in assay buffer for 10 minutes at room temperature with gentle agitation, before reading CFP (425 nm and 485 nm excitation and emission wavelengths) or YPET (485 nm and 535 nm) fluorescence in a plate reader. Concentration ranges used were 0.1- 5.0 µM for $^{N\Delta17}$*Hs*ARF1-CFP (**Figure 16A**), 1.0 – 5.0 µM for $^{N\Delta17}$*Pf*ARF1-CFP (**Figure 16B**), 0.5 – 4.5 µM for YPET-GGA3^{GAT} (**Figure 16C**) and 0.5-5.0 µM for CFP (**Figure 16D**).

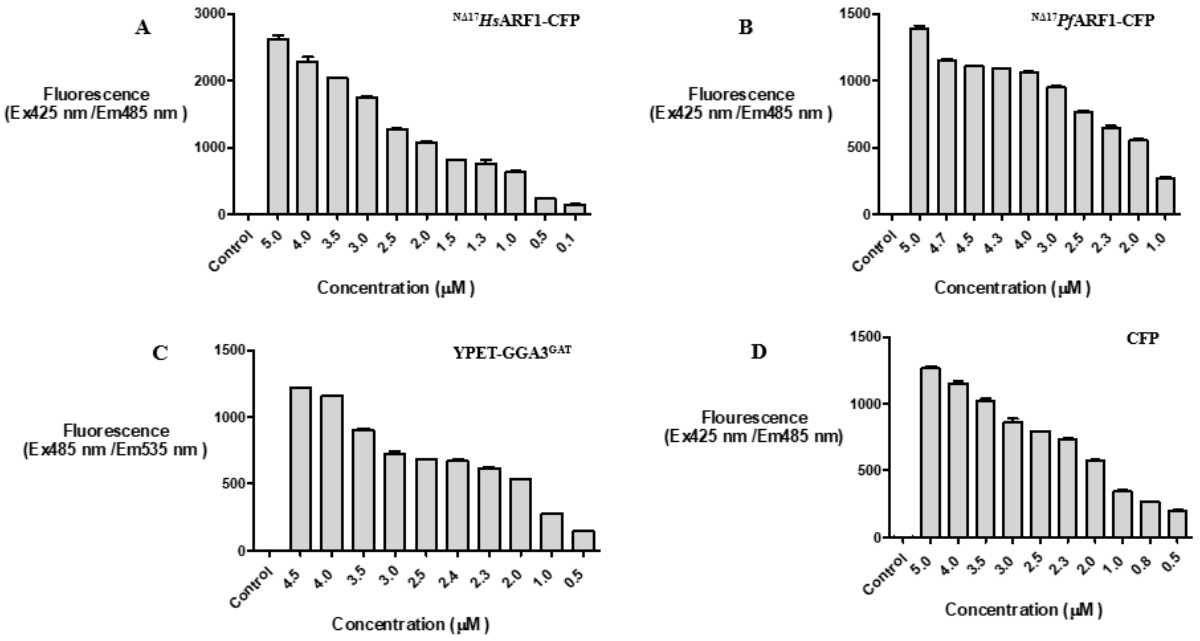

Figure 16: Fluorescence yield analysis of $^{N\Delta17}$*Hs*ARF1-CFP, $^{N\Delta17}$*Pf*ARF1-CFP, YPET-GGA3^{GAT} and CFP. Various concentrations of $^{N\Delta17}$*Hs*ARF1-CFP (**A**), $^{N\Delta17}$*Pf*ARF1-CFP (**B**), YPET-GGA3^{GAT} (**C**) and CFP (**D**) were incubated in assay buffer in a standard 96 well black plate for 10 minutes at room temperature. Following the incubation, the fluorescence was measured using excitation and emission wavelengths of 425 nm and 485 nm respectively for the CFP proteins and 485 nm and 535 nm for YPET-GGA3^{GAT}. As a background control the assay buffer was incubated alone and readings subtracted from those obtained for wells containing protein. Each bar represents the average mean ± standard deviation of fluorescence readings obtained from incubations carried out in triplicate.

Following the fluorescence yield determination for the different proteins to be used for the FRET assay, concentrations of each recombinant CFP-tagged protein that emitted the same fluorescence intensity as its intended FRET partner (YPET-GGA3^{GAT}) were chosen to conduct future FRET assays. Two pairs of concentrations were chosen, a lower concentration and a higher concentration. To confirm that these concentration pairs would yield similar CFP and YPET fluorescence yields, the proteins were incubated in separate wells at the selected concentrations and fluorescence measured. The selected concentrations for the different FRET combinations were 0.1 and 1.0 μM $^{N\Delta17}$*Hs*ARF1-CFP and 0.5 and 2.5 μM YPET-GGA3^{GAT} respectively (**Figure 17A**), 1.0 and 2.3 μM $^{N\Delta17}$*Pf*ARF1-CFP and 1.0 and 2.4 μM YPET-GGA3^{GAT} (**Figure 17B**) and 0.8 and 2.3 μM CFP and 1.0 and 3.0 μM YPET-GGA3^{GAT} (**Figure 17C**). The concentrations chosen produced similar fluorescence yields (**Figure 17A-C**). These concentrations were used in further analyses to set up the FRET reactions.

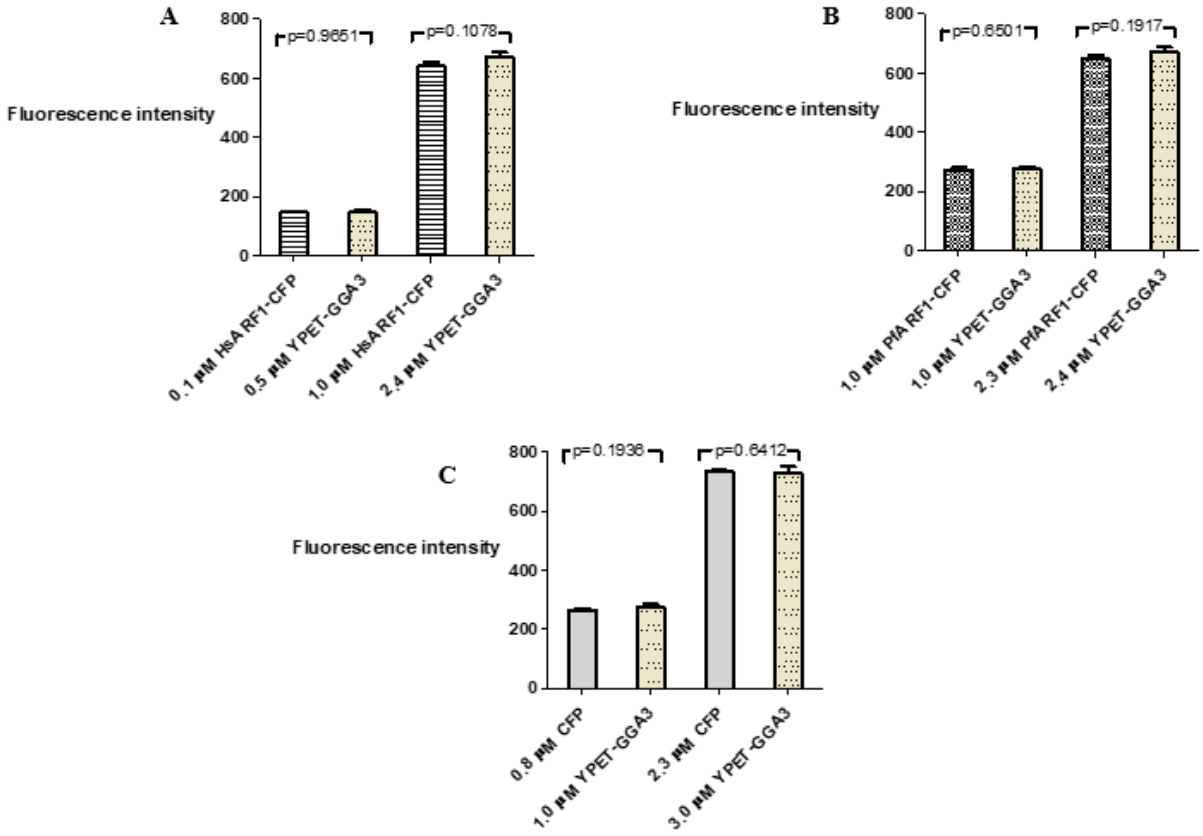

Figure 17: $^{N\Delta17}$*Hs*ARF1-CFP, $^{N\Delta17}$*Pf*ARF1-CFP, CFP and YPET-GGA3^{GAT} concentrations used for FRET analysis. Following the fluorescence yield determination, concentrations of each recombinant protein that emitted the same fluorescence intensity as its intended FRET partner were chosen: $^{N\Delta17}$*Hs*ARF1-CFP and YPET-GGA3^{GAT} (**A**), $^{N\Delta17}$*Pf*ARF1-CFP and YPET-GGA3^{GAT} (**B**) and CFP and YPET-GGA3^{GAT} (**C**) In each case, CFP fluorescence was measured at excitation and emission wavelengths of 425 nm and 485 nm respectively, and YPET at 485 nm and 535 nm. Each bar represents the average mean ± standard deviation of fluorescence readings obtained from incubations carried out in triplicate.

The final step to establish the FRET assay was to determine whether the assay was able to distinguish between active (GTP-bound) $^{N\Delta17}$*Hs*ARF1-CFP and $^{N\Delta17}$*Pf*ARF1-CFP and their inactive (GDP-bound) forms. This assay format is attractive for the high throughput screening of chemical libraries for potential novel therapeutics for cancer and malaria since it requires no additional reagents except the recombinant proteins and is homogeneous (it does not require sequential pipetting and washing steps). YPET-GGA3^{GAT} was mixed with its FRET partners $^{N\Delta17}$*Hs*ARF1-CFP GTP/GDP (**Figure 18**), $^{N\Delta17}$*Pf*ARF1-CFP GTP/GDP (**Figure 19**) or CFP (**Figure 20**) using the lower and higher concentration combinations established previously. The untagged CFP incubation was used as a negative control - no signal was expected as the construct lacks ARF1. All incubations were conducted in assay buffer for 25 minutes at room temperature in a standard black 96 well plate with gentle agitation. The fluorescence was

subsequently measured at an excitation wavelength of 425 nm and at an emission wavelength of 485 nm for the detection of CFP fluorescence and at an excitation wavelength of 425 nm and at an emission wavelength of 535 nm for the detection of FRET-induced YPET fluorescence. The FRET signal was expressed as the ratio of YPET fluorescence and CFP fluorescence, that is the fluorescence signal produced at an excitation wavelength of 425 nm and at an emission wavelength of 535 nm divided by the fluorescence signal measured at an excitation wavelength of 425 nm and emission wavelength of 485 nm. The fluorescence signals used to express the FRET signal were corrected by subtracting background signals obtained from ARF1-CFP GTP/GDP alone (in the absence of YPET-GGA3^{GAT}) from signals produced when there was YPET-GGA3^{GAT} present. When using the lower concentration combinations, there was no statistically significant difference in the FRET signals obtained with the GTP vs. GDP-bound forms of $^{N\Delta17}$*Hs*ARF1-CFP (p=0.1647, **Figure 18A**) or $^{N\Delta17}$*Pf*ARF1-CFP (p=0.2753, **Figure 19A**). At the higher concentration combinations, however, 33% difference in signals was observed in the case of $^{N\Delta17}$*Hs*ARF1-CFP (p<0.0001, **Figure 18B**) as well as a 10% difference in signals for $^{N\Delta17}$*Pf*ARF1-CFP (p=0.0008, **Figure 19B**), which suggested a FRET occurrence and that YPET-GGA3^{GAT} was preferentially binding to the active GTP-bound forms of the ARF1 proteins. As expected, the FRET signals obtained with the CFP negative control (**Figure 20**) were considerably lower than those found in the ARF1 experiments, suggesting that in the latter case FRET signals were due to the binding of GGA3^{GAT} to ARF1.

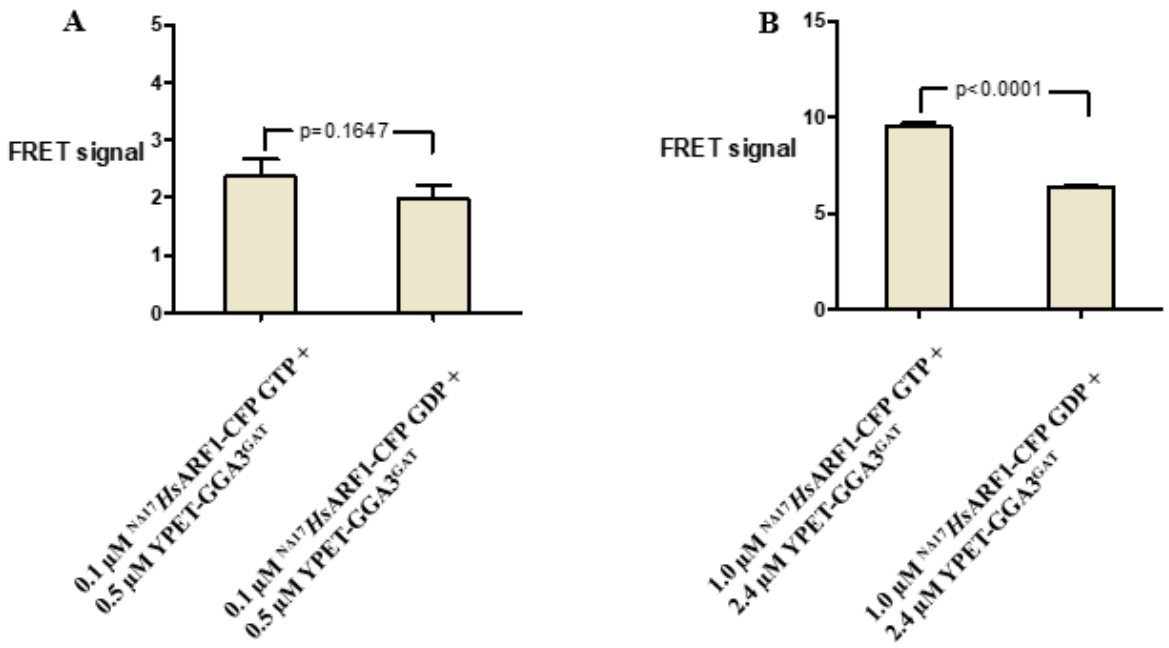

Figure 18: *Hs*ARF1 FRET assay. The background controls were $^{N\Delta17}$*Hs*ARF1-CFP GTP and $^{N\Delta17}$*Hs*ARF1-CFP GDP incubated alone in assay buffer. The background readings were subtracted from the corresponding FRET signals measured. The FRET signal is expressed as the fluorescence signal measured at Ex425 nm/ Em535 nm divided by the fluorescence signal measured at Ex425 nm/ Em485 nm. **A: FRET analysis conducted at lower concentrations of $^{N\Delta17}$*Hs*ARF1-CFP and YPET-GGA3^{GAT}**.The difference in signals measured when 0.1 µM $^{N\Delta17}$*Hs*ARF1-CFP GTP and $^{N\Delta17}$*Hs*ARF1-CFP GDP incubated with 0.5 µM YPET-GGA3^{GAT} were statistically insignificant (p=0.1647, n=3). **B: FRET analysis conducted at higher concentrations of $^{N\Delta17}$*Hs*ARF1-CFP and YPET-GGA3^{GAT}**.The difference in signals measured when 1.0 µM $^{N\Delta17}$*Hs*ARF1-CFP GTP and $^{N\Delta17}$*Hs*ARF1-CFP GDP incubated with 2.4 µM YPET-GGA3^{GAT} were statistically significant (p<0.0001, n=3). Each bar represents the average mean ± standard deviation of fluorescence readings obtained from incubations carried out in triplicate wells.

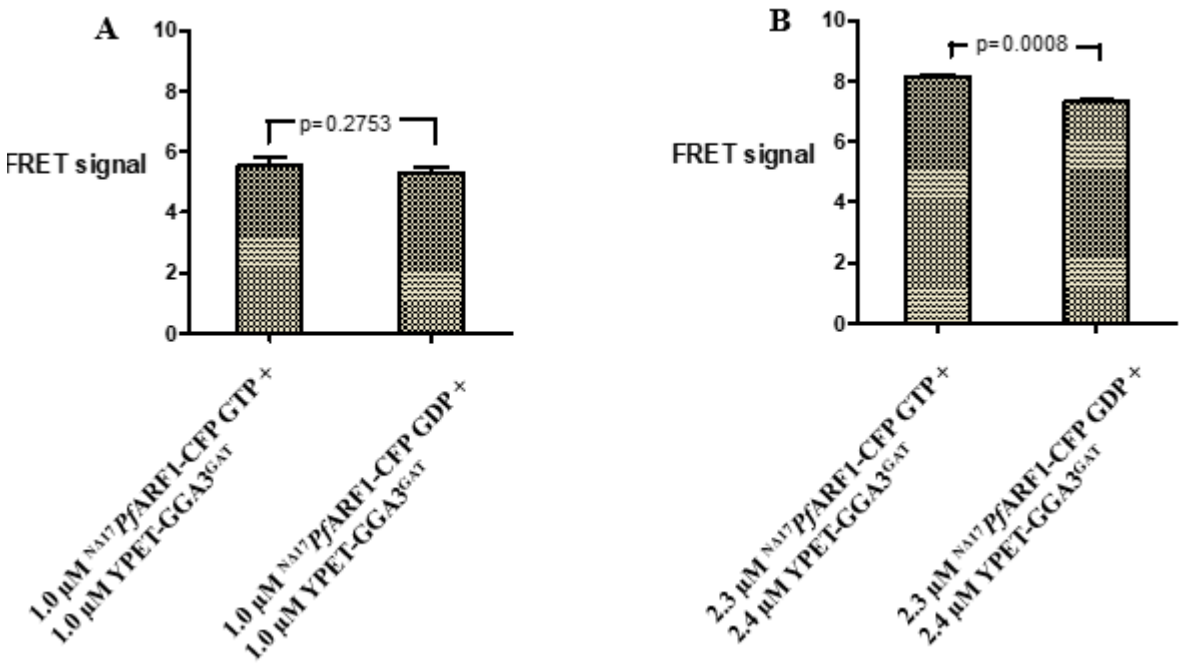

Figure 19: *Pf*ARF1 FRET assay. The background controls were $^{N\Delta17}$*Pf*ARF1-CFP GTP and $^{N\Delta17}$*Pf*ARF1-CFP GDP incubated alone in assay buffer. The background readings were subtracted from the corresponding FRET signals measured. The FRET signal is expressed as the fluorescence signal measured at Ex425nm/ Em535 nm divided by the fluorescence signal measured at Ex425 nm/ Em485 nm. **A: FRET analysis conducted at lower concentrations of $^{N\Delta17}$*Pf*ARF1-CFP and YPET-GGA3^{GAT}**. The difference in signals measured when 1.0 µM $^{N\Delta17}$*Pf*ARF1-CFP GTP and $^{N\Delta17}$*Pf*ARF1-CFP GDP incubated with 1.0 µM YPET-GGA3^{GAT} were statistically insignificant (p=0. 2753, n=3). **B: FRET analysis conducted at higher concentrations of $^{N\Delta17}$*Pf*ARF1-CFP and YPET-GGA3^{GAT}**. The difference in signals measured when 2.3 µM $^{N\Delta17}$*Pf*ARF1-CFP GTP and $^{N\Delta17}$*Pf*ARF1-CFP GDP incubated with 2.4 µM YPET-GGA3^{GAT} were statistically significant (p=0.0008, n=3). Each bar represents the average mean ± standard deviation of fluorescence readings obtained from incubations carried out in triplicate wells.

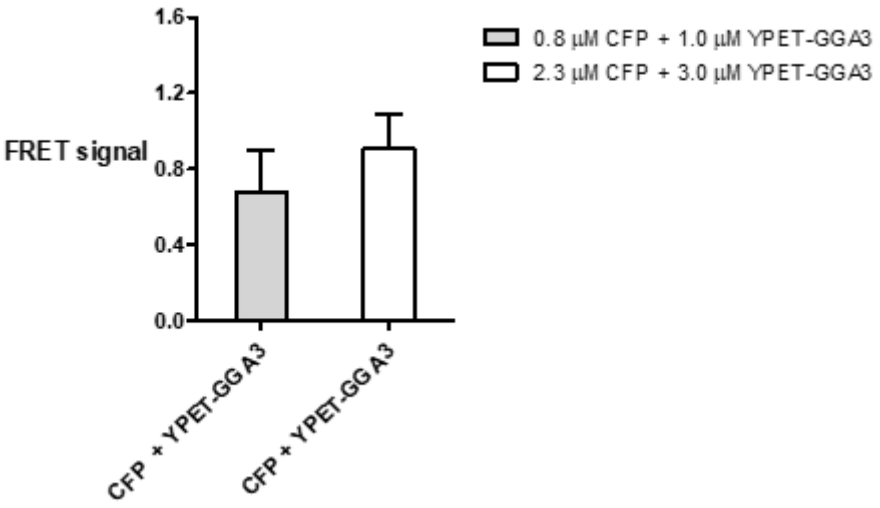

Figure 20: No FRET detected for CFP and YPET-GGA3^{GAT}. The pET-CFP construct served as the negative control reaction for all FRET experiments. The background control was the assay buffer incubated alone. The background readings were subtracted from the FRET signals measured. The FRET signal is expressed as the fluorescence signal measured at Ex425 nm/ Em535 nm divided by the fluorescence signal measured at Ex425 nm/ Em485 nm. Each bar represents the average mean ± standard deviation of fluorescence readings obtained from incubations carried out in triplicate wells.

.

3.4. DISCUSSION AND FUTURE WORK

The aim of this study was to develop a FRET assay to measure and monitor the activation status of ARF1 in real time. The overall goal would be to use this assay for high throughput screening (HTS) of chemical libraries and identify novel inhibitors of ARF effectors, ARF-GEFs and ARF-GAPs. A more interesting research question driving the motivation of this study was to answer the question of whether drug inhibitors that are aimed as an anti-cancer strategy could be used simultaneously as an anti-malarial strategy.

A key consideration in establishing a FRET signal was the stoichiometry of the donor: acceptor. Ideally, equimolar concentrations of the donor and acceptor would be desired so that the same number of molecules are present in the reaction system and to promote binding events between the donor and acceptor fluorescent proteins. Since the FRET signal is a measure of YFP fluorescence and CFP fluorescence, finding the concentrations which would yield similar fluorescence intensity signals needed to be addressed as an imbalance in fluorescence intensity would skew the results, for example excess CFP fluorescence yield would bleed through into the YFP emission channel and obscure FRET signals. If the CFP fluorescence was dominant, this would skew the results negatively as this would result in a low FRET signal which would suggest that there is no interaction between the effector- YPET-GGA3^{GAT} and active ARF GTPase. Conversely, if the YFP fluorescence was dominant, this would skew the results positively as this would result in a high FRET signal which would suggest that there is an interaction between the effector- YPET-GGA3^{GAT} and active ARF GTPase. Donor: acceptor stoichiometry that is outside the range of 10:1 to 1:10 can limit FRET detectability (Berney and Danuser, 2003; Chen *et al*., 2006). The stoichiometry of all test reactions fell within this range. Thus, the stoichiometry was addressed to eliminate one of the first hurdles in FRET detection. More limitations will be discussed shortly.

FRET assays to measure the activation status for $^{N\Delta17}$*Hs*ARF1 and $^{N\Delta17}$*Pf*ARF1 were established. The question of whether the assays were robust enough, that is if the window between the signals obtained for GDP- and GTP-bound ARF1 was sufficient to launch screening campaigns, was investigated by determining the Z-factor values. The Z-factor is a biostatical parameter routinely used to predict whether small, pilot studies of an assay are suitable for HTS assays by determining whether the background signal is sufficiently different from the assay signal. Z-factor scores above 0.5 qualitatively describe the assay as an 'excellent' assay (Zhang, 1999). Both the human and malarial FRET assays could be

qualitatively described as excellent assays for HTS owing to Z-factor values of 0.776 and 0.508 respectively (**Table 2**).

Table 2: High throughput screening potential of human and malarial ARF1 FRET assays

Assay	Z Factor
*Hs*ARF1 FRET assay	0.776
*Pf*ARF1 FRET assay	0.508

Refer to the supplementary information for calculation of Z-Factors and interpretation.

The assays seemed to be robust enough for screening and in particular the human ARF FRET assay shows greater potential then the malarial ARF1 FRET assay. Nonetheless, care should be taken in exploiting FRET assays for screening. We provide some scenarios that could lead to sub-optimal FRET signals in general and for the case observed here in our study for the malarial ARF1 FRET assay.

The quantification of FRET signals produced relatively small differences between the negative control and the test reactions as the FRET assay techniques are often plagued by background noise (spectral cross talk or bleed-through between the fluorophores) (Woehler, 2013). Background noise can arise when the acceptor molecule is excited directly with the light that has been chosen to excite the donor molecule, which refers to the spectral cross talk, or the fluorescence from the donor molecule can leak into the detection channel for the acceptor fluorescence (Piston and Kremers, 2007). If the cross-talk is high then background signals may be higher than signals from the energy transfer which makes it difficult to detect positive FRET signals. To overcome this problem, fluorophores that are spectrally separated (see section 3.1.3.4. for fluorophores with larger Stokes shifts) reduces cross-talk but reduces the overlap integral which in practice decreases the detectability of the FRET signal more than it helps eliminate the cross-talk problem (Piston and Kremers, 2007).

Sub-optimal FRET signals can be observed due to the effector protein used in this study. YPET-GGA3 and specifically the GAT domain of GGA3 was unable to fully distinguish between active, GTP loaded $^{N\Delta17}$*Hs*ARF1-CFP and $^{N\Delta17}$*Pf*ARF1-CFP and inactive, GDP loaded $^{N\Delta17}$*Hs*ARF1-CFP and $^{N\Delta17}$*Pf*ARF1-CFP. This is suggested by the fact that the FRET signals obtained with the negative control CFP were much lower than signals obtained with the GDP-bound ARF proteins. This suggests that the GGA3 is also binding, to some extent, to

GDP-ARF1. Additionally, the presence of contaminant proteins in the final YPET-GGA3^{GAT} preparation could have affected the binding with the ARF1 protein. We provide two further explanations that can lead to sub-optimal FRET signals.

Firstly, FRET signals can be reduced if the two fluorophores are not aligned (referring to orientation) or not in close proximity (referring to the distance between the fluorophores) (Sekar and Periasamy, 2003). The conformational orientations of the interacting proteins may lock them in a state that is unfavourable for the transfer of energy from one fluorophore to another. The proteins could be interacting but the fluorescent labels are not close enough for the energy transfer to take place (Piston and Kremers, 2007). Therefore, a negative result does not mean that the two proteins are not interacting or bound.

Secondly, for assays of protein-protein interactions, it is important to ensure that the fluorescent proteins interact minimally on their own. YPET has been shown to exist as a dimer or tetramer (Makwardt *et al*., 2011; Shaner *et al*., 2013) while CFP exists as a monomer (Goedhart *et al*., 2012). An *in vitro* test for aggregation can be done to investigate the quaternary structure of YPET through SDS-PAGE analysis under non-denaturing conditions. However, the detection of these complexes may be complicated as the formation of complexes depends on homodimer affinity as well as the concentration of the protein. In future, mutations that eliminate fluorescent protein dimerization should be introduced through site directed mutagenesis by replacing the hydrophobic residues by positively charged residues (Zacharias *et al*., 2002).

So far explanations for sub-optimal FRET signal have been largely attributed to looking at the factors that affect the protein interactions and how absence of the interactions can be the cause of sub-optimal FRET signals. The transfer of energy from the donor to the acceptor can also be affected by factors that affect the fluorophores and some of them will be discussed shortly.

The fluorescence quantum yield is another important consideration that has been shown to limit FRET based approaches. The fluorescence quantum yield is the number of photons emitted per number of photons absorbed of the donor and the closer this value is to 1 the better (Laverdant *et al.*, 2011; Hamilton and Sanabria, 2019). CFP has been shown to have a high quantum yield with a reported value of 0.80 (Makwardt *et al*., 2011; Goedhart *et al*., 2012). The quantum yield of YPET has been reported to be 0.77 (Shaner *et al*., 2013), which is a value that is higher than other YFP derivatives. Fluorescence quantum yields can be improved by introducing mutation on specific residues using site directed mutagenesis. For example, mutations T65S and H148G

were introduced as these two mutations increased the fluorescence quantum yield values to a value as high as 0.89 for another CFP variant (Erard *et al*., 2013).

CFP-YFP tags suffer from photo-instability. This phenomenon leads to the destruction of the fluorophore when excited as they can undergo side reactions. The loss of fluorescence over time is what is known as photobleaching. The rapidity of photobleaching is non-linear and depends on the excitation wavelength and time that the fluorophore is illuminated (Cranfill *et al*., 2016). For shorter time period measurements such as the measurements taken in this study, photobleaching may be of little concern but still may be possible. As previously mentioned (refer to section 3.1.4.2), photobleaching of the acceptor can be used as a tool for FRET detection. Future studies can employ acceptor photobleaching of YPET and measure the energy transfer by observing the change in CFP fluorescence. This method has also been reported to have its own set of limitations as there could be increased background signals, as with the case of sensitized emission, arising from photoconversion of YFPs to CFP like artifacts which can result in false positives (Malkani and Schmid, 2011). This method is also destructive and cannot be used for dynamic FRET measurements.

Two final strategies can be employed to improve FRET signals. The first strategy is to design weak helper interactions between the fluorescent proteins themselves to bring the donor and acceptor into close proximity. Grünberg *et al*. (2012) used computational methods to create electrostatic interactions between Citrine and mCherry. This approach can be applied to this study to map out electrostatic interactions that can bring the fluorescent proteins in close proximity. The second strategy would look at how to improve the interactions between the ARF GTPases and the effector protein GGA3. The VHS domain of GGA3 has been shown to help bind to ARF1 and thus a new plasmid construct with GGA3-VHS, currently available on Addgene, can be used in future studies (Collins *et al*., 2003; Ren *et al*., 2010).

To summarize findings, the activation status of ARF1 was detected based on the FRET approaches used in this study. The human ARF1 assay results suggest that the assay can be used to launch screening campaigns to find possible drug targets for cancer and malarial therapeutics if the reproducibility with different batches of proteins can be confirmed. Bill *et al* (2011) conceptualized a FRET assay that was used to screen for ARNO (a GEF) inhibitors and FRET signals produced in this study were similar to the FRET signals found in our study. The FRET signals produced for the malarial ARF1 FRET assay were sub-optimal. Possible reasons for the sub-optimal FRET signals are given above. Reasons that pertain to the ARF

GTPases and the effector GGA3 include stoichiometry and oligomerization. Possible explanations that pertain to the fluorescent proteins include photobleaching, conformational orientations and fluorescence quantum yield. Possible strategies to overcome these limitations were suggested which could be used in future studies.

Chapter 4: The development of a novel *in vitro* guanine nucleotide exchange factor assay to explore the drug target status of ARF1

4.1. INTRODUCTION

An ongoing interest in the research group is to confirm the status of ARF1 as a potential drug target for cancer and malaria. The approach being explored is chemical validation, which entails the discovery of novel ARF1 inhibitors and assessing their effects on cancer cells and malaria parasites, in this case. This requires the development of assays that can be used to screen compound libraries for inhibitors to be employed in subsequent cell-based validation experiments. While the previous chapter focused on the development of a fluorescence resonance energy transfer assay, this chapter focuses on the development of a novel plate-based immobilised protein interaction assay. The main reason for developing these assays is to find an answer to the pertinent research question, posed in the previous chapter: could an ARF1 inhibitor be used to target cancer and malaria, thus establishing ARF1 as a pleiotropic disease target?

The search for effective anti-cancer therapeutics includes: i) traditional drug discovery approaches – the search for novel synthetic and natural chemical compounds that compromise tumour cell growth, metastasis and/or viability, and ii) the development of biologicals – *inter alia* antibodies, RNAi molecules, aptamers and viral genomic constructs that specifically target cancer cells. From a traditional drug discovery point of view, an important component is the identification and validation of new drug targets, *i.e.* proteins that counteract the tumour-promoting properties of cells when their function(s) are inhibited by drug-like chemical compounds (Cragg *et al*., 2009; Bauer and Brönstrup, 2014; Prieto-Dominguez *et al*., 2019). As previously mentioned, promising putative cancer targets are ADP-ribosylation factor (ARF) GTPases. There are six isoforms of ARF GTPases in mammalian cells of which ARF1 and ARF6 are the most prevalent. While both have been proposed as potential cancer drug targets, this chapter focuses on ARF1, which is involved in the secretory pathway (Peyroche *et al*., 1999; Gu and Gruenberg *et al*., 2000; D'Souza-Schorey and Chavrier, 2006). In addition, evidence suggests that it may be involved in cell signalling pathways that are important in cancer cell proliferation, e.g. the MAP Kinase and PI-3-kinase pathways. It is highly upregulated in many cancer cell types and genetic manipulation experiments (gene silencing,

overexpression or use of dominant negative mutants) suggest it plays a key role in the establishment of cancer-promoting properties in cells ((Boulay *et al*., 2008; Boulay *et al*., 2011; Casalou *et al*., 2016; Davis *et al*., 2016). Moreover, ARF1 inhibitors inhibit cancer cell viability, proliferation and metastasis characteristics, for example cell detachment, migration and invasion, and growth of tumours in mouse models (Sausville *et al*., 1996; Ohashi *et al*., 2012; Ohashi *et al*., 2016; Prieto-Dominguez *et al*., 2019).

An additional feature of ARF1 as a potential drug target is that it is highly conserved in all eukaryotes. ARF1 inhibitors could thus be developed as therapeutics against all eukaryotic pathogens, including fungi and parasites. Moreover, there is considerable evidence that ARF1 is required for a wide range of RNA viruses to replicate in human cells, including Hepatitis C, Herpes and polio virus, suggesting that inhibitors of human ARF1 function may have antiviral properties in addition to cancer therapy (Wessels *et al*., 2006; Belov *et al*., 2007; Lanke *et al*., 2009; Bui *et al*., 2009; Hsu *et al*., 2010; Matto *et al*., 2011; Panda *et al*., 2011; Zhang *et al*., 2012).

4.1.1. Current high throughput screening methods for human ARF1

An attractive feature of ARFs is that they present multiple conceptual avenues to disrupt ARF1 function with inhibitors. Modalities for inhibiting ARF functions with drug compounds may include: i) directly binding to the ARF GTPase and inhibiting its ability to release GDP, bind to GTP or hydrolyse GTP, ii) inhibition of ARF-effector interactions, iii) inhibition of ARF-GAP interactions, iv) inhibition of ARF- GEF interactions. The search for therapeutic ARF1 inhibitors has focussed on disrupting ARF-GEF interactions since that is the mode of action of the canonical inhibitor, BFA (Zeghouf *et al*., 2005). BFA causes tumour regression in mouse models but poor bioavailability has hindered further development in preclinical trials (Sausville *et al*., 1996; Anadu *et al*., 2006; Seehafer *et al*., 2013). This has led to the development of BFA derivatives for cancer therapy and, in addition, at least 5 new chemotypes which mimic BFA have been reported, namely: LM11, AG1478, Golgicide A, LG186 and AMF-26 (Viaud *et al*., 2007; Pan *et al*., 2008; Sáenz *et al*., 2009; Boal *et al*., 2010; Ohashi *et al*., 2012). These inhibitors were discovered through cell-based screens and *in silico* docking studies by taking advantage of the available crystal structures for ARFs and ARF GEFs. To date, to increase throughput and facilitate compound screening, protein based *in vitro* protein interaction assays have been described - a FRET assay for GEF activity (Bill *et al*., 2011), a fluorescence

polarization assay for GAP activity (Sun *et al*., 2011) and a fluorescence polarisation aptamer displacement assay which is specific for the cytohesin class of ARFGEFs and was used to identify SecinH3 (Hafner *et al*., 2006). To support inhibitor discovery, a colorimetric assay was conceptualized (described below) and explored in this chapter.

4.1.2. Conceptualisation of assay formats

One of the effector proteins of ARF1 is the *trans*-Golgi network protein GGA3 (Golgi Associated, Gamma Adaptin Ear containing, ARF Binding Protein 3). In particular, the GAT (GGA and Tom1) domain of GGA3 is known to bind ARF1 and ARF6 but only if the ARF is in its GTP-bound (active) form. This feature has been widely used as an experimental tool to detect active ARF1 (GTP-bound) vs. inactive ARF1 (GDP-bound) in cells using pull-down (co-precipitation) assays that employ the GGA3 GAT domain immobilized on beads (Puertollano *et al*., 2001; Collins *et al*., 2003; Hirsch *et al*., 2003; Shiba *et al*., 2004; Cohen and Donaldson, 2010). To determine if the selective binding of GST-GGA3^{GAT} to ARF1 GTP can be further exploited to determine the activation status of purified recombinant ARF1 proteins (human and malarial) in a microtiter plate format, we conceptualised an assay format (**Figure 21**) in which ARF1 proteins, expressed and purified as histidine tagged truncated forms (truncation of the first 17 amino acids of the N-terminal alpha helix is routinely practiced to prepare soluble forms of ARF1 proteins), are immobilized on nickel- NTA coated 96-well plates, followed by incubation with GST-GGA3^{GAT}. The amount GST-GGA3^{GAT} immobilized (and thus indirectly the amount of active ARF) can be determined by using a colorimetric GST substrate solution containing 1-chloro-2,4-dinitrobenzene (CDNB) and reduced L-glutathione (GSH). The dinitrophenol thioester (GS-DNB) conjugation product produced by active GST can be measured at an absorbance wavelength of 340 nm (Habig *et al*., 1974; Mannervik *et al*., 1988; Wilce and Parker, 1994). Once the immobilisation assays are developed then the assay can be adopted to follow the activation of ARF1 by ARF GEFs. The catalytic Sec7 domains of three GEFs were used in this study: two large ARF GEFs *Pf*ARFGEF^{Sec7} and BIG1^{Sec7}, which are BFA sensitive, and one small GEF: ARNO^{Sec7}, which is BFA insensitive. The sequence alignments of ARNO, which is BFA insensitive, and BFA sensitive BIG1 are shown in **Figure S41 and S42** respectively. The N-terminals were aligned to show the conserved catalytic glutamic acid (*highlighted red*) required for GEF activity. The C-terminal alignments show the residues that render BIG1 BFA sensitive which are not present in the ARNO sequence

(*residues shown in red text*). The C-terminal sequence alignments of BIG1 and *Pf*ARFGEF are shown in **Figure S42**. This alignment was done to show that the residues required for BFA sensitivity (*highlighted in green*) are present on the *Pf*ARFGEF, despite its unusual tertiary structure.

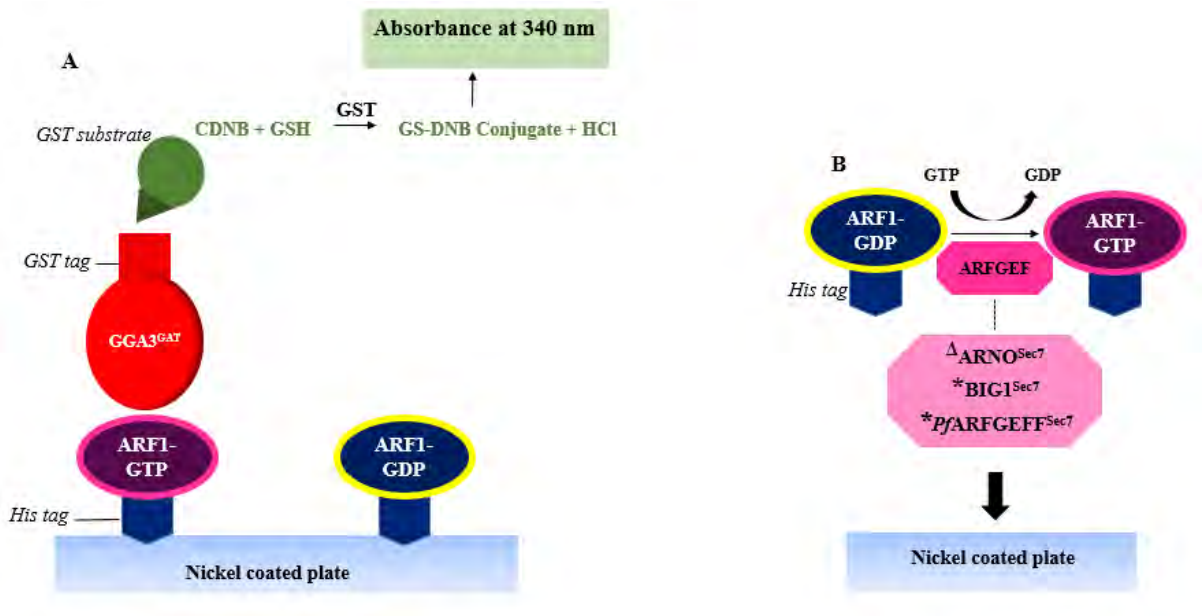

Figure 21: Ni-NTA immobilised ARF1 interaction assay principle. A: Schematic of NI-NTA immobilised ARF1 interaction assay. Active ARF1 (*dark purple*) and inactive ARF1 (*dark blue*), expressed as His-tagged recombinant proteins and nucleotide loaded by EDTA-mediated nucleotide exchange, are immobilized on a nickel-NTA pre-blocked plate. The effector protein, the GAT domain of GGA3 (*orange*), which binds active ARF GTPases, is expressed as a recombinant, GST-tagged protein. Following the immobilisation of ARF GTPases on Ni-NTA plates, there is a further incubation with GST-GGA3^{GAT}, reaction mixtures are aspirated and wells washed to reduce nonspecific binding and to remove any unbound proteins. The plate is incubated with a GST substrate solution (*light green*) containing CDNB and GSH and the conjugation product GS-DNB is measured at an absorbance wavelength of 340 nm. Since GST-GGA3^{GAT} selectively binds to active (GTP-bound) ARFs, the signals measured are indicative of the levels of active ARF1 immobilised on the plate. **B: Schematic principle of the activation of ARF1 by ARF GEFs.** GDP-preloaded inactive ARF1 is incubated with GTP in the presence of an ARF GEF (*light pink octagon: ARF GEFs used*) in round bottom plates. The ARF GEF catalyses the exchange of GDP for GTP, thus the transition of ARF1 from an inactive to an active form. These reactions are then transferred to a Ni-NTA plate and Ni-NTA ARF1 immobilised assay is conducted to detect the amount of active ARF1 in the reaction mix. *BFA sensitive GEF. $^{\Delta}$BFA insensitive GEF.

4.2. AIMS AND OBJECTIVES

Aim of the study: From a drug discovery point of view, the main aim is to identify compounds that disrupt the ARF GEF-mediated activation of ARF1, while inhibition of ARF GAP-mediated ARF deactivation may also be a source of potential therapeutics (T. Swart, PhD thesis in preparation). A small number of compounds have been identified that inhibit the former, *i.e.* ARF GEF mediated ARF1 activation, and includes BFA and AMF-26, both of which have been shown to inhibit tumour growth in mouse models. The main question addressed in this chapter was whether the activation of ARF1 by the catalytic Sec7 domains of three GEFs (human ARNO, human BIG1 and the putative *P. falciparum* ARFGEF) can be detected using the assay format described above. If successful, the assay could be exploited to screen compound libraries for inhibitors of GEF-mediated ARF1 activation.

Specific aims/ objectives and experimental approaches:

1. Express and purify the recombinant proteins as His-tagged or GST-tagged proteins in soluble and pure forms. The analytical scale conditions for optimal expression were scaled up for the preparative scale purification of recombinant proteins.
2. Prepare GTP- and GDP-loaded human and malaria ARF1 using EDTA-mediated nucleotide exchange for use in subsequent assays.
3. Determine whether GST-GGA3^{GAT} can be used to selectively detect activated ARF1 immobilised on nickel-coated microtiter plates.
4. Determine if the Ni-NTA immobilised ARF1 interaction assay can be further exploited to detect the activation of ARF1 by the Sec7 domains of the three ARF GEFs chosen for this study.

4.3. RESULTS

Preparation of DNA constructs to be used in the development of ARF1 GEF assays. Six recombinant proteins were required for this study: $^{N\Delta17}$*Hs*ARF1 and $^{N\Delta17}$*Pf*ARF1 (His-tagged human and malaria ARF1 truncated at the N-terminus), GST-GGA3^{GAT} (the GAT domain of human GGA3 fused at the N-terminus with GST) and ARNO^{Sec7}, BIG1^{Sec7} and *Pf*ARFGEF^{Sec7} (the Sec7 domains of the three GEFs selected for this study). The pET-28a-$^{N\Delta17}$*Hs*ARF1 and pET-28a-$^{N\Delta17}$*Pf*ARF1 N terminally truncated protein expression constructs were prepared and donated by T. Swart (PhD thesis in preparation). The pGEX-4T-2/hGGA3^{GAT} was obtained from Addgene. The pET-28a-ARNO^{Sec7}, pET-28a-BIG1^{Sec7} and pET-28a-*Pf*ARFGEF^{Sec7} plasmid constructs were custom prepared by Genscript (Hong Kong), codon optimised for bacterial expression. The latter constructs were obtained as lyophilized powders, resuspended in water, used to transform XL-10 Gold *E. coli* competent cells and colonies cultured overnight. Overnight cultures of the ARF1 and GST-GGA3^{GAT} constructs in XL-10 Gold *E. coli* were prepared from existing glycerol stocks. The plasmids were purified using alkaline lysis miniprep from the overnight cultures. Restriction digestions to confirm the constructs were conducted and digestion products were analysed using agarose gel electrophoresis. Theoretically, digestions of pET-28a-$^{N\Delta17}$*Hs*ARF1 and pET-28a-$^{N\Delta17}$*Pf*ARF1 constructs by *Nhe*I and *Xho*I should result in two linearized bands which represent the pET-28a vector (5369 bp) and $^{N\Delta17}$*Hs*ARF1 or $^{N\Delta17}$*Pf*ARF1 (500 bp) coding sequences. Two digestion products with sizes of 5400 bp and 500 bp which corresponded with the digestion pattern predicted were observed (**Figure 22A**, Lane 2 for pET-28a-$^{N\Delta17}$*Hs*ARF1 and **Figure 22B,** Lane 2 for pET-28a-$^{N\Delta17}$*Pf*ARF1). The pGEX-4T-2/hGGA3^{GAT} construct was digested with BamHI and *Xho*I. which should have yielded two digestion products representing pGEX-4T-2 (5150 bp) and hGGA3^{GAT} (355 bp) coding sequences. The observed banding pattern showed two digestion products of 5000 bp and 350 bp corresponding with the expected banding pattern (**Figure 22C,** Lane 2).

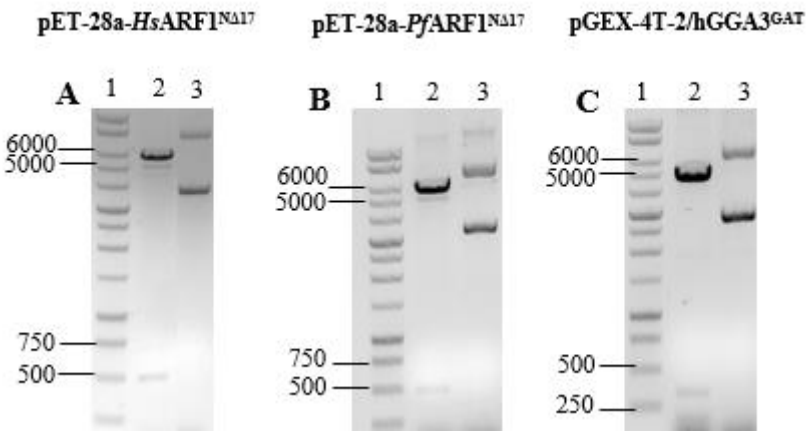

Figure 22: Diagnostic restriction digestion analysis of pET-28a-$^{N\Delta17}$*Hs*ARF1, pET-28a-$^{N\Delta17}$*Pf*ARF1 and pGEX-4T-2/hGGA3^{GAT} constructs. All the restriction digestion products were run on a 0.8 % (w/v) agarose gel at 95 V for approximately 75 minutes. The DNA bands were stained with ethidium bromide, visualized under UV light and photographed using a ChemiDoc XRS+ gel documentation system (Bio-Rad). For all gels: Lane 1: Promega 1 kbp DNA ladder (molecular weights are shown in bp). **A: pET-28a-$^{N\Delta17}$*Hs*ARF1.** Lane 2: pET-28a-$^{N\Delta17}$*Hs*ARF1 construct double digested with BamHI and *Nhe*I and Lane 3: Undigested pET-28a-$^{N\Delta17}$*Hs*ARF1 construct. **B:pET-28a-$^{N\Delta17}$*Pf*ARF1.** Lane 2: pET-28a-$^{N\Delta17}$*Pf*ARF1 construct double digested with BamHI and *Nhe*I and Lane 3: Undigested pET-28a-$^{N\Delta17}$*Pf*ARF1 construct. **C:pGEX-4T-2/hGGA3^{GAT}.** Lane 2: pGEX-4T-2/hGGA3^{GAT} construct double digested with BamHI and *Xho*I and Lane 3: Undigested pGEX-4T-2/hGGA3^{GAT} construct.

The pET-28a-ARNO^{Sec7} construct was previously analysed by a digestion with *Nhe*I and *Xho*I (A. Ntlantsana, BSc (Hons) report). In principle, the diagnostic restriction should have yielded two linearized bands representing the pET-28a vector (5369 bp) and ARNO^{Sec7} (624 bp) coding sequences. Two linearized bands of approximately 5400 bp and 600 bp were observed (**Figure S38** *see supplementary information*). The pET-28a-BIG1^{Sec7} and pET-28a-*Pf*ARFGEF^{Sec7} constructs digested with *Nhe*I and *Xho*I should yield the pET-28a plasmid backbone (5369 bp) and the coding sequence inserts (636 bp and 1629 bp for the BIG1 and *Pf*ARFGEF Sec7 domains, respectively). The respective diagnostic digests conformed to the expected results (**Figure 23A and B**, Lane 2).

In summary, the results suggested that plasmid constructs were successfully prepared for bacterial protein expression in *E.coli* cells.

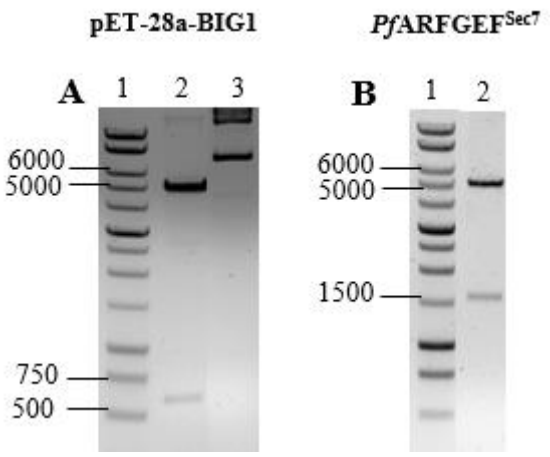

Figure 23: Diagnostic restriction digestion analysis of pET-28a-BIG1^{Sec7}, pET-28a-*Pf*ARFGEF^{Sec7} constructs. All the restriction digestion products were run on a 0.8 % (w/v) agarose gel at 95 V for approximately 75 minutes. The DNA bands were stained with ethidium bromide, visualized under UV light and photographed using a ChemiDoc XRS+ gel documentation system (Bio-Rad). For all gels: Lane 1: Promega 1 kbp DNA ladder (molecular weights are shown in bp). **A: pET-28a-BIG1^{Sec7} construct.** Lane 2: pET-28a- BIG1^{Sec7} construct double digested with *Nhe*I and *Xho*I and Lane 3: Uncut pET-28a-BIG1^{Sec7} construct. **B: pET-28a-*Pf*ARFGEF^{Sec7} construct.** Lane 2: pET-28a-*Pf*ARFGEF^{Sec7} construct double digested with *Nhe*I and *Xho*I.

Analytical scale expression of the recombinant proteins used in the GEF assays for ARF1. The main objective of this part of this work was to establish the conditions to express soluble proteins required for the ARF1 GEF assay. The expression constructs, previously used to transform XL-10 Gold competent *E. coli* cells for storage purposes and prepared by alkaline lysis miniprep, were transformed into T7 Express lysY/I_q competent *E. coli* cells and cells cultured overnight at 37 ºC. The analytical scale expression cultures were prepared by inoculating (1 in 20 inoculum) 8 mL Luria broth containing kanamycin with the overnight starter culture. Once the bacterial expression cultures had achieved a bacterial density with an OD_{600} reading of 0.5-0.9, protein expression was induced by the addition of IPTG to final concentrations between 0.4- 1 mM and at 18, 25, 30 and 37 ºC for 18, 16, 6 and 3 hours to optimize protein expression conditions. Soluble and insoluble bacterial fractions were prepared and analysed by SDS-PAGE. The molecular weights of the recombinant proteins were determined by preparing a standard curve of log molecular weight versus migration distance of the molecular weight marker used (*results not shown*). The His-tagged $^{N\Delta17}$HsARF1 recombinant protein had a predicted molecular mass of 23 kDa. The protein was concluded to be soluble as dark protein bands of 19 kDa were present in the induced soluble fractions in the analytical scale expression profiles of *E.coli* cells harbouring the pET-28a- $^{N\Delta17}$*Hs*ARF1 construct (**Figure 24A** *indicated by arrow*). The protein band was not present in the uninduced

insoluble and soluble fractions. Western blotting analysis was conducted to confirm the presence of $^{N\Delta17}$*Hs*ARF1 in the soluble fractions using the analytical scale expression profile samples. The proteins resolved on a SDS-PAGE gel were transferred to a nitrocellulose membrane probed for His-tagged proteins with nickel-HRP detector followed with incubation in TMB membrane peroxidase substrate. A band with a molecular mass of 20 kDa was present in the induced soluble fractions (**Figure 24C** *indicated by arrow*). No bands were present in the uninduced insoluble and soluble fractions. The His-tagged $^{N\Delta17}$*Pf*ARF1 recombinant protein had a predicted molecular weight of 21.1 kDa. Analytical scale expression profiles of *E.coli* cells harbouring the pET-28a- $^{N\Delta17}$*Pf*ARF1 construct showed no prominent obvious bands at the expected molecular weight (**Figure 25**). A western blot to analyse the samples of the analytical scale expression profile was done. The proteins resolved on a SDS-PAGE gel were transferred to a nitrocellulose membrane probed for ARF1 proteins using anti-ARF1 mouse primary antibodies and anti-mouse secondary antibodies conjugated to HRP followed with an incubation in TMB membrane peroxidase substrate. Prominent bands with a molecular mass of 18 kDa were present in the induced soluble fractions and induced insoluble fractions at the chosen concentrations of IPTG used to induced protein expression (**Figure 25C** *indicated by arrow*). The bands were not present in the uninduced insoluble and soluble fractions.

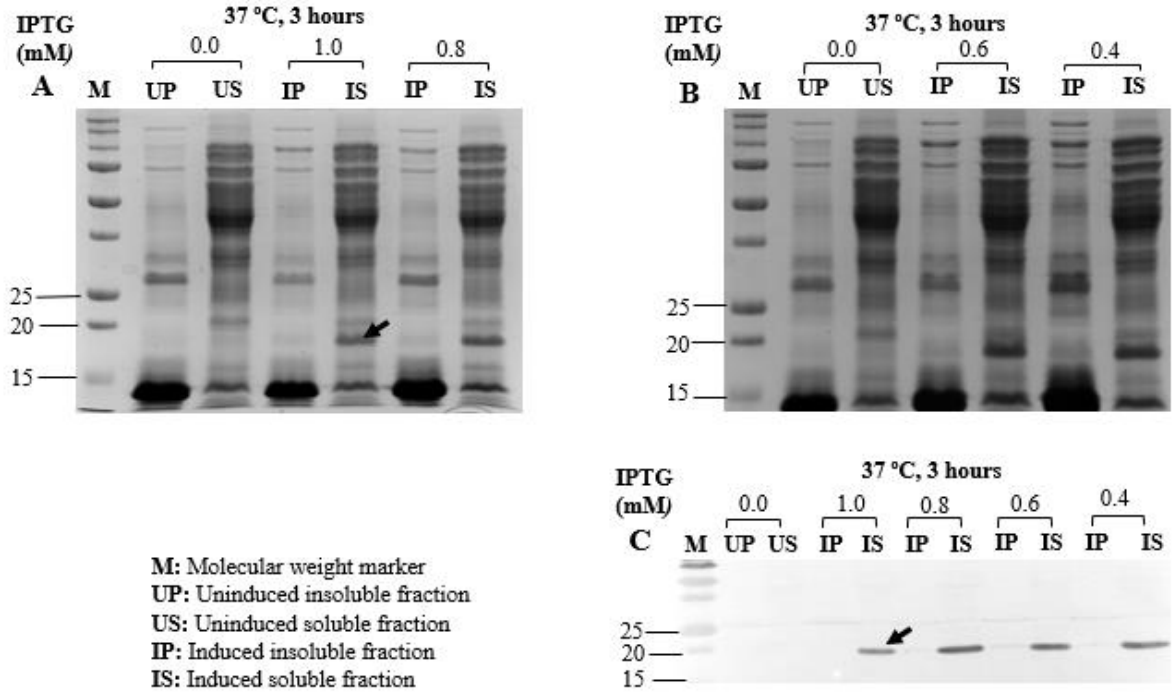

Figure 24: Analytical scale protein expression analysis of $^{N\Delta17}$*Hs*ARF1. *E. coli* (T7 Express lysY/I_q) was transformed with pET-28a-$^{N\Delta17}$*Hs*ARF1. The transformed cells were cultured at 37 °C until the logarithmic growth phase. Protein expression was induced by the addition of IPTG to final concentrations ranging from 0.4- 1.0 mM, while parallel cultures lacking IPTG served as uninduced controls. The uninduced and induced cultures were lysed and soluble and insoluble protein fractions were obtained by centrifugation. All samples were prepared in SDS sample loading buffer and resolved on a 15% SDS- PAGE gel run at 115 V for approximately 1.5 hours. For all gels: **M:** Molecular weight marker: Precision Plus protein standard (Bio-Rad #161-0373) (molecular weights are shown in kDa) **A and B: Expression conducted at 37 ºC**. **C: Western Blotting analysis of $^{N\Delta17}$*Hs*ARF1 expressed at 37 °C.**

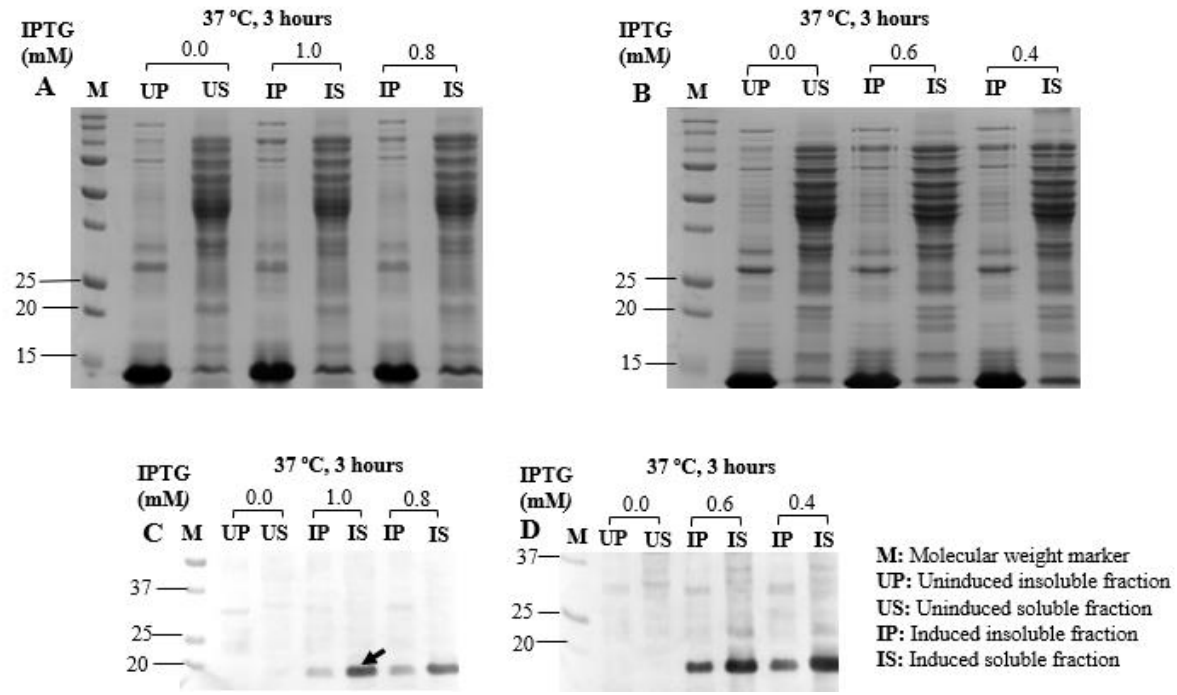

Figure 25: Analytical scale protein expression analysis of $^{N\Delta17}$*Pf*ARF1. *E. coli* (T7 Express lysY/I_q) was transformed with pET-28a-$^{N\Delta17}$*Pf*ARF1. The transformed cells were cultured at 37 °C until the logarithmic growth phase. Protein expression was induced by the addition of IPTG to final concentrations ranging from 0.4- 1.0 mM, while parallel cultures lacking IPTG served as uninduced controls. The uninduced and induced cultures were lysed and soluble and insoluble protein fractions were obtained by centrifugation. All samples were prepared in SDS sample loading buffer and resolved on a 15% SDS- PAGE gel run at 115 V for approximately 1.5 hours. For all gels: **M:** Molecular weight marker: Precision Plus protein standard (Bio-Rad #161-0373) (molecular weights are shown in kDa). **A and B: Expression of conducted at 37 ºC. C and D: Western Blotting analysis of $^{N\Delta17}$*Pf*ARF1 expressed at 37 °C.**

The His-tagged BIG1^{Sec7} recombinant protein had a predicted molecular mass of 26.1 kDa. The protein was concluded to be soluble as overexpressed bands with a molecular mass of 24.8 kDa were present in the induced soluble fractions in the analytical scale expression profiles of *E. coli* cells harbouring the pET-28a-BIG1^{Sec7} construct (**Figure 26A** *indicated by arrow*). The protein band was not present in the uninduced insoluble and soluble fractions. The analytical scale expression analysis for GST-tagged GGA3^{GAT} (**Figure S39** *see supplementary information*) was previously conducted by T.Swart (PhD thesis) while the analytical scale expression analysis for His-tagged ARNO^{Sec7} (**Figure S40** *see supplementary information*) was conducted by A. Ntlantsana in a previous study (B.Sc Honours report). The analytical scale conditions for GST-tagged GGA3^{GAT} and His-tagged ARNO^{Sec7} previously determined were scaled up for preparative scale purification.

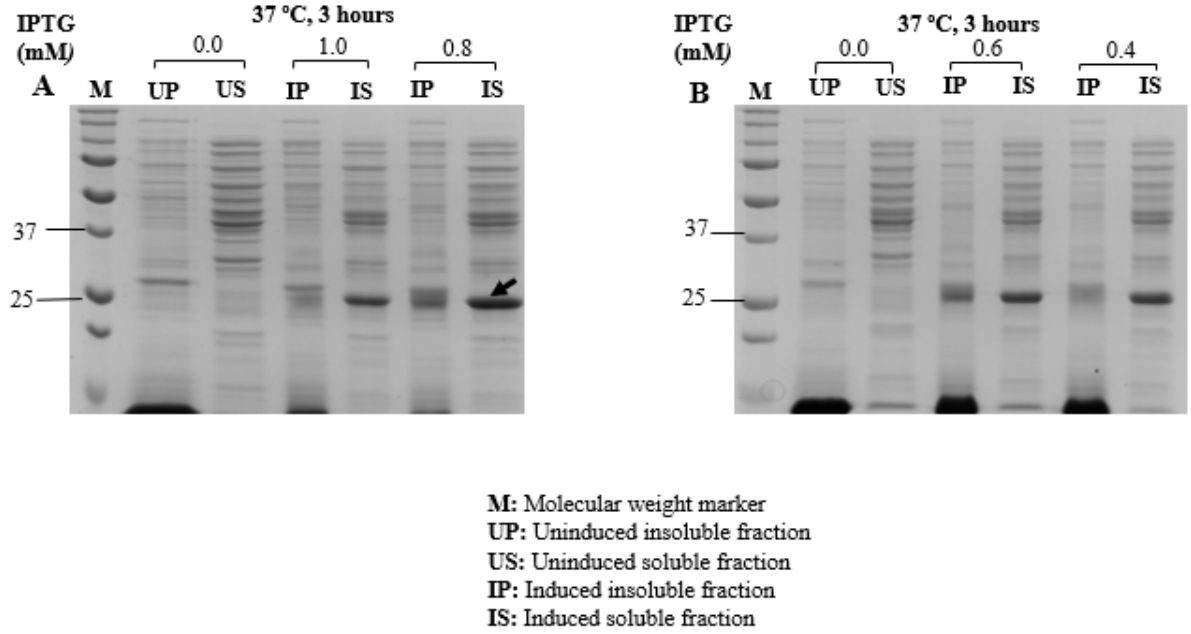

Figure 26: Analytical scale protein expression analysis of BIG1^{Sec7}. *E. coli* (T7 Express lysY/I_q) was transformed with pET-28a-BIG1^{Sec7}. The transformed cells were cultured at 37 °C until the logarithmic growth phase. Protein expression was induced by the addition of IPTG to final concentrations ranging from 0.4-1.0 mM, while parallel cultures lacking IPTG served as uninduced controls. The uninduced and induced cultures were lysed and soluble and insoluble protein fractions were obtained by centrifugation. All samples were prepared in SDS sample loading buffer and resolved on a 15% SDS- PAGE gel run at 100 V for approximately 1.5 hours. For all gels: **M:** Molecular weight marker: Precision Plus protein standard (Bio-Rad #161-0373) (molecular weights are shown in kDa). **A and B: Analytical scale expression of BIG1^{Sec7} conducted at 37 ºC.**

To improve protein expression of *Pf*ARFGEF^{Sec7}, three different competent cell lines (T7 Express lysY/I_q, XL-1 Blue and Rosetta DE3) were used at varying concentrations of IPTG and varying temperatures. The His-tagged *Pf*ARFGEF^{Sec7} recombinant protein had a predicted molecular mass of 64.7 kDa. For the Rosetta DE3 *E.coli* competent cells, general protein expression was superior to that of the other bacterial strains at all temperatures tested. A protein band with a molecular mass 66 kDa was present in the induced soluble and insoluble fractions when expression was conducted at 25 ºC (**Figure 27C** *indicated by arrow*). Although an *E. coli* protein migrated to the same position in the uninduced soluble fraction, it was absent from the uninduced insoluble pellet. This suggests that the *Pf*ARFGEF^{Sec7} was being expressed, but it was inconclusive whether it was entirely insoluble or there was sufficient soluble protein to attempt purification. To address this, western blotting analysis on the analytical scale expression profile samples was conducted to confirm the presence of protein in the induced fractions obtained by expression at 25°C. The proteins resolved on a SDS-PAGE gel were transferred to a nitrocellulose membrane probed for His-tagged proteins using HisDetector followed by incubation in TMB membrane peroxidase substrate. Prominent bands with a

molecular mass of 65 kDa were present in the induced soluble fractions and induced insoluble fractions at the chosen concentrations of IPTG used to induced protein expression (**Figure 27E** *indicated by arrow*). The bands were not present in the uninduced insoluble and soluble fractions. The analytical scale results for the other bacterial strains are in the supplementary information section and overall protein expression at the different temperatures was lower and a unique band at the expected *Pf*ARFGEF^{Sec7} position could not be confidently discerned (**Figures: S43 and S44**)

In summary, the results suggested that the analytical scale expression analysis conducted at 37 ºC (for $^{N\Delta17}$*Hs*ARF1, $^{N\Delta17}$*Pf*ARF1, GGA3^{GAT}, BIG1^{Sec7}) and 25 ºC (for *Pf*ARFGEF^{Sec7}) for 3 hours (for $^{N\Delta17}$*Hs*ARF1, $^{N\Delta17}$*Pf*ARF1, GGA3^{GAT}, BIG1^{Sec7}) and 16 hours (for *Pf*ARFGEF^{Sec7}) at 1 mM IPTG concentration (for $^{N\Delta17}$*Hs*ARF1, $^{N\Delta17}$*Pf*ARF1, GGA3^{GAT}) and 0.8 mM IPTG concentration (for BIG1^{Sec7}, *Pf*ARFGEF^{Sec7}) suggested that these conditions could be scaled up for preparative scale purification and that sufficient amounts of each recombinant protein could be obtained for use to set up the human and malarial ARF1 GEF assays.

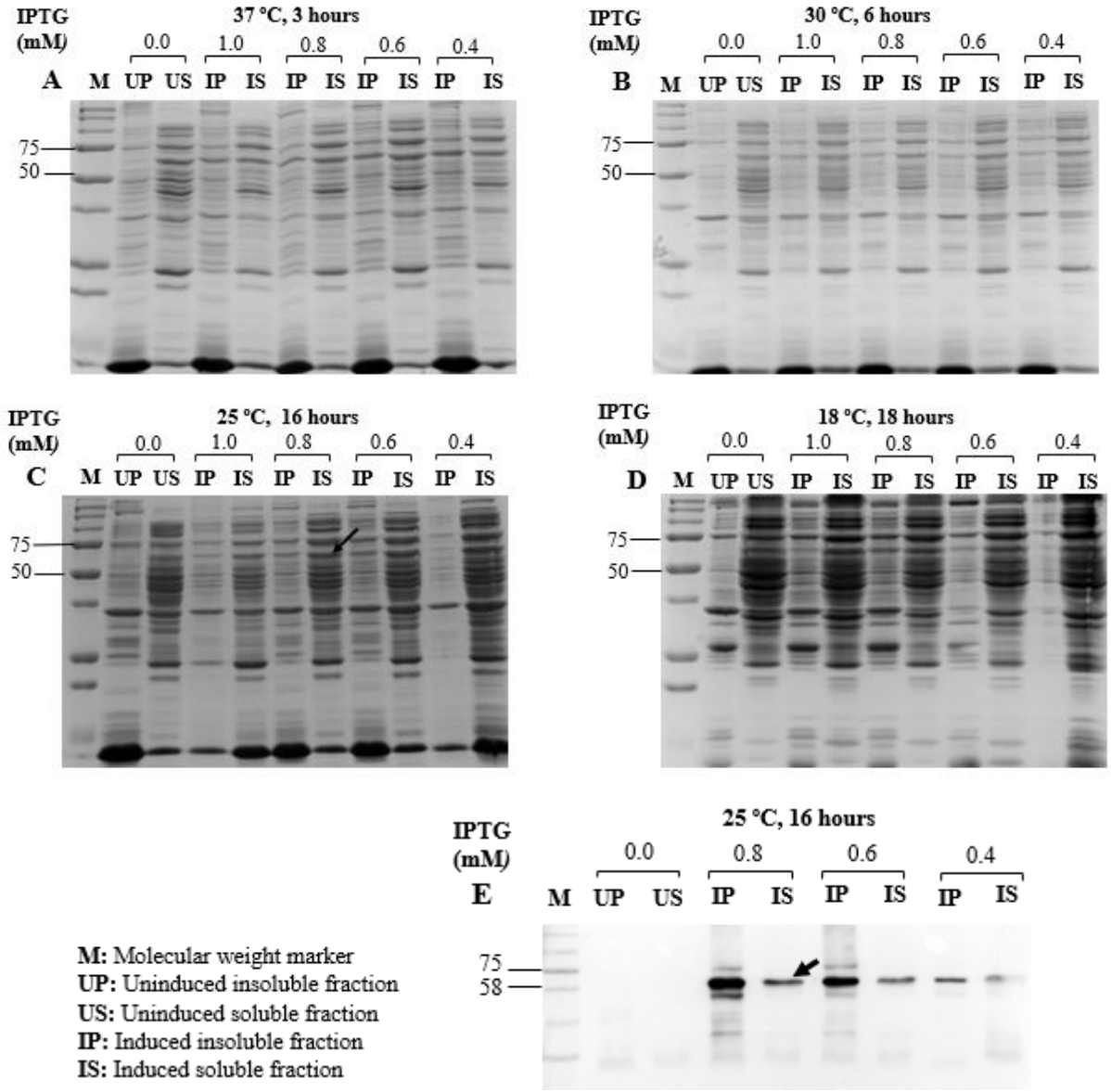

Figure 27: Analytical scale protein expression analysis of *Pf*ARFGEF^{Sec7} in Rosetta DE3 competent cells. *E. coli* (Rosetta DE3) was transformed with pET-28a-*Pf*ARFGEF^{Sec7}. The transformed cells were cultured at 37 °C until the logarithmic growth phase. Protein expression was induced at different temperatures by the addition of IPTG to final concentrations ranging from 0.4- 1.0 mM, while parallel cultures lacking IPTG served as uninduced controls. The uninduced and induced cultures were lysed and soluble and insoluble protein fractions were obtained by centrifugation. All samples were prepared in SDS sample loading buffer and resolved on a 12% SDS- PAGE gel run at 100 V for approximately 1.5 hours. For: **A-D**: **M:** Molecular weight marker: Precision Plus protein standard (Bio-Rad #161-0373) and **E: M:** Molecular weight marker: Blue protein standard (New England Biolabs #P7706) (molecular weights are shown in kDa) **A: Expression at: A: 37 ºC, B: 30 ºC, C: 25 ºC** and **D 18 ºC**. **E: Western Blotting analysis of *Pf*ARFGEF^{Sec7} expressed at 25 ºC.**

Preparative scale purification of recombinant proteins for ARF1 GEF Assays. The main objective of this component of the work was to produce $^{N\Delta17}$*Hs*ARF1, $^{N\Delta17}$*Pf*ARF1, ARNO^{Sec7}, BIG1^{Sec7} and *Pf*ARFGEF^{Sec7} as His-tagged recombinant proteins and GGA3^{GAT} as a GST-tagged recombinant protein which will be used to set up human and malarial ARF1 GEF assays. The expression conditions which were established by analytical scale expression analysis ($^{N\Delta17}$*Hs*ARF1, $^{N\Delta17}$*Pf*ARF1, ARNO^{Sec7} protein expression induced using 1 mM IPTG for 3 hours at 37 ºC, BIG1^{Sec7} protein expression induced using 0.8 mM IPTG for 3 hours at 37 ºC, *Pf*ARFGEF^{Sec7} protein expression induced using 0.8 mM IPTG for 16 hours at 25 ºC) were adopted for preparative scale expression and purification in 250 mL, 500 mL or 1000 mL cultures. Protein expression was induced with IPTG using these aforementioned *E. coli* cultures. The *E. coli* were harvested, lysed and the soluble fraction was prepared. In summary, $^{N\Delta17}$*Hs*ARF1, $^{N\Delta17}$*Pf*ARF1, ARNO^{Sec7} and BIG1^{Sec7} were successfully purified using Ni-NTA chromatography and buffer-exchanged into assay buffer using size exclusion chromatography. GST-GGA3^{GAT} was successfully purified using glutathione affinity chromatography and buffer-exchanged into assay buffer using size exclusion chromatography. The *Pf*ARFGEF^{Sec7} purification was unsuccessful as there were three other protein bands present in the final eluate (**Figure 29C**, Lane 7). The protein concentration was determined using a Bradford assay (BSA standard curve with $R^2 \geq 0.99$). SDS-PAGE analysis was conducted to assess the purification profiles of the recombinant proteins and assess the purity of the final desalted eluate. The sizes of the purified recombinant proteins were determined by a standard curve of Log (molecular weight) versus relative migration distance of the molecular weight marker used (*results not shown*). The average protein concentrations of all the recombinant proteins are described as some were expressed and purified on multiple occasions.

A protein product for the $^{N\Delta17}$*Hs*ARF1 recombinant protein was expected at 23 kDa and sufficient soluble protein was purified as there was a prominent band present at 20 kDa in the SDS-PAGE purification profile (**Figure 28A**, Lane 7 *indicated by arrow*). In the wash steps, there was some unbound protein that was eluted as there are bands of protein of expected molecular weight (**Figure 28A**, Lanes 4-5). The banding pattern showed minimal amounts of non-specific proteins in both eluate and desalted fractions and a dark band was observed corresponding to high yields of recombinant protein in the eluate and desalted samples. (**Figure 28A**, Lanes 6-7). A protein product for the $^{N\Delta17}$*Pf*ARF1 recombinant protein was expected at 21.1 kDa and sufficient soluble protein was purified as there was a prominent band present at 19 kDa (**Figure 28B,** Lane 7 *indicated by arrow*). Total volumes of 4 mL $^{N\Delta17}$*Hs*ARF1 and $^{N\Delta17}$*Pf*ARF1 with concentrations of 2.21 mg. mL^{-1} and 1.14 mg. mL^{-1} were purified from 250

mL and 500 mL protein expression cultures respectively. A protein product for the GST-GGA3^{GAT} recombinant protein was expected at 44 kDa and sufficient soluble protein was purified as there was a prominent band present at 48 kDa (**Figure 28C,** Lane 9). In the wash steps, there was some unbound protein that was eluted as there are faint bands of protein of expected molecular weight (**Figure 28C,** Lane 4-5). The banding pattern showed negligible amounts of non-specific proteins in the eluate fractions (**Figure 28C,** Lanes 6-8) and desalted fractions and a dark band was observed corresponding to a high yield of the recombinant protein purified (**Figure 28C,** Lane 9 *indicated by arrow*). A total volume of 3 mL GST-GGA3^{GAT} with a concentration of 3.21 mg. mL^{-1} was purified from a 250 mL protein expression culture.

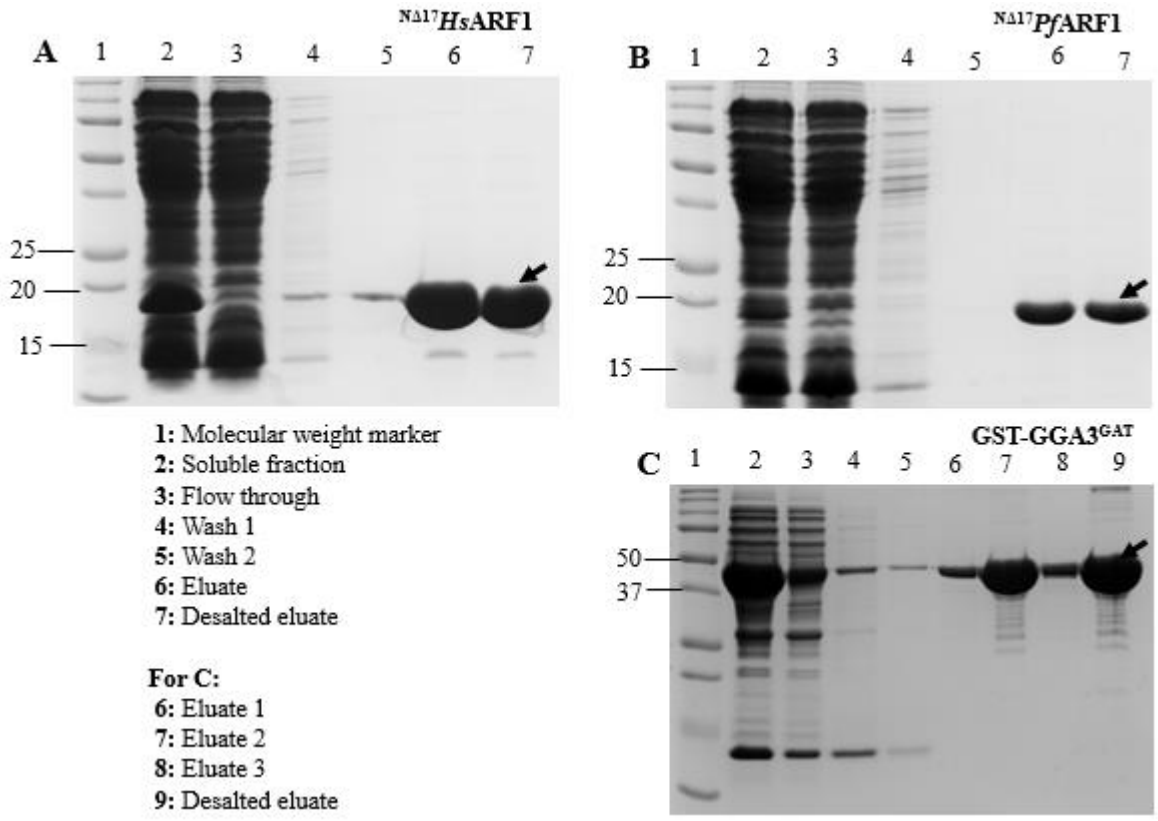

Figure 28: Preparative scale purification of $^{N\Delta17}$*Hs*ARF1, $^{N\Delta17}$*Pf*ARF1 by Ni-NTA affinity chromatography and GST-GGA3^{GAT} by glutathione affinity chromatography. All expression constructs were transformed into competent *E. coli* (T7 Express lysY/I_q cells). The transformed cells were cultured at 37 ºC until the logarithmic growth phase. Protein expression was induced by the addition of 1mM IPTG at 37 ºC for 4 hours. The cells were harvested by centrifugation, lysed and soluble fractions prepared by centrifugation and filtration for purification by Ni-NTA and glutathione affinity chromatography. All samples were prepared in SDS sample loading buffer and resolved on a 15% SDS-PAGE gel for $^{N\Delta17}$*Hs*ARF1, $^{N\Delta17}$*Pf*ARF1 and a 12% SDS-PAGE gel for GST-GGA3^{GAT} which were run at 115- 120 V for approximately 1.5 hours and stained with Coomassie. For all gels: Lane 1: Precision Plus protein standard (Bio-Rad #161-0373) (molecular weights are shown in kDa). **A and B**: Lane 2: soluble fraction; Lane 3: column flow-through; Lane 4: first wash; Lane 5: second wash; Lane 6: eluate and Lane 7: desalted eluate. **C:** Lane 2: soluble fraction; Lane 3: flow-through; Lane 4: first wash; Lane 5: second wash; Lane 6: first eluate; Lane 7: second eluate; Lane 8: third eluate and Lane 9: desalted eluate. **A: His-tagged $^{N\Delta17}$*Hs*ARF1. B: His-tagged $^{N\Delta17}$*Pf*ARF1. C: GST-tagged GGA3^{GAT}.**

A protein product was expected at 23.3 kDa for the ARNO^{Sec7} recombinant protein and sufficient soluble amounts of target protein were purified as there was a prominent band present at 22.6 kDa (**Figure 29A**, Lane 7 *indicated by arrow*). The banding pattern showed negligible amounts of non-specific proteins in both eluate and desalted fractions and a dark band was observed corresponding to a high yield of the recombinant protein in the eluate samples (**Figure 29A,** Lanes 6-7). A total volume of 4 mL ARNO^{Sec7} with a concentration of 2.68 mg. mL^{-1} was purified from a 250 mL protein expression culture. A protein product for the BIG1^{Sec7} recombinant protein was expected at 26.1 kDa and sufficient soluble protein was purified as there is a prominent band present at 28.5 kDa (**Figure 29B**, Lane 7 *indicated by arrow*). In the wash steps, there was some unbound protein was eluted as there are dark bands of protein of expected size (**Figure 29B**, Lanes 4-5). The banding pattern showed minimal amounts of non-specific proteins in both eluate and desalted fractions and a dark band was observed corresponding to high yields of recombinant protein in the eluate samples (**Figure 29B**, Lanes 6-7). A total volume of 4 mL BIG1^{Sec7} with a concentration of 2.30 mg. mL^{-1} was purified from a 250 mL protein expression culture. A protein product for the *Pf*ARFGEF^{Sec7} recombinant protein was expected at 64.7 kDa. The eluted and desalted samples contained a protein band at the expected molecular wdeight, but there were also three contaminating proteins with similar or greater concentrations (**Figure 29C**, Lane 6 and 7). This result was considered inconclusive. To confirm the presence of the *Pf*ARFGEF^{Sec7} requires western blotting analysis. ARNO^{Sec7} and BIG1^{Sec7} were used in the GEFs assays as the *Pf*ARFGEF^{Sec7}expression and purification requires further optimisation. Proteins were stored in 40 % (v/v) glycerol at -20 ºC.

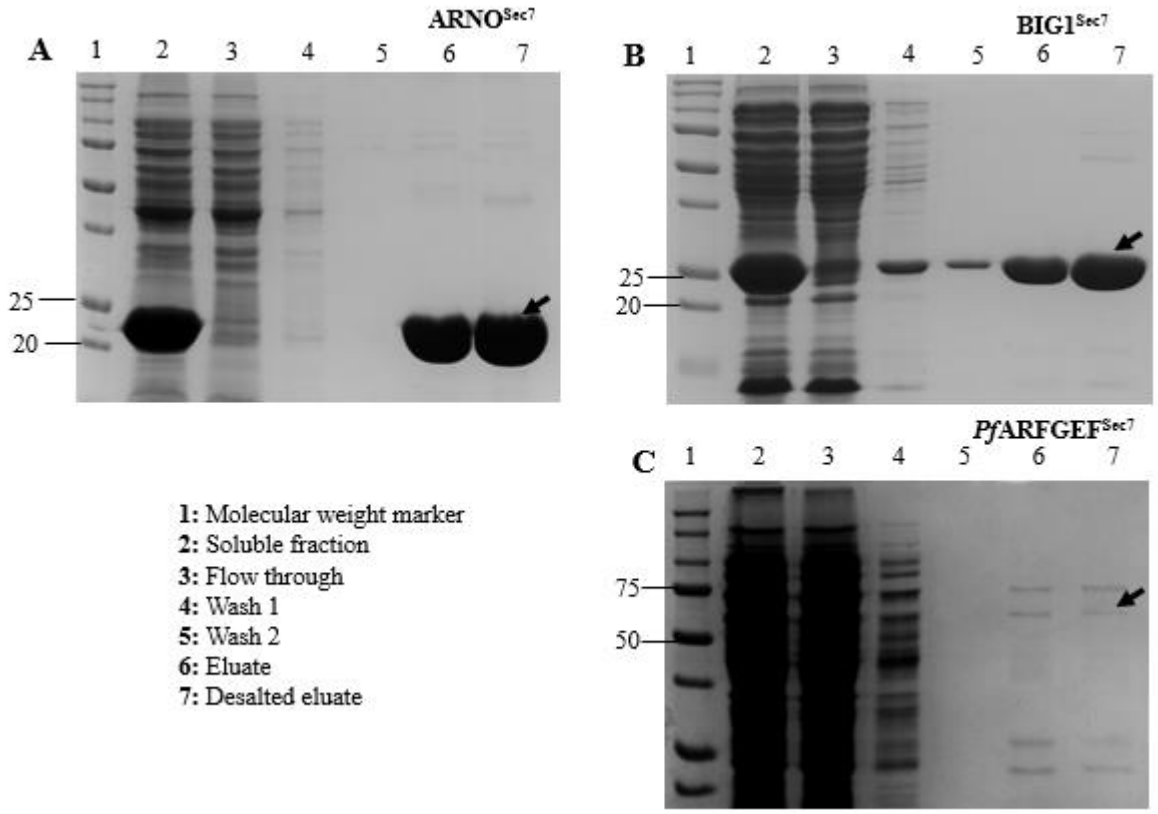

Figure 29: Preparative scale purification of guanine nucleotide exchange factors by Ni-NTA affinity chromatography. All expression constructs were transformed into competent *E. coli* (T7 Express lysY/I_q cells for ARNO^{Sec7} and BIG1^{Sec7} and Rosetta DE3 for *Pf*ARFGEF^{Sec7}). The transformed cells were cultured at 37 ºC until the logarithmic growth phase. Protein expression was induced by the addition of: 1mM IPTG at 37 ºC for 4 hours for ARNO^{Sec7}, 0.8 mM IPTG at 37 ºC for 4 hours for BIG1^{Sec7} and 0.8 mM IPTG at 25 ºC for 16 hours for *Pf*ARFGEF^{Sec7}. The cells were harvested by centrifugation, lysed and soluble fractions were prepared centrifugation and filtration for purification by Ni-NTA affinity chromatography. All samples were prepared in SDS sample loading buffer and resolved on a 15% SDS-PAGE gel for ARNO^{Sec7} and on a 12% SDS-PAGE gel for BIG1^{Sec7} and *Pf*ARFGEF^{Sec7} which were run at approximately 115- 120 V for approximately 1.5 hours. For all gels: Lane 1: Precision Plus protein standard (Bio-Rad #161-0373) (molecular weights are shown in kDa). **A: Purification profile of His-tagged ARNO^{Sec7}. B: Purification profile of His-tagged BIG1^{Sec7}. C: Purification profile of His-tagged *Pf*ARFGEF^{Sec7}.**

EDTA-mediated nucleotide exchange of $^{N\Delta17}$*Pf*ARF1 and $^{N\Delta17}$*Hs*ARF1. The protocol used for the nucleotide exchange reactions was developed by T. Swart (PhD thesis in preparation) with further modifications. The nucleotide exchange reactions were carried out to prepare GTP- and GDP-loaded $^{N\Delta17}$*Pf*ARF1 and $^{N\Delta17}$*Hs*ARF1. GDP-loaded (inactive) forms of the proteins were required as substrates and negative controls for the GEF-mediated nucleotide exchange assays, while GTP-loaded (active) proteins were required as positive controls for successful GEF-mediated nucleotide exchange. EDTA mediated nucleotide exchange was conducted by incubating 5 µM $^{N\Delta17}$*Pf*ARF1 and $^{N\Delta17}$*Hs*ARF1 with 50 µM GTP or GDP in the presence of 20 mM EDTA for $^{N\Delta17}$*Pf*ARF1 and 2 mM EDTA for $^{N\Delta17}$*Hs*ARF1 at 25 ºC in a black 96 well plate. The tryptophan fluorescence (Ex298 nm/ Em340 nm) was measured in a plate reader for 90 minutes at 5-minute intervals, with gentle agitation between readings. Kinetic readings were carried out to monitor the real-time activation and deactivation status of $^{N\Delta17}$*Pf*ARF1 (**Figure 30A**) and $^{N\Delta17}$*Hs*ARF1 (**Figure 31A**). $MgCl_2$ was added to a final concentration of 30 mM to stabilize the nucleotide loaded $^{N\Delta17}$*Pf*ARF1 proteins and to a final concentration of 3 mM to stabilize the $^{N\Delta17}$*Hs*ARF1 nucleotide complexes. To follow the stabilization of the $^{N\Delta17}$*Pf*ARF1 GTP, $^{N\Delta17}$*Pf*ARF1 GDP, $^{N\Delta17}$*Hs*ARF1 GTP and $^{N\Delta17}$*Hs*ARF1 GDP complexes, kinetic readings of the tryptophan fluorescence were measured for 30 minutes at 2-minute intervals after addition of $MgCl_2$, with gentle agitation between readings **(Figure 30B** for $^{N\Delta17}$*Pf*ARF1 and **Figure 31B** for $^{N\Delta17}$*Hs*ARF1**)**. The nucleotide exchange was finally assessed by intrinsic tryptophan fluorescence readings as an endpoint. The results suggested that over time $^{N\Delta17}$*Pf*ARF1 and $^{N\Delta17}$*Hs*ARF1 were successfully loaded with GTP and GDP in the presence of EDTA indicated by the significantly lower tryptophan fluorescence readings obtained for the GDP-loaded proteins. The $MgCl_2$ was able to stabilize the $^{N\Delta17}$*Pf*ARF1 and $^{N\Delta17}$*Hs*ARF1 GTP and GDP complexes as there was no change in the intrinsic tryptophan fluorescence over time.

To determine to what extent the $^{N\Delta17}$*Pf*ARF1 and $^{N\Delta17}$*Hs*ARF1 recombinant proteins were originally purified in a GTP or GDP loaded form, they were included in the nucleotide exchange reactions, but without the addition of excess GTP or GDP. The kinetic and end-point readings suggest that $^{N\Delta17}$*Pf*ARF1 was purified as a mixture of GTP- and GDP-bound forms, since its tryptophan fluorescence readings were midway between that of the GTP and GDP loading reactions (**Figure 31A** and **B**, purple lines). By contrast, $^{N\Delta17}$*Hs*ARF1 was purified as predominantly GTP-bound, since its fluorescence readings mirrored that obtained in the GTP loading reaction (**Figure 32A** and **B**, purple lines). Thus, GTP loading the $^{N\Delta17}$*Hs*ARF1 purified protein may not be a necessary step.

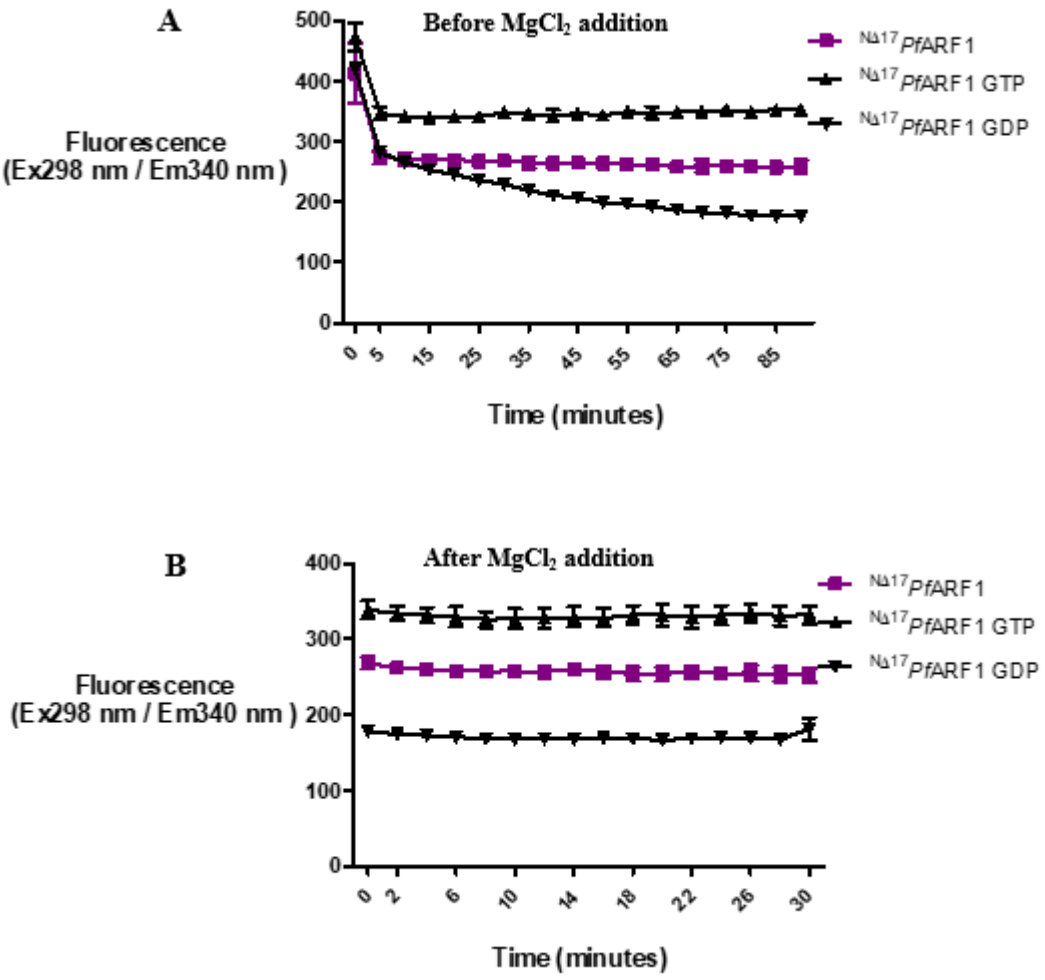

Figure 30: EDTA mediated nucleotide exchange on $^{N\Delta17}$*Pf*ARF1. A: Intrinsic tryptophan fluorescence profile of $^{N\Delta17}$*Pf*ARF1 before the addition of magnesium chloride. 5 µM $^{N\Delta17}$*Pf*ARF1 was incubated at 25 ºC with 50 µM GTP or GDP in the presence of 20 mM EDTA in a black 96 well plate and the tryptophan fluorescence (Exc298 nm/ Emm340 nm) was measured in a plate reader for 90 minutes at 5-minute intervals. 5 µM $^{N\Delta17}$*Pf*ARF1 without the addition of GTP and GDP was also included as a positive control and was incubated in assay buffer only. Background controls contained GTP or GDP and all reaction components without the recombinant protein. Readings from these wells were subtracted from the $^{N\Delta17}$*Pf*ARF1 GTP and $^{N\Delta17}$*Pf*ARF1 GDP signals respectively. The nucleotide exchange reactions were conducted in triplicate wells and all data points represent the mean fluorescence ± standard deviations. **B: Intrinsic tryptophan fluorescence profile of $^{N\Delta17}$*Pf*ARF1 after the addition of magnesium chloride.** Following the addition of 30 mM $MgCl_2$, a further incubation was conducted and the tryptophan fluorescence was measured in a plate reader for 30 minutes at 2-minute intervals.

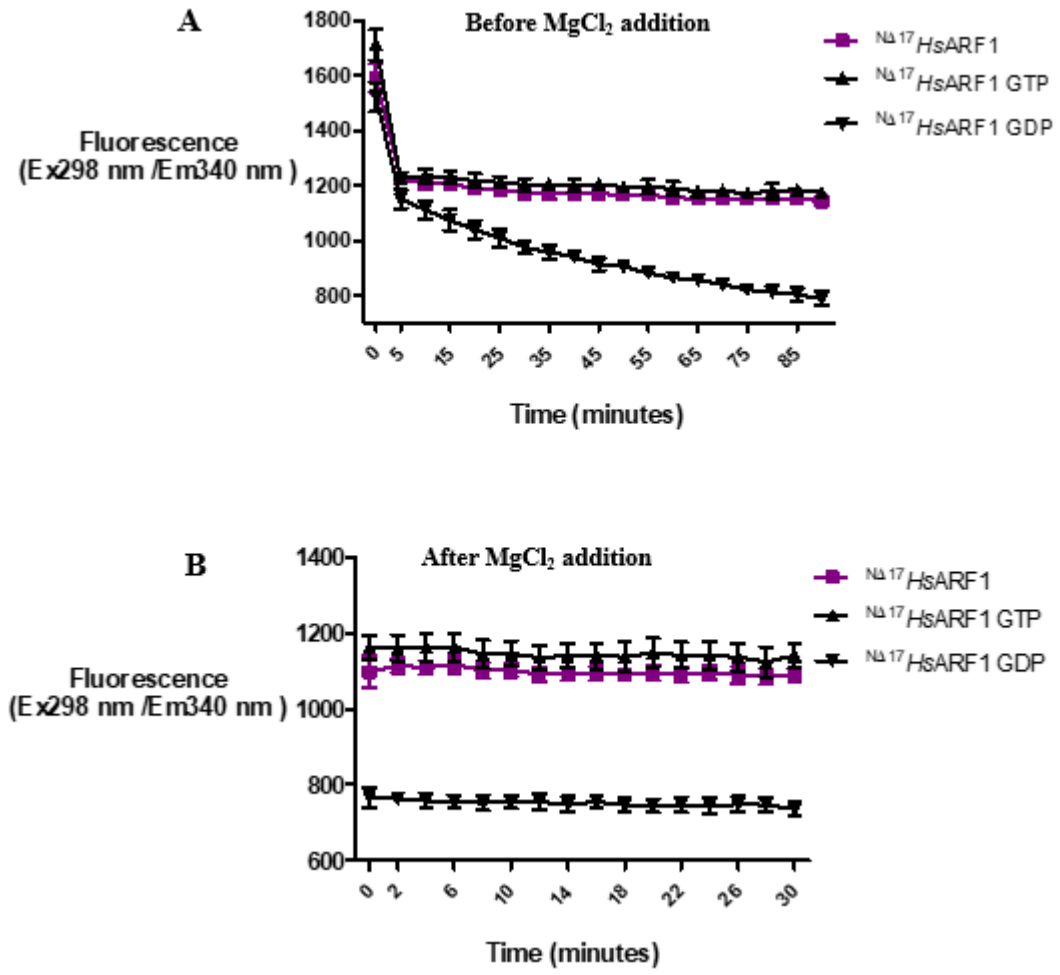

Figure 31: EDTA mediated nucleotide exchange on $^{N\Delta17}$*Hs*ARF1. A: Intrinsic tryptophan fluorescence profile of $^{N\Delta17}$*Hs*ARF1 before the addition of magnesium chloride. 5 µM $^{N\Delta17}$*Hs*ARF1 was incubated at 25 ºC with 50 µM GTP or GDP in the presence of 2 mM EDTA in a black 96 well plate and the tryptophan fluorescence (Ex298 nm/ Em340 nm) was measured in a plate reader for 90 minutes at 5-minute intervals. 5 µM $^{N\Delta17}$*Hs*ARF1 without the addition of GTP and GDP was also included as a positive control and was incubated in assay buffer only. Background controls contained GTP or GDP and all reaction components without the recombinant protein. Readings from these wells were subtracted from the $^{N\Delta17}$*Hs*ARF1 GTP and $^{N\Delta17}$*Hs*ARF1 GDP signals respectively. The nucleotide exchange reactions were conducted in triplicate wells and all data points represent the mean fluorescence ± standard deviations. **B: Intrinsic tryptophan fluorescence profile of $^{N\Delta17}$*Hs*ARF1 after the addition of magnesium chloride.** Following the addition of 3 mM $MgCl_2$, a further incubation was conducted and the tryptophan fluorescence was measured in a plate reader for 30 minutes at 2-minute intervals.

Ni-NTA immobilised ARF1-GGA3^{GAT} interaction assay established for use in the GEF Assays. The development of the immobilisation assay for ARF1 was primarily done by T. Swart (manuscript submitted for publication). This work has demonstrated that the assay can be used to detect the modulation of malarial ARF1 by Sec7 and ARFGAP domains *in vitro*. The main objective of this work was to use this novel assay to detect the modulation of ARF1 by the Sec7 domains *in vitro* and to launch drug screening campaigns to evaluate the drug target status of ARF1. To detect whether GST-GGA3^{GAT} was able to detect the activation status of human ARF1 ($^{N\Delta17}$*Hs*ARF1) and malarial ARF1 ($^{N\Delta17}$*Pf*ARF1) (as for the FRET assay, the N terminal 17 amino acids containing the myristylation site and amphipathic α-helix were omitted) using the ARF1 immobilised assay, 1 µM GTP and GDP loaded $^{N\Delta17}$*Hs*ARF1 or 1 µM GTP and GDP loaded $^{N\Delta17}$*Pf*ARF1 were transferred to a Ni-NTA coated 96 well plates, incubated for 30 minutes at 4 ºC with gentle agitation. Sequential incubations carried out with 1 µM GST-GGA3^{GAT} for 60 minutes at 4 ºC with gentle agitation, and a colorimetric GST substrate (containing CDNB and GSH), with several washing steps before the addition of the GST substrate. The end point absorbance at 340 nm signal was measured after 30 minutes following the room temperature incubation with GST substrate to measure the formation of the GS-DNB conjugation product produced by active immobilised GST. The controls consisted of assay buffer and GST-GGA3^{GAT} in the absence of GTP and GDP loaded $^{N\Delta17}$*Hs*ARF1 or $^{N\Delta17}$*Pf*ARF1. Additionally, a positive control of His-tagged GST (previously prepared by L. Wambua, M.Sc dissertation) was used to confirm that the Ni-NTA plates can capture His tagged proteins (r*esults not shown*) and this control was used in all experiments. The difference in signals between active $^{N\Delta17}$*Hs*ARF1 GTP and inactive $^{N\Delta17}$*Hs*ARF1 GDP were statistically significant (**Figure 32A,** $p<0.0001$, $n=3$), as was the difference in signals between active $^{N\Delta17}$*Pf*ARF1 GTP and inactive $^{N\Delta17}$*Pf*ARF1 GDP (**Figure 32B,** $p<0.0001$, $n=3$). These results suggested that the GST-GGA3^{GAT} was able to detect the activation status of $^{N\Delta17}$*Hs*ARF1 and $^{N\Delta17}$*Pf*ARF1 using the Ni-NTA immobilised assay.

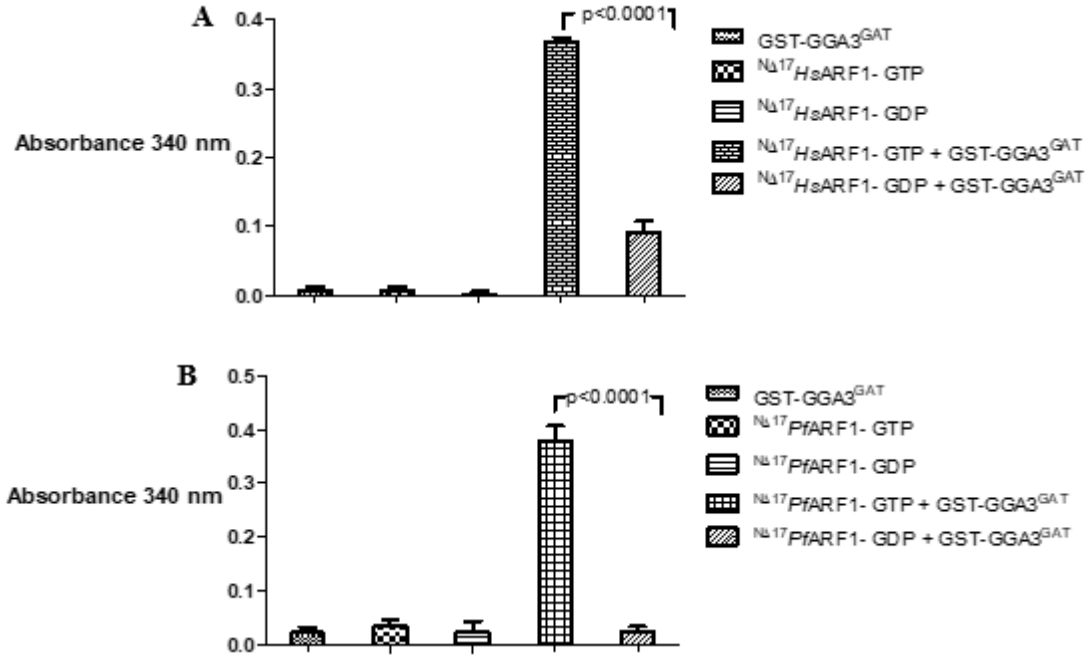

Figure 32: Ni-NTA immobilised ARF1-GGA3^{GAT} interaction assay can distinguish between active and inactive ARF1. The background was assay buffer incubated alone. All reactions were incubated with a final concentration of 1 µM GST-GGA3^{GAT}. The GST signals were corrected by the average background readings. **A: ^{NΔ17}*Hs*ARF1 -GGA3^{GAT} interaction assay. B: ^{NΔ17}*Pf*ARF1 -GGA3^{GAT} interaction assay.** Incubations were carried out in triplicate wells and bars represent the mean absorbance 340 nm ± standard deviation.

Concentration of GTP optimised to use for the human and malarial GEF assay. Since the human and malarial immobilised ARF1-GGA3^{GAT} interaction assays were established, the next step was to optimise the concentration of GTP used stimulate the exchange of GDP for GTP on ARF1 in the presence of an ARF GEF. This was investigated as preliminary analysis suggested that there is a spontaneous exchange of GDP for GTP on $^{N\Delta17}$*Hs*ARF1 or $^{N\Delta17}$*Pf*ARF1 - despite the presence of $MgCl_2$ to stabilise the existing bound GDP nucleotide – when the GDP-bound proteins were incubated with GTP in the absence of a GEF. We thus sought to find the concentration of GTP that would result in GGA3^{GAT} interaction signals that were similar to those obtained with GDP loaded $^{N\Delta17}$*Hs*ARF1 or $^{N\Delta17}$*Pf*ARF1 control incubated without GTP. This would aid in discerning whether the observed positive signals obtained in subsequent GEF assays are due to Sec7 domain catalytic activity and not spontaneous GDP-GTP nucleotide exchange. 1 µM GDP loaded $^{N\Delta17}$*Hs*ARF1 or 1 µM GDP loaded $^{N\Delta17}$*Pf*ARF1 was incubated at various concentrations GTP. The reactions were incubated for 45 minutes at 37 ºC with gentle agitation. The controls consisted of GTP and GDP loaded $^{N\Delta17}$*Hs*ARF1 and $^{N\Delta17}$*Pf*ARF1 in the absence of GTP. The reactions were transferred to a nickel NTA plate and the immobilised ARF1-GGA3^{GAT} interaction assay carried out as described previously. The results suggested that at a concentration of 5 µM GTP, there was no spontaneous exchange of GDP for GTP on $^{N\Delta17}$*Hs*ARF1 GDP (**Figure 33A**) and $^{N\Delta17}$*Pf*ARF1 GDP **(Figure 33B**), while higher concentrations of GTP resulted in increased GST-GGA3^{GAT} interaction, likely due to the conversion of ARF1 GDP to ARF1 GTP despite the absence of a GEF. These conditions (5 µM GTP) were used for the analysis of GEF activity on human and malarial ARF1.

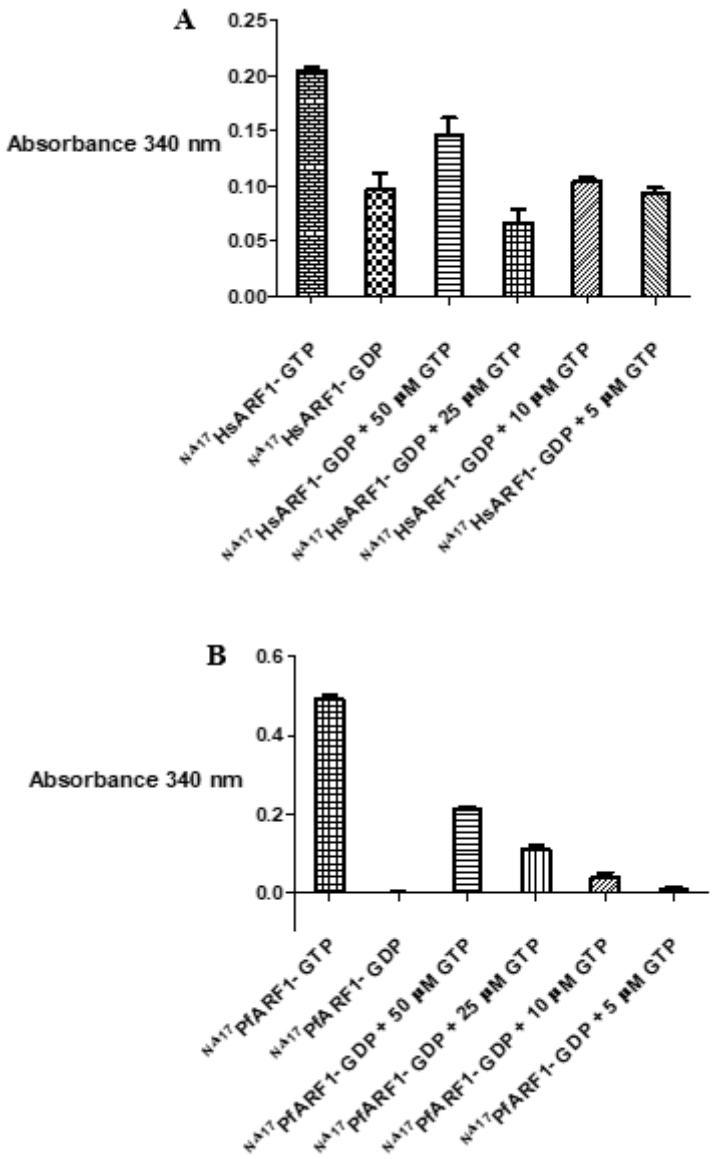

Figure 33: Effect of GTP on differential GGA3 interaction with ARF1-GTP and ARF1-GDP. 1 µM $^{N\Delta17}$*Hs*ARF1 GDP or 1 µM $^{N\Delta17}$*Pf*ARF1 GDP was incubated in assay buffer alone or in the presence of varying concentrations of GTP for 45 minutes at 37 ºC and added to Ni-NTA coated 96 well plates for 30 minutes at 4 ºC. 1 µM GST-GGA3^{GAT} was added and incubation continued for 60 minutes at 4 º C. Following washing steps, GST substrate was added and absorbance readings measured at 340 nm. The GST signals were corrected by the average background readings obtained from wells incubated with 1 µM GST-GGA3^{GAT} in the absence of immobilised ARF1. **A: $^{N\Delta17}$*Hs*ARF1. B: $^{N\Delta17}$*Pf*ARF1.** Incubations were carried out in triplicate wells and bars represent the mean absorbance 340 nm ± standard deviation.

ARNO^{Sec7} and BIG1^{Sec7} mediated exchange on ARF1 was moderately detectable by the immobilised ARF1-GGA3^{GAT} interaction assay. Since the human and malarial immobilised ARF1-GGA3^{GAT} interaction assays and the concentration of GTP to be used to stimulate the exchange of GDP for GTP on ARF1 in the presence of an ARF GEF were established, the next question was whether the ARF GEFs would stimulate nucleotide exchange of GDP for GTP and the activation status of ARF1 subsequently be detected using the immobilised ARF1-GGA3^{GAT} interaction assay. To investigate if the assay could be exploited to detect the activation of ARF1 by ARF GEFs *in vitro*, 1 µM GDP loaded $^{N\Delta17}$*Hs*ARF1 or $^{N\Delta17}$*Pf*ARF1 was incubated in the presence of the Sec7 domain of ARNO^{Sec7} and BIG1^{Sec7} at varying concentrations of the ARF GEFs and with 5 µM GTP. The reactions were incubated for 45 minutes at 37 ºC with gentle agitation. The controls consisted of GTP and GDP loaded $^{N\Delta17}$*Hs*ARF1 and $^{N\Delta17}$*Pf*ARF1 in the absence of GTP and GDP loaded $^{N\Delta17}$*Hs*ARF1 and $^{N\Delta17}$*Pf*ARF1 in the presence of GTP, but without the addition of the Sec7 domains. The reactions were transferred to a nickel NTA plate and the immobilised ARF1-GGA3^{GAT} interaction assay described previously carried out. The expected result was that incubation of the GDP loaded ARF1 proteins with GTP in the presence of the Sec7 domains would increase GGA3^{GAT} binding (and thus Abs340 nm) compared to the corresponding incubations without the Sec7 domains, due to the formation of GTP loaded ARF1 caused by the Sec7 domain GEF activity. In the case of $^{N\Delta17}$*Hs*ARF1, the results suggested that Sec7 domain of ARNO^{Sec7} and BIG1^{Sec7} could moderately stimulate catalytic activity (exchange of GDP for GTP) on $^{N\Delta17}$*Hs*ARF1 using different concentrations of ARNO^{Sec7} (**Figure 34A**) and BIG1^{Sec7} (**Figure 35A**) as the incubations with ARNO^{Sec7} and BIG1^{Sec7} yielded Abs340 nm values that were slightly higher and statistically significant ($p<0.05$) compared to those obtained with $^{N\Delta17}$*Hs*ARF1-GDP without ARNO^{Sec7} and BIG1^{Sec7}. In the case of $^{N\Delta17}$*Pf*RF1, the results suggested that the Sec7 domain of ARNO^{Sec7} and BIG1^{Sec7} was able to stimulate catalytic activity on $^{N\Delta17}$*Pf*ARF1 when concentrations of 0.5 and 0.8 µM of ARNO^{Sec7} (**Figure 35B**) and 0.8 µM BIG1^{Sec7} (**Figure 36B**) were used as the incubations with ARNO^{Sec7} and BIG1^{Sec7} yielded Abs340 nm values that were slightly higher and statistically significantly different($p<0.05$) than those obtained with $^{N\Delta17}$*Pf*ARF1-GDP without ARNO^{Sec7} and BIG1^{Sec7}. However, the Sec7 domain of ARNO^{Sec7} and BIG1^{Sec7} could not stimulate catalytic activity on $^{N\Delta17}$*Pf*ARF1 at a concentration of 0.2 µM ARNO^{Sec7} (**Figure 35B**) and concentrations of 0.2 and 0.5 µM BIG1^{Sec7} (**Figure 36B**) as the incubations with ARNO^{Sec7} and BIG1^{Sec7} yielded Abs340 nm values that were not statistically significantly different ($p>0.05$) than those obtained with $^{N\Delta17}$*Pf*ARF1-GDP without ARNO^{Sec7} and BIG1^{Sec7}.

A possible confounding factor was that increasing the ARNO^{Sec7} concentration led to Abs340 nm values below those obtained with the GDP loaded ARF1 controls. This could be due to competition of the Sec7 domain (which is also His-tagged) with the ARF1 for binding to the nickel-coated plate which could, in turn, have masked the presence of successfully activated ARF1-GTP. A similar result was obtained with the Sec7 domain of BIG1 (**Figure 35A** and **B**).

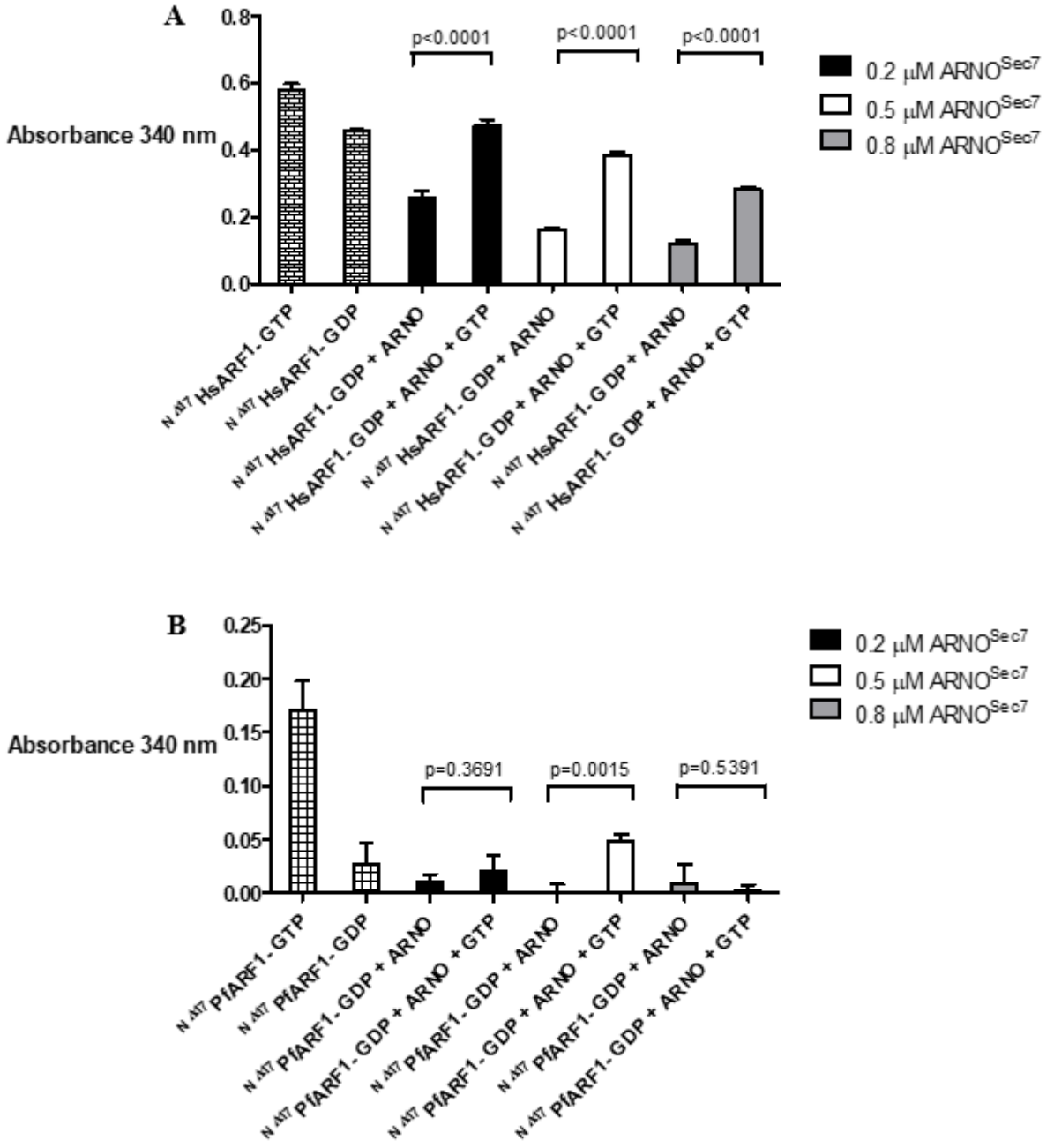

Figure 34: Ni-NTA immobilised ARF1-GGA3^{GAT} interaction assay to detect ARNO^{Sec7}-mediated exchange on human and malarial ARF1. 1 µM ^{NΔ17}*Hs*ARF1 GDP or 1 µM ^{NΔ17}*Pf*ARF1 GDP was incubated with 0.2, 0.5 and 0.8 µM ARNO^{Sec7} in the presence of 5 µM GTP for 45 minutes at 37 ºC and added to Ni-NTA coated 96 well plates for 30 minutes at 4 ºC. 1 µM GST-GGA3^{GAT} was added and incubation continued for 60 minutes at 4 ºC, followed by washing steps, incubation with GST substrate and absorbance readings measured at 340 nm. The GST signals were corrected by the average background readings obtained from wells incubated with 1 µM GST-GGA3^{GAT} alone. Controls consisted of incubations conducted with 1 µM ^{NΔ17}*Hs*ARF1 GTP (positive control) and 1 µM ^{NΔ17}*Hs*ARF1 GDP (negative control). The same controls were included for ^{NΔ17}*Pf*ARF1. **A: ^{NΔ17}*Hs*ARF1 incubations. B: ^{NΔ17}*Pf*ARF1 incubations.** Incubations were carried out in triplicate wells and bars represent the mean absorbance at 340 nm ± standard deviation.

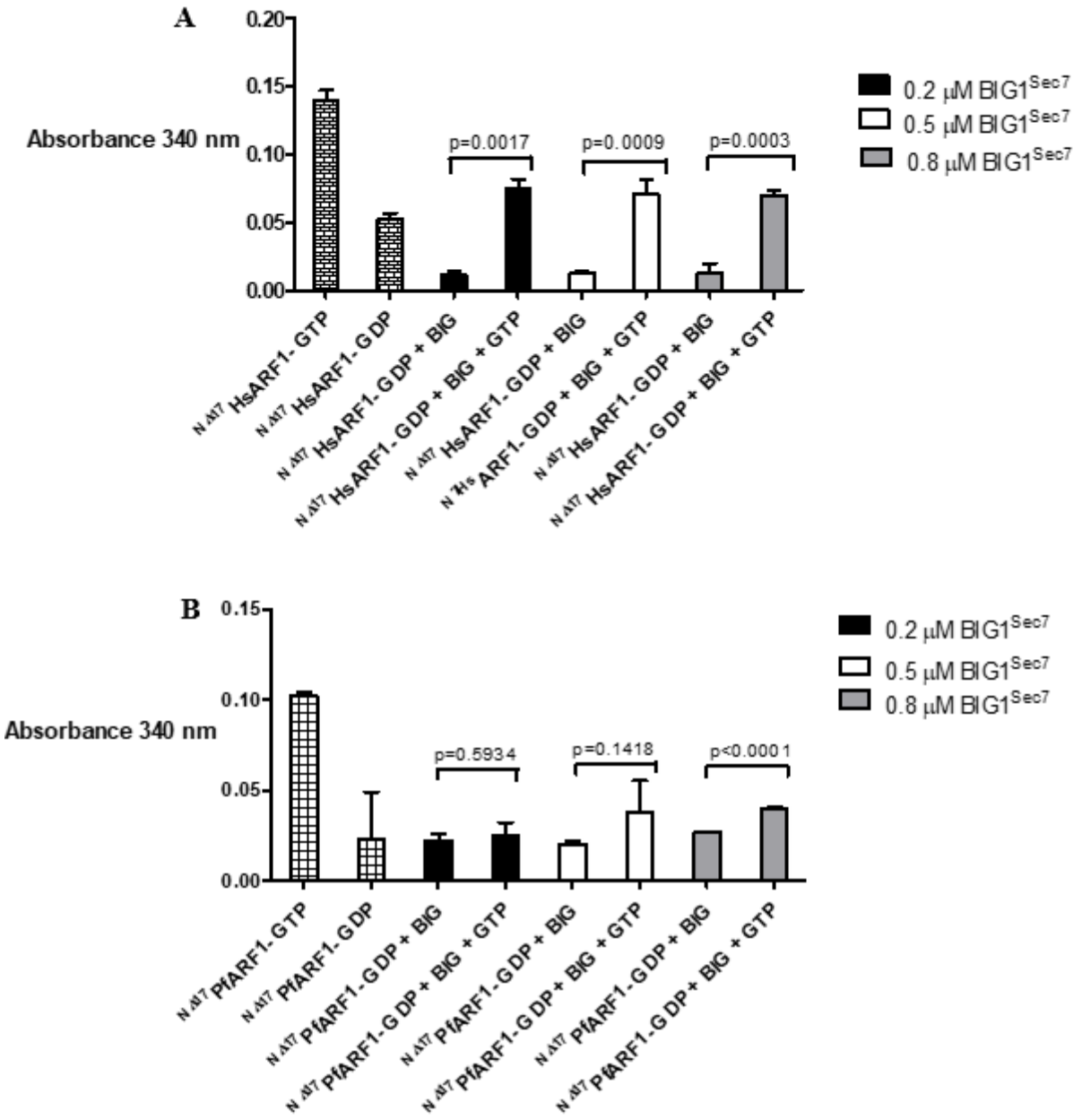

Figure 35: Ni-NTA immobilised ARF1-GGA3^{GAT} interaction assay to detect BIG1^{Sec7}-mediated exchange on human and malarial ARF1. 1 µM ^{NΔ17}*Hs*ARF1 GDP or 1 µM ^{NΔ17}*Pf*ARF1 GDP was incubated with 0.2, 0.5 and 0.8 µM BIG1^{Sec7} in the presence of 5 µM GTP for 45 minutes at 37 ºC and added to Ni-NTA coated 96 well plates for 30 minutes at 4 ºC. 1 µM GST-GGA3^{GAT} was added and incubation continued for 60 minutes at 4 ºC, followed by washing steps, incubation with GST substrate and absorbance readings measured at 340 nm. The GST signals were corrected by the average background readings obtained from wells incubated with 1 µM GST-GGA3^{GAT} alone. Controls consisted of incubations conducted with 1 µM ^{NΔ17}*Hs*ARF1 GTP (positive control) and 1 µM ^{NΔ17}*Hs*ARF1 GDP (negative control). The same controls were included for ^{NΔ17}*Pf*ARF1. **A: ^{NΔ17}*Hs*ARF1 incubations. B: ^{NΔ17}*Pf*ARF1 incubations.** Incubations were carried out in triplicate wells and bars represent the mean absorbance at 340 nm ± standard deviation.

4.4. DISCUSSION AND FUTURE WORK

The overall aim of this study was to develop a robust immobilised ARF1 interaction assay to employ for high-throughput screening (HTS) of chemical libraries to identify novel inhibitors of ARF1 effectors and ARF1 GEF interactions. Although targeting ARF GEF interactions has been proposed for cancer, a question we asked is whether it would also be a strategy that can be used to simultaneously target other diseases and in this case, we sought to target malaria.

The human and malarial ARF1-GGA3^{GAT} interaction assays were developed as robust signals that discriminate between active (GTP bound) and inactive (GDP bound) ARF1 proteins were detected. In addition to being reproducible, the ARF1-GGA3 interaction assays may also suitable for high throughput screening of compounds that disrupt the binding of ARF1 to effector proteins (GGA3 in this case). Z-factor scores above 0.5 qualitatively describe the assay as an 'excellent' assay (Zhang, 1999). Ni-NTA immobilised $^{N\Delta17}$*Hs*ARF1-GGA3^{GAT} and $^{N\Delta17}$*Pf*ARF1-GGA3^{GAT} interaction assays were both reproducible and can be qualitatively determined to be excellent assays for HTS owing to their Z-factor values of 0.916 and 0.876 respectively (**Table 3**).

Table 3: High throughput screening potential analysis of the immobilised ARF-GGA3 interaction assays.

Assay	**Z-Factor**
Ni-NTA immobilised $^{N\Delta17}$*Hs*ARF1 -GGA3^{GAT} interaction assay	0.916
Ni-NTA immobilised $^{N\Delta17}$*Pf*ARF1 -GGA3^{GAT} interaction assay	0.876

*Refer to the supplementary information for Z-Factor calculations and interpretation.

The next question was whether the ability of the assay to discriminate between GDP and GTP bound ARF1 could be exploited to detect the nucleotide exchange action of GEFs on ARF1. The principle of the assay was to incubate inactive ARF1 GDP with GTP in the presence of the catalytic Sec7 domains of GEFs and measure resultant ARF1 GTP levels using the GGA3^{GAT} interaction assay. However, spontaneous exchange of GDP for GTP on human and malarial ARF1 would mask Sec7 effects. Experiments were therefore conducted by incubating ARF1 GDP with various concentrations of GTP in the absence of Sec7 domains. The results suggested that at a concentration of 5 μM GTP, there was no spontaneous exchange of GDP

for GTP, but it did occur at higher GTP concentrations. The results are in alignment with the concentrations that have been used in other studies for GEF assays (Franco *et al*., 1995). Franco *et al*. (1995) observed a spontaneous exchange of GDP for GTP on ARF1 in the presence of phospholipid vesicles at physiological levels of Mg^{2+}. Given that one of the assay buffer components is $MgCl_2$ and $MgCl_2$ was used to stabilize the nucleotide/ARF1 complexes, this could provide a possible explanation why there seemed to be a spontaneous exchange of GDP for GTP in the absence of an ARF GEF. Additionally, ARFs could potentially possess intrinsic GEF activity. While this has not been shown in studies conducted previously, it could provide a possible explanation for the observations made in this study. Although not attempted in this study, a possible means for discriminating between spontaneous vs. GEF-mediated nucleotide exchange in future could be to include known GEF inhibitors, e.g. SecinH3, BFA and Golgicide A.

To find inhibitors that can be used in cancer and malarial therapies, high throughput screening assays need to be developed to measure the activation of ARF1 by ARF GEFs. Robust signals to confirm the activation of ARF1 due to GEF action could not be detected in this study. Studies done show conflicting results concerning substrate specificity of $ARNO^{Sec7}$ *in vitro* and *in vivo*. *In vitro* studies show that $ARNO^{Sec7}$ is able to activate ARF6 but catalyse the activation more efficiently on class I ARFs, of which ARF1 is one of the isoforms. However, *in vivo* studies show $ARNO^{Sec7}$ preferentially co-localizes with ARF6 (Frank *et al*., 1998; Venkateswarlu *et al*., 1998; Langille *et al*., 1999; Santy and Casanova, 2001). $BIG1^{Sec7}$ has been shown to activate ARF1 and ARF3, so it has a specificity for class I ARFs (Zhoa *et al*., 2002; Pacheco-Rodriguez *et al*., 2002; Ishizaki *et al*., 2008). These published reports show that ARF1 is a likely substrate for $ARNO^{Sec7}$ and $BIG1^{Sec7}$, but this could not be confirmed in this study. Interestingly, the *P. falciparum* genome encodes for a single Sec7 domain containing putative ARF GEF, which should be specific for malarial proteins (Baumgartner *et al*., 2001; Wiek *et al*., 2004). In addition to sequence homology, the conclusion that the protein product of this gene is an ARFGEF is supported by the fact that BFA (a canonical ARFGEF inhibitor) sensitivity in malaria parasites is determined by a single point mutation in this coding sequence. However, a direct demonstration of the GEF activity of this protein has not been reported. The unusual secondary structure arrangement of the $Pf ARFGEF^{Sec7}$ (Baumgartner *et al*., 2001; Wiek *et al*., 2004; Supplementary figures S41 and S42) could affect its ability to activate ARF1.

The Sec7 domain is the minimal fragment required to promote nucleotide exchange ARF GEF activity (Béraud-Dufour *et al*., 1998; Jackson and Casanova, 2000). While this domain may be

the minimal fragment this does suggest that potentially there are other domains which are responsible in stimulating nucleotide exchange. Active ARF1 has been shown to recruit the Sec7 domain to the *trans*-Golgi network via interaction with the HDS1 domain of the ARF GEF (Richardson *et al*., 2012). Additionally, N-terminal DCB/HUS domains facilitate membrane activation of ARF1 (Richardson *et al*., 2016). Cohen *et al*. (2007) also demonstrated that ARF GTPases recruit ARNO/Cytohesin GEFs to the plasma membrane by binding via their PH domains. This result suggests that ARF could interact with ARF GEF regions other than the Sec7 domain responsible for nucleotide exchange.

In summary, the human and malarial ARF-GGA3^{GAT} immobilised assays were established and are excellent assays that can be employed for HTS. ARNO^{Sec7} and BIG1^{Sec7} mediated exchange on ARF1 was moderately detectable by the immobilised ARF1-GGA3^{GAT} interaction assay but the attempt to use this assay to clearly demonstrate changes to ARF1 activity in response to a GEF was, so far, unsuccessful. While the effects seen may be an indication that the GEF assays could work but they cannot be employed in launching screening campaigns to find inhibitors to confirm the drug status of ARF1 as the signals detected were not sufficiently robust.

Overall conclusion

In conclusion, the human ARF1 FRET assay can be used to explore the activation status of ARF1 by GEFs and attempt to find inhibitors by launching screening campaigns. However, because of the sub-optimal FRET signals observed for the malarial ARF1 FRET assays, the signals are not robust enough to suggest the exploration of the activation of malarial ARF by GEFs. With the human and malarial ARF1 immobilised $GGA3^{GAT}$ interaction assays, the activation of ARF could be detected but detection of the activation of ARF1 by GEFs was not robust enough to launch screening assays without further optimisation.

Supplementary information

Chapter 3:

Z-factor score (adapted from Zhang *et al*. (1999))

Formula:

$$\text{Z-factor} = 1 - \frac{3(\sigma p - \sigma n)}{|\mu p - \mu n|}$$

Key:

σ_P = standard deviation of the positive control

σ_n = standard deviation of the negative control

μ_p = mean of the positive control

μ_n = mean of the negative control

Interpretation:

Z factor = 1.0 Ideal

1.0 > Z factor > 0.5 Excellent assay

0.0 > Z factor > 0.5 Marginal assay

Z factor < 0 Assay format is not useful

DNA Sequencing confirmation of the pET-28a-$^{N\Delta17}$*Hs*ARF1-CFP and pET-28a-$^{N\Delta17}$*Pf*ARF1-CFP constructs

Human ARF1-CFP plasmid -T7 promoter primer

TTTGTTTAACTTTAAGAAGGAGATATACCATGGGCAGCAGCCRTCATCMYCWTCATCACAGCAGSGGCCTGG
TGCCGCGCGGCAGCCATATGGCTAGCATGCGCATCCTCATGGTGGGCCTGGATGCTGCAGGGAAGACCACGA
TCCTCTACAAGCTTAAGCTGGGTGAGATCGTGACCACCATTCCCACCATAGGCTTCRACGTGGAAACCGTGGA
GTACAAGAACATCAGCTTCACTGTGTGGGACGTGGGTGGCCAGGACAAGATCCGGCCCCTGTGGCGCCACTA
CTTCCAGAACACACAAGGCCTGATCTTCGTGGTGGACAGCAATGACAGAGAGCGTGTGAACGAGGCCCGTGA
GGAGCTCATGAGGATGCTGGCCGAGGACGAGCTCCGGGATGCTGTCCTCCTGGTGTTCGCCAACAAGCAGGA
CCTCCCCAACGCCATGAATGCGGCCGAGATCACAGACAAGCTGGGGCTGCACTCACTACGCCACAGGAACTG
GTACATTCRGGCCACCTGCGCCACCAGCGGCGACGGGCTCTATGAAGGACTGGACTGGCTGTCCAATCAGCTC
CGGAACCAGAAGGGATCCATGGTGAGCAAGGGCGAGGAGCTGTTCACCGGGGTGGTGCCCATCCTGGTCGA
GCTGGACGGCGACGTAAACGGCCACAAGTTCAGCGTGTCCGGCGAGGGCGAGGGCGATGCCACCTACGGCA
AGCTGACCCTGAAGTTCATCTGCACCACCGGCAAGCTGCCCGTGCCCTGGCCCACCCTCGTGACCACCCTGAC
CTGGGGCGTGCAGTGCTTCGCCCGCTACCCCGACCACATGAAGCAGCACGACTTCTTCAAGTCCGCCATGCCC
GAAGGCTACGTCCAGGAGCGCACCATCTTCTTCAAGGACGACGGCAACTACAAGACCCGCGCCGAGGTGAAG
TTCGAGGG

Human ARF1-CFP plasmid-T7-terminator primer

CGGATCTCAGTGGTGGTGGTGGTGGTGCTCGAGTTACTTGTACASCTYGTCCWTGCCGAGAGTGATCCCGGC
GGCGGTCACGAACTCCAGCAGGACCATGTGATCGCGCTTCTCGTTGGGGTCTTTGCTCAGCTTGGACTGGGTG
CTCAGGTAGTGGTTGTCGGGCAKCAGCACGGGGCCGTCGCCGATGGGGGTGTTCTGCTGGTAGTGGTCGGC
GAGCTGCACGCTGCCGTCCTCRATGTTGTGGCGGATCTTGAAGTTGGCCTTGATGCCGTTCTTCTGCTTGTCGG
CGGTGATATAGACGTTGTCGCTGATGGCGTTGTACTCCAGCTTGTGCCCCAGGATGTTGCCGTCCTCCTTGAA
GTCKATGCCCTTCAGCTCGATGCGGTTCACCAGGGTGTCGCCCTCGAACTTCACCTCGGCGCGGGTCTTGTAG
TTGCCGTCGTCCTTGAAGAAGATGGTGCGCTCCTGGACGTAGCCTTCGGGCATGGCGGACTTGAAGAAGTCG
TGCTGCTTCATGTGGTCGGGGTAGCGGGCGAAGCACTGCACGCCCCAGGTCAGGGTGGTCACGAGGGTGGG
CCAGGGCACGGGCAGCTTGCCGGTGGTGCAGATGAACTTCAGGGTCAGCTTGCCGTAGGTGGCATCGCCCTC
GCCCTCGCCGGACACGCTGAACTTGTGGCCGTTTACGTCGCCGTCCAGCTCGACCAGGATGGGCACCACCCCG
GTGAACAGCTCCTCGCCCTTGCTCACCATGGATCCCTTCTGGTTCCGGAGCTGATTGGACAGCCAGTCCAGTCC
TTCATAGAGCCCGTCGCCGCTGGTGGCGCAGGTGGCCTGAATGTACCAGTTCCTGTGGCGTAGTGAGTGCAG
CCCCAGCTTGTCTGTGATCTCGGCCGCATTCATGGCGTTGGGGAGGTCCTGCTTGTTGGCGAACACCA

Figure S36: Human ARF1-CFP plasmid sequencing. The cloned human ARF1-CFP plasmid was sequenced by Inqaba Biotech. The restriction sites are highlighted in yellow. The CFP sequence is highlighted in cyan. The ARF sequence is highlighted in grey. The T7 promoter primer was used to amplify the ARF1 sequence while T7 terminator primer was used to amplify the CFP sequence.

Malarial ARF1-CFP-T7 terminator primer

GCCGGATCTCAGTGGTGGTGGTGGTGGTGCTCGAGTTACTTGTACASCTYGTCCWTGCCGAGAGTGATCCCG
GCGGCGGTCACGAACTCCAGCAGGACCATGTGATCGCGCTTCTCGTTGGGGTCTTTGCTCAGCTTGGACTGGG
TGCTCAGGTAGTGGTTGTCGGGCAKCAGCACGGGGCCGTCGCCGATGGGGGTGTTCTGCTGGTAGTGGTCG
GCGAGCTGCACGCTGCCGTCCTCGATGTTGTGGCGGATCTTGAAGTTGGCCTTGATGCCGTTCTTCTGCTTGTC
GGCGGTGATATAGACGTTGTCGCTGATGGCGTTGTACTCCAGCTTGTGCCCCAGGATGTTGCCGTCCTCCTTG
AAGTCGATGCCCTTCAGCTCGATGCGGTTCACCAGGGTGTCGCCCTCGAACTTCACCTCGGCGCGGGTCTTGT
AGTTGCCGTCGTCCTTGAAGAAGATGGTGCGCTCCTGGACGTAGCCTTCGGGCATGGCGGACTTGAAGAAGT
CGTGCTGCTTCATGTGGTCGGGGTAGCGGGCGAAGCACTGCACGCCCCAGGTCAGGGTGGTCACGAGGGTG
GGCCAGGGCACGGGCAGCTTGCCGGTGGTGCAGATGAACTTCAGGGTCAGCTTGCCGTAGGTGGCATCGCC
CTCGCCCTCGCCGGACACGCTGAACTTGTGGCCGTTTACGTCGCCGTCCAGCTCGACCAGGATGGGCACCACC
CCGGTGAACAGCTCCTCGCCCTTGCTCACCATGGATCCCTTGGCGTTGTTCAGGTGGGTGGTCAGCCAGTCGA
AGCCCTCGTACAGGCCGTCGCCCCTGGTGGCGCAGGTGCTCTGGATGAACCAGTTCCTTTCCCTGATAGTGTT
CAGATGCAGCTTCTCGGTCACCTCGGCTGCGCTCATGGCATTGGGCAGGTCCTGTTTGTTGG

Malarial ARF1-CFP plasmid-T7 promoter primer

TTTTGTTTAACTTTAAGAAGGAGATATACCATGGGCAGCAGCCATCATCMYCATYATCACAGCAGSGGCCTGG
TGCCGCGCGGCAGCCATATGGCTAGCGTGAGAATCCTGRTGGTCGGCCTGGACGCCGCTGGGAAGACTACCA
TTCTGTACAAGGTGAAGCTGGGCGAGGTGGTGACCACAATCCCCACCATCGGCTTCAACGTGGAGACCGTGG
AGTTCAGGAACATCTCCTTCACCGTGTGGGACGTGGGAGGCCAGGACAAGATCAGGCCACTGTGGAGGCACT
ACTACAGCAATACCGACGGGCTGATTTTCGTGGTGGACAGCAACGACAGGGAGAGGATCGACGACGCCAGG
GAGGAGCTGCACAGGATGATTAACGAGGAAGAGCTGAAAGACGCCATTATCCTGGTGTTTGCCAACAAACAG
GACCTGCCCAATGCCATGAGCGCAGCCGAGGTGACCGAGAAGCTGCATCTGAACACTATCAGGGAAAGGAA
CTGGTTCATCCAGAGCACCTGCGCCACCAGGGGCGACGGCCTGTACGAGGGCTTCGACTGGCTGACCACCCA
CCTGAACAACGCCAAGGGATCCATGGTGAGCAAGGGCGAGGAGCTGTTCACCGGGGTGGTGCCCATCCTGG
TCGAGCTGGACGGCGACGTAAACGGCCACAAGTTCAGCGTGTCCGGCGAGGGCGAGGGCGATGCCACCTAC
GGCAAGCTGACCCTGAAGTTCATCTGCACCACCGGCAAGCTGCCCGTGCCCTGGCCCACCCTCGTGACCACCC
TGACCTGGGGCGTGCAGTGCTTCGCCCGCTACCCCGACCACATGAAGCAGCACGACTTCTTCAAGTCCGCCAT
GCCCGAAAGGCTACGTCCAGGAGCGCACCATCTTCTTCAAGGACGACGGCAACTACAAGACCCGCG

Figure S37: Malarial ARF1-CFP plasmid sequencing. The cloned malarial ARF1-CFP plasmid was sequenced by Inqaba Biotech. The restriction sites are highlighted in yellow. The CFP sequence is highlighted in cyan. The ARF sequence is highlighted in grey. The T7 promoter primer was used to amplify the ARF1 sequence while T7 terminator primer was used to amplify the CFP sequence.

Chapter 4:

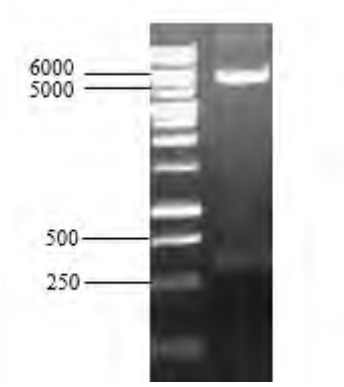

Figure S38: Diagnostic restriction digestion analysis of pET-28a-ARNO^{Sec7} constructs. All the restriction digestion products were run on a 0.8 % (w/v) agarose gel at 95 V for approximately 75 minutes. The DNA bands were stained with ethidium bromide, visualized under UV light and photographed using a ChemiDoc XRS+ gel documentation system (Bio-Rad). For all gels: Lane 1: Promega 1Kb DNA ladder (molecular weights are shown in bp). Lane 2: pET-28a- ARNO^{Sec7} construct double digested with *Nhe*I and *Xho*I.

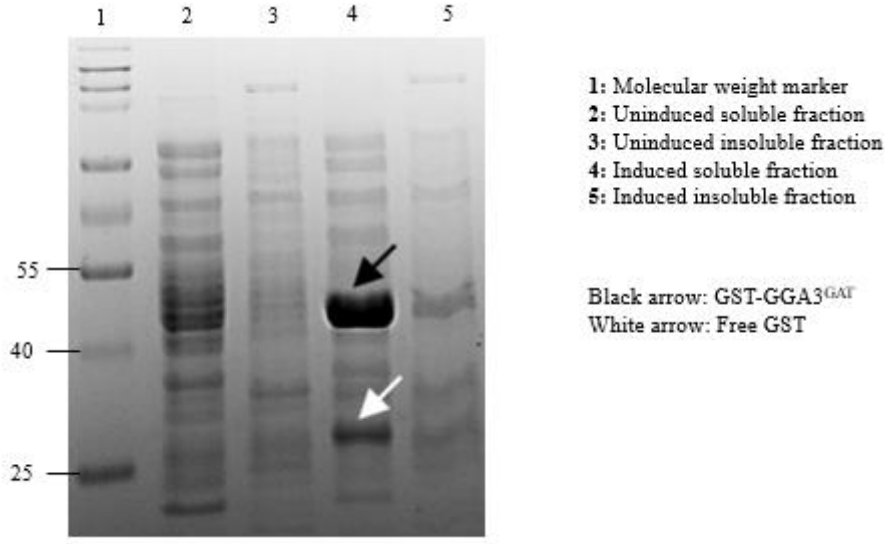

Figure S39: Analytical scale protein expression analysis of GST-GGA3^{GAT}. *E. coli* (T7 Express lysY/I_q) was transformed with pGEX-4T-2/hGGA3^{GAT}. The transformed cells were cultured at 37 °C until the logarithmic growth phase. Protein expression was induced at 37 °C by the addition of IPTG to final concentration of 1.0 mM, while parallel cultures lacking IPTG served as uninduced controls. The uninduced and induced cultures were lysed and soluble and insoluble protein fractions were obtained by centrifugation. All samples were prepared in SDS sample loading buffer and resolved on a 12% SDS- PAGE gel run at 120 V for approximately 1.5 hours. Molecular weight marker (ProSieve QuadColor Protein Marker Fisher Scientific) (molecular weights are shown in kDa).

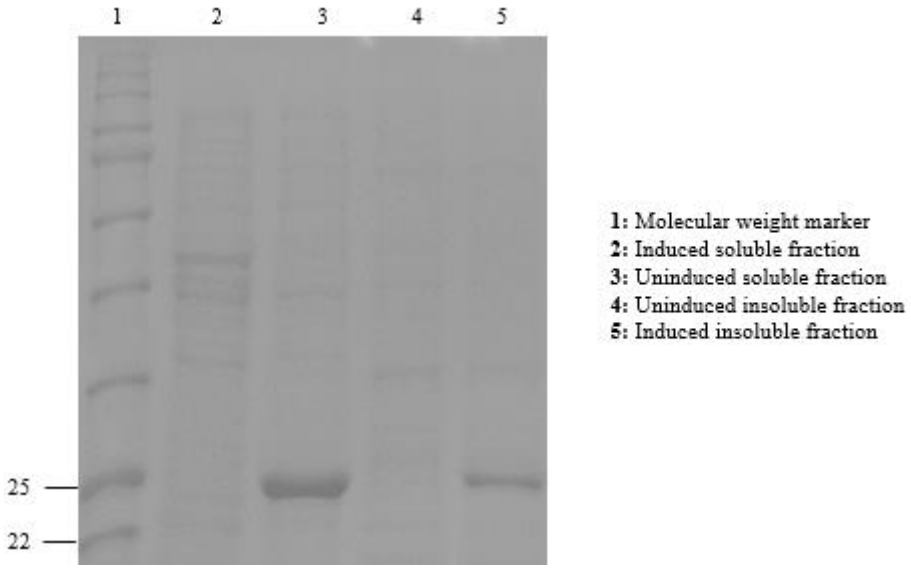

Figure S40: Analytical scale protein expression analysis of ARNO^{Sec7}. *E. coli* (T7 Express lysY/I_q) was transformed with pET-28a-ARNO^{Sec7}. The transformed cells were cultured at 37 °C until the logarithmic growth phase. Protein expression was induced at 37 °C by the addition of IPTG to final concentration of 1.0 mM, while parallel cultures lacking IPTG served as uninduced controls. The uninduced and induced cultures were lysed and soluble and insoluble protein fractions were obtained by centrifugation. All samples were prepared in SDS sample loading buffer and resolved on a 12% SDS- PAGE gel run at 120 V for approximately 1.5 hours. Molecular weight marker (New England Biolabs P7712S) (molecular weights are shown in kDa).

Sequence and secondary structure analysis of the putative *Pf*ARFGEF.

The Sec7 domains of mammalian ARF GEFs consist of a characteristic stretch of 10 sequential alpha helices. The putative *P. falciparum* ARFGEF is unusual in that the sequences encoding helices 1-7 and 8-10 align well with the corresponding regions of human Sec7 domains (alignment of the N-terminal helices 1-7 and C-terminal helices 8-10 with the ARNO Sec7 domain shown in **Figure S41**), but these two stretches of conserved alpha helices are separated by a *P. falciparum*-specific insert of 146 amino acids that is not found in other ARFGEFs. The critical glutamic acid residue required for GEF activity (displacing GDP from ARF1) is conserved in the *P. falciparum* Sec7 domain and – as in ARNO – resides at the start of helix 7 (E1296, highlighted in red). In addition, unlike the ARNO Sec7 domain, the predicted *Pf*ARFGEF Sec7 domain is thought to be BFA sensitive. This was concluded based on a study that found a single point mutation in this region (M1473I in helix 8) conferred resistance of malaria parasites to the parasiticidal effect of BFA (Baumgartner *et al*., 2001). Further evidence for this is the conservation of amino acid residues thought to be critical for BFA binding in the region C-terminal to the 146 amino acid insert (i.e. containing helices 8-10). This is illustrated in the alignment of this region with the corresponding sequence of human BIG1, which is a BFA sensitive GEF (**Figure S42**). The BFA binding residues (YS, M, D and M) are highlighted in green in the BIG1 and malarial sequences. Note that these residues are replaced by FA, M, S and P in BFA-insensitive ARNO (indicated by red letters in **Figure S41**). The alignment of the *P. falciparum* Sec7 domain N-terminal to the 146 amino acid sequence (helices 1-7) with the corresponding region of human BIG1 is also shown.

Alignment: ARNO and *Pf*Sec7 (predicted Sec7 domain of the putative *Pf*ARFGEF)

N-terminal alignment (helices 1-7) (ARNO 51 - 181; PfSec7 1200 – 1314)

```
Length: 130
# Identity:       41/130 (31.5%)
# Similarity:     69/130 (53.1%)
# Gaps:           22/130 (16.9%)
```

Alpha helices are underlined and numbered

```
                                          1          2              3
ARNO      51 --eanegsktlqrnrkmamgrkkfnmdpkkgiqflvenellqntpeeiar  98
               :|:|...::..|    ..:|.|....|..   |:|:|..   .:.:|:
PfSec7  1201 HMKASEIISSVAHN----FSKKHFKHSTKNN---LMEDEYF---VKSMAK  1240
                  1                2                    3
                          4              5              6
ARNO      99 flykgeglnktaigdylgereelnlavlhafvdlheftdlnlvqalrqfl  148
             |:.....|:|..:|:|:..|:.:||  |..:|.|.:|.:|:|:.:||.||
PfSec7  1241 FVRYNPFLDKEFVGEYISHRKNVNL--LKRYVRLFDFCNLSLLSSLRLFL  1288
                          4              5                    6
                                  7
ARNO     149 wsfrlpgeaqkidrmmeafaqryclcnpgvfqs  181
             ..|:||||||.|:|::|.|:    ||   .|.|
PfSec7  1289 RCFKLPGEAQLIERILEHFS----LC---FFYS  1314
                                  7
```

C-terminal alignment (helices 8-10) (ARNO 182 - 270; PfSec7 1461 – 1545)

```
# Length: 89
# Identity:       35/89 (39.3%)
# Similarity:     52/89 (58.4%)
# Gaps:            4/89 ( 4.5%)
```

```
                        8                   9
ARNO     182 tdtcyvlsfavimlntslhnpnvrdkpglerfvamnrgineggdlpeell  231
             :|..::|::::|||||.|||..|::|..||.|:..|||||.|.::....|
PfSec7  1461 SDVIFILTYSIIMLNTDLHNNQVKNKMKLEEFIKNNRGINNGKNIDRIYL  1510
                        8                   9
                10
ARNO     232 rnlydsirnepfkipeddgndlthtffnpdregwllklg  270
             .|||:.|.||..|:..:..|    |:.|.|:...||...
PfSec7  1511 ENLYNCILNEEIKLFSNTQN----TYTNDDQYWKLLDQK  1545
                10
```

Figure S41: Conservation of glutamic residue and residues required for BFA sensitivity.

The putative *P. falciparum* ARF GEF N-terminal protein sequence (PlasmoDB code: PF3D7_1442900) was aligned with the human ARNO N-terminal protein sequence (Accession code: NP_004219.3) using MUSCLE pairwise alignment tool. The N-terminal sequences house the conserved glutamic residue required for GEF activity (*highlighted in red*). The C-terminals of the putative *P. falciparum* ARF GEF and ARNO were aligned. The residues required for BFA sensitivity are signposted using red text on the putative *P. falciparum* ARF GEF sequence and the residues that render ARNO BFA insensitive are shown with red text on the human ARNO sequence.

Alignment: BIG1 and *Pf*Sec7

C-terminal alignment

```
# Length: 74
# Identity:     33/74 (44.6%)
# Similarity:   45/74 (60.8%)

BIG1        1 adtayvlaysiimlttdlhspqvknkmtkeqyikmnrgindskdlpeeyl     50
              :|..::|.||||||.||||:.||||||..|::||.|||||:.|::...||
PfSec7      1 SDVIFILTYSIIMLNTDLHNNQVKNKMKLEEFIKNNRGINNGKNIDRIYL     50

BIG1       51 saiyneiagkki------------     62
              ..:||.|..::|
PfSec7     51 ENLYNCILNEEIKLFSNTQNTYTN     74
```

Figure S42: Residues required for BFA sensitivity. The putative *P. falciparum* ARF GEF C-terminal protein sequence (PlasmoDB code: PF3D7_1442900) was aligned with the human BIG1 C-terminal protein sequence (Accession code: NP_006412.2) using MUSCLE pairwise alignment tool. The C-terminals of the putative *P. falciparum* ARF GEF and BIG1 were aligned. The residues required for BFA sensitivity are highlighted green on the putative *P. falciparum* ARF GEF sequence and human BIG1 sequence.

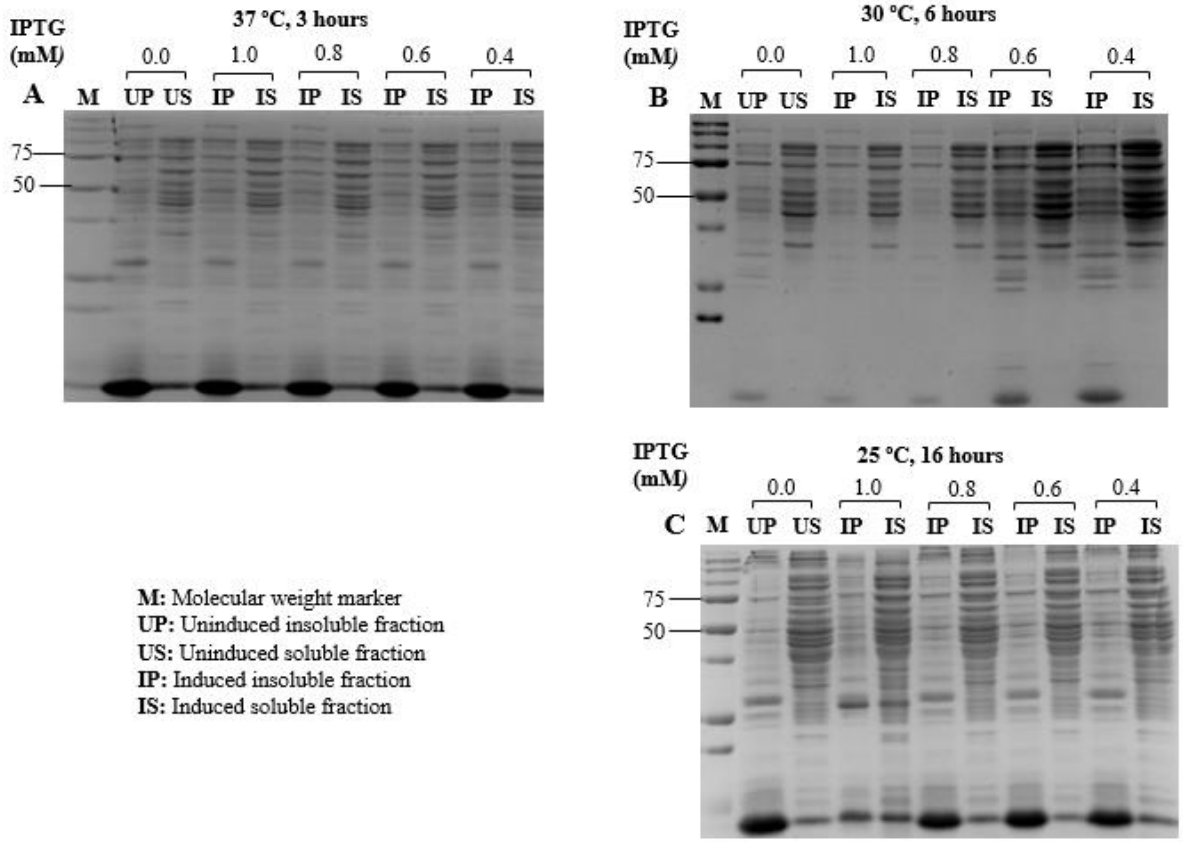

Figure S43: Analytical scale protein expression analysis of *Pf*ARFGEF^{Sec7} in T7 Express LysY/I$_q$ competent cells. *E. coli* (T7 Express lysY/I$_q$) was transformed with pET-28a-*Pf*ARFGEF^{Sec7}. The transformed cells were cultured at 37 °C until the logarithmic growth phase. Protein expression was induced at different temperatures by the addition of IPTG to final concentrations ranging from 0.4- 1.0 mM, while parallel cultures lacking IPTG served as uninduced controls. The uninduced and induced cultures were lysed and soluble and insoluble protein fractions were obtained by centrifugation. All samples were prepared in SDS sample loading buffer and resolved on a 12% SDS- PAGE gel run at 100 V for approximately 1.5 hours. For all gels: **M:** Molecular weight marker: Precision Plus protein standard (Bio-Rad #161-0373) (molecular weights are shown in kDa) **A: Expression at 37 ºC. B: Expression at 30 ºC. C: Expression at 25 ºC.**

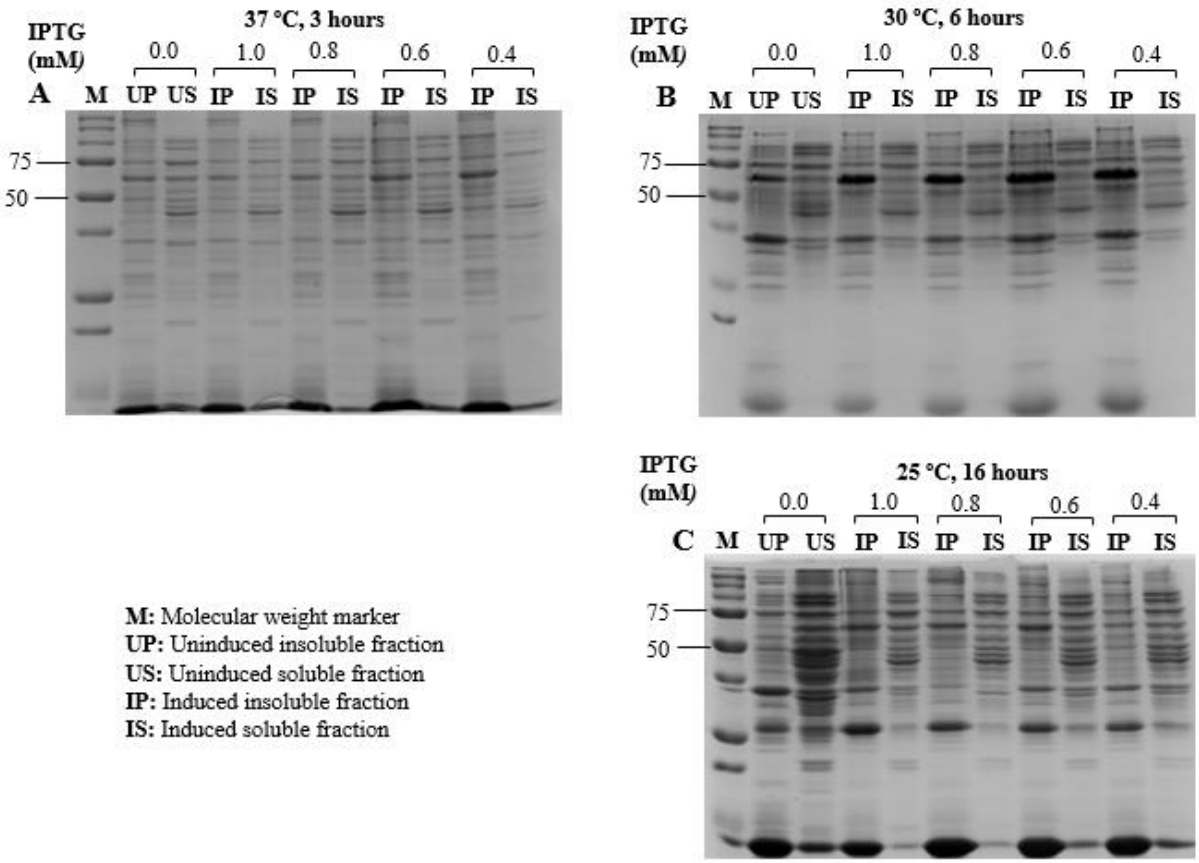

Figure S44: Analytical scale protein expression analysis of *Pf*ARFGEF^{Sec7} in XL-1 Blue competent cells. *E. coli* (XL-1 Blue) was transformed with pET-28a-*Pf*ARFGEF^{Sec7}. The transformed cells were cultured at 37 °C until the logarithmic growth phase. Protein expression was induced at different temperatures by the addition of IPTG to final concentrations ranging from 0.4- 1.0 mM, while parallel cultures lacking IPTG served as uninduced controls. The uninduced and induced cultures were lysed and soluble and insoluble protein fractions were obtained by centrifugation. All samples were prepared in SDS sample loading buffer and resolved on a 12% SDS- PAGE gel run at 100 V for approximately 1.5 hours. For all gels: **M:** Molecular weight marker: Precision Plus protein standard (Bio-Rad #161-0373) (molecular weights are shown in kDa) **A: Expression at 37 ºC. B: Expression at 30 ºC. C: Expression at 25 ºC.**

References

Abraham, B. G., Sarkisyan, K. S., Mishin, A. S., Santala, V., Tkachenko, N. V., & Karp, M. (2015). Fluorescent protein based FRET pairs with improved dynamic range for fluorescence lifetime measurements. *PloS one*, *10*(8), e0134436.

Ahn, J. Y., Hu, Y., Kroll, T. G., Allard, P., & Ye, K. (2004). PIKE-A is amplified in human cancers and prevents apoptosis by up-regulating Akt. *Proceedings of the National Academy of Sciences*, *101*(18), 6993-6998.

Ai, H. W., Henderson, J. N., Remington, S. J., & Campbell, R. E. (2006). Directed evolution of a monomeric, bright and photostable version of Clavularia cyan fluorescent protein: structural characterization and applications in fluorescence imaging. *Biochemical Journal*, *400*(3), 531-540.

Aikawa, Y., & Martin, T. F. (2003). ARF6 regulates a plasma membrane pool of phosphatidylinositol (4, 5) bisphosphate required for regulated exocytosis. *The Journal of cell biology*, *162*(4), 647-659.

Altan-Bonnet, N., Phair, R. D., Polishchuk, R. S., Weigert, R., & Lippincott-Schwartz, J. (2003). A role for Arf1 in mitotic Golgi disassembly, chromosome segregation, and cytokinesis. *Proceedings of the National Academy of Sciences*, *100*(23), 13314-13319.

Anadu, N. O., Davisson, V. J., & Cushman, M. (2006). Synthesis and anticancer activity of brefeldin A ester derivatives. *Journal of medicinal chemistry*, *49*(13), 3897-3905.

Antonny, B., Beraud-Dufour, S., Chardin, P., & Chabre, M. (1997). N-terminal hydrophobic residues of the G-protein ADP-ribosylation factor-1 insert into membrane phospholipids upon GDP to GTP exchange. *Biochemistry*, *36*(15), 4675-4684.

Bai, M., Gad, H., Turacchio, G., Cocucci, E., Yang, J. S., Li, J., ... & Collawn, J. F. (2011). ARFGAP1 promotes AP-2-dependent endocytosis. *Nature cell biology*, *13*(5), 559-567.

Bajar, B. T., Wang, E. S., Lam, A. J., Kim, B. B., Jacobs, C. L., Howe, E. S., ... & Chu, J. (2016). Improving brightness and photostability of green and red fluorescent proteins for live cell imaging and FRET reporting. *Scientific reports*, *6*, 20889.

Bar-Sagi, D., & Hall, A. (2000). Ras and Rho GTPases: a family reunion. *Cell*, *103*(2), 227-238.

Bauer, A., & Brönstrup, M. (2014). Industrial natural product chemistry for drug discovery and development. *Natural product reports*, *31*(1), 35-60.

Baumgartner, F., Wiek, S., Paprotka, K., Zauner, S., & Lingelbach, K. (2001). A point mutation in an unusual Sec7 domain is linked to brefeldin A resistance in a Plasmodium falciparum line generated by drug selection. *Molecular microbiology*, *41*(5), 1151-1158.

Beck, R., Ravet, M., Wieland, F. T., & Cassel, D. (2009). The COPI system: molecular mechanisms and function. *FEBS letters*, *583*(17), 2701-2709.

Belov, G. A., Altan-Bonnet, N., Kovtunovych, G., Jackson, C. L., Lippincott-Schwartz, J., & Ehrenfeld, E. (2007). Hijacking components of the cellular secretory pathway for replication of poliovirus RNA. *Journal of virology*, *81*(2), 558-567.

Belov, G. A., Feng, Q., Nikovics, K., Jackson, C. L., & Ehrenfeld, E. (2008). A critical role of a cellular membrane traffic protein in poliovirus RNA replication. *PLoS pathogens*, *4*(11).

Belov, G. A., Habbersett, C., Franco, D., & Ehrenfeld, E. (2007). Activation of cellular Arf GTPases by poliovirus protein 3CD correlates with virus replication. *Journal of virology*, *81*(17), 9259-9267.

Béraud-Dufour, S., Robineau, S., Chardin, P., Paris, S., Chabre, M., Cherfils, J., & Antonny, B. (1998). A glutamic finger in the guanine nucleotide exchange factor ARNO displaces Mg2+ and the β-phosphate to destabilize GDP on ARF1. *The EMBO journal*, *17*(13), 3651-3659.

Béraud-Dufour, S., Robineau, S., Chardin, P., Paris, S., Chabre, M., Cherfils, J., & Antonny, B. (1998). A glutamic finger in the guanine nucleotide exchange factor ARNO displaces Mg2+ and the β-phosphate to destabilize GDP on ARF1. *The EMBO journal*, *17*(13), 3651-3659.

Bergmans, H.E.N., Van Die, I.M., Hoekstra, W.P.M. (1981). Transformation in Escherichia coli: stages in the process. J. Bacteriol. 146, 564–570.

Berney, C., & Danuser, G. (2003). FRET or no FRET: a quantitative comparison. *Biophysical journal*, *84*(6), 3992–4010.

Bertolin, G., Sizaire, F., Déméautis, C., Chapuis, C., Mérola, F., Erard, M., & Tramier, M. (2019). Optimized FRET Pairs and Quantification Approaches To Detect the Activation of Aurora Kinase A at Mitosis. *ACS sensors*, *4*(8), 2018-2027.

Betz, S. F., Schnuchel, A., Wang, H., Olejniczak, E. T., Meadows, R. P., Lipsky, B. P., ... & Fesik, S. W. (1998). Solution structure of the cytohesin-1 (B2–1) Sec7 domain and its interaction with the GTPase ADP ribosylation factor 1. *Proceedings of the National Academy of Sciences*, *95*(14), 7909-7914.

Bharti, S., Inoue, H., Bharti, K., Hirsch, D. S., Nie, Z., Yoon, H. Y., ... & Randazzo, P. A. (2007). Src-dependent phosphorylation of ASAP1 regulates podosomes. *Molecular and cellular biology*, *27*(23), 8271-8283.

Bi, X., Schmitz, A., Hayallah, A. M., Song, J. N., & Famulok, M. (2008). Affinity-Based Labeling of Cytohesins with a Bifunctional SecinH3 Photoaffinity Probe. *Angewandte Chemie International Edition*, *47*(49), 9565-9568.

Bienz, K., Egger, D., Rasser, Y., & Bossart, W. (1983). Intracellular distribution of poliovirus proteins and the induction of virus-specific cytoplasmic structures. *Virology*, *131*(1), 39-48.

Bigay, J., & Antonny, B. (2005). Real-Time Assays for the Assembly–Disassembly Cycle of COP Coats on Liposomes of Defined Size. *Methods in enzymology*, *404*, 95-107.

Bigay, J., Casella, J. F., Drin, G., Mesmin, B., & Antonny, B. (2005). ArfGAP1 responds to membrane curvature through the folding of a lipid packing sensor motif. *The EMBO journal*, *24*(13), 2244-2253.

Bill, A., Blockus, H., Stumpfe, D., Bajorath, J., Schmitz, A., & Famulok, M. (2011). A homogeneous fluorescence resonance energy transfer system for monitoring the activation of a protein switch in real time. *Journal of the American Chemical Society*, *133*(21), 8372-8379.

Bill, A., Schmitz, A., König, K., Heukamp, L. C., Hannam, J. S., & Famulok, M. (2012). Anti-proliferative effect of cytohesin inhibition in gefitinib-resistant lung cancer cells. *PloS one*, *7*(7).

Boal, F., Guetzoyan, L., Sessions, R. B., Zeghouf, M., Spooner, R. A., Lord, J. M., ... & Stephens, D. J. (2010). LG186: An inhibitor of GBF1 function that causes Golgi disassembly in human and canine cells. *Traffic*, *11*(12), 1537-1551.

Boman, A. L. (2001). GGA proteins: new players in the sorting game. *Journal of cell science*, *114*(19), 3413-3418.

Bonifacino, J. S., & Glick, B. S. (2004). The mechanisms of vesicle budding and fusion. *cell*, *116*(2), 153-166.

Bonifacino, J. S., & Lippincott-Schwartz, J. (2003). Coat proteins: shaping membrane transport. *Nature reviews Molecular cell biology*, *4*(5), 409-414.

Bos, J. L., Rehmann, H., & Wittinghofer, A. (2007). GEFs and GAPs: critical elements in the control of small G proteins. *Cell*, *129*(5), 865-877.

Bottanelli, F., Kilian, N., Ernst, A. M., Rivera-Molina, F., Schroeder, L. K., Kromann, E. B., ... & Bewersdorf, J. (2017). A novel physiological role for ARF1 in the formation of bidirectional tubules from the Golgi. *Molecular biology of the cell*, *28*(12), 1676-1687.

Boulay, P. L., Cotton, M., Melançon, P., & Claing, A. (2008). ADP-ribosylation factor 1 controls the activation of the phosphatidylinositol 3-kinase pathway to regulate epidermal growth factor-dependent growth and migration of breast cancer cells. *Journal of Biological Chemistry*, *283*(52), 36425-36434.

Boulay, P. L., Schlienger, S., Lewis-Saravalli, S., Vitale, N., Ferbeyre, G., & Claing, A. (2011). ARF1 controls proliferation of breast cancer cells by regulating the retinoblastoma protein. *Oncogene*, *30*(36), 3846.

Bourgoin, S. G., & El Azreq, M. A. (2012). Small inhibitors of ADP-ribosylation factor activation and function in mammalian cells. *World Journal of Pharmacology*, *1*(4), 55-64.

Bourne, H. R., Sanders, D. A., & McCormick, F. (1991). The GTPase superfamily: conserved structure and molecular mechanism. Nature, 349(6305), 117.

Bouvet, S., Golinelli-Cohen, M. P., Contremoulins, V., & Jackson, C. L. (2013). Targeting of the Arf-GEF GBF1 to lipid droplets and Golgi membranes. *J Cell Sci*, *126*(20), 4794-4805.

Brown, F. D., Rozelle, A. L., Yin, H. L., Balla, T., & Donaldson, J. G. (2001). Phosphatidylinositol 4, 5-bisphosphate and Arf6-regulated membrane traffic. *The Journal of cell biology*, *154*(5), 1007-1018.

Bui, Q. T., Golinelli-Cohen, M. P., & Jackson, C. L. (2009). Large Arf1 guanine nucleotide exchange factors: evolution, domain structure, and roles in membrane trafficking and human disease. *Molecular Genetics and Genomics*, *282*(4), 329-350.

Cai, H., Reinisch, K., & Ferro-Novick, S. (2007). Coats, tethers, Rabs, and SNAREs work together to mediate the intracellular destination of a transport vesicle. *Developmental cell*, *12*(5), 671-682.

Carter, A. P. (2013). Crystal clear insights into how the dynein motor moves. *Journal of cell science*, *126*(3), 705-713.

Casalou, C., Faustino, A., & Barral, D. C. (2016). Arf proteins in cancer cell migration. *Small GTPases*, *7*(4), 270-282.

Casanova, J. E. (2007). Regulation of Arf activation: the Sec7 family of guanine nucleotide exchange factors. *Traffic*, *8*(11), 1476-1485.

Chan, S. H., Huang, W. C., Chang, J. W., Chang, K. J., Kuo, W. H., Wang, M. Y., ... & Jang, T. H. (2014). MicroRNA-149 targets GIT1 to suppress integrin signaling and breast cancer metastasis. *Oncogene*, *33*(36), 4496-4507.

Chaudhuri, S., Kumar, A., & Berger, M. (2001). Association of ARF and Rabs with complement receptor Type-1 storage vesicles in human neutrophils. *Journal of leukocyte biology*, *70*(4), 669-676.

Chavrier, P., & Goud, B. (1999). The role of ARF and Rab GTPases in membrane transport. *Current opinion in cell biology*, *11*(4), 466-475.

Chen, H., Puhl, H. L., 3rd, Koushik, S. V., Vogel, S. S., & Ikeda, S. R. (2006). Measurement of FRET efficiency and ratio of donor to acceptor concentration in living cells. *Biophysical journal*, *91*(5), L39–L41.

Chen, P. W., Jian, X., Heissler, S. M., Le, K., Luo, R., Jenkins, L. M., ... & Randazzo, P. A. (2016). The Arf GTPase-activating protein, ASAP1, binds nonmuscle myosin 2A to control remodeling of the actomyosin network. *Journal of Biological Chemistry*, *291*(14), 7517-7526.

Chen, X., Zehnbauer, B., Gnirke, A., & Kwok, P. Y. (1997). Fluorescence energy transfer detection as a homogeneous DNA diagnostic method. *Proceedings of the National Academy of Sciences of the United States of America*, *94*(20), 10756–10761.

Chen, Y., Mauldin, J. P., Day, R. N., & Periasamy, A. (2007). Characterization of spectral FRET imaging microscopy for monitoring nuclear protein interactions. *Journal of microscopy*, *228*(Pt 2), 139–152.

Cherfils, J. (2014). Arf GTPases and their effectors: assembling multivalent membrane-binding platforms. *Current opinion in structural biology*, *29*, 67-76.

Cherfils, J., & Chardin, P. (1999). GEFs: structural basis for their activation of small GTP-binding proteins. *Trends in biochemical sciences*, *24*(8), 306-311.

Cherfils, J., & Zeghouf, M. (2013). Regulation of small gtpases by gefs, gaps, and gdis. *Physiological reviews*, *93*(1), 269-309.

Cherfils, J., Menetrey, J., Mathieu, M., Le Bras, G., Robineau, S., Béraud-Dufour, S., ... & Chardin, P. (1998). Structure of the Sec7 domain of the Arf exchange factor ARNO. *Nature*, *392*(6671), 101.

Chu, J., Haynes, R. D., Corbel, S. Y., Li, P., González-González, E., Burg, J. S., ... & Davidson, M. W. (2014). Non-invasive intravital imaging of cellular differentiation with a bright red-excitable fluorescent protein. *Nature methods*, *11*(5), 572.

Claude, A., Zhao, B. P., Kuziemsky, C. E., Dahan, S., Berger, S. J., Yan, J. P., ... & Melançon, P. (1999). GBF1: A novel Golgi-associated BFA-resistant guanine nucleotide exchange factor that displays specificity for ADP-ribosylation factor 5. *The Journal of cell biology*, *146*(1), 71-84.

Clegg, R. M. (1995). Fluorescence resonance energy transfer. *Current opinion in biotechnology*, *6*(1), 103-110.

Cohen, L. A., & Donaldson, J. G. (2010). Analysis of Arf GTP-binding protein function in cells. *Current protocols in cell biology*, *48*(1), 14-12.

Cohen, L. A., Honda, A., Varnai, P., Brown, F. D., Balla, T., & Donaldson, J. G. (2007). Active Arf6 recruits ARNO/cytohesin GEFs to the PM by binding their PH domains. *Molecular biology of the cell*, *18*(6), 2244-2253.

Cohen, S. N., Chang, A. C., Boyer, H. W., & Helling, R. B. (1973). Construction of biologically functional bacterial plasmids in vitro. *Proceedings of the National Academy of Sciences*, *70*(11), 3240-3244.

Collins, B. M., Watson, P. J., & Owen, D. J. (2003). The structure of the GGA1-GAT domain reveals the molecular basis for ARF binding and membrane association of GGAs. Developmental cell, 4(3), 321-332.

Collins, B. M., Watson, P. J., & Owen, D. J. (2003). The structure of the GGA1-GAT domain reveals the molecular basis for ARF binding and membrane association of GGAs. *Developmental cell*, *4*(3), 321-332.

Cox, R., Mason-Gamer, R. J., Jackson, C. L., & Segev, N. (2004). Phylogenetic analysis of Sec7-domain-containing Arf nucleotide exchangers. *Molecular biology of the cell*, *15*(4), 1487–1505.

Cragg, G. M., Grothaus, P. G., & Newman, D. J. (2009). Impact of natural products on developing new anti-cancer agents. *Chemical reviews*, *109*(7), 3012-3043.

Cranfill, P. J., Sell, B. R., Baird, M. A., Allen, J. R., Lavagnino, Z., de Gruiter, H. M., … Piston, D. W. (2016). Quantitative assessment of fluorescent proteins. *Nature methods*, *13*(7), 557–562.

Crary, J. L., & Haldar, K. (1992). Brefeldin A inhibits protein secretion and parasite maturation in the ring stage of Plasmodium falciparum. *Molecular and biochemical parasitology*, *53*(1-2), 185-192.

Cukierman, E., Huber, I., Rotman, M., & Cassel, D. (1995). The ARF1 GTPase-activating protein: zinc finger motif and Golgi complex localization. *Science*, *270*(5244), 1999-2002.

Davis, J. E., Xie, X., Guo, J., Huang, W., Chu, W. M., Huang, S., ... & Wu, G. (2016). ARF1 promotes prostate tumorigenesis via targeting oncogenic MAPK signaling. *Oncotarget*, *7*(26), 39834.

Day, R. N., & Davidson, M. W. (2012). Fluorescent proteins for FRET microscopy: monitoring protein interactions in living cells. *BioEssays : news and reviews in molecular, cellular and developmental biology*, *34*(5), 341–350.

De Matteis, M. A., & Godi, A. (2004). Protein–lipid interactions in membrane trafficking at the Golgi complex. *Biochimica et Biophysica Acta (BBA)-Biomembranes*, *1666*(1-2), 264-274.

Dickinson, M. E., Bearman, G., Tille, S., Lansford, R., & Fraser, S. E. (2001). Multi-spectral imaging and linear unmixing add a whole new dimension to laser scanning fluorescence microscopy. *Biotechniques*, *31*(6), 1272-1278.

DiPilato, L. M., Cheng, X., & Zhang, J. (2004). Fluorescent indicators of cAMP and Epac activation reveal differential dynamics of cAMP signaling within discrete subcellular compartments. *Proceedings of the National Academy of Sciences*, *101*(47), 16513-16518.

Donaldson, J. G., & Jackson, C. L. (2000). Regulators and effectors of the ARF GTPases. *Current opinion in cell biology*, *12*(4), 475-482.

Donaldson, J. G., & Jackson, C. L. (2011). ARF family G proteins and their regulators: roles in membrane transport, development and disease. *Nature reviews Molecular cell biology*, *12*(6), 362-375.

Drin, G., Morello, V., Casella, J. F., Gounon, P., & Antonny, B. (2008). Asymmetric tethering of flat and curved lipid membranes by a golgin. *Science*, *320*(5876), 670-673.

D'Souza, R. S., & Casanova, J. E. (2016). The BRAG/IQSec family of Arf GEFs. *Small GTPases*, *7*(4), 257-264.

D'Souza-Schorey, C., & Chavrier, P. (2006). ARF proteins: roles in membrane traffic and beyond. *Nature reviews Molecular cell biology*, *7*(5), 347.

D'Souza-Schorey, C., & Chavrier, P. (2006). ARF proteins: roles in membrane traffic and beyond. *Nature reviews Molecular cell biology*, *7*(5), 347-358.

Ducharme, N. A., & Bickel, P. E. (2008). Minireview: lipid droplets in lipogenesis and lipolysis. *Endocrinology*, *149*(3), 942-949.

Dunphy, J. L., Ye, K., & Casanova, J. E. (2007). Nuclear functions of the Arf guanine nucleotide exchange factor BRAG2. *Traffic*, *8*(6), 661-672.

Elliott, S. J., Krejany, E. O., Mellies, J. L., Robins-Browne, R. M., Sasakawa, C., & Kaper, J. B. (2001). EspG, a novel type III system-secreted protein from enteropathogenic Escherichia coli with similarities to VirA of Shigella flexneri. *Infection and Immunity*, *69*(6), 4027-4033.

Ellong, E. N., Soni, K. G., Bui, Q. T., Sougrat, R., Golinelli-Cohen, M. P., & Jackson, C. L. (2011). Interaction between the triglyceride lipase ATGL and the Arf1 activator GBF1. *PloS one*, *6*(7).

Erard, M., Fredj, A., Pasquier, H., Beltolngar, D. B., Bousmah, Y., Derrien, V., ... & Merola, F. (2013). Minimum set of mutations needed to optimize cyan fluorescent proteins for live cell imaging. *Molecular BioSystems*, *9*(2), 258-267.

Fan, C., Tian, Y., Miao, Y., Lin, X., Zhang, X., Jiang, G., ... & Wang, E. (2014). ASAP3 expression in non-small cell lung cancer: association with cancer development and patients' clinical outcome. *Tumor Biology*, *35*(2), 1489-1494.

Fensome, A., Whatmore, J., Morgan, C., Jones, D., & Cockcroft, S. (1998). ADP-ribosylation factor and Rho proteins mediate fMLP-dependent activation of phospholipase D in human neutrophils. *Journal of Biological Chemistry*, *273*(21), 13157-13164.

Ferland, R. J., Batiz, L. F., Neal, J., Lian, G., Bundock, E., Lu, J., ... & Brown, P. J. (2009). Disruption of neural progenitors along the ventricular and subventricular zones in periventricular heterotopia. *Human molecular genetics*, *18*(3), 497-516.

Filonov, G. S., Piatkevich, K. D., Ting, L. M., Zhang, J., Kim, K., & Verkhusha, V. V. (2011). Bright and stable near-infrared fluorescent protein for in vivo imaging. *Nature biotechnology*, *29*(8), 757.

Flisiak, S., Zeeh, J. C., Guibert, B., Cherfils, J., & Zeghouf, M. (2008). An Arf1 GTPase mutant with different responses to GEF inhibitors. *Biochemical and biophysical research communications*, *377*(1), 156-160.

Förster, T. (1965). Delocalized excitation and excitation transfer. *Modern Quantum Chemistry. (3)*, 93–137.

Franco, M., Chardin, P., Chabre, M., & Paris, S. (1995). Myristoylation of ADP-ribosylation factor 1 facilitates nucleotide exchange at physiological Mg levels. *Journal of Biological Chemistry*, *270*(3), 1337-1341.

Franco, M., Chardin, P., Chabre, M., & Paris, S. (1996). Myristoylation-facilitated binding of the G protein ARF1 to membrane phospholipids is required for its activation by a soluble nucleotide exchange factor. *Journal of Biological Chemistry*, *271*(3), 1573-1578.

Frank, S., Upender, S., Hansen, S. H., & Casanova, J. E. (1998). ARNO is a guanine nucleotide exchange factor for ADP-ribosylation factor 6. *Journal of Biological Chemistry*, *273*(1), 23-27.

Frigerio, G., Grimsey, N., Dale, M., Majoul, I., & Duden, R. (2007). Two human ARFGAPs associated with COP-I-coated vesicles. *Traffic*, *8*(11), 1644-1655.

Fuss, B., Becker, T., Zinke, I., & Hoch, M. (2006). The cytohesin Steppke is essential for insulin signalling in Drosophila. *Nature*, *444*(7121), 945-948.

Gamara, J., Chouinard, F., Davis, L., Aoudjit, F., & Bourgoin, S. G. (2015). Regulators and effectors of Arf GTPases in neutrophils. *Journal of immunology research*, *2015*.

Ganesan, S., Ameer-beg, S. M., Ng, T. T., Vojnovic, B., & Wouters, F. S. (2006). A dark yellow fluorescent protein (YFP)-based Resonance Energy-Accepting Chromoprotein (REACh) for Förster resonance energy transfer with GFP. *Proceedings of the National Academy of Sciences*, *103*(11), 4089-4094.

Gazina, E. V., Mackenzie, J. M., Gorrell, R. J., & Anderson, D. A. (2002). Differential requirements for COPI coats in formation of replication complexes among three genera of Picornaviridae. *Journal of virology*, *76*(21), 11113-11122.

Gehart, H., Goginashvili, A., Beck, R., Morvan, J., Erbs, E., Formentini, I., ... & Ricci, R. (2012). The BAR domain protein Arfaptin-1 controls secretory granule biogenesis at the trans-Golgi network. *Developmental cell*, *23*(4), 756-768.

Germer, K., Leonard, M., & Zhang, X. (2013). RNA aptamers and their therapeutic and diagnostic applications. *International journal of biochemistry and molecular biology*, *4*(1), 27.

Gillingham, A. K., & Munro, S. (2007). The small G proteins of the Arf family and their regulators. *Annu. Rev. Cell Dev. Biol.*, *23*, 579-611.

Gillingham, A. K., Tong, A. H. Y., Boone, C., & Munro, S. (2004). The GTPase Arf1p and the ER to Golgi cargo receptor Erv14p cooperate to recruit the golgin Rud3p to the cis-Golgi. *The Journal of cell biology*, *167*(2), 281-292.

Goedhart, J., von Stetten, D., Noirclerc-Savoye, M., Lelimousin, M., Joosen, L., Hink, M. A., … Royant, A. (2012). Structure-guided evolution of cyan fluorescent proteins towards a quantum yield of 93%. *Nature communications*, *3*, 751.

Goldberg, J. (1998). Structural basis for activation of ARF GTPase: mechanisms of guanine nucleotide exchange and GTP–myristoyl switching. *Cell*, *95*(2), 237-248.

Greasley, S. E., Jhoti, H., Teahan, C., Solari, R., Fensome, A., Thomas, G. M., ... & Bax, B. (1995). The structure of rat ADP-ribosylation factor-1 (ARF-1) complexed to GDP determined from two different crystal forms. *Nature structural biology*, *2*(9), 797-806.

Griesbeck, O., Baird, G. S., Campbell, R. E., Zacharias, D. A., & Tsien, R. Y. (2001). Reducing the environmental sensitivity of yellow fluorescent protein mechanism and applications. *Journal of Biological Chemistry*, *276*(31), 29188-29194.

Grünberg, R., Burnier, J. V., Ferrar, T., Beltran-Sastre, V., Stricher, F., Van Der Sloot, A. M., ... & Serrano, L. (2013). Engineering of weak helper interactions for high-efficiency FRET probes. *Nature methods*, *10*(10), 1021.

Gu, F., & Gruenberg, J. (2000). ARF1 regulates pH-dependent COP functions in the early endocytic pathway. *Journal of Biological Chemistry*, *275*(11), 8154-8160.

Habig, W. H., Pabst, M. J., & Jakoby, W. B. (1974). Glutathione S-transferases the first enzymatic step in mercapturic acid formation. *Journal of biological Chemistry*, *249*(22), 7130-7139.

Hafner, M., Schmitz, A., Grüne, I., Srivatsan, S. G., Paul, B., Kolanus, W., ... & Famulok, M. (2006). Inhibition of cytohesins by SecinH3 leads to hepatic insulin resistance. *Nature*, *444*(7121), 941.

Hahn, I., Fuss, B., Peters, A., Werner, T., Sieberg, A., Gosejacob, D., & Hoch, M. (2013). The Drosophila Arf GEF Steppke controls MAPK activation in EGFR signaling. *Journal of cell science*, *126*(11), 2470-2479.

Hamilton, G., & Sanabria, H. (2019). Multiparameter fluorescence spectroscopy of single molecules. In *Spectroscopy and Dynamics of Single Molecules* (pp. 269-333). Elsevier.

Hayashi, M., Taniguchi, S., Ishizuka, Y., Kim, H. S., Wataya, Y., Yamamoto, A., & Moriyama, Y. (2001). A Homologue of N-Ethylmaleimide-sensitive Factor in the Malaria ParasitePlasmodium falciparum Is Exported and Localized in Vesicular Structures in the Cytoplasm of Infected Erythrocytes in the Brefeldin A-sensitive Pathway. *Journal of Biological Chemistry*, *276*(18), 15249-15255.

He, B., Wang, Y., Zheng, Y., Chen, W., & Zhu, Q. (2013). Synthesis and cytotoxic evaluation of acylated brefeldin a derivatives as potential anticancer agents. *Chemical biology & drug design*, *82*(3), 307-316.

He, L., Gao, L., Shay, C., Lang, L., Lv, F., & Teng, Y. (2019). Histone deacetylase inhibitors suppress aggressiveness of head and neck squamous cell carcinoma via histone acetylation-independent blockade of the EGFR-Arf1 axis. *Journal of Experimental & Clinical Cancer Research*, *38*(1), 84.

Heim, R., & Tsien, R. Y. (1996). Engineering green fluorescent protein for improved brightness, longer wavelengths and fluorescence resonance energy transfer. *Current biology*, *6*(2), 178-182.

Heim, R., Prasher, D. C., & Tsien, R. Y. (1994). Wavelength mutations and posttranslational autoxidation of green fluorescent protein. *Proceedings of the National Academy of Sciences*, *91*(26), 12501-12504.

Hirsch, D. S., Stanley, K. T., Chen, L. X., Jacques, K. M., Puertollano, R., & Randazzo, P. A. (2003). Arf regulates interaction of GGA with mannose-6-phosphate receptor. *Traffic*, *4*(1), 26-35.

Hoffman, G. R., Nassar, N., Oswald, R. E., & Cerione, R. A. (1998). Fluoride activation of the Rho family GTP-binding protein Cdc42Hs. *Journal of Biological Chemistry*, *273*(8), 4392-4399.

Hong, J. X., Lee, F. J. S., Patton, W. A., Lin, C. Y., Moss, J., & Vaughan, M. (1998). Phospholipid-and GTP-dependent activation of cholera toxin and phospholipase D by human ADP-ribosylation factor-like protein 1 (HARL1). *Journal of Biological Chemistry*, *273*(25), 15872-15876.

Hongu, T., Yamauchi, Y., Funakoshi, Y., Katagiri, N., Ohbayashi, N., & Kanaho, Y. (2016). Pathological functions of the small GTPase Arf6 in cancer progression: Tumor angiogenesis and metastasis. *Small GTPases*, *7*(2), 47-53.

Hou, T., Yang, C., Tong, C., Zhang, H., Xiao, J., & Li, J. (2014). Overexpression of ASAP1 is associated with poor prognosis in epithelial ovarian cancer. *International journal of clinical and experimental pathology*, *7*(1), 280.

Hsu, N. Y., Ilnytska, O., Belov, G., Santiana, M., Chen, Y. H., Takvorian, P. M., ... & Cameron, C. E. (2010). Viral reorganization of the secretory pathway generates distinct organelles for RNA replication. *Cell*, *141*(5), 799-811.

Huang, B., Bates, M., & Zhuang, X. (2009). Super-resolution fluorescence microscopy. *Annual review of biochemistry*, *78*, 993-1016.

Inoue, H., & Randazzo, P. A. (2007). Arf GAPs and their interacting proteins. *Traffic*, *8*(11), 1465-1475.

Isabet, T., Montagnac, G., Regazzoni, K., Raynal, B., El Khadali, F., England, P., ... & Ménétrey, J. (2009). The structural basis of Arf effector specificity: the crystal structure of ARF6 in a complex with JIP4. *The EMBO journal*, *28*(18), 2835-2845.

Ishizaki, R., Shin, H. W., Mitsuhashi, H., & Nakayama, K. (2008). Redundant roles of BIG2 and BIG1, guanine-nucleotide exchange factors for ADP-ribosylation factors in membrane traffic between the trans-Golgi network and endosomes. *Molecular biology of the cell*, *19*(6), 2650-2660.

Ismail, S. A., Vetter, I. R., Sot, B., & Wittinghofer, A. (2010). The structure of an Arf-ArfGAP complex reveals a Ca2+ regulatory mechanism. *Cell*, *141*(5), 812-821.

Jackson, C. L. (2018). Activators and Effectors of the Small G Protein Arf1 in Regulation of Golgi Dynamics During the Cell Division Cycle. *Frontiers in Cell and Developmental Biology*, *6*, 29.

Jackson, C. L. (2018). Activators and effectors of the small G protein Arf1 in regulation of Golgi dynamics during the cell division cycle. *Frontiers in Cell and Developmental Biology*, *6*, 29.

Jackson, C. L., & Bouvet, S. (2014). Arfs at a glance.

Jackson, C. L., & Casanova, J. E. (2000). Turning on ARF: the Sec7 family of guanine-nucleotide-exchange factors. *Trends in cell biology*, *10*(2), 60-67.

Jackson, C. L., & Casanova, J. E. (2000). Turning on ARF: the Sec7 family of guanine-nucleotide-exchange factors. *Trends in cell biology*, *10*(2), 60-67.

Jian, X., Brown, P., Schuck, P., Gruschus, J. M., Balbo, A., Hinshaw, J. E., & Randazzo, P. A. (2009). Autoinhibition of Arf GTPase-activating protein activity by the BAR domain in ASAP1. *Journal of Biological Chemistry*, *284*(3), 1652-1663.

Jiménez-Sánchez, A. (2016). Coevolution of RAC small GTPases and their regulators GEF proteins. *Evolutionary Bioinformatics*, *12*, EBO-S38031.

Junnila, S., Kokkola, A., Karjalainen-Lindsberg, M. L., Puolakkainen, P., & Monni, O. (2010). Genome-wide gene copy number and expression analysis of primary gastric tumors and gastric cancer cell lines. *BMC cancer*, *10*(1), 73.

Kahn, R. A., & Gilman, A. G. (1984). Purification of a protein cofactor required for ADP-ribosylation of the stimulatory regulatory component of adenylate cyclase by cholera toxin. *Journal of Biological Chemistry*, *259*(10), 6228-6234.

Kahn, R. A., Bruford, E., Inoue, H., Logsdon Jr, J. M., Nie, Z., Premont, R. T., ... & Cassel, D. (2008). Consensus nomenclature for the human ArfGAP domain-containing proteins. *The Journal of cell biology*, *182*(6), 1039-1044.

Kahn, R. A., Cherfils, J., Elias, M., Lovering, R. C., Munro, S., & Schurmann, A. (2006). Nomenclature for the human Arf family of GTP-binding proteins: ARF, ARL, and SAR proteins. *The Journal of cell biology*, *172*(5), 645-650.

Kawai, H., Suzuki, T., Kobayashi, T., Sakurai, H., Ohata, H., Honda, K., ... & Nakamura, R. (2005). Simultaneous real-time detection of initiator-and effector-caspase activation by double fluorescence resonance energy transfer analysis. *Journal of pharmacological sciences*, *97*(3), 361-368.

Kawamoto, K., Yoshida, Y., Tamaki, H., Torii, S., Shinotsuka, C., Yamashina, S., & Nakayama, K. (2002). GBF1, a guanine nucleotide exchange factor for ADP-ribosylation factors, is localized to the cis-Golgi and involved in membrane association of the COPI coat. *Traffic*, *3*(7), 483-495.

Khan, A. R., & Ménétrey, J. (2013). Structural biology of Arf and Rab GTPases' effector recruitment and specificity. *Structure*, *21*(8), 1284-1297.

Klebe, C., Prinz, H., Wittinghofer, A., & Goody, R. S. (1995). The kinetic mechanism of Ran-nucleotide exchange catalyzed by RCC1. *Biochemistry*, *34*(39), 12543-12552.

Koronakis, V., Hume, P. J., Humphreys, D., Liu, T., Hørning, O., Jensen, O. N., & McGhie, E. J. (2011). WAVE regulatory complex activation by cooperating GTPases Arf and Rac1. *Proceedings of the National Academy of Sciences*, *108*(35), 14449-14454.

Koushik, S. V., Chen, H., Thaler, C., Puhl III, H. L., & Vogel, S. S. (2006). Cerulean, Venus, and VenusY67C FRET reference standards. *Biophysical journal*, *91*(12), L99-L101.

Kremers, G. J., Goedhart, J., van Munster, E. B., & Gadella, T. W. (2006). Cyan and yellow super fluorescent proteins with improved brightness, protein folding, and FRET Förster radius. *Biochemistry*, *45*(21), 6570-6580.

Kremers, G. J., Hazelwood, K. L., Murphy, C. S., Davidson, M. W., & Piston, D. W. (2009). Photoconversion in orange and red fluorescent proteins. *Nature methods*, *6*(5), 355–358.

Kumari, S., & Mayor, S. (2008). ARF1 is directly involved in dynamin-independent endocytosis. *Nature cell biology*, *10*(1), 30-41.

Laemmli, U.K., 1970. Cleavage of structural proteins during the assembly of the head of bacteriophage T4. *Nature*, 15;227(5259):680-685.

Lai, C. C., Boguski, M., Broek, D., & Powers, S. (1993). Influence of guanine nucleotides on complex formation between Ras and CDC25 proteins. *Molecular and cellular biology*, *13*(3), 1345-1352.

Lakowicz, J. R. (Ed.). (2013). *Principles of fluorescence spectroscopy*. Springer Science & Business Media.

Lam, A. J., St-Pierre, F., Gong, Y., Marshall, J. D., Cranfill, P. J., Baird, M. A., ... & Tsien, R. Y. (2012). Improving FRET dynamic range with bright green and red fluorescent proteins. *Nature methods*, *9*(10), 1005.

Lang, L., Shay, C., Zhao, X., & Teng, Y. (2017). Combined targeting of Arf1 and Ras potentiates anticancer activity for prostate cancer therapeutics. *Journal of Experimental & Clinical Cancer Research*, *36*(1), 112.

Langhans, M., Marcote, M. J., Pimpl, P., Virgili-López, G., Robinson, D. G., & Aniento, F. (2008). In vivo trafficking and localization of p24 proteins in plant cells. *Traffic*, *9*(5), 770-785.

Langille, S. E., Patki, V., Klarlund, J. K., Buxton, J. M., Holik, J. J., Chawla, A., ... & Czech, M. P. (1999). ADP-ribosylation factor 6 as a target of guanine nucleotide exchange factor GRP1. *Journal of Biological Chemistry*, *274*(38), 27099-27104.

Lanke, K. H., van der Schaar, H. M., Belov, G. A., Feng, Q., Duijsings, D., Jackson, C. L., ... & van Kuppeveld, F. J. (2009). GBF1, a guanine nucleotide exchange factor for Arf, is crucial for coxsackievirus B3 RNA replication. *Journal of virology*, *83*(22), 11940-11949.

Laverdant, J., Marcillac, W. D., Barthou, C., Chinh, V. D., Schwob, C., Coolen, L., … Maître, A. (2011). Experimental Determination of the Fluorescence Quantum Yield of Semiconductor Nanocrystals. *Materials (Basel, Switzerland)*, *4*(7), 1182–1193.

Lawley, T. D., & Walker, A. W. (2013). Intestinal colonization resistance. *Immunology*, *138*(1), 1-11.

Lebensohn, A. M., & Kirschner, M. W. (2009). Activation of the WAVE complex by coincident signals controls actin assembly. *Molecular cell*, *36*(3), 512-524.

Leber, W., Skippen, A., Fivelman, Q. L., Bowyer, P. W., Cockcroft, S., & Baker, D. A. (2009). A unique phosphatidylinositol 4-phosphate 5-kinase is activated by ADP-ribosylation factor in Plasmodium falciparum. *International journal for parasitology*, *39*(6), 645-653.

Lecoq, J., & Schnitzer, M. J. (2011). An infrared fluorescent protein for deeper imaging. Nature biotechnology, 29(8), 715.

Lee, F. J. S., Patton, W. A., Lin, C. Y., Moss, J., Vaughan, M., Goldman, N. D., & Syin, C. (1997). Identification and characterization of an ADP-ribosylation factor in Plasmodium falciparum. *Molecular & Biochemical Parasitology*, *2*(87), 217-223.

Lee, M. C., Miller, E. A., Goldberg, J., Orci, L., & Schekman, R. (2004). Bi-directional protein transport between the ER and Golgi. *Annu. Rev. Cell Dev. Biol.*, *20*, 87-123.

Lee, S. Y., Yang, J. S., Hong, W., Premont, R. T., & Hsu, V. W. (2005). ARFGAP1 plays a central role in coupling COPI cargo sorting with vesicle formation. *The Journal of cell biology*, *168*(2), 281-290.

Li, J., Malaby, A. W., Famulok, M., Sabe, H., Lambright, D. G., & Hsu, V. W. (2012). Grp1 plays a key role in linking insulin signaling to glut4 recycling. *Developmental cell*, *22*(6), 1286-1298.

Li, M., Tian, L., Yao, H., Lu, J., Ge, J., Guo, Y., ... & Xiao, H. (2014). ASAP1 mediates the invasive phenotype of human laryngeal squamous cell carcinoma to affect survival prognosis. *Oncology reports*, *31*(6), 2676-2682.

Lin, D., Watahiki, A., Bayani, J., Zhang, F., Liu, L., Ling, V., ... & Gout, P. W. (2008). ASAP1, a gene at 8q24, is associated with prostate cancer metastasis. *Cancer research*, *68*(11), 4352-4359.

Liu, X., Hu, Y., Hao, C., Rempel, S. A., & Ye, K. (2007). PIKE-A is a proto-oncogene promoting cell growth, transformation and invasion. *Oncogene*, *26*(34), 4918-4927.

Liu, Y., Kahn, R. A., & Prestegard, J. H. (2009). Structure and membrane interaction of myristoylated ARF1. *Structure*, *17*(1), 79-87.

Liu, Y., Kahn, R. A., & Prestegard, J. H. (2010). Dynamic structure of membrane-anchored Arf• GTP. *Nature structural & molecular biology*, *17*(7), 876.

Macia, E., Chabre, M., & Franco, M. (2001). Specificities for the small G proteins ARF1 and ARF6 of the guanine nucleotide exchange factors ARNO and EFA6. *Journal of Biological Chemistry*, *276*(27), 24925-24930.

Majoul, I., Straub, M., Hell, S. W., Duden, R., & Soeling, H. D. (2001). KDEL-cargo regulates interactions between proteins involved in COPI vesicle traffic: measurements in living cells using FRET. *Developmental cell*, *1*(1), 139-153.

Malkani, N., & Schmid, J. A. (2011). Some secrets of fluorescent proteins: distinct bleaching in various mounting fluids and photoactivation of cyan fluorescent proteins at YFP-excitation. *PloS one*, *6*(4), e18586.

Man, Z., Kondo, Y., Koga, H., Umino, H., Nakayama, K., & Shin, H. W. (2011). Arfaptins are localized to the trans-Golgi by interaction with Arl1, but not Arfs. *Journal of Biological Chemistry*, *286*(13), 11569-11578.

Mannervik, B., Helena Danielson, U., & Ketterer, B. (1988). Glutathione transferases—structure and catalytic activit. *Critical Reviews in Biochemistry*, *23*(3), 283-337.

Manolea, F., Claude, A., Chun, J., Rosas, J., & Melançon, P. (2008). Distinct functions for Arf guanine nucleotide exchange factors at the Golgi complex: GBF1 and BIGs are required for assembly and maintenance of the Golgi stack and trans-Golgi network, respectively. *Molecular biology of the cell*, *19*(2), 523-535.

Mao, L., Li, N., Guo, Y., Xu, X., Gao, L., Xu, Y., ... & Liu, W. (2013). AMPK phosphorylates GBF1 for mitotic Golgi disassembly. *Journal of cell science*, *126*(6), 1498-1505.

Markwardt ML, Kremers G-J, Kraft CA, Ray K, Cranfill PJC, Wilson KA, Day RN, Wachter RM, Davidson MW, Rizzo MA (2011). An improved cerulean fluorescent protein with enhanced brightness and reduced reversible photoswitching. PLoS One *6*, e17896.

Mastop, M., Bindels, D. S., Shaner, N. C., Postma, M., Gadella, T. W., & Goedhart, J. (2017). Characterization of a spectrally diverse set of fluorescent proteins as FRET acceptors for mTurquoise2. *Scientific reports*, *7*(1), 1-18.

Matto, M., Sklan, E. H., David, N., Melamed-Book, N., Casanova, J. E., Glenn, J. S., & Aroeti, B. (2011). Role for ADP ribosylation factor 1 in the regulation of hepatitis C virus replication. *Journal of virology*, *85*(2), 946-956.

Mayer, G., Blind, M., Nagel, W., Böhm, T., Knorr, T., Jackson, C. L., ... & Famulok, M. (2001). Controlling small guanine–nucleotide-exchange factor function through cytoplasmic RNA intramers. *Proceedings of the National Academy of Sciences*, *98*(9), 4961-4965.

Mena, M. A., Treynor, T. P., Mayo, S. L., & Daugherty, P. S. (2006). Blue fluorescent proteins with enhanced brightness and photostability from a structurally targeted library. *Nature biotechnology*, *24*(12), 1569-1571.

Ménétrey, J., Macia, E., Pasqualato, S., Franco, M., & Cherfils, J. (2000). Structure of Arf6–GDP suggests a basis for guanine nucleotide exchange factors specificity. *Nature structural biology*, *7*(6), 466-469.

Mesmin, B., Drin, G., Levi, S., Rawet, M., Cassel, D., Bigay, J., & Antonny, B. (2007). Two lipid-packing sensor motifs contribute to the sensitivity of ArfGAP1 to membrane curvature. *Biochemistry*, *46*(7), 1779-1790.

Meyers, J. A., Sanchez, D. A. V. I. D., Elwell, L. P., & Falkow, S. T. A. N. L. E. Y. (1976). Simple agarose gel electrophoretic method for the identification and characterization of plasmid deoxyribonucleic acid. *Journal of Bacteriology*, *127*(3), 1529-1537.

Mittal, R., Ahmadian, M. R., Goody, R. S., & Wittinghofer, A. (1996). Formation of a transition-state analog of the Ras GTPase reaction by Ras· GDP, tetrafluoroaluminate, and GTPase-activating proteins. *Science*, *273*(5271), 115-117.

Miyawaki, A. (2011). Development of probes for cellular functions using fluorescent proteins and fluorescence resonance energy transfer. Annual review of biochemistry, 80, 357-373.

Miyawaki, A., Llopis, J., Heim, R., McCaffery, J. M., Adams, J. A., Ikura, M., & Tsien, R. Y. (1997). Fluorescent indicators for Ca 2+ based on green fluorescent proteins and calmodulin. *Nature*, *388*(6645), 882.

Molina, S., Sanz, M. A., Madan, V., Ventoso, I., Castelló, A., & Carrasco, L. (2007). Differential inhibition of cellular and Sindbis virus translation by brefeldin A. *Virology*, *363*(2), 430-436.

Morohashi, Y., Balklava, Z., Ball, M., Hughes, H., & Lowe, M. (2010). Phosphorylation and membrane dissociation of the ARF exchange factor GBF1 in mitosis. *Biochemical Journal*, *427*(3), 401-412.

Mossessova, E., Corpina, R. A., & Goldberg, J. (2003). Crystal structure of ARF1• Sec7 complexed with Brefeldin A and its implications for the guanine nucleotide exchange mechanism. *Molecular cell*, *12*(6), 1403-1411.

Mossessova, E., Gulbis, J. M., & Goldberg, J. (1998). Structure of the guanine nucleotide exchange factor Sec7 domain of human arno and analysis of the interaction with ARF GTPase. *Cell*, *92*(3), 415-423.

Mouratou, B., Biou, V., Joubert, A., Cohen, J., Shields, D. J., Geldner, N., ... & Cherfils, J. (2005). The domain architecture of large guanine nucleotide exchange factors for the small GTP-binding protein Arf. *BMC genomics*, *6*(1), 20.

Müller, T., Stein, U., Poletti, A., Garzia, L., Rothley, M., Plaumann, D., ... & Pankratz, M. (2010). ASAP1 promotes tumor cell motility and invasiveness, stimulates metastasis formation in vivo, and correlates with poor survival in colorectal cancer patients. *Oncogene*, *29*(16), 2393-2403.

Mullis, K., Faloona, F., Scharf, S., Saiki, R. K., Horn, G. T., & Erlich, H. (1986, January). Specific enzymatic amplification of DNA in vitro: the polymerase chain reaction. In *Cold Spring Harbor symposia on quantitative biology* (Vol. 51, pp. 263-273). Cold Spring Harbor Laboratory Press.

Murakoshi, H., & Shibata, A. C. (2017). ShadowY: a dark yellow fluorescent protein for FLIM-based FRET measurement. *Scientific reports*, *7*(1), 1-10.

Murakoshi, H., Lee, S. J., & Yasuda, R. (2008). Highly sensitive and quantitative FRET–FLIM imaging in single dendritic spines using improved non-radiative YFP. *Brain cell biology*, *36*(1-4), 31-42.

Murakoshi, H., Shibata, A. C., Nakahata, Y., & Nabekura, J. (2015). A dark green fluorescent protein as an acceptor for measurement of Förster resonance energy transfer. *Scientific reports*, *5*, 15334.

Nalla, A. K., Williams, T. F., Collins, C. P., Rae, D. T., & Trobridge, G. D. (2016). Lentiviral vector-mediated insertional mutagenesis screen identifies genes that influence androgen independent prostate cancer progression and predict clinical outcome. *Molecular carcinogenesis*, *55*(11), 1761-1771.

Natsume, W., Tanabe, K., Kon, S., Yoshida, N., Watanabe, T., Torii, T., & Satake, M. (2006). Smap2, a novel arf gtpase-activating protein, interacts with clathrin and clathrin assembly protein and functions on the ap-1–positive early endosome/trans-golgi network. *Molecular biology of the cell*, *17*(6), 2592-2603.

Nguyen, A. W., & Daugherty, P. S. (2005). Evolutionary optimization of fluorescent proteins for intracellular FRET. *Nature biotechnology*, *23*(3), 355.

Nie, Z., & Randazzo, P. A. (2006). Arf GAPs and membrane traffic. *Journal of cell science*, *119*(7), 1203-1211.

Nie, Z., Hirsch, D. S., & Randazzo, P. A. (2003). Arf and its many interactors. *Current opinion in cell biology*, *15*(4), 396-404.

Niu, T. K., Pfeifer, A. C., Lippincott-Schwartz, J., & Jackson, C. L. (2005). Dynamics of GBF1, a Brefeldin A-sensitive Arf1 exchange factor at the Golgi. *Molecular biology of the cell*, *16*(3), 1213-1222.

Ogun, S. A., & Holder, A. A. (1994). Plasmodium yoelii: brefeldin A-sensitive processing of proteins targeted to the rhoptries. *Experimental parasitology*, *79*(3), 270-278.

Oh, S. J., & Santy, L. C. (2010). Differential effects of cytohesins 2 and 3 on β1 integrin recycling. *Journal of Biological Chemistry*, *285*(19), 14610-14616.

Ohashi, Y., Iijima, H., Yamaotsu, N., Yamazaki, K., Sato, S., Okamura, M., ... & Yamori, T. (2012). AMF-26, a novel inhibitor of the Golgi system, targeting ADP-ribosylation factor 1 (Arf1) with potential for cancer therapy. *Journal of Biological Chemistry*, *287*(6), 3885-3897.

Ohashi, Y., Okamura, M., Hirosawa, A., Tamaki, N., Akatsuka, A., Wu, K. M., ... & Dan, S. (2016). M-COPA, a Golgi disruptor, inhibits cell surface expression of MET protein and exhibits antitumor activity against MET-addicted gastric cancers. *Cancer research*, *76*(13), 3895-3903.

Onodera, Y., Hashimoto, S., Hashimoto, A., Morishige, M., Mazaki, Y., Yamada, A., ... & Wada, H. (2005). Expression of AMAP1, an ArfGAP, provides novel targets to inhibit breast cancer invasive activities. *The EMBO journal*, *24*(5), 963-973.

Pacheco-Rodriguez, G., Moss, J., & Vaughan, M. (2002). BIG1 and BIG2: brefeldin A-inhibited guanine nucleotide-exchange proteins for ADP-ribosylation factors. *Methods in enzymology*, *345*, 397.

Padilla, P. I., Pacheco-Rodriguez, G., Moss, J., & Vaughan, M. (2004). Nuclear localization and molecular partners of BIG1, a brefeldin A-inhibited guanine nucleotide-exchange protein for ADP-ribosylation factors. *Proceedings of the National Academy of Sciences*, *101*(9), 2752-2757.

Padilla, P. I., Uhart, M., Pacheco-Rodriguez, G., Peculis, B. A., Moss, J., & Vaughan, M. (2008). Association of guanine nucleotide-exchange protein BIG1 in HepG2 cell nuclei with nucleolin, U3 snoRNA, and fibrillarin. *Proceedings of the National Academy of Sciences*, *105*(9), 3357-3361.

Pan, H., Yu, J., Zhang, L., Carpenter, A., Zhu, H., Li, L., ... & Yuan, J. (2008). A novel small molecule regulator of guanine nucleotide exchange activity of the ADP-ribosylation factor and golgi membrane trafficking. *Journal of Biological Chemistry*, *283*(45), 31087-31096.

Pan, T., Sun, J., Hu, J., Hu, Y., Zhou, J., Chen, Z., ... & Zhang, S. (2014). Cytohesins/ARNO: the function in colorectal cancer cells. *PLoS One*, *9*(3).

Pan, T., Sun, J., Zhou, J., Fu, Z., Hu, Y., Zheng, S., & Zhang, S. (2013). Function and mode of action of cytohesins in the epidermal growth factor pathway in colorectal cancer cells. *Oncology letters*, *5*(2), 521-526.

Panda, D., Das, A., Dinh, P. X., Subramaniam, S., Nayak, D., Barrows, N. J., ... & Pattnaik, A. K. (2011). RNAi screening reveals requirement for host cell secretory pathway in infection by diverse families of negative-strand RNA viruses. *Proceedings of the National Academy of Sciences*, *108*(47), 19036-19041.

Paris, S., Béraud-Dufour, S., Robineau, S., Bigay, J., Antonny, B., Chabre, M., & Chardin, P. (1997). Role of protein-phospholipid interactions in the activation of ARF1 by the guanine nucleotide exchange factor Arno. Journal of Biological Chemistry, 272(35), 22221-22226.

Pasqualato, S., Renault, L., & Cherfils, J. (2002). Arf, Arl, Arp and Sar proteins: a family of GTP-binding proteins with a structural device for 'front–back'communication. *EMBO reports*, *3*(11), 1035-1041.

Pauloin, A., Adenot, P., Hue-Beauvais, C., & Chanat, E. (2016). The perilipin-2 (adipophilin) coat of cytosolic lipid droplets is regulated by an Arf1-dependent mechanism in HC11 mouse mammary epithelial cells. *Cell biology international*, *40*(2), 143-155.

Peng, H., Dara, L., Li, T. W., Zheng, Y., Yang, H., Tomasi, M. L., ... & Lu, S. C. (2013). MAT2B-GIT1 interplay activates MEK1/ERK 1 and 2 to induce growth in human liver and colon cancer. *Hepatology*, *57*(6), 2299-2313.

Peurois, F., Veyron, S., Ferrandez, Y., Ladid, I., Benabdi, S., Zeghouf, M., ... & Cherfils, J. (2017). Characterization of the activation of small GTPases by their GEFs on membranes using artificial membrane tethering. *Biochemical Journal*, *474*(7), 1259-1272.

Peyroche, A., Antonny, B., Robineau, S., Acker, J., Cherfils, J., & Jackson, C. L. (1999). Brefeldin A acts to stabilize an abortive ARF–GDP–Sec7 domain protein complex: involvement of specific residues of the Sec7 domain. *Molecular cell*, *3*(3), 275-285.

Piatkevich, K. D., Malashkevich, V. N., Almo, S. C., & Verkhusha, V. V. (2010). Engineering ESPT pathways based on structural analysis of LSSmKate red fluorescent proteins with large Stokes shift. *Journal of the American Chemical Society*, *132*(31), 10762-10770.

Piston, D. W., & Kremers, G. J. (2007). Fluorescent protein FRET: the good, the bad and the ugly. *Trends in biochemical sciences*, *32*(9), 407-414.

Prieto-Dominguez, N., Parnell, C., & Teng, Y. (2019). Drugging the small GTPase pathways in cancer treatment: promises and challenges. *Cells*, *8*(3), 255.

Puertollano, R., Randazzo, P. A., Presley, J. F., Hartnell, L. M., & Bonifacino, J. S. (2001). The GGAs promote ARF-dependent recruitment of clathrin to the TGN. *Cell*, *105*(1), 93-102.

Randazzo, P. A., & Hirsch, D. S. (2004). Arf GAPs: multifunctional proteins that regulate membrane traffic and actin remodelling. *Cellular signalling*, *16*(4), 401-413.

Randazzo, P. A., Andrade, J., Miura, K., Brown, M. T., Long, Y. Q., Stauffer, S., ... & Cooper, J. A. (2000). The Arf GTPase-activating protein ASAP1 regulates the actin cytoskeleton. *Proceedings of the National Academy of Sciences*, *97*(8), 4011-4016.

Randazzo, P. A., Inoue, H., & Bharti, S. (2007). Arf GAPs as regulators of the actin cytoskeleton. *Biology of the Cell*, *99*(10), 583-600.

Raychaudhuri, S., & Prinz, W. A. (2010). The diverse functions of oxysterol-binding proteins. *Annual review of cell and developmental biology*, *26*, 157-177.

Ren, X., & Hurley, J. H. (2010). VHS domains of ESCRT-0 cooperate in high-avidity binding to polyubiquitinated cargo. *The EMBO journal*, *29*(6), 1045-1054.

Renault, L., Guibert, B., & Cherfils, J. (2003). Structural snapshots of the mechanism and inhibition of a guanine nucleotide exchange factor. *Nature*, *426*(6966), 525.

Reviriego-Mendoza, M. M., & Santy, L. C. (2015). The cytohesin guanosine exchange factors (GEF s) are required to promote HGF-mediated renal recovery after acute kidney injury (AKI) in mice. *Physiological reports*, *3*(6), e12442.

Richardson, B. C., & Fromme, J. C. (2015). Biochemical methods for studying kinetic regulation of Arf1 activation by Sec7. In *Methods in cell biology* (Vol. 130, pp. 101-126). Academic Press.

Richardson, B. C., Halaby, S. L., Gustafson, M. A., & Fromme, J. C. (2016). The Sec7 N-terminal regulatory domains facilitate membrane-proximal activation of the Arf1 GTPase. *Elife*, *5*, e12411.

Richardson, B. C., McDonold, C. M., & Fromme, J. C. (2012). The Sec7 Arf-GEF is recruited to the trans-Golgi network by positive feedback. Developmental cell, 22(4), 799-810.

Ríos, R. M., Sanchís, A., Tassin, A. M., Fedriani, C., & Bornens, M. (2004). GMAP-210 recruits γ-tubulin complexes to cis-Golgi membranes and is required for Golgi ribbon formation. *Cell*, *118*(3), 323-335.

Sáenz, J. B., Sun, W. J., Chang, J. W., Li, J., Bursulaya, B., Gray, N. S., & Haslam, D. B. (2009). Golgicide A reveals essential roles for GBF1 in Golgi assembly and function. *Nature chemical biology*, *5*(3), 157.

Salonen, A. N. N. E., Ahola, T. E. R. O., & Kääriäinen, L. E. E. V. I. (2004). Viral RNA replication in association with cellular membranes. In *Membrane trafficking in viral replication* (pp. 139-173). Springer, Berlin, Heidelberg.

Sangar, F., Schreurs, A. S., Umaña-Diaz, C., Clapéron, A., Desbois-Mouthon, C., Calmel, C., ... & Praz, F. (2014). Involvement of small ArfGAP1 (SMAP1), a novel Arf6-specific GTPase-activating protein, in microsatellite instability oncogenesis. *Oncogene*, *33*(21), 2758-2767.

Santy, L. C., & Casanova, J. E. (2001). Activation of ARF6 by ARNO stimulates epithelial cell migration through downstream activation of both Rac1 and phospholipase D. *The Journal of cell biology*, *154*(3), 599-610.

Santy, L. C., Ravichandran, K. S., & Casanova, J. E. (2005). The DOCK180/Elmo complex couples ARNO-mediated Arf6 activation to the downstream activation of Rac1. *Current biology*, *15*(19), 1749-1754.

Sattarzadeh, A., Saberianfar, R., Zipfel, W. R., Menassa, R., & Hanson, M. R. (2015). Green to red photoconversion of GFP for protein tracking in vivo. *Scientific reports*, *5*(1), 1-8.

Sausville, E. A., Duncan, K. L., Senderowicz, A., Plowman, J., Randazzo, P. A., Kahn, R., ... & Grever, M. R. (1996). Antiproliferative effect in vitro and antitumor activity in vivo of brefeldin A. *CANCER JOURNAL-NEW YORK-*, *2*, 52-58.

Schlienger, S., Ramirez, R. A. M., & Claing, A. (2015). ARF1 regulates adhesion of MDA-MB-231 invasive breast cancer cells through formation of focal adhesions. *Cellular signalling*, *27*(3), 403-415.

Seehafer, K., Rominger, F., Helmchen, G., Langhans, M., Robinson, D. G., zata, B., ... & Klein, C. D. (2013). Synthesis and biological properties of novel brefeldin A analogues. *Journal of medicinal chemistry*, *56*(14), 5872-5884.

Sekar, R. B., & Periasamy, A. (2003). Fluorescence resonance energy transfer (FRET) microscopy imaging of live cell protein localizations. *The Journal of cell biology*, *160*(5), 629–633.

Selvin, P. R. (2000). The renaissance of fluorescence resonance energy transfer. *Nature structural biology*, *7*(9), 730-734.

Shaner, N. C., Lambert, G. G., Chammas, A., Ni, Y., Cranfill, P. J., Baird, M. A., ... & Davidson, M. W. (2013). A bright monomeric green fluorescent protein derived from Branchiostoma lanceolatum. *Nature methods*, *10*(5), 407.

Shcherbakova, D. M., Hink, M. A., Joosen, L., Gadella, T. W., & Verkhusha, V. V. (2012). An orange fluorescent protein with a large Stokes shift for single-excitation multicolor FCCS and FRET imaging. *Journal of the American Chemical Society*, *134*(18), 7913-7923.

Shcherbo, D., Murphy, C. S., Ermakova, G. V., Solovieva, E. A., Chepurnykh, T. V., Shcheglov, A. S., ... & Lukyanov, S. (2009). Far-red fluorescent tags for protein imaging in living tissues. *Biochemical journal*, *418*(3), 567-574.

Sheen, V. L., Ganesh, V. S., Topcu, M., Sebire, G., Bodell, A., Hill, R. S., ... & Guerrini, R. (2004). Mutations in ARFGEF2 implicate vesicle trafficking in neural progenitor proliferation and migration in the human cerebral cortex. *Nature genetics*, *36*(1), 69-76.

Shiba, Y., & Randazzo, P. A. (2012). ArfGAP1 function in COPI mediated membrane traffic: currently debated models and comparison to other coat-binding ArfGAPs.

Shiba, Y., & Randazzo, P. A. (2014). ArfGAPs: key regulators for receptor sorting. *Receptors & clinical investigation*, *1*(5), e158.

Shiba, Y., Katoh, Y., Shiba, T., Yoshino, K., Takatsu, H., Kobayashi, H., ... & Nakayama, K. (2004). GAT (GGA and Tom1) domain responsible for ubiquitin binding and ubiquitination. *Journal of Biological Chemistry*, *279*(8), 7105-7111.

Shiina, I., Umezaki, Y., Ohashi, Y., Yamazaki, Y., Dan, S., & Yamori, T. (2013). Total synthesis of AMF-26, an antitumor agent for inhibition of the Golgi system, targeting ADP-ribosylation factor 1. *Journal of medicinal chemistry*, *56*(1), 150-159.

Shinotsuka, C., Yoshida, Y., Kawamoto, K., Takatsu, H., & Nakayama, K. (2002). Overexpression of an ADP-ribosylation factor-guanine nucleotide exchange factor, BIG2, uncouples brefeldin A-induced adaptor protein-1 coat dissociation and membrane tubulation. *Journal of Biological Chemistry*, *277*(11), 9468-9473.

Shu, X., Royant, A., Lin, M. Z., Aguilera, T. A., Lev-Ram, V., Steinbach, P. A., & Tsien, R. Y. (2009). Mammalian expression of infrared fluorescent proteins engineered from a bacterial phytochrome. *Science*, *324*(5928), 804-807.

Sirirattanakul, S., Wannakrairot, P., Tencomnao, T., & Santiyanont, R. (2015). Gene expression profile in breast cancer comprising predictive markers for metastatic risk. *Genetics and Molecular Research*, *14*(3), 10929-10936.

Song, Y., Madahar, V., & Liao, J. (2011). Development of FRET assay into quantitative and high-throughput screening technology platforms for protein–protein interactions. *Annals of biomedical engineering*, *39*(4), 1224-1234.

Soni, K. G., Mardones, G. A., Sougrat, R., Smirnova, E., Jackson, C. L., & Bonifacino, J. S. (2009). Coatomer-dependent protein delivery to lipid droplets. *Journal of cell science*, *122*(11), 1834-1841.

Sorieul, M., Langhans, M., Guetzoyan, L., Hillmer, S., Clarkson, G., Lord, J. M., ... & Frigerio, L. (2011). An Exo2 Derivative Affects ER and Golgi Morphology and Vacuolar Sorting in a Tissue-Specific Manner in Arabidopsis. *Traffic*, *12*(11), 1552-1562.

Spang, A., Shiba, Y., & Randazzo, P. A. (2010). Arf GAPs: gatekeepers of vesicle generation. FEBS letters, 584(12), 2646-2651.

Spooner, R. A., Watson, P., Smith, D. C., Boal, F., Amessou, M., Johannes, L., ... & Roberts, L. M. (2008). The secretion inhibitor Exo2 perturbs trafficking of Shiga toxin between endosomes and the trans-Golgi network. *Biochemical Journal*, *414*(3), 471-484.

Stafford, W. H., Stockley, R. W., Ludbrook, S. B., & Holder, A. A. (1996). Isolation, expression and characterization of the gene for an ADP-ribosylation factor from the human malaria parasite, Plasmodium falciparum. European journal of biochemistry, 242(1), 104-113.

Struck, D. K., Hoekstra, D., & Pagano, R. E. (1981). Use of resonance energy transfer to monitor membrane fusion. Biochemistry, 20(14), 4093-4099.

Sun, W., Vanhooke, J. L., Sondek, J., & Zhang, Q. (2011). High-throughput fluorescence polarization assay for the enzymatic activity of GTPase-activating protein of ADP-ribosylation factor (ARFGAP). *Journal of biomolecular screening*, *16*(7), 717-723.

Sztul, E., Chen, P. W., Casanova, J. E., Cherfils, J., Dacks, J. B., Lambright, D. G., ... & Wilhelmi, I. (2019). ARF GTPases and their GEFs and GAPs: concepts and challenges. *Molecular biology of the cell*, *30*(11), 1249-1271.

Szul, T., Grabski, R., Lyons, S., Morohashi, Y., Shestopal, S., Lowe, M., & Sztul, E. (2007). Dissecting the role of the ARF guanine nucleotide exchange factor GBF1 in Golgi biogenesis and protein trafficking. *Journal of cell science*, *120*(22), 3929-3940.

Tai, A. W., Benita, Y., Peng, L. F., Kim, S. S., Sakamoto, N., Xavier, R. J., & Chung, R. T. (2009). A functional genomic screen identifies cellular cofactors of hepatitis C virus replication. *Cell host & microbe*, *5*(3), 298-307.

Tanabe, K., Kon, S., Natsume, W., Torii, T., Watanabe, T., & Satake, M. (2006). Involvement of a novel ADP-ribosylation factor GTPase-activating protein, SMAP, in membrane trafficking: Implications in cancer cell biology. *Cancer science*, *97*(9), 801-806.

Tang, W., Tam, J. H., Seah, C., Chiu, J., Tyrer, A., Cregan, S. P., ... & Pasternak, S. H. (2015). Arf6 controls beta-amyloid production by regulating macropinocytosis of the Amyloid Precursor Protein to lysosomes. *Molecular brain*, *8*(1), 41.

Tarricone, C., Xiao, B., Justin, N., Walker, P. A., Rittinger, K., Gamblin, S. J., & Smerdon, S. J. (2001). The structural basis of Arfaptin-mediated cross-talk between Rac and Arf signalling pathways. *Nature*, *411*(6834), 215-219.

Terskikh, A., Fradkov, A., Ermakova, G., Zaraisky, A., Tan, P., Kajava, A. V., ... & Weissman, I. (2000). " Fluorescent timer": protein that changes color with time. *Science*, *290*(5496), 1585-1588.

Thavayogarajah, T., Gangopadhyay, P., Rahlfs, S., Becker, K., Lingelbach, K., Przyborski, J. M., & Holder, A. A. (2015). Alternative protein secretion in the malaria parasite Plasmodium falciparum. *PloS one*, *10*(4).

Thiam, A. R., Antonny, B., Wang, J., Delacotte, J., Wilfling, F., Walther, T. C., ... & Pincet, F. (2013). COPI buds 60-nm lipid droplets from reconstituted water–phospholipid–triacylglyceride interfaces, suggesting a tension clamp function. *Proceedings of the National Academy of Sciences*, *110*(33), 13244-13249.

Toda, T., Watanabe, M., Kawato, J., Kadin, M. E., Higashihara, M., Kunisada, T., ... & Horie, R. (2015). Brefeldin A exerts differential effects on anaplastic lymphoma kinase positive anaplastic large cell lymphoma and classical Hodgkin lymphoma cell lines. *British journal of haematology*, *170*(6), 837-846.

Truong, R. M., Francis, S. E., Chakrabarti, D., & Goldberg, D. E. (1997). Cloning and characterization of Plasmodium falciparum ADP-ribosylation factor and factor-like genes. *Molecular and biochemical parasitology*, *84*(2), 247-253.

Tsuchiya, M., Price, S. R., Tsai, S. C., Moss, J., & Vaughan, M. (1991). Molecular identification of ADP-ribosylation factor mRNAs and their expression in mammalian cells. *Journal of Biological Chemistry*, *266*(5), 2772-2777.

Turner, C. E. (2000). Paxillin interactions. *Journal of cell science*, *113*(23), 4139-4140.

Vallee, R. B., McKenney, R. J., & Ori-McKenney, K. M. (2012). Multiple modes of cytoplasmic dynein regulation. *Nature cell biology*, *14*(3), 224-230.

Venkateswarlu, K., P.B. Oatey, J.M. Tavare, and P.J. Cullen. 1998. Insulin-dependent translocation of ARNO to the plasma membrane of adipocytes requires phosphatidylinositol 3-kinase. *Curr. Biol*. 8:463–466.

Verkhusha, V. V., Otsuna, H., Awasaki, T., Oda, H., Tsukita, S., & Ito, K. (2001). An enhanced mutant of red fluorescent protein DsRed for double labeling and developmental timer of neural fiber bundle formation. *Journal of Biological Chemistry*, *276*(32), 29621-29624.

Vetter, I. R., & Wittinghofer, A. (2001). The guanine nucleotide-binding switch in three dimensions. *Science*, *294*(5545), 1299-1304.

Viaud, J., Zeghouf, M., Barelli, H., Zeeh, J. C., Padilla, A., Guibert, B., ... & Chavanieu, A. (2007). Structure-based discovery of an inhibitor of Arf activation by Sec7 domains through targeting of protein–protein complexes. *Proceedings of the National Academy of Sciences*, *104*(25), 10370-10375.

Vigil, D., Cherfils, J., Rossman, K. L., & Der, C. J. (2010). Ras superfamily GEFs and GAPs: validated and tractable targets for cancer therapy?. *Nature Reviews Cancer*, *10*(12), 842-857.

Wang, L., Jackson, W. C., Steinbach, P. A., & Tsien, R. Y. (2004). Evolution of new nonantibody proteins via iterative somatic hypermutation. *Proceedings of the National Academy of Sciences*, *101*(48), 16745-16749.

Watson, P. J., Frigerio, G., Collins, B. M., Duden, R., & Owen, D. J. (2004). γ-COP appendage domain–structure and function. *Traffic*, *5*(2), 79-88.

Wessels, E., Duijsings, D., Niu, T. K., Neumann, S., Oorschot, V. M., de Lange, F., ... & Melchers, W. J. (2006). A viral protein that blocks Arf1-mediated COP-I assembly by inhibiting the guanine nucleotide exchange factor GBF1. *Developmental cell*, *11*(2), 191-201.

Western, L. M., & Rose, S. J. (1991). A novel DNA joining activity catalyzed by T4 DNA ligase. *Nucleic acids research*, *19*(4), 809-813.

White, D. T., McShea, K. M., Attar, M. A., & Santy, L. C. (2010). GRASP and IPCEF promote ARF-to-Rac signaling and cell migration by coordinating the association of ARNO/cytohesin 2 with Dock180. *Molecular biology of the cell*, *21*(4), 562-571.

Wickham, M. E., Rug, M., Ralph, S. A., Klonis, N., McFadden, G. I., Tilley, L., & Cowman, A. F. (2001). Trafficking and assembly of the cytoadherence complex in Plasmodium falciparum-infected human erythrocytes. *The EMBO journal*, *20*(20), 5636-5649.

Wiek, S., Cowman, A. F., & Lingelbach, K. (2004). Double cross-over gene replacement within the sec 7 domain of a GDP–GTP exchange factor from Plasmodium falciparum allows the generation of a transgenic brefeldin A-resistant parasite line. *Molecular and biochemical parasitology*, *138*(1), 51-55.

Wilce, M. C., & Parker, M. W. (1994). Structure and function of glutathione S-transferases. *Biochimica et Biophysica Acta (BBA)-Protein Structure and Molecular Enzymology*, *1205*(1), 1-18.

Wilfling, F., Thiam, A. R., Olarte, M. J., Wang, J., Beck, R., Gould, T. J., ... & Walther, T. C. (2014). Arf1/COPI machinery acts directly on lipid droplets and enables their connection to the ER for protein targeting. *Elife*, *3*, e01607.

Willis, S., Villalobos, V. M., Gevaert, O., Abramovitz, M., Williams, C., Sikic, B. I., & Leyland-Jones, B. (2016). Single gene prognostic biomarkers in ovarian cancer: a meta-analysis. *PloS one*, *11*(2).

Woehler, A. (2013). Simultaneous quantitative live cell imaging of multiple FRET-based biosensors. *PLoS One*, *8*(4).

Wong, M., & Munro, S. (2014). The specificity of vesicle traffic to the Golgi is encoded in the golgin coiled-coil proteins. *Science*, *346*(6209), 1256898.

Wright, J., Kahn, R. A., & Sztul, E. (2014). Regulating the large Sec7 ARF guanine nucleotide exchange factors: the when, where and how of activation. *Cellular and molecular life sciences*, *71*(18), 3419-3438.

Wu, B., Piatkevich, K. D., Lionnet, T., Singer, R. H., & Verkhusha, V. V. (2011). Modern fluorescent proteins and imaging technologies to study gene expression, nuclear localization, and dynamics. *Current opinion in cell biology*, *23*(3), 310-317.

Xie, X., Tang, S. C., Cai, Y., Pi, W., Deng, L., Wu, G., ... & Teng, Y. (2016). Suppression of breast cancer metastasis through the inactivation of ADP-ribosylation factor 1. *Oncotarget*, *7*(36), 58111.

Yadav, S., Puthenveedu, M. A., & Linstedt, A. D. (2012). Golgin160 recruits the dynein motor to position the Golgi apparatus. *Developmental cell*, *23*(1), 153-165.

Yagi, R., Tanaka, M., Sasaki, K., Kamata, R., Nakanishi, Y., Kanai, Y., & Sakai, R. (2011). ARAP3 inhibits peritoneal dissemination of scirrhous gastric carcinoma cells by regulating cell adhesion and invasion. *Oncogene*, *30*(12), 1413-1421.

Yang, J. S., Lee, S. Y., Gao, M., Bourgoin, S., Randazzo, P. A., Premont, R. T., & Hsu, V. W. (2002). ARFGAP1 promotes the formation of COPI vesicles, suggesting function as a component of the coat. *The Journal of cell biology*, *159*(1), 69-78.

Zacharias, D. A., Violin, J. D., Newton, A. C., & Tsien, R. Y. (2002). Partitioning of lipid-modified monomeric GFPs into membrane microdomains of live cells. *Science*, *296*(5569), 913-916.

Zeeh, J. C., Zeghouf, M., Grauffel, C., Guibert, B., Martin, E., Dejaegere, A., & Cherfils, J. (2006). Dual specificity of the interfacial inhibitor brefeldin a for arf proteins and sec7 domains. *Journal of Biological Chemistry*, *281*(17), 11805-11814.

Zeghouf, M., Guibert, B., Zeeh, J. C., & Cherfils, J. (2005). Arf, Sec7 and Brefeldin A: a model towards the therapeutic inhibition of guanine nucleotide-exchange factors.

Zhang, C. J., Cavenagh, M. M., & Kahn, R. A. (1998). A family of Arf effectors defined as suppressors of the loss of Arf function in the yeast Saccharomyces cerevisiae. Journal of Biological Chemistry, 273(31), 19792-19796.

Zhang, G. F., Patton, W. A., Lee, F. J. S., Liyanage, M., Han, J. S., Rhee, S. G., ... & Vaughan, M. (1995). Different ARF domains are required for the activation of cholera toxin and phospholipase D. *Journal of Biological Chemistry*, *270*(1), 21-24.

Zhang, J. H. (1999). chung, TD; oldenburg, K. r. a simple statistical Parameter for Use in evaluation and validation of High Throughput screening assays. *J. Biomol. Screen*, *4*(2), 67-73.

Zhang, L., Hong, Z., Lin, W., Shao, R. X., Goto, K., Hsu, V. W., & Chung, R. T. (2012). ARF1 and GBF1 generate a PI4P-enriched environment supportive of hepatitis C virus replication. *PLoS One*, *7*(2), e32135.

Zhao, H., Ahirwar, D. K., Oghumu, S., Wilkie, T., Powell, C. A., Nasser, M. W., ... & Ganju, R. K. (2016). Endothelial Robo4 suppresses breast cancer growth and metastasis through regulation of tumor angiogenesis. *Molecular oncology*, *10*(2), 272-281.

Zhao, X., Claude, A., Chun, J., Shields, D. J., Presley, J. F., & Melançon, P. (2006). GBF1, a cis-Golgi and VTCs-localized ARF-GEF, is implicated in ER-to-Golgi protein traffic. *Journal of cell science*, *119*(18), 3743-3753.

Zhao, X., Lasell, T. K., & Melancİon, P. (2002). Localization of large ADP-ribosylation factor-guanine nucleotide exchange factors to different Golgi compartments: evidence for distinct functions in protein traffic. *Molecular biology of the cell*, *13*(1), 119-133.

Zimmermann, T., Rietdorf, J., & Pepperkok, R. (2003). Spectral imaging and its applications in live cell microscopy. *FEBS letters*, *546*(1), 87-92.